ABSORPTION OF ATOMIC HYDROGEN IN A STRONG MAGNETIC FIELD

A thesis submitted for the degree of

Doctor of Philosophy

in

the University of London

by

Stephanie M. Kara, B.Sc. (London)

June 1981

ABSTRACT

The photoabsorption of atomic hydrogen in a strong static magnetic field is studied. The bound states are considered in some detail, approximating the wavefunctions by a set of unperturbed, spherical hydrogenic functions and a set of simple separable functions of cylindrical symmetry. Results are presented for the energy eigenvalues of fourteen low lying states in the range of magnetic field strengths $10^7 \leq B \leq 2.35 \times 10^9$ G. The eigenfunctions corresponding to the bound states are used to obtain electric dipole transition probabilities. For strong transitions ($A_{mn} > 0.1 \times 10^8$ s^{-1}), transition probabilities in the two approximations agree at fields of 10^7 and 10^8 G. However, at $5 \times 10^8 \leq B \leq 2.35 \times 10^9$ G, the cylindrical basis proves to give a better description of the system, producing a lower set of energy eigenvalues, and the agreement between the two sets of transition probabilities is not so good. Relativistic and spin effects are neglected here.

The simple cylindrical functions are used to calculate photoionization cross sections, enabling, in the case of the pure Landau continuum, all the matrix elements occurring in these cross sections to be calculated analytically. A second, more appropriate model for the continuum, in the range of fields considered, is also used, in which the Coulomb attraction of the nucleus is considered in the plane perpendicular to the field direction. Wavefunctions and energy eigenvalues for the discrete states in this second continuum model are calculated numerically, from a two point boundary value equation. Calculations of the photoionization of the lowest even and odd parity bound states at photon energies from the (field dependent) ionization threshold to 8γ rydbergs above it are reported, where $\gamma = \hbar\omega_c$. The appropriate generalization of the Wigner threshold law is given. Resonances are found at each embedded discrete

continuum level in the absence of broadening, and secondary maxima associated with the motion along the field are predicted, and confirmed in a simple model. Results for the two continuum models are compared and the differences discussed in some detail.

ACKNOWLEDGEMENTS

I should like to express my thanks and appreciation to Professor M R C McDowell for his guidance and advice throughout the course of this work. I am also grateful to Dr L A Morgan for her assistance with computational problems, and to Professor E S Chang for helpful discussions at an early stage on the bound-bound transitions.

I am indebted to the Science Research Council for their financial support in the form of a research studentship, and to the University of London Computing Centre for the facilities provided by them.

Finally, I acknowledge all those involved in the compilation of this thesis, including Mrs G Dickerson for her contribution to the typing, despite a difficult manuscript, Mrs M Dixon for typing some of the tables, and Mr W Kara for his generous help during the finishing stages.

CONTENTS

CHAPTER 1

INTRODUCTION

§ 1.1 General Background

Since the first discovery of the existence of strong magnetic fields in a white dwarf by Kemp et al 1970 and Kemp, 1970, much work has been carried out on the properties of atoms and ions in such strong fields. Kemp estimated that a field of about 10^7 Gauss is present in the white dwarf Grw + $70^{\circ}8247$, and since then, the existence of large magnetic fields in pulsars thought to be up to 10^{12} Gauss at the surface, have also been demonstrated (Ruderman, 1972).

The study of atoms and ions in strong magnetic fields is also of importance in solid state physics where the effects of high fields may be observed at low fields. This is due to two properties of solids: (i) the mass of an electron in motion in a solid must be represented by the effective mass m^*, which may be several orders of magnitude smaller than m, the mass of the electron in free space and (ii) the dielectric constant of a solid is not unity, as in the case of free space, but may have a value in the range 10 to 50 (Praddaude, 1972). Both of these facts contribute significantly to the change in the ratio of the magnetic energy to the Coulomb energy (denoted by γ) from the case where the atom exists in free space. We have,

$$\gamma = \frac{\hbar \omega_c}{2\,Ry^*} \quad \text{a.u.} \tag{1.1}$$

where $\omega_c = \frac{eB}{m^*}$ is the cyclotron frequency and $Ry^* = \frac{m^* e^4}{2\hbar^2 D^2}$ is the effective Rydberg with D the dielectric constant. Now if we suppose

$D = 50$ and $m^* = 0.1m$, then it is clearly seen that γ is a factor of 2.5×10^5 greater than for the case where $D = 1$ and $m = m^*$. In other words, if a magnetic field of strength 10^4G (a fairly weak field) was applied to the solid, the effects observed, would be those of a field of 2.5×10^9G (a strong field) in free space.

More recently, fairly intense magnetic fields of $10^4 - 5 \times 10^4$G have been produced over large volumes in magnetically confined, controlled thermonuclear fusion experimental devices. The effects of these fields on the atomic properties of the trapped plasma is of considerable importance. Laboratory magnetic fields of 2×10^5G have now been achieved. Very strong magnetic fields are also known to exist in the ablation layers of targets used in inertial fusion experiments (Lawson, 1979), where such physical processes as photoionization of atomic hydrogen (as deuterium and tritium) and of highly stripped (hydrogenic) ions occur.

It is the effect of these strong magnetic fields on atomic hydrogen that is studied here. It is necessary, at this point, to define what is meant by a "strong magnetic field". A weak magnetic field will be referred to as one in which the Coulomb force of the nucleus dominates the magnetic field such that the ordinary Zeeman level splitting occurs, and the quadratic Zeeman effect is negligible. The region of field strengths in which this occurs is approximately $0 < B < 10^7$G. We will define a strong magnetic field as one in which the Coulomb and magnetic interactions become comparable, the quadratic Zeeman term being non-negligible ie $10^7 < B < 10^{11}$G. Above about 10^{11}G, the magnetic field completely dominates the Coulomb field and we move into what is known as the quasi-Landau regime, where the motion of electrons is close to that of free electrons in a magnetic field. These regions, and the effects on the bound and free levels are described more fully by Garstang, 1977.

It is the strong field case which proves to be the most difficult to solve, as neither the Coulomb nor the magnetic field can be treated as a perturbation. The resulting problem to be solved in order to calculate the energies and wavefunctions of the electron of the hydrogen atom, proves to be non-separable, and as a result, no exact solution can be found.

§1.2 Effect of the Magnetic Field on the Bound States of Atomic Hydrogen

Firstly, we will consider the problem of finding the bound state energies and corresponding wavefunctions of the hydrogen atom in a strong static magnetic field. It is a well-known result of quantum mechanics that the equation to be solved is the (time-independent) Schrodinger equation:

$$H \psi_j = E_j \psi_j \qquad (1.2)$$

where E_j is the energy of the bound state $|j\rangle$, ψ_j the corresponding quadratically integrable wavefunction and H the Hamiltonian of the system. Now the Hamiltonian for this system is the sum of the zero field Hamiltonian, a term denoting the electron spin orbit interaction, a term linear in the magnetic field strength B, and a quadratic term in B, the last two terms denoting the interaction of the atom with the external magnetic field. The linear term in B gives rise to the linear Zeeman effect, and the quadratic term gives rise to the quadratic Zeeman effect (Landau and Lifshitz, 1975, Ch.XIV). For a detailed account of the structure of the atom in magnetic fields of various strengths, see Garstang, 1977. It is sufficient to say here, that for the range of magnetic field strengths which we are considering (ie between 10^7 and 10^9 Gauss), the quadratic term in B cannot be neglected. In fact, at fields as strong as 10^9G, it will be seen later, that this term is very important to the structure of the bound, and indeed the free, states.

It is seen in section §2.2 that, due to the nature of the Hamiltonian, equation (1.2) is non-separable and so cannot be solved exactly. Unlike the case of the classical Zeeman effect in which the principal, angular momentum and magnetic quantum numbers remain good quantum numbers, the magnetic field is too strong to be treated as a perturbation and the states can only be labelled by principle quantum number n,m, the magnetic quantum number and parity π. In practice, however, we continue for convenience to label the bound states with their corresponding zero field labels (n,ℓ,m), preserving the same order for n and ℓ as at zero field for each m and parity.

As perturbation theory becomes inadequate at the fieldstrengths considered here, the variational method must be used in order to find an approximate solution to equation (1.2). This involves expanding the wavefunctions in a suitable basis. If this basis is complete, then the calculated energy eigenvalues and wavefunctions will be exact, but it will be seen that it is not practical to use a complete basis set. If we expand the wavefunction of the ground state (Ψ_{1s_o}) in terms of a set of basis functions $\{\phi_j : j = 1,2\ldots\}$, then we have the following trial solution:

$$\Psi_{1s_o} = \sum_j a_j \phi_j \tag{1.3}$$

where the a_j are constants. Now it has been shown by Hylleraas and Undheim, 1930, and MacDonald, 1933, that the exact energy of the ground state is always a lower bound on the energy obtained using a (normalized) trial function such as that of equation (1.3). That is,

$$E_{1s_o} \leq \frac{\int \Psi^*_{1s_o} H \Psi_{1s_o} d\tau}{\int |\Psi_{1s_o}|^2 d\tau} \tag{1.4}$$

where E_{1s_o} is the exact energy of the ground state. This simple variational method is concerned with finding an expression for Ψ_{1s_o} in

terms of the ϕ_j , of the form given by equation (1.3), such that the right hand side of equation (1.4) is a minimum. The trial function for ψ_{1s_o} will be dependent on one or more parameters, which may be varied until a minimum trial energy eigenvalue is obtained. If the chosen trial function is close to the true nature of the exact wavefunction, then the corresponding energy will also be close to the exact energy. For a detailed discussion see Dalgarno in Bates, Quantum Theory Vol.1. It is important therefore, to consider very carefully, the nature of the physical situation before choosing appropriate trial solutions.

Trial wavefunctions for the higher excited states can also be found, but care must be taken to ensure that all the ψ_i form an orthonormal set. To be more specific, all states of given (m,π) must be orthogonal. The calculations involved in the solution of equation (1.2) are discussed in more detail in chapters 2 and 3.

In choosing suitable trial solutions for the wavefunctions of the bound states of the hydrogen atom, the effect of the magnetic field on the orbit of the electron must be considered. In order to do this, we first consider the free motion of an electron in a magnetic field.

In classical mechanics, it is found that the force exerted by an external magnetic field on a particle, is proprotional to the product of the charge of the particle and the velocity of the particle in the plane perpendicular to the direction of the field. In fact

$$F = evB \qquad (1.5)$$

where B is the field strength and v the component of velocity perpendicular to the field. If we take the field to be in the z direction, then v will be the velocity in the (x - y) plane. As the force exerted by this field acts in a direction perpendicular to the velocity, only

the direction of the velocity will change, and not the magnitude. The motion is therefore circular in the (x - y) plane with constant radius r and (again from the results of classical mechanics) we have

$$F = \frac{mv^2}{r} \quad . \tag{1.6}$$

Combining equations (1.5) and (1.6) we find that

$$r = \frac{mv}{eB} \quad . \tag{1.7}$$

The classical angular frequency is defined as v/r and this can be written

$$\omega_c = \frac{eB}{m} \tag{1.8}$$

where ω_c is known as the cyclotron frequency.

The Schrodinger equation for a free electron in a magnetic field $B\underline{z}$ has been solved by Dingle, 1952, who shows that the energy of the electron is unquantized in the z- direction, but that it can only take allowed values in the (x - y) plane. From equation (1.7) it can be seen that if we write

$$E = \frac{mv^2}{2} \tag{1.9}$$

then the radius of the motion in the (x - y) plane is dependent on the energy of the electron. This implies that the radius of the orbit of the electron about the field direction, can also only take certain allowed values. In fact, it has been shown by Dingle, 1952, that the energies in the x - y plane are given by

$$E_n = (n + \tfrac{1}{2})\hbar\omega_c \tag{1.10}$$

where n = 0,1,2..... Substituting equations (1.10) and (1.9) into equation (1.7), we obtain

$$\bar{r}_n = \left(\frac{\hbar}{eB}\right)^{\frac{1}{2}} (2n + 1)^{\frac{1}{2}} \tag{1.11}$$

and the cyclotron radius is defined by

$$R = \left(\frac{\hbar}{eB}\right)^{\frac{1}{2}} \quad . \tag{1.12}$$

The discrete energy levels occupied by the electron in the x - y plane are known as the Landau levels, and these levels are equally spaced by $\hbar\omega_c$ a.u. ($= 2\hbar\omega_c$ Ry).

To summarize, to a first approximation, a free electron in a magnetic field will describe a helical orbit about the field direction, the radius of the orbit in the plane perpendicular to the field direction, and the energy of the electron being quantized according to equations (1.10) and (1.11), but the guiding centre of the orbit "gitterbugs" as m changes.

Returning to the problem of the hydrogen atom in a magnetic field, we would expect, in the limit as $B \to \infty$, that the Coulomb attraction of the nucleus would become relatively negligible, and that the electron would behave as a free electron in a magnetic field. It has already been seen that this free motion is cylindrically symmetric about the field direction, and so, as the magnetic field strength becomes greater, we would expect that the orbit described by the electron becomes more and more elongated in the z- direction, as it approaches the Landau limit, departing from the zero field spherical symmetry. Once the symmetry of the system has been established, it should then be possible to describe, with great accuracy, the wave-functions in terms of a basis of either cylindrical or spherical functions. In practice, however, a region exists in which the orbits are ovoid in shape, the major axis lying along the field direction, and in this case, the system possesses neither cylindrical or spherical symmetry, and it is this region of field strengths which is the primary topic of study here.

Throughout, the magnetic field strength will be measured in terms of the parameter γ, where

$$\gamma = \frac{\hbar\omega_c}{2(Ry)}, \quad \gamma = 1 \text{ when } B = 2.35 \times 10^9 G. \qquad (1.13)$$

In fact, γ is the ratio of the square of the radius of the first Bohr orbit (a_0) to the square of the cyclotron radius. Now as R^2 is inversely proportional to B, it would appear that the cyclotron radius decreases with increasing field strength, thus γ increases as B increases. We consider three cases: firstly, if $\gamma \ll 1$, then $a_0^2 \ll R^2$, ie for the ground state of the hydrogen atom, the region to which the magnetic field confines the electron is large compared to the dimensions of the atom, and so the effect of this field on the ground state wavefunction is minimal. For higher excited states, however, where the size of the orbit of the electron at zero field can approach the cyclotron radius, the magnetic field becomes more important. In this situation, the effects of a high magnetic field are observed at low fields. For instance, at $B = 2.35 \times 10^4 G$ (ie $\gamma = 10^{-5}$), the atomic radius approaches the cyclotron radius at states with principle quantum number 58 (Garstang, 1977). As γ approaches unity, the cyclotron and Bohr radii become comparable and the effects of the field on the wavefunctions of all the bound states are significant. The fields which are considered here, lie in the range $4.3 \times 10^{-3} \leq \gamma \leq 1$, which fall in this region. For $\gamma \gg 1$, the cyclotron radius becomes much smaller than the Bohr radius and in this case, the magnetic field becomes the dominant force.

It is the region around $\gamma = 1$ where it is the most difficult to find suitable trial wavefunctions for the bound states as, for the states of lower energy, the orbit of the electron becomes ovoid and cannot be described exactly by a set of either cylindrical or spherical functions.

However, both approaches are considered here. We first take a set of basis functions containing unperturbed spherical, hydrogenic functions, and also a set of cylindrical functions and compare the two sets of results, to see which is the more accurate within the range of fields considered, ie which produces the lower set of energy eigenvalues.

The basis of hydrogenic states was first used by Brandi, 1975, whose results for the ground state energies are found to be in excellent agreement with the results of Cabib et al, 1972 in the range of field strengths $2.35 \times 10^8 \leq B \leq 2.35 \times 10^9$G (ie $0.1 \leq \gamma \leq 1$), and substantially better than those obtained by Yafet et al, 1956 who used a very simple cylindrical basis. It will, however, be seen that this is not the case with states of higher energies, and that for these higher states, the wavefunctions are much better described by a basis of cylindrical functions for $B \geq 5 \times 10^8$G.

A spherical basis has also been used by Smith et al, 1972, but numerical results for energies are not presented and so comparison is impossible. However, results are presented for bound-bound transition probabilities for which comparison is possible with those obtained in the hydrogenic and cylindrical bases (see Chapter 3 for a detailed discussion of these results).

Praddaude, 1972, applied a basis of more complicated cylindrical functions to the problem, which give the correct asymptotic behaviour of the wavefunctions as $r \to \infty$ and as $r \to 0$. The results obtained compare well with those of the simple cylindrical basis used here (Kara and McDowell, 1980) and these are discussed in more detail in Chapter 3. The complicated functions of Praddaude, however, are non-separable and therefore not of practical use in the calculation of such matrix elements

as those occurring in the bound-bound transition probabilities and oscillator strengths.

Perturbation calculations have been carried out by Ruder et al, 1981, who show that a perturbation treatment of the magnetic field is adequate up to fields of the order of 10^7G and obtain very good agreement with the results of Praddaude, 1972, Cabib et al, 1972 and Kara and McDowell, 1980, at this field strength.

Much work has also been carried out in the very high field region, although such high fields are not considered in detail here. For instance, Simola and Virtamo, 1978, have used a basis of Landau orbitals for their wavefunctions and consider fields in the region $\gamma \gg 1$. Results are given for ground state binding energies and ionization energies for seven excited states and are 4-5% better than those obtained by the simple cylindrical basis of Yafet et al, 1956, in the range $10 < \gamma < 100$. Numerous other variational calculations such as those of Pokatilov and Rusanov, 1969, Bhaduri et al, 1977, and Dos Santos and Brandi, 1976, who used a basis of three dimensional harmonic oscillator functions, have also been carried out in this region. The results of Dos Santos and Brandi, 1976, in fact, are shown to be more accurate than the hydrogenic functions for $10^9 < B < 10^{11}$G, which is exactly what we would expect. Their results are also in good agreement with those of Praddaude, 1972. This work has also been extended by Brandi and Koiller, 1978, who add a variational scaling parameter to each basis set (ie the hydrogenic and three dimensional harmonic oscillator sets) to improve them, but still do not achieve the accuracy of the cylindrical bases used by Kara and McDowell, 1980, and Praddaude, 1972, etc. for high fields ($B \gg 5 \times 10^8$G).

An additional problem is prevalent at very high fields, and that is one concerning the relativistic effects on the bound states of such

a system. This has been studied by Glasser and Kaplan, 1975, who show that relativistic effects may be significant at fields as low as 10^{10}G for the excited states of atomic hydrogen.

Another technique for dealing with the very high field problem has been studied by Pavlov-Verevkin and Zhilinskii, 1980 who use a method based on perturbation theory. Their first order wavefunction is a product of Landau functions and eigenfunctions of the Hamiltonian describing motion in a one-dimensional Coulomb potential to a finite distance away from the nucleus. The motion due to the Coulomb field outside the cyclotron radius is treated as a perturbation. The range of field strengths studied is $B \gg 10^{10}$G and much complicated numerical work is involved. Results compare favourably with those of Simola and Virtamo, 1978, and Praddaude, 1972, for $B > 5 \times 10^{9}$G, and it is shown that for $B \geq 10^{10}$G, third order perturbation theory is sufficient.

High Rydberg states have also been a subject of much study as, due to the diminishing effect of the Coulomb field as the electron moves further away from the nucleus, electrons in these states, even at low fields possess the properties of those at lower energies in higher fields. This quadratic Zeeman effect has been observed experimentally by Garton and Tomkins, 1969, Lu, Tomkins and Garton, 1978 and others, and was considered theoretically by Edmonds, 1970 who adopted a semiclassical approach, which is appropriate in this region.

In a further study by Edmonds, 1973, a somewhat different approach was used, in that the Schrodinger equation was solved, expanding the wavefunctions in a basis of Sturmian functions. These functions have the advantage that they form a discrete complete basis set, and so the continuum states are effectively included, which are significant for the high Rydberg states. The basis must be truncated in order that the problem

be finite and results for fairly low states have been compared with those obtained using the hydrogenic basis at about 10^4G. It was found that the two sets of results were not significantly different, and the hydrogenic basis, only requiring a few terms, was preferable to the basis of Sturmian functions which requires an extremely large number of terms in order that convergence may be obtained on the eigenvalues. However, it is expected that the Sturmian basis will be far more accurate than the hydrogenic basis for higher states. This work has been extended by Clark and Taylor, 1980, who use a similar basis and calculate oscillator strengths for dipole transitions from the ground state to states lying above n = 16 at B = 47 kG, and illustrate the inter-ℓ mixing occuring at high levels due to the presence of the quadratic Zeeman term.

Having obtained the energy levels for atomic hydrogen, it is then easy to obtain energies for any other one electron system, as has been shown by Surmelian and O'Connell, 1974. They derive the basic result

$$E(Z,B) = Z^2 E(1,B') \tag{1.14}$$

where $B' = B/Z^2$ and Z is the charge on the nucleus. $E(1,B')$ of course, are the energies of the states of the hydrogen atom.

A scaling law for the bound-bound transition probabilities and oscillator strengths for different nuclear charges has been derived by Wunner, et al, 1980 and can be written

$$D_{if}(Z,B) = \frac{1}{Z^2} D_{if}\left(1, \frac{B}{Z^2}\right) \tag{1.15}$$

where D_{if} is the dipole matrix element. So the bound-bound transition probabilities and oscillator strengths for similar systems such as He^+ can now be calculated directly from those of the simple atomic hydrogen case. Wunner et al, 1980, used a polynomial approximation for

Fig. 1.1

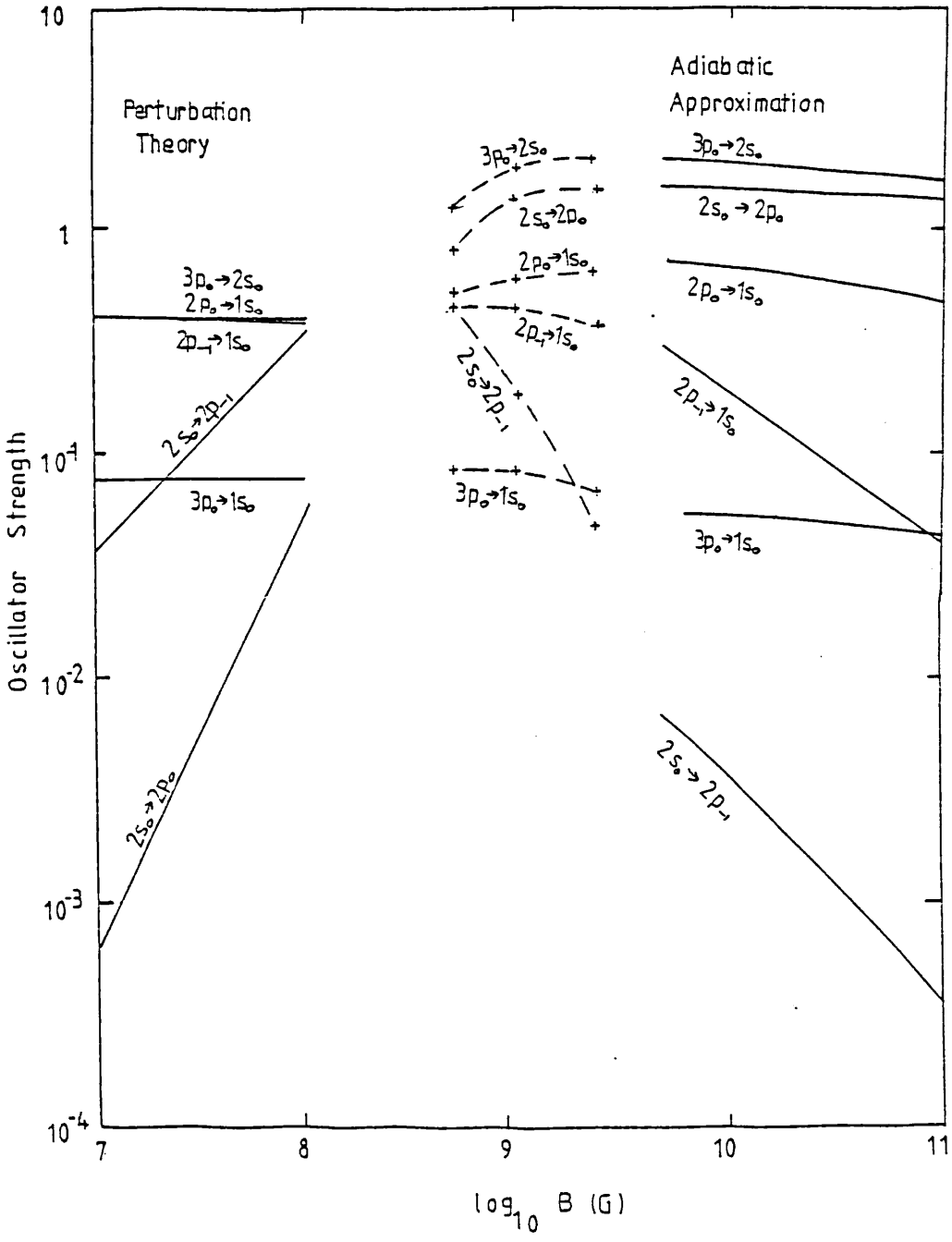
Perturbation Theory
Adiabatic Approximation
$3p_0 \to 2s_0$
$2p_0 \to 1s_0$
$2p_{-1} \to 1s_0$
$2s_0 \to 2p_{-1}$
$3p_0 \to 1s_0$
$2s_0 \to 2p_0$
$2p_0 \to 1s_0$
$2p_{+1} \to 1s_0$
$2s_0 \to 2p_{-1}$
$3p_0 \to 1s_0$
$3p_0 \to 2s_0$
$2s_0 \to 2p_0$
$2p_0 \to 1s_0$
$2p_{+1} \to 1s_0$
$2s_0 \to 2p_{-1}$
$3p_0 \to 1s_0$
Oscillator Strength
10
1
10^{-1}
10^{-2}
10^{-3}
10^{-4}
7
8
9
10
11
$\log_{10}$ B (G)

Figure 1.1

Oscillator strengths of some bound-bound transitions as a function of magnetic field strength. The perturbation theory results in the low field region and the adiabatic approximation results in the very high field region have been given by Wunner et al 1980, whilst the broken line represents the cylindrical basis results calculated in the electric dipole approximation (Kara and McDowell, 1980).

the dipole matrix elements and excellent agreement is obtained for results for some oscillator strengths at $B = 10^7$G with those of our spherical wavefunctions (see chapter 4).

Throughout this thesis, the electric dipole approximation for transitions has been used, ie the wavelength of the emitted radiation is considered to be large compared with the dimensions of the hydrogen atom. However, an adiabatic approximation (Wunner, 1980) is appropriate at very high fields ($\gamma \gg 1$) and it is shown in figure (1.1) that the oscillator strengths go smoothly into those calculated in the adiabatic approximation at high fields. There is also reasonable agreement with the perturbation theory calculations at low fields (Wunner et al, 1980), showing that this cylindrical basis gives a good description of the wavefunctions in the range of field strengths $5 \times 10^8 \leq B \leq 2.35 \times 10^9$G.

Two electron systems such as He, Li^+ etc. have also been studied by various authors, but no discussion of them will be given here. For a full discussion refer to Garstang, 1977.

§1.3 Effect of the Magnetic Field on the Continuum States and the Photoionization Spectrum

The effect of the magnetic field on the free electron has already been discussed in the previous section, and it was found that such an electron is confined to Landau levels in the plane perpendicular to the field lines, with the possibility of escape in the field direction. We consider the effect of a Coulomb field on these Landau levels. It has been shown, by a semiclassical argument (Starace, 1973) that if the motion in the (ρ , ϕ) plane in cylindrical polar coordinates (we assume $\underline{B} = B\underline{z}$), is decoupled from that in the z direction, and the

Coulomb force exerted by the nucleus is approximated by a term $-\frac{1}{\rho}$ a.u., then applying the semiclassical Bohr-Sommerfeld quantization condition, gives an energy spacing of about $1.5\hbar\omega_c$ a.u., in the threshold region for each value of the magnetic quantum number m_f. However, as one moves away from threshold, the Landau limit is eventually reached where the spacing is $\hbar\omega_c$ a.u. This effect was first observed experimentally by Garton and Tomkins, 1969, in Ba. Experiments have also been carried out on Rb (Economou et al, 1979), Sr (Fonk et al, 1978 and Lu et al, 1978) and most recently, on Cs by Gay et al, 1980 who give results up to 8×10^4G. All have observed this threshold spacing. In fact, it is true that whenever there is a mixing of fields, a pattern of equally spaced levels near threshold will be seen (Rau, 1979). This implies that the structure of the continuum in a semiclassical approximation is significantly changed by the presence of a Coulomb field and this is clearly observed in the results presented in Chapter 6. The energies calculated by the Bohr - Sommerfeld quantization condition

$$\int_{\rho_1}^{\rho_2} \left\{ E_n - \frac{m^2}{\rho^2} + \frac{\gamma^2\rho^2}{4} - \frac{2e^2}{r} \right\}^{\frac{1}{2}} d\rho = (n+\tfrac{1}{2})\pi \qquad (1.16)$$

where $n = 0,1.....$ and ρ_1 , ρ_2 are the zeros of the integrand, correspond to the wavefunctions calculated by the semiclassical WKB method (Akimoto and Hasegawa, 1967).

On calculating the continuum wavefunctions we do not consider the semi-classical method, but rather, solve the Schrodinger equation directly, by numerical means, to obtain an exact solution. We use the same approximation for the Coulomb field as Starace, 1973, Rau, 1979, etc. and this renders the Schrodinger equation separable. However, as is shown in Chapter 6, the WKB method gives a good first approximation to the energy eigenvalues for these calculations.

The effect of the Coulomb field on these continuum state functions, is to draw them to smaller ρ, thus significantly changing the form of the wavefunction in the region of overlap with the bound states (which is approximately $0 \leq \rho \leq 8\ a_0$). It also has the dramatic effect of changing considerably, the energy E_n corresponding to the state $|n\rangle$, particularly at lower magnetic fields, but the Landau limit is approached as $B \to \infty$. Results for the continuum wavefunctions and energies are discussed in greater detail in Chapter 6.

Photoionization cross-sections have been studied extensively for zero magnetic field and results for many atoms and ions have been tabulated for a wide range of energies. For example, the hydrogen atom has been dealt with by Burgess et al, 1964 and many other systems are considered by Peach, 1967 and Peach, 1970. However, little is known about the cross sections when a magnetic field is switched on.

Only limited experimental work has been carried out in fields of interest here, due to the difficulties in obtaining high fields in the laboratory. At present, fields up to about 10^5G have been obtained. Amongst the experiments carried out in this field, are those performed by Blumberg et al, 1978. They consider the photodetachment cross-section for S^- in fields up to 15.7kG. Results for both π and σ polarized light are given. They observe peaks at the discrete continuum levels, a phenomenum first predicted in the simple theoretical approach of Wallis and Bowlden, 1956, where the ground state wavefunction was taken to be of the simple form

$$\Psi_{1s_0} = N e^{-\delta r^2} \tag{1.17}$$

and the continuum was represented by pure Landau levels.

We study the photoionization cross-section with both the Landau and the Coulomb modified continua, and study in detail the behaviour of the cross-section at the discrete levels. (Kara and McDowell, 1981). We find, in fact, that in our approximation, and in the absence of broadening due to the velocity of the residual ion, that the behaviour of the cross section at the discrete energy levels goes as $1/k_z$ or k_z depending on the parity and magnetic quantum number of the initial and final states. This is in agreement with the theoretical prediction of Blumberg et al, 1979, on S^-. On including the broadening effects due to the motion of the ion, agreement is obtained with previous experimental results.

More recently, some theoretical results have been presented by Schmidt et al, 1981. They, however, only consider photoionization to final states whose energies lie in the interval $[\hbar\omega_c, 2\hbar\omega_c]$ ry, ie up to the second Landau level. The initial state is a Landau type orbital as the field strengths studied are in the range $2.35 \times 10^{11} < B < 4.7 \times 10^{13}$, ie $100 < \gamma < 2 \times 10^4$. These are far higher than those studied here and, due to the dominance of the magnetic interaction, it is assumed that the continuum contains pure Landau levels in the (ρ, ϕ) plane, with the Coulomb field only considered along the z axis. An interesting discovery here, is that the behaviour of the cross-section at the threshold $\hbar\omega = \hbar\omega_c$, is constant with respect to E_z, which is in agreement with the prediction of Wigner, 1948, in the presence of a Coulomb field.

In a recent publication (McDowell, 1981) it has been shown that the scaling law, relating cross sections for different nuclear charges, is exactly the same as that given in equation (1.15) for the dipole

matrix elements. The cross sections are related by

$$\frac{a_{\nu_1}(Z_1, B_1)}{a_{\nu_2}(Z_2, B_2)} = \left(\frac{Z_2}{Z_1}\right)^2 \tag{1.18}$$

where

$$\nu_i = Z_i^2 \nu \tag{1.19}$$

and

$$B_i = \frac{B}{Z_i^2} \tag{1.20}$$

Z_1 and Z_2 being the charges of two hydrogenic ions, and $h\nu$ being the energy of the incident photon.

Cross sections for other hydrogenic ions can now be calculated directly from those of atomic hydrogen which are given in Chapters 5 and 6.

CHAPTER 2

ENERGIES AND BOUND-BOUND TRANSITIONS USING A BASIS OF UNPERTURBED HYDROGENIC STATES

§2.1 Introduction

This chapter is concerned with the calculation of energies and bound-bound transitions of atomic hydrogen in a strong static magnetic field, the wavefunctions being expanded in a basis of unperturbed hydrogenic functions. The reason for this choice of basis functions is discussed in the introductory chapter. Section §2.2 derives an expression for the Hamiltonian which includes a linear and a quadratic term in B (the magnetic field strength). At the field strengths we are considering, the quadratic term is not negligible. The eigenvalue equation is also derived, from which the energies and wave functions can be calculated. The next section calculates all the matrix elements required to solve the eigenvalue equation derived in §2.2, and section §2.4 describes the numerical methods used in solving this equation. In order to solve the equation, the matrix elements must all be reduced to a form in which they can easily be computed. This is achieved in section §2.5. The remainder of the chapter is devoted to deriving formulae to calculate the bound-bound transition probabilities and oscillator strengths. The same matrix elements occur in the transition probabilities and oscillator strengths, and these are calculated in section §2.7.

§2.2 The Hamiltonian And Energy Eigenvalue Equation

The Hamiltonian of a particle of mass μ, charge -e and momentum $p = -i\hbar\nabla$, moving in the Coulomb potential of a proton, $-\frac{e^2}{r}$ (infinite

mass assumed) is

$$H_o = \frac{1}{2\mu} \underline{p}^2 - \frac{e^2}{r} = -\frac{\hbar^2}{2\mu} \nabla^2 - \frac{e^2}{r} \quad . \tag{2.1}$$

When a magnetic field $\underline{B}$ is imposed on the system, by a well-known result of classical mechanics (Goldstein, 1950, p222), the Hamiltonian is obtained by replacing $\underline{p}$ by $\underline{p} + \frac{e\underline{A}}{c}$ where

$$\underline{A} = \underline{A}(\hat{r},t) \tag{2.2}$$

is the (time dependent) vector potential which represents the interaction between the electron and the magnetic field. The Hamiltonian then becomes

$$H = \frac{1}{2\mu} \left(\underline{p} + \frac{e\underline{A}}{c} \right)^2 - \frac{e^2}{r}$$

$$\text{i.e.} \quad H = H_o + \frac{1}{2\mu} \left\{ \frac{e}{c} \left(\underline{p}.\underline{A} + \underline{A}.\underline{p} \right) + \frac{e^2 A^2}{c^2} \right\} \quad . \tag{2.3}$$

But, by elementary vector analysis we have

$$\underline{p}.\underline{A}\phi = -i\hbar\nabla.\underline{A}\phi = -i\hbar\phi\nabla.\underline{A} - i\hbar\underline{A}.\nabla\phi = \underline{A}.\underline{p}\phi \tag{2.4}$$

therefore,

$$H = H_o + \frac{e}{\mu c} \underline{p}.\underline{A} + \frac{e^2}{2\mu c^2} A^2 \quad . \tag{2.5}$$

The problem we are considering is the interaction of a <u>static</u> magnetic field $\underline{B} = B\hat{z}$ with the hydrogen atom. $\underline{A}$ then becomes $\underline{A}(\hat{r})$ and it is easy to show that $\underline{A} = \frac{1}{2}\underline{B} \times \underline{r}$ satisfies $B\hat{z} = \nabla \times \underline{A}$ and so

$$H = H_o + \frac{ie\hbar B}{2\mu c} L_z + \frac{e^2}{2\mu c^2} \tfrac{1}{4}(\underline{B} \times \underline{r})^2 \tag{2.6}$$

where $\underline{L} = -i\hbar\underline{r} \times \nabla$ and L_z is the z component of $\underline{L}$.

Now setting $\cos\theta = \underline{B} \times \underline{r}$, i.e. taking $\underline{B}$ along the $\theta = 0$ axis, we obtain $(\underline{B} \times \underline{r})^2 = B^2 r^2 \sin^2\theta$. Throughout, the magnetic field will be measured in terms of γ, where

$$\gamma = \frac{\mu_B B}{Ry} = \frac{\hbar\omega_c}{2Ry} . \tag{2.7}$$

B is measured in Gauss, μ_B is the Bohr magneton and the cyclotron frequency is

$$\omega_c = \frac{eB}{\mu} . \tag{2.8}$$

Ry is the Rydberg and we find that $|\underline{B}|_{\gamma=1} = 2.35 \times 10^9$ Gauss = 2.35×10^5 Tesla.

We must also add to the Hamiltonian, a term representing the spin interaction. The spin magnetic moment of the electron is

$$\underline{\alpha} = -g_e \frac{e\underline{S}}{2\mu c} \tag{2.9}$$

where $\underline{S}$ is the spin angular momentum vector and g_e is the Landé-g factor corresponding to the electron. According to Dirac relativistic theory, g_e can be taken to have the value 2 (Bethe and Salpeter, 1977, p207). The term to be added to the Hamiltonian to represent spin interaction is then

$$-\underline{\alpha}.\underline{B} = g_e \frac{e}{2\mu c} \underline{B}.\underline{S} = \frac{e}{\mu c} BS_z = 2\gamma S_z . \tag{2.10}$$

The Hamiltonian is now

$$H = H_o + \gamma(L_z + 2S_z) + \frac{\gamma^2}{4} r^2 \sin^2\theta . \tag{2.11}$$

The time-independent Schrödinger equation,

$$H\Psi = E\Psi \tag{2.12}$$

is not exactly soluble and so an approximation for the wave function Ψ must be found. Let this approximation be such that

$$\Psi_p = \sum_j a_{jp} \phi_j \tag{2.13}$$

where $\{ \phi_j : j = 1, 2 .... N \}$ is a linearly independent set of basis functions.

At relatively low fields, i.e. $B < 10^8$ G, where the atom retains its spherical symmetry and the bound states retain some of their zero-field character, it would seem logical to assume that a basis set of unperturbed hydrogenic states will give good results in this region. This set of basis states was used by Brandi (1975), but in his paper, results for the energies of the 14 lowest bound states are only presented graphically. To obtain more accurate results for the energies, and in order to go on and calculate bound-bound transition probabilities, it was necessary to repeat the work of Brandi. The basis set functions are:

$$\phi_j = R_{n_j \ell_j}(r)\, Y_{\ell_j m_{\ell_j}}(\hat{r})\, \chi_{s_j m_{s_j}} \qquad (2.14)$$

$R_{n\ell}$ is the unperturbed hydrogenic radial function, $Y_{\ell m_\ell}$ the spherical harmonic function and χ_{sm_s} the spin function. n_j, ℓ_j, m_{ℓ_j}, s_j, m_{s_j} are the principal, angular momentum, magnetic, spin angular momentum and spin magnetic quantum numbers respectively, of the unperturbed state.

Equation (2.12) must be solved in order to find the energy eigenvalues $E_j : j = 1, 2 \ldots N$ and the a_{jp} of equation (2.13) which are the eigenvectors; $a_{jp} : j = 1, 2 \ldots N$ are the elements of the p'th column of the eigenvector matrix.

Equation (2.12) can be rewritten

$$\langle \Psi_p \mid H \mid \Psi_q \rangle = E \langle \Psi_p \mid \Psi_q \rangle \qquad (2.15)$$

where the integration is over all space and H is given by equation (2.11).

§2.3 Calculation of Matrix Elements $\langle \Psi_p | H | \Psi_q \rangle$ and $\langle \Psi_p | \Psi_q \rangle$

(i) Matrix Element of H_o

As the ϕ_j are mutually orthogonal functions, we have

$$\langle \sum_j a_{jp}\, \phi_j \mid H_o \mid \sum_k a_{kq}\, \phi_k \rangle = \sum_j a_{jp}^{*}\, a_{jq}\, E_j^{(o)} \qquad (2.16)$$

where $E_j^{(o)}$ is the energy of the unperturbed state ϕ_j.

(ii) Matrix Element of $(L_z + 2S_z)$

We know that

$$L_z \, Y_{\ell_j m_{\ell_j}}(\hat{r}) = m_{\ell_j} \hbar \, Y_{\ell_j m_{\ell_j}}(\hat{r}) \tag{2.17}$$

and

$$S_z \, \chi_{s_j m_{s_j}} = m_{s_j} \hbar \, \chi_{s_j m_{s_j}} \tag{2.18}$$

and again using the fact that the ϕ_j are orthogonal, we have

$$\langle \sum_j a_{jp} \, \phi_j | (L_z + 2S_z) | \sum_k a_{kq} \, \phi_k \rangle = \sum_j a_{jp}^* a_{jq} \gamma \, (m_{\ell_j} + 2m_{s_j}) \tag{2.19}$$

(iii) Matrix Element of $\frac{1}{4}\gamma^2 r^2 \sin^2\theta$

Noting that $\sin^2\theta = \frac{2}{3}\left(1 - 2\left(\frac{\pi}{5}\right)^{\frac{1}{2}} Y_{20}(\hat{r})\right)$ (Edmonds, 1965, p124), we have

$$\langle \sum_j a_{jp} \, \phi_j | \tfrac{1}{4}\gamma^2 r^2 \sin^2\theta | \sum_k a_{kq} \, \phi_k \rangle = \tfrac{1}{4}\gamma^2 \sum_{j,k} a_{jp}^* a_{kq} \, R'_{jk} \, \frac{2}{3} \times$$

$$\int \{ Y_{\ell_j m_{\ell_j}}(\hat{r})^* \, Y_{\ell_k m_{\ell_k}}(\hat{r}) - 2\left(\frac{\pi}{5}\right)^{\frac{1}{2}} Y_{\ell_j m_{\ell_j}}(\hat{r})^* \, Y_{\ell_k m_{\ell_k}}(\hat{r}) \, Y_{20}(\hat{r}) \} \times$$

$$\chi_{s_j m_{s_j}}^* \, \chi_{s_k m_{s_k}} \, d\hat{r} \tag{2.20}$$

where

$$R'_{jk} = \int_0^\infty R_{n_j \ell_j}(r) \, R_{n_k \ell_k}(r) \, r^4 \, dr \, . \tag{2.21}$$

Both $Y_{\ell m}(\hat{r})$ and $\chi_{s m_s}$ are orthogonal polynomials and also (Edmonds, 1965, p63)

$$\int Y_{\ell_1 m_{\ell_1}}(\hat{r})^* \, Y_{\ell_2 m_{\ell_2}}(\hat{r}) \, Y_{\ell_3 m_{\ell_3}}(\hat{r}) \sin\theta \, d\theta \, d\phi = \{(2\ell_1+1)(2\ell_2+1)(2\ell_3+1)\}^{\frac{1}{2}}$$

$$\times \; (-1)^{-m_{\ell_1}} \begin{pmatrix} \ell_1 & \ell_2 & \ell_3 \\ 0 & 0 & 0 \end{pmatrix} \begin{pmatrix} \ell_1 & \ell_2 & \ell_3 \\ -m_{\ell_1} & m_{\ell_2} & m_{\ell_3} \end{pmatrix} \tag{2.22}$$

where $\begin{pmatrix} a & b & c \\ d & e & f \end{pmatrix}$ is the Wigner 3-j symbol (Edmonds, 1965). Now

using these facts and also $Y_{\ell,-m}(\hat{r}) = (-1)^m Y^*_{\ell,m}(\hat{r})$, equation (2.15) becomes:

$$\langle \sum_j a_{jp}\,\phi_j \left| \frac{\gamma^2}{4} r^2 \sin^2\theta \right| \sum_k a_{kq}\,\phi_k \rangle = \frac{\gamma^2}{6} \sum_{j,k} a_{jp}^* a_{kq} R'_{jk} \times$$

$$\{ \delta_{\ell_j \ell_k} \delta_{m_{\ell_j} m_{\ell_k}} - (-1)^{-m_{\ell_j}} ((2\ell_j+1)(2\ell_k+1))^{\frac{1}{2}} \begin{pmatrix} \ell_j & \ell_k & 2 \\ 0 & 0 & 0 \end{pmatrix} \begin{pmatrix} \ell_j & \ell_k & 2 \\ -m_{\ell_j} & m_{\ell_k} & 0 \end{pmatrix} \}$$

$$\times \delta_{s_j s_k} \delta_{m_{s_j} m_{s_k}} \qquad (2.23)$$

From the results of sections (i), (ii) and (iii), i.e. equations (2.16), (2.19) and (2.20), the total Hamiltonian matrix element becomes:

$$H_{pq} = \frac{\gamma^2}{6} \sum_{j,k} a_{jp}^* a_{kq} R'_{jk} \Theta_{jk} \delta_{m_{s_j} m_{s_k}} \delta_{s_j s_k} + \sum_j a_{jp}^* a_{jq} \times$$

$$(E_j^{(o)} + \gamma m_{\ell_j} + 2\gamma m_{s_j}) \qquad (2.24)$$

where

$$\Theta_{jk} = \{ \delta_{\ell_j \ell_k} \delta_{m_{\ell_j} m_{\ell_k}} - (-1)^{-m_{\ell_j}} ((2\ell_j+1)(2\ell_k+1))^{\frac{1}{2}} \begin{pmatrix} \ell_j & \ell_k & 2 \\ 0 & 0 & 0 \end{pmatrix}$$

$$\times \begin{pmatrix} \ell_j & \ell_k & 2 \\ -m_{\ell_j} & m_{\ell_k} & 0 \end{pmatrix} \qquad (2.25)$$

Consider the two vector-coupling coefficients contained in the expression for Θ_{jk} (equation (2.25)): from the properties of 3-j coefficients, the term $\begin{pmatrix} \ell_j & \ell_k & 2 \\ -m_j & m_k & 0 \end{pmatrix}$ must be zero unless $m_{\ell_k} = m_{\ell_j}$ and $|\ell_j - 2| \leq \ell_k \leq \ell_j + 2$ (i.e. the triangular rule is satisfied) and $\ell_j + \ell_k + 2$ is even. Similarly for $\begin{pmatrix} \ell_j & \ell_k & 2 \\ 0 & 0 & 0 \end{pmatrix}$, but in this case the condition $m_{\ell_j} = m_{\ell_k}$ does not apply. So the rules governing the coupling of states are that the state $|n,\ell,m_\ell,s,m_s\rangle$ can only couple to itself and $|n,\ell\pm2,m_\ell,s,m_s\rangle$. The only exceptions are that $\ell=0$ states can only couple to $\ell=0$ and $\ell=2$ states and $\ell=1$ states can only couple to $\ell=1$ and $\ell=3$ states. So H_{pq} (the matrix element of the Hamiltonian $\langle \psi_p \mid H \mid \psi_q \rangle$)

will form a square matrix $\{H_{pq}\}$ of dimension D given in table 2.1.

ℓ_j	Possible Choices of ℓ_k	D
0	0,2	$2N_1$
1	1,3	$2N_2$
$\ell(>1)$	ℓ, $\ell\pm2$	$3N_3$

Table 2.1

This table gives the dimension of the matrix of matrix elements of the Hamiltonian for the 3 possible cases of ℓ_j. N_1, N_2 and N_3 are the sums of the total numbers of basis elements for each possible coupled state.

In all the following calculations with this basis set, spin is omitted, the primary reason for this being that the omission of spin enables the results to be compared with those of other workers such as Praddaude (1972), Smith et al (1973) who also neglected spin. It is easy to add the spin energy shift $\Delta E = 2\gamma m_{s_j}$ later.

So the equation to be solved now, in order to find the energy eigenvalues E, and the eigenvectors $\underline{x}$, is

$$\begin{aligned} &(\{H_{pq}\} - \{\langle\phi_p|E|\phi_q\rangle\})\ \underline{x} = (\{H_{pq}\} - E\{\langle\phi_p|\phi_q\rangle\})\ \underline{x} \\ &= (\{H_{pq}\} - E\ \{S_{pq}\})\ \underline{x} = \underline{0} \end{aligned} \tag{2.26}$$

where $\{A_{pq}\}$ represents the matrix whose (p,q)'th element is A_{pq}. Due to the nature of the angular part of the unperturbed hydrogenic functions, they form an orthonormal basis set, i.e.

$$\int \phi_j^* \phi_k \, d\hat{r} \, dr = \delta_{j,k} \ . \tag{2.27}$$

This indicates that the matrix elements S_{pq} form the identity matrix.

The eigenvalue problem is then reduced to the form:

$$\{H_{pq}\}\ \underline{x} = E\ \underline{x} \tag{2.28}$$

where $\{H_{pq}\}$ is symmetric (i.e. $\int \phi_j H \phi_k \, d\hat{r}dr = \int \phi_k H \phi_j \, d\hat{r}dr$). This is because

$$\begin{aligned} &< \phi_j | H_o | \phi_k > \ = \ < \phi_j | \phi_k > \ = \ E\ \delta_{j,k} \quad , \\ &< \phi_j | \gamma L_z | \phi_k > \ = \ \gamma\ m_{\ell_k} < \phi_j | \phi_k > \ = \ \gamma\ m_{\ell_k}\ \delta_{j,k} \quad , \\ &\Theta_{jk} \ = \ \Theta_{kj} \quad \text{(from equation (2.25))} \ . \end{aligned} \tag{2.29}$$

§2.4 Numerical Methods Used to Solve the Eigenvalue Equation

The numerical routine used to solve this eigenvalue equation (i.e. equation (2.28)) is taken from the NAG library and a brief description of the methods used is given here. The routine used in these calculations is F02ABF.

The n×n symmetric, positive definite matrix $\{H_{pq}\}$ is reduced to tridiagonal form by applying n-2 orthogonal transformations of the form

$$A_{i+1} = P_i\ A_i\ P_i \quad , \quad i = 1, 2 \ \ldots\ n-2 \tag{2.30}$$

where A_i is the matrix $\{H_{pq}\}$ after i transformations. This reducing scheme is known as Householders Algorithm (Wilkinson and Reinsch, 1971, pp212). P_r is of the form

$$P_r = I - 2w_r w_r^t \tag{2.31}$$

with $w_r^t = (0, 0, \ldots 0, x_{r+1}, x_{r+2}, \ldots x_n)$, where w_r is a normalized vector. The transformations are such that if

$$A_1 = \begin{pmatrix} a_{11}^{(1)} & a_{12}^{(1)} & \ldots\ldots & a_{1n}^{(1)} \\ a_{21}^{(1)} & & & \\ \vdots & & & \\ a_{n1}^{(1)} & \ldots\ldots\ldots & & a_{nn}^{(1)} \end{pmatrix} \tag{2.32}$$

then,

$$A_2 = \begin{pmatrix} a_{11}^{(2)} & a_{12}^{(2)} & 0 & 0 & \cdots & 0 \\ a_{21}^{(2)} & a_{22}^{(2)} & a_{23}^{(2)} & \cdots & & a_{2n}^{(2)} \\ 0 & a_{32}^{(2)} & a_{34}^{(2)} & \cdots & & a_{3n}^{(2)} \\ 0 & & & & & \\ \vdots & & & & & \\ 0 & a_{n2}^{(2)} & a_{n3}^{(2)} & \cdots & & a_{nn}^{(2)} \end{pmatrix} \quad \text{, and} \qquad (2.33)$$

$$A_3 = \begin{pmatrix} a_{11}^{(3)} & a_{12}^{(3)} & 0 & 0 & \cdots & 0 \\ a_{21}^{(3)} & a_{22}^{(3)} & a_{23}^{(3)} & 0 & \cdots & 0 \\ 0 & a_{32}^{(3)} & a_{33}^{(3)} & \cdots & & a_{3n}^{(3)} \\ 0 & 0 & a_{43}^{(3)} & \cdots & & a_{4n}^{(3)} \\ \vdots & & & & & \\ 0 & 0 & a_{n3}^{(3)} & \cdots & & a_{nn}^{(3)} \end{pmatrix} \qquad (2.34)$$

etc., until tridiagonal form is reached. So the matrix A_r contains n-r-1 elements in the r'th row and column which have to be reduced to zero by P_r. We now have n-r-1 equations for x_{r+1}, x_{r+2} ... x_n. Also the normalization condition is another equation which means that we now have n-r equations in n-r variables. Thus the matrix A_1 can be reduced to tridiagonal form in this way.

Example

Consider the matrix

$$A_1 = \begin{pmatrix} a & b & c \\ b & d & e \\ c & e & f \end{pmatrix} . \qquad (2.35)$$

We have $A_2 = P_1 A_1 P_1$, where $P_1 = I - 2 w_1 w_1^t$, $w_1^t = (0, x_2, x_3)$ and $x_2^2 + x_3^2 = 1$, and in this case, A_2 is the tridiagonal form. Now,

$$P_1 = \begin{pmatrix} 1 & 0 & 0 \\ 0 & 1-2x_2^2 & -2x_2x_3 \\ 0 & -2x_2x_3 & 1-2x_3^2 \end{pmatrix} \qquad (2.36)$$

$$A_1 P_1 = \begin{pmatrix} a & b(1-2x_2^2) - 2cx_2x_3 & -2bx_2x_3 + c(1-2x_3^2) \\ b & d(1-2x_2^2) - 2ex_2x_3 & -2dx_2x_3 + e(1-2x_3^2) \\ c & e(1-2x_2^2) - 2fx_2x_3 & -2ex_2x_3 + f(1-2x_3^2) \end{pmatrix} . \quad (2.37)$$

The first row must remain unchanged on premultiplying $A_1 P_1$ by P_1, so in order that $P_1 A_1 P_1$ is tridiagonal, we must have

$$c - 2x_3(cx_3+bx_2) = 0 . \quad (i)$$

Since P_1 is orthogonal, the moduli of the row vectors is invariant i.e.

$$a^2 + (b + 2x_2(bx_2+cx_3))^2 = a^2 + b^2 + c^2 . \quad (ii)$$

From (i) and (ii) we have,

$$cx_2 - bx_3 = x_3(b^2 + c^2)^{\frac{1}{2}} \quad (iii)$$

and also

$$x_2^2 + x_3^2 = 1 . \quad (iv)$$

For convenience, take the positive square root in equation (iii). Equations (iii) and (iv) give two equations in 2 variables so x_2 and x_3 can be found in terms of b and c, therefore P_2 can be found in terms of b and c and the tridiagonal matrix A_2 is easily calculated.

Now as the matrices A_1 and A_n are similar, the eigenvalues of A_n will be the same as those of A_1. The eigenvalues of the tridiagonal matrix A_n are calculated by the QL method. This method is a trivial adaptation of the QR method which was devised by, and is discussed at some length by, Francis (1961), so only a brief outline is given here. Basically, it relies on the fact that a symmetric, tridiagonal matrix can be written as the product of a unitary matrix and a lower triangular matrix. Let $A_n = B_1$, then after k transformations B_k is formed and

$$B_k = Q_k L_k \quad (2.38)$$

where Q_k is unitary and L_k is lower triangular.

$$B_{k+1} = Q_k^* B_k Q_k = Q_k^* Q_k L_k Q_k = L_k Q_k$$

and $$B_{k+1} = Q_k^* Q_{k-1}^* \cdots Q_1^* B Q_1 Q_2 \cdots Q_k . \quad (2.39)$$

It is shown by an adaption of the proof by Francis (1961) that as

$k \to \infty$, the matrix B_k tends to a lower triangular matrix, the diagonal elements of which, are the eigenvalues of B_k. But B_k is similar to B_1 which in turn is similar to A_1 so the diagonal elements of B_k are actually the required eigenvalues of A_1.

In the Householder reduction routine, the best results are obtained from a 'balanced' matrix, i.e. if the moduli of the row and column vectors of A_1 vary considerably, then using row and column operations, A_1 is manipulated such that the last row and column vectors have the largest modulus. As a consequence of this, the tridiagonal matrix will have the largest elements in the bottom right hand corner. This necessitates the use of the QL rather than the QR transformation.

The original matrix A_1 is related to B_k by the orthogonal transformation P and the unitary transformation Q:

$$B_k = Q^* B Q = Q^* P A_1 P Q = S^{-1} A_1 S , \qquad (2.40)$$

where $S = PQ$. The eigenvectors are calculated by direct substitution of the corresponding eigenvalue into the equations

$$\begin{aligned} B_k \underline{y} &= \lambda \underline{y} \\ S^{-1} \underline{y} &= \underline{x} \end{aligned} \qquad (2.41)$$

where $\underline{y}$ is the eigenvector of B_k corresponding to the eigenvalue λ and $\underline{x}$ is the eigenvector of A_1 corresponding to the eigenvalue λ (i.e. the required eigenvector). The eigenvectors produced by the appropriate NAG routines, are normalized.

In our case, it is unnecessary to balance the matrix $\{H_{pq}\}$ as the moduli of the column vectors do not vary by more than two orders of magnitude.

§2.5 Computation of the Matrix $\{H_{pq}\}$

The methods used in the computation of the terms occurring in the matrix element H_{pq}, an expression for which is given in equation (2.24), are given below.

(i) Computation of R'_{jk}

R'_{jk} is defined in equation (2.21) as being the integral over r of the product of two hydrogenic radial functions and r^2. The radial functions can be written:

$$R_{nl}(r) = N\, e^{-r/n}\, r^{\ell}\, F(-n+\ell+1,\ 2\ell+2,\ \frac{2r}{n}) \quad , \tag{2.42}$$

where

$$N = \frac{2^{\ell+1}}{n^{\ell+2}\,(2\ell+1)!}\left\{\frac{(n+\ell)!}{(n-\ell-1)!}\right\}^{\frac{1}{2}} \tag{2.43}$$

and $F(\alpha,\beta,x)$ is a confluent hypergeometric function (Landau and Lifshitz, 1975, p118). Now, the confluent hypergeometric function can be written as a power series in x

$$F(\alpha,\beta,x) = \sum_{p=0}^{\infty} \frac{(\alpha+p-1)!}{(\alpha-1)!}\,\frac{(\beta-1)!}{(\beta+p-1)!}\,\frac{x^p}{p!} \tag{2.44}$$

where β is strictly positive. Writing $\alpha=\ell-n+1$, and $\beta=2\ell+2$ and $x=\frac{2r}{n}$, we have

$$F(-n+\ell+1,\ 2\ell+2,\ \frac{2r}{n}) = \sum_{p=0}^{\infty} \frac{(\ell-n+p)!}{(\ell-n)!}\,\frac{(2\ell+1)}{(2\ell+1+p)!}\,(\frac{2}{n})^p\,\frac{r^p}{p!} \quad . \tag{2.45}$$

This expression can be written in the form $\sum_p a_p\, r^p$ where a_p satisfies the recursion relation

$$a_{p+1} = \frac{2(\ell-n+p+1)}{n(p+1)(2\ell+2+p)}\,a_p, \qquad a_o = 1 \ . \tag{2.46}$$

This shows that the maximum value of p such that a_p is non-zero is $n-\ell-1$. So R'_{jk} now becomes

$$R'_{jk} = \int_o^{\infty} N_j\, N_k\, e^{-\gamma_{jk} r}\, r^{\ell_j+\ell_k+4} \sum_{p=0}^{n_j-\ell_j-1} \sum_{q=0}^{n_k-\ell_k-1} a_p^{(j)}\, a_q^{(k)}\, r^{p+q}\, dr \tag{2.47}$$

where

$$\gamma_{jk} = \frac{1}{n_j} + \frac{1}{n_k} \quad . \tag{2.48}$$

Performing the integral over r, we obtain

$$R'_{jk} = \sum_{p=0}^{n_j-\ell_j-1} \sum_{q=0}^{n_k-\ell_k-1} N_j\, N_k\, a_p^{(j)}\, a_q^{(k)} \left\{\frac{(\ell_j+\ell_k+p+q+4)!}{\gamma_{jk}^{\ell_j+\ell_k+p+q+5}}\right\}. \tag{2.49}$$

In program HYDROGN, R'_{jk} is calculated in SUBROUTINE RMAT, the coefficients $a_p^{(j)}$ and $a_q^{(k)}$ being calculated recursively and stored in arrays AC and BC respectively. N_j and N_k are stored in AN and BN and the final sum R'_{jk} in SUM. See Appendix (I) for details of program HYDROGN.

(ii) Computation of Θ_{jk}

The expression for Θ_{jk} is given by equation (2.25). Firstly, consider the diagonal elements, i.e. when $\ell_j = \ell_k = \ell$, say.

$$\Theta_{jk} = 1 - (-1)^m (2\ell+1) \begin{pmatrix} \ell & \ell & 2 \\ 0 & 0 & 0 \end{pmatrix} \begin{pmatrix} \ell & \ell & 2 \\ -m & m & 0 \end{pmatrix} \tag{2.50}$$

where $$\begin{pmatrix} \ell & \ell & 2 \\ 0 & 0 & 0 \end{pmatrix} = (-1)^{\ell+1} \left\{\frac{4}{2\ell+3}\right\}^{\frac{1}{2}} \tag{2.51}$$

and $$\begin{pmatrix} \ell & \ell & 2 \\ -m & m & 0 \end{pmatrix} = (-1)^{2\ell+2+m} \frac{2(3m^2 - 2(\ell+1)(2\ell+3))}{\{(4\ell+7)(4\ell+6)(4\ell+5)(4\ell+4)(4\ell+3)\}^{\frac{1}{2}}}. \tag{2.52}$$

For the off-diagonal elements, previously calculated selection rules state that $\ell_k = \ell_j \pm 2$. Θ_{jk} then reduces to

$$\Theta_{jk} = (-1)^{m+1} ((2\ell_j \pm 2+1)(2\ell_j+1))^{\frac{1}{2}} \begin{pmatrix} \ell_j & \ell_j \pm 2 & 2 \\ 0 & 0 & 0 \end{pmatrix} \begin{pmatrix} \ell_j & \ell_j \pm 2 & 2 \\ -m & m & 0 \end{pmatrix} \tag{2.53}$$

where

$$\begin{pmatrix} \ell_j & \ell_j+2 & 2 \\ 0 & 0 & 0 \end{pmatrix} = (-1)^{\ell_j} \sqrt{6}\, (\ell_j+2)(\ell_j+1) \frac{1}{f(\ell_j)}$$

$$\begin{pmatrix} \ell_k+2 & \ell_k & 2 \\ 0 & 0 & 0 \end{pmatrix} = (-1)^{\ell_k} \sqrt{6}\, (\ell_k+2)(\ell_k+1) \frac{1}{f(\ell_k)}$$

$$\begin{pmatrix} \ell_j & \ell_j+2 & 2 \\ -m & m & 0 \end{pmatrix} = (-1)^{\ell_j - m} \{6(\ell_j+m+2)(\ell_j+m+1)(\ell_j-m+2)(\ell_j-m+1)\}^{\frac{1}{2}} \frac{1}{f(\ell_j)}$$

$$\begin{pmatrix} \ell_k+2 & \ell_k & 2 \\ -m & m & 0 \end{pmatrix} = (-1)^{\ell_k+m} \{6(\ell_k-m+2)(\ell_k-m+1)(\ell_k+m+2)(\ell_k+m+1)\}^{\frac{1}{2}} \frac{1}{f(\ell_k)}$$

with $f(x) = ((2x+5)(2x+4)(2x+3)(2x+2)(2x+1))^{\frac{1}{2}}$.

Θ_{jk} is now in computable form and $((2\ell_j+1)(2\ell_k+1))^{\frac{1}{2}} \begin{pmatrix} \ell_j & \ell_k & 2 \\ 0 & 0 & 0 \end{pmatrix} \begin{pmatrix} \ell_j & \ell_k & 2 \\ -m & m & 0 \end{pmatrix}$ is calculated in SUBROUTINE THREEJ of program HYDROGN, (see Appendix (I)).

Computation of other terms occurring in the matrix elements H_{pq} is straightforward.

§2.6 Transition Probabilities

Consider the spontaneous transition from a state m' with energy $E_{m'}$, to a state m, with energy E_m, in a uniform static magnetic field $\underline{B}$ with the emission of one photon. Both states are bound, hydrogenic states and m' and m represent all the quantum numbers of the two states. The angular frequency of the emitted photon is

$$\omega_{m'm} = \frac{1}{\hbar}(E_{m'} - E_m). \tag{2.54}$$

The method for finding E_m and $E_{m'}$ has already been described in section §2.2. Now, let the interaction between the radiation field and the electron be represented by a vector potential $\underline{A}'$, where

$$\underline{A}' = \underline{A}'(r,t). \tag{2.55}$$

Including this in the expression for the Hamiltonian given by equation (2.3), we get:

$$H' = \frac{1}{2\mu}\{\underline{p} + \frac{e}{2c}\underline{B} \times \underline{r} + \frac{e}{c}\underline{A}'\}^2 - \frac{e^2}{r^2} \tag{2.56}$$

and so

$$H' = H + \frac{e}{2\mu c}(\underline{p}.\underline{A}' + \underline{A}'.\underline{p}) + \frac{e}{2\mu c^2}A'^2 + \frac{e}{2\mu c^2}\underline{A}'.\underline{B} \times \underline{r} \tag{2.57}$$

where H is the Hamiltonian of a hydrogen atom in a uniform magnetic field only. Choosing our gauge such that $\underline{p}.\underline{A}' = \underline{A}'.\underline{p}$, we have

$$H' = H + \frac{e}{\mu c}\underline{A}'.(\underline{p} + \frac{e}{2c}\underline{B} \times \underline{r}) + \frac{e^2A'^2}{2\mu c^2} \tag{2.58}$$

We can eliminate the term A'^2 by means of a unitary transformation U, which does not in any way change the problem, but merely converts the wavefunction Ψ to a different basis. We can write

$$\psi = U\Psi \tag{2.59}$$

and choose U to be of the form

$$U = \exp\{C\int_0^t A'(\tau)^2 dt\} . \tag{2.60}$$

The time dependent Schrodinger equation ($H'\Psi = i\hbar\dot{\Psi}$) can now be written

$$\{H + \frac{e}{\mu c}\underline{A}'.(\underline{p} + \frac{e}{2c}\underline{B}\times\underline{r}) + \frac{e\,A'^2}{2\mu c^2}\}\,U\psi = i\hbar(U\dot{\psi} + CA'^2U\psi) \tag{2.61}$$

which can be reduced to

$$\{H + \frac{e}{\mu c}\underline{A}'.(\underline{p} + \frac{e}{2c}\underline{B}\times\underline{r})\}\psi = i\hbar\dot{\psi} \tag{2.62}$$

where we have written

$$C = \frac{e^2}{2\mu c^2 i\hbar} . \tag{2.63}$$

The additional term in the Hamiltonian due to the interaction between the electron and the electromagnetic field can now be treated as a perturbation, i.e. if

$$H' = H + H_{int} \tag{2.64}$$

then we treat H_{int} as a perturbation, where

$$H_{int} = \frac{e}{\mu c}\underline{A}'.(\underline{p} + \omega_L\,\mu\,\hat{B}\times\underline{r}) . \tag{2.65}$$

In order to find the transition probability in the length formulation, we need to find

$$\langle m'|H_{int}|m\rangle$$

in terms of

$$\langle m'|\underline{r}|m\rangle .$$

This may be achieved by considering the commutator $\{\underline{r},H\}$ where

$$H = \frac{\hbar^2}{2\mu}\nabla^2 - \frac{e^2}{r} + \gamma L_z + \frac{\gamma^2}{4} r^2 \sin^2\theta \ . \qquad (2.66)$$

Consider the components of the matrix element of the commutator $\{\underline{r},H\}$:

(i) $\langle m'|\underline{r}\nabla^2 - \nabla^2\underline{r}|m\rangle$

Taking the x component of the above matrix element, we obtain

$$\langle m'|x\frac{\partial^2}{\partial x^2} - \frac{\partial^2}{\partial x^2}x|m\rangle = \int_{-\infty}^{\infty} \{\psi_{m'}^{*} \, x \, \psi_m^{(2)} - \psi_{m'}^{*} \, (\psi_m x)^{(2)}\} \, dx \qquad (2.67)$$

where ψ_m is the wavefunction corresponding to the state $|m\rangle$ and superscript (n) denotes the n'th derivative with respect to x.

Performing the differentiation on the second term in the integrand we get:

$$\langle m'|x\frac{\partial^2}{\partial x^2} - \frac{\partial^2}{\partial x^2}x|m\rangle = \int_{-\infty}^{\infty} \{\psi_{m'}^{*} \, x \, \psi_m^{(2)} - 2\psi_{m'}^{*} \, \psi_m^{(1)} - \psi_{m'}^{*} \, x \, \psi_m^{(2)}\} \, dx$$

$$= -2 \int_{-\infty}^{\infty} \psi_{m'}^{*} \, \psi_m^{(1)} \, dx \ . \qquad (2.68)$$

By similarly considering the y and z components, we obtain the final result

$$\langle m'|\underline{r}\nabla^2 - \nabla^2\underline{r}|m\rangle = -2\langle m'|\nabla|m\rangle \qquad (2.69)$$

(ii) $\langle m'|\underline{r}(\hat{B} \times \underline{r})^2 - (\hat{B} \times \underline{r})^2\underline{r}|m\rangle$

Now, remembering that the magnetic field is taken to be in the z direction, we can write $\hat{B}$ as the vector (0,0,1) in cartesian coordinates, and so

$$(\hat{B} \times \underline{r})^2 = y^2 + x^2 \ . \qquad (2.70)$$

It is now obvious that the matrix element of the commutator $\{\underline{r},(\hat{B} \times \underline{r})^2\}$ is zero.

(iii) $\langle m'|\underline{r}\frac{e^2}{r} - \frac{e^2}{r}\underline{r}|m\rangle$

It is immediately obvious that this matrix element is also zero.

(iv) $\langle m'|\underline{r}L_z - L_z\underline{r}|m\rangle$

L_z is given by $xp_y - yp_x$, where p_x and p_y are the x and y components of momentum respectively, i.e.

$$L_z = -i\hbar x\frac{\partial}{\partial y} + i\hbar y\frac{\partial}{\partial x} \ . \qquad (2.71)$$

Considering the x component of this matrix element, we have

$$\langle m'|xL_z - L_z x|m\rangle = -i\hbar \int \psi_{m'}^{*}\, y\, \psi_m \, d\tau \quad , \tag{2.72}$$

and considering the y component, we have

$$\langle m'|yL_z - L_z y|m\rangle = i\hbar \int \psi_{m'}^{*}\, x\, \psi_m \, d\tau \quad . \tag{2.73}$$

As the partial derivatives involved in L_z are only with respect to x or y, it obvious that the z component of this matrix element must be zero. Therefore the total matrix element is

$$\begin{aligned} \langle m'|\underline{r}L_z - L_z\underline{r}|m\rangle &= i\hbar \langle m'|(-y,x,0)|m\rangle \\ &= i\hbar \langle m'|\hat{B} \times \underline{r}|m\rangle \quad . \end{aligned} \tag{2.74}$$

From equation (2.66) and the results of (i), (ii), (iii) and (iv), we can write down the following expression for the matrix element of the commutator $\{\underline{r},H\}$:

$$\langle m'|\{\underline{r},H\}|m\rangle = \langle m'|\frac{\hbar^2}{\mu}\nabla + i\hbar\omega_L \hat{B} \times \underline{r}|m\rangle \tag{2.75}$$

Now H_{int}, the part of the Hamiltonian representing the interaction between the electron and the radiation field, can be written (equation (2.62))

$$H_{int} = -\frac{ie}{c\hbar}\underline{A}' \cdot (\frac{\hbar^2}{\mu}\nabla + i\hbar\omega_L \hat{B} \times \underline{r}) \quad . \tag{2.76}$$

So, from equations (2.75) and (2.76) we can write

$$\langle m'|H_{int}|m\rangle = -\frac{ie}{c\hbar}\underline{A}' \cdot \langle m'|\{\underline{r},H\}|m\rangle \quad . \tag{2.77}$$

Also, we can write the Schrodinger equation,

$$H\,\psi_m = E_m\,\psi_m \tag{2.78}$$

where E_m is the energy of the electron corresponding to state ψ_m. Premultiplying this equation by $\psi_{m'}$, $\underline{r}$ and integrating over all space, we obtain

$$\int \psi_{m'}^{*}\, \underline{r}H\, \psi_m \, d\tau = E_m \int \psi_{m'}^{*}\, \underline{r}\, \psi_m \, d\tau \quad , \tag{2.79}$$

and post-multiplying by $\underline{r}$ and premultiplying by $\psi_{m'}^{*}$ and integrating over all space, we obtain

$$\int \psi_{m'}^{*} H\underline{r}\, \psi_m \, d\tau = \int (H^{*} \psi_{m'})^{*} (\underline{r}\, \psi_m) \, d\tau$$

$$= E_{m'} \int \psi_{m'}^{*} \underline{r}\, \psi_m \, d\tau \quad , \tag{2.80}$$

using the fact that H is hermitian. From equations (2.79) and (2.80) we have the result

$$\langle m' | \{\underline{r}, H\} | m \rangle = (E_m - E_{m'}) \langle m' | \underline{r} | m \rangle \quad . \tag{2.81}$$

So finally, we can combine the results of equations (2.77) and (2.81) to get the following expression for the matrix element of H_{int},

$$\langle m' | H_{int} | m' \rangle = - \frac{ie}{c} \omega_{mm'} \underline{A}' . \langle m' | \underline{r} | m \rangle \, . \tag{2.82}$$

So it has now been shown that the matrix element of H_{int} can be written in terms of the matrix element of $\underline{r}$, which is the correct form of the matrix element in order that the transition probability may be calculated in the length formulation. This expression, in fact, is exactly the same as the equivalent expression for the zero field case, (Eyring, Walter and Kimball, 1957, p111). From this expression (equation (2.82)) it has been shown by several authors (for example, Condon and Shortley, 1963, Eyring, Walter and Kimbal, 1957) that the transition probability per unit time in the magnetic field (which is exactly analogous to the zero field case), taking into account emission of radiation in all directions, can be written

as

$$A_{m'm} = \frac{4e^2}{3\hbar c^3}\omega_{m'm}^3 \left|\langle m'| \sum_{i=-1}^{1} \underline{r}.\hat{e}_i^* |m\rangle\right|^2 . \qquad (2.83)$$

(Cf. Eyring, Walter and Kimbal, 1957, p115).

There has been some dispute as to the correct form of the Einstein 'A' coefficient, the original formulation of Smith et al (1973) being in error: see Smith et al (1973) and Brandi et al (1976). The result of equation (2.83), which is the length form of the transition probability, agrees with the formula obtained by dos Santos and Brandi (1976) which is the correct result. The result of Smith et al (1973) was later corrected (Smith et al (1975)).

Converting the expression given by equation (2.83) to atomic units (i.e. putting length in terms a_o and frequency in terms of $\frac{me^4}{\hbar^3}$) we obtain

$$A_{m'm} = \frac{4e^2}{3\hbar c^3}\omega_{m'm}^3 \left(\frac{me^4}{\hbar^3}\right)^3 \left|\langle m'| \sum_{i=-1}^{1} \underline{r}.\hat{e}_i^* |m\rangle\right|^2 \left(\frac{\hbar^2}{me^2}\right)^2 \qquad (2.84)$$

i.e. $$A_{m'm} = \frac{4}{3}\frac{\alpha^3}{\tau_o}\omega_{m'm}{}^3 \left|\langle m'\right| \sum_{i=-1}^{1} \underline{r}.\hat{e}_i^{\,*} \left|m\rangle\right|^2$$

where $\alpha = \frac{1}{137.0373}$ (the fine structure constant) and $\tau_o = 2.4187\times10^{-17}$ seconds, so that the final result is

$$A_{m'm} = 2.14210301\times10^{10}\ \omega_{m'm}{}^3 \left|\langle m'\right| \sum_{i=-1}^{1} \underline{r}.\hat{e}_i^{\,*} \left|m\rangle\right|^2 . \qquad (2.85)$$

The $\hat{e}_i$ are defined by

$$\hat{e}_{\pm1} = \mp\frac{1}{\sqrt{2}}(e_x \pm ie_y), \qquad \hat{e}_o = e_z \qquad (2.86)$$

where

$$e_x = (1,0,0), \quad e_y = (0,1,0), \quad e_z = (0,0,1) \qquad (2.87)$$

in cartesian coordinates.

The formula of equation (2.85) can be checked with the known zero-field results given by Bethe, H.A. and Salpeter, E.E. (1977). Considering the $2p_o$ - $1s_o$ transition, we have

$$\omega_{2p,1s} = \tfrac{1}{2}(1-\tfrac{1}{4}) = 0.375 \text{ a.u.}$$

$$\left|\langle 2p\right| \sum_{i=-1}^{1} \underline{r}.\hat{e}_i^{\,*} \left|1s\rangle\right|^2 = \frac{2^{15}}{3^9}$$ (Bethe, H.A. and Salpeter, E.E., 1977, p262).

Therefore,

$$A_{2p,1s} = 2.14210301\times10^{10} \times (0.375)^3 \times \frac{2^{15}}{3^9} \times \frac{1}{3}$$
$$= 6.2681 \times 10^8\ s^{-1} \qquad (2.88)$$

which agrees with Bethe, H.A. and Salpeter, E.E. (1977) p266.

So this result for the transition probabilities (equation (2.85)) of atomic hydrogen in a magnetic field $\underline{B}$ tends to the true zero field result as $|\underline{B}| \to 0$, unlike those of Brandi who neglect the integration over all directions of polarization, and in consequence, their results corresponding to zero-field are a factor of $\frac{8\pi}{3}$ from the true results of Bethe, H.A. and Salpeter, E.E. (1977) p266. In fact, in order to compare our results with those of Brandi et al (1976) and Smith et al (1973) it was necessary to include this factor of $\frac{8\pi}{3}$ in their results.

§2.7 Computation of Transition Probabilities

In order to find the transition probabilities, an expression for which is given in equation (2.85), we need to evaluate the matrix elements of the form $\langle m'|r_\mu|m\rangle$, where $r_\mu = \underline{r}.\hat{e}_\mu$. From equations (2.13) and (2.14), we have (ignoring spin)

$$\langle m'|r_\mu|m\rangle = \sum_{j,k} a_{jm'} a_{km} \langle R_{n_j\ell_j}(r)\, Y_{\ell_j m_{\ell_j}}(\hat{r})|r_\mu|R_{n_k\ell_k}(r)\, Y_{\ell_k m_{\ell_k}}(\hat{r})\rangle . \quad (2.89)$$

Now $\mu = 0$, 1 or -1 and we have (from Edmonds, 1965)

$$\begin{aligned} r_0 &= z = r\cos\theta = \sqrt{(\tfrac{4\pi}{3})}\, r\, Y_{1,0} \\ r_1 &= -\frac{1}{\sqrt{2}}(x + iy) = -\frac{r}{\sqrt{2}}\sin\theta\, e^{i\phi} = \sqrt{(\tfrac{4\pi}{3})}\, r\, Y_{1,1} \\ r_{-1} &= \frac{1}{\sqrt{2}}(x - iy) = \frac{r}{\sqrt{2}}\sin\theta\, e^{-i\phi} = \sqrt{(\tfrac{4\pi}{3})}\, r\, Y_{1,-1} \end{aligned} \quad (2.90)$$

and so generally, we have

$$r_\mu = \sqrt{(\tfrac{4\pi}{3})}\, r\, Y_{1,\mu} \quad . \quad (2.91)$$

The matrix element now becomes

$$\langle m'|r_\mu|m\rangle = \sum_{j,k} a^*_{jm'} a_{km} \sqrt{(\tfrac{4\pi}{3})} \int_0^\infty R_{n_j\ell_j}(r)\, r\, R_{n_k\ell_k}(r)\, r^2\, dr \times \int Y^*_{\ell_j m_{\ell_j}}(\hat{r})\, Y_{1\mu}(\hat{r})\, Y_{\ell_k m_{\ell_k}}(\hat{r})\, d\Omega \quad (2.92)$$

where $d\Omega = \sin^2\theta d\theta d\phi$. Writing

$$I_3(j,k) = \int_0^\infty R_{n_j\ell_j}(r)\, R_{n_k\ell_k}(r)\, r^3\, dr \quad (2.93)$$

and using equation (2.22) to evaluate the angular integral, we obtain

$$\langle m'|r_\mu|m\rangle = (-1)^{m_{\ell_j}} I_3(j,k) \sqrt{((2\ell_j+1)(2\ell_k+1))} \begin{pmatrix} \ell_j & 1 & \ell_k \\ 0 & 0 & 0 \end{pmatrix} \times \begin{pmatrix} \ell_j & 1 & \ell_k \\ -m_{\ell_j} & 0 & m_{\ell_k} \end{pmatrix} . \quad (2.94)$$

Consider the two 3j symbols in equation (2.94); the second 3j symbol is zero unless $|\ell_j - 1| \leq \ell_k \leq \ell_j + 1$ (i.e. the triangular rule is satisfied), $m_{\ell_k} - m_{\ell_j} + \mu = 0$ and $\ell_j + \ell_k + 1$ is even, the last condition also applying to the first 3j symbol. From these selection

rules it can be seen that transitions can only occur between states of different parity, in fact only when $\Delta\ell = 1$. Also, the selection rule $\Delta m = \mu = 0, 1$ or -1 must be obeyed. This rule governing the magnetic quantum number shows that for each transition, there is only one value of μ for which $\langle m'|r_\mu|m\rangle$ is non-zero.

It should be noted that, at zero field, the energies of states $|n,\ell,m\rangle$ where $m = -2\ell-1, -2\ell \ldots 2\ell+1$ coincide and this should be taken into account when evaluating the transition probabilities by summing over the magnetic quantum number of the state with the lower energy.

The total expression for the transition probability now becomes

$$A_{m'm} = 2.14210301\times10^{10}\ \omega_{m'm}{}^3\ (2\ell_j+1)(2\ell_k+1)\ \{I_3(j,k)\ \begin{pmatrix} \ell_j & 1 & \ell_k \\ 0 & 0 & 0 \end{pmatrix} \times \begin{pmatrix} \ell_j & 1 & \ell_k \\ -m_{\ell_j} & \mu & m_{\ell_k} \end{pmatrix} \}^2 \qquad (2.95)$$

(i) Computation of $I_3(j,k)$

$I_3(j,k)$ is computed in a very similar way to that of R'_{jk}, the radial matrix element occurring in the calculation of the energy levels (see section §2.5). The final result is

$$I_3(j,k) = \sum_{p=0}^{n_j-\ell_j-1} \sum_{q=0}^{n_k-\ell_k-1} N_j\ N_k\ a_p^{(j)}\ a_q^{(k)}\ \{\frac{(\ell_j+\ell_k+p+q+3)!}{\gamma_{jk}{}^{\ell_j+\ell_k+p+q+4}}\} \qquad (2.96)$$

where, as before,

$$N_i = \frac{2^{\ell_i+1}}{n_i{}^{\ell_i+2}(2\ell_i+1)!}\ \{\frac{(n_i+\ell_i)!}{(n_i-\ell_i-1)!}\}^{\frac{1}{2}} \qquad (2.97)$$

$$a_{p+1}^{(i)} = \frac{2(\ell_i-n_i+p+1)\ a_p^{(i)}}{n_i(p+1)(2\ell_i+2+p)}\ , \qquad a_o = 1 \qquad (2.98)$$

and

$$\gamma_{jk} = \frac{1}{n_j} + \frac{1}{n_k} \qquad (2.99)$$

(ii) Computation of $\begin{pmatrix} \ell_j & 1 & \ell_k \\ 0 & 0 & 0 \end{pmatrix}^2$

Let $\ell_k = \ell$ and $m_{\ell k} = m$ throughout.

Case I: $\ell_j = \ell_k - 1$

$$\begin{pmatrix} \ell-1 & 1 & \ell \\ 0 & 0 & 0 \end{pmatrix}^2 = \frac{\ell}{(2\ell+1)(2\ell-1)} \tag{2.100}$$

Case II: $\ell_j = \ell_k + 1$

$$\begin{pmatrix} \ell+1 & 1 & \ell \\ 0 & 0 & 0 \end{pmatrix}^2 = \frac{2(\ell+1)}{(2\ell+3)(2\ell+2)(2\ell+1)} \tag{2.101}$$

(iii) Computation of $\begin{pmatrix} \ell_j & 1 & \ell_k \\ -m_{\ell j} & \mu & m_{\ell k} \end{pmatrix}^2$

Case I: $\ell_j = \ell_k - 1$

(a) $\mu = 0$ i.e. $m_j = m_k$

$$\begin{pmatrix} \ell-1 & 1 & \ell \\ -m & 0 & 0 \end{pmatrix}^2 = \frac{2(\ell+m)(\ell-m)}{2\ell(2\ell+1)(2\ell-1)} \tag{2.102}$$

(b) $\mu = 1$ i.e. $m_j = m_k + 1$

$$\begin{pmatrix} \ell-1 & 1 & \ell \\ -m-1 & 1 & m \end{pmatrix}^2 = \frac{(\ell-1-m)(\ell-m)}{(2\ell+1)(2\ell)(2\ell-1)} \tag{2.103}$$

(c) $\mu = -1$ i.e. $m_j = m_k - 1$

$$\begin{pmatrix} \ell-1 & 1 & \ell \\ 1-m & -1 & m \end{pmatrix}^2 = \frac{(\ell+m)(\ell+m-1)}{(2\ell+1)(2\ell)(2\ell-1)} \tag{2.104}$$

Case II: $\ell_j = \ell_k + 1$

(a) $\mu = 0$ i.e. $m_j = m_k$

$$\begin{pmatrix} \ell+1 & 1 & \ell \\ -m & 0 & m \end{pmatrix}^2 = \frac{2(\ell+m+1)(\ell+m+2)}{(2\ell+3)(2\ell+2)(2\ell+1)} \tag{2.105}$$

(b) $\mu = 1$ i.e. $m_j = m_k + 1$

$$\begin{pmatrix} \ell+1 & 1 & \ell \\ -m-1 & 1 & m \end{pmatrix}^2 = \frac{(\ell+m+1)(\ell+m+2)}{(2\ell+3)(2\ell+2)(2\ell+1)} \tag{2.106}$$

(c) $\mu = -1$ i.e. $m_j = m_k - 1$

$$\begin{pmatrix} \ell+1 & 1 & \ell \\ 1-m & -1 & m \end{pmatrix}^2 = \frac{(\ell-m+2)(\ell-m+1)}{(2\ell+3)(2\ell+2)(2\ell+1)} \tag{2.107}$$

If we now consider the zero field case where, to obtain the total transition probability, we must sum over all m_j, we have

Case I: $\ell_j = \ell_k - 1$

$$|\langle m'| \sum_{\mu=-1}^{1} r_\mu |m\rangle|^2 = (I_3(j,k))^2 \ (2\ell+1)(2\ell-1) \left\{\left(\frac{\ell}{(2\ell+1)(2\ell-1)}\right) \times \left(\frac{2(\ell+m)(\ell-m) + (\ell-1-m)(\ell-m) + (\ell+m)(\ell+m-1)}{2\ell(2\ell+1)(2\ell-1)}\right)\right\}$$

$$= (I_3(j,k))^2 \left(\frac{\ell}{2\ell+1}\right) \qquad (2.108)$$

Case II: $\ell_j = \ell_k + 1$

$$|\langle m'| \sum_{=-1}^{1} r_\mu |m\rangle|^2 = (I_3(j,k))^2 \ (2\ell+1)(2\ell+3) \left\{\left(\frac{2(\ell+1)^2}{(2\ell+3)(2\ell+2)(2\ell+1)}\right) \left(\frac{2(\ell+m+1)(\ell-m+1)+(\ell+m+1)(\ell+m+2)+(\ell-m+2)(\ell-m+1)}{(2\ell+3)(2\ell+2)(2\ell+1)}\right)\right\}$$

$$= (I_3(j,k))^2 \left(\frac{\ell+1}{2\ell+1}\right) \qquad (2.109)$$

and in this zero field case, the transition is between pure hydrogenic states $|n_j,\ell_j\rangle$ and $|n_k,\ell_k\rangle$.

§2.8 Wavelengths and Oscillator Strengths

(i) Wavelengths

The wavelength of a transition from state m' with energy $E_{m'}$ to a state m with energy E_m can be written

$$\lambda = \frac{hc}{|E_{m'} - E_m|} \qquad (2.110)$$

with energies in Joules, $h = 6.626\times10^{-34}$ J. sec, $c = 2.99793\times10^{8}$ ms^{-1} and λ in metres. Transforming the energy into Rydbergs and λ into Å we have

$$\lambda = \frac{911.3487}{|E_{m'} - E_m|} \text{ Å} . \qquad (2.111)$$

(ii) Oscillator Strengths

From Bethe, H.A. and Salpeter, E.E. (1977), p250, we have the following expression for the oscillator strength of a transition from state m' to state m

$$f_{m'm} = \frac{2\mu}{\hbar} \omega_{m'm} |\langle m'|r_\mu|m\rangle|^2 \quad . \tag{2.112}$$

Converting $\omega_{m'm}$ to a.u. by multiplying by $\frac{me^4}{\hbar^3}$ and the matrix element to a.u. by multiplying by a_o^2 $(= \frac{\hbar^2}{me^2})$ we have

$$f_{m'm} = 2\, \omega_{m'm} |\langle m'|r_\mu|m\rangle|^2 \, . \tag{2.113}$$

It has already been shown how to calculate $|\langle m'|r_\mu|m\rangle|^2$, and so it is easy to compute the wavelengths and oscillator strengths for the bound-bound transitions.

CHAPTER 3

ENERGIES AND BOUND-BOUND TRANSITIONS USING A BASIS OF CYLINDRICAL STATES

§3.1 Introduction

As described in Chapter 1, in very strong magnetic fields, the electron of the hydrogen atom describes a cylindrical, rather than a spherical, orbit. At high field strengths, therefore, it would seem more appropriate to describe the motion of the electron with a set of cylindrically symmetric, rather than the previously used spherically symmetric (hydrogenic) basis functions.

This chapter describes the construction of such a basis set, and the methods used in calculating the bound energies and transition probabilities between the bound states (Kara and McDowell, 1980). Unlike the case where the basis states were unperturbed hydrogenic functions, this set of states contains elements with three variable parameters (labelled α, β and δ)which must be carefully assigned values in order that parity is conserved, the functions have the same angular dependence as the zero field functions at low fields, and also so that the energies tend to the zero field limit as $|\underline{B}| \rightarrow 0$ and to the Landau limit as $|\underline{B}| \rightarrow \infty$.

Transition probabilities are calculated in the velocity as well as the length formulation in order to ascertain the accuracy of the wave functions.

§3.2 Construction of the Basis Set

The new set of functions must form an odd parity basis set representing the states corresponding to the zero field p, f etc. states and an even parity basis set representing the states corresponding to the zero field s, d etc states. We must also have the following orthogonality conditions:

$$\int \psi_{odd}^{*} \psi_{even} \, d\tau = 0 \tag{3.1}$$

$$\int \psi_{odd}^{*} \psi_{odd} \, d\tau = 1$$

$$\int \psi_{even}^{*} \psi_{even} \, d\tau = 1$$

where ψ_{odd} is any odd parity wave function and ψ_{even} is any even parity wave function. The trial solutions for the wave functions are of the form

$$\psi_j^{(m,\Pi)} = \sum_{\alpha_j,\beta_j,\delta_j} C_{\alpha_j\beta_j\delta_j} \chi_{\alpha_j\beta_j\delta_j}^{(m,\Pi)} (\underline{r}) \tag{3.2}$$

where m is the magnetic quantum number, Π parity and α_j, β_j and δ_j are three variational parameters. The basis functions $\chi_{\alpha\beta\delta}^{(m,\Pi)} (\underline{r})$ are chosen to be

$$\chi_{\alpha\beta\delta}^{(m,\Pi)} (\underline{r}) = z^{\alpha} \rho^{\beta} e^{-\delta r^2} e^{im\phi} \, . \tag{3.3}$$

in cylindrical polar coordinates (ρ,z,ϕ). If we let Π' be a parity operator (reflection about the (x,y) plane), then

$$\begin{aligned} \Pi'(\rho) &= \rho \\ \Pi'(z) &= -z \\ \Pi'(\phi) &= \pi+\phi \end{aligned} \tag{3.4}$$

So, on applying Π' to $\chi_{\alpha\beta\delta}^{(m,\Pi)} (\underline{r})$, we see that it is α that determines the sign of $\Pi'(\chi_{\alpha\beta\delta}^{(m,\Pi)} (\underline{r}))$. From this, we can conclude that α must be an integer for a state to have definite parity and for even parity basis functions α must be even, and for odd parity basis functions α must be odd. Also, considering the matrix element $\langle \chi_1 | \chi_2 \rangle$ where

$$\chi_i = \chi^{(m_i,\Pi_i)}_{\alpha_i\beta_i\delta_i}(\underline{r}) \quad , \tag{3.5}$$

we see that the integral over z, i.e.

$$\int_{-\infty}^{\infty} z^A e^{-\Delta z^2} dz \quad , \tag{3.6}$$

where $A = \alpha_1 + \alpha_2$ and $\Delta = \delta_1 + \delta_2$, is zero if A is odd as the integrand is then an odd function, and non-zero if A is even, as the integrand is then an even function. As the only occassions on which A is odd are when χ_1 and χ_2 have different parity, the conditions in equations (3.1) must be satisfied (that is if the coefficients of the basis functions are chosen such that the total wave function is normalised).

§3.3 Calculation of the Matrix Elements Occurring in the Energy Eigenvalue Equation

In order that the energies and wave functions of the bound states may be calculated, it is again necessary to solve the eigenvalue equation, i.e. equation (2.12).

The non-relativistic Hamiltonian operator for a hydrogen atom in a uniform, static, magnetic field is given by equation (2.11). Neglecting spin effects and adopting cylindrical polar coordinates (ρ,z,ϕ), this Hamiltonian can be rewritten

$$H = -\frac{\partial^2}{\partial\rho^2} - \frac{1}{\rho}\frac{\partial}{\partial\rho} - \frac{1}{\rho^2}\frac{\partial^2}{\partial\phi^2} - \frac{\partial^2}{\partial z^2} + \gamma L_z + \frac{\gamma^2}{4}\rho^2 - \frac{2}{r} \tag{3.7}$$

where $r^2 = \rho^2 + z^2$ and atomic units (i.e. $e = \hbar = \mu = c = 1$) are used. The z component of angular momentum can be written in cylindrical polar coordinates,

$$L_z = -i\frac{\partial}{\partial\phi} \, . \tag{3.8}$$

In order to solve the energy eigenvalue equation, we need to evaluate the matrix element $\langle\chi_1|H|\chi_2\rangle$, where χ_1 and χ_2 are two basis elements. We begin by operating the Hamiltonian, H, on the function χ_2 :

$$
\begin{aligned}
H\,\chi_2 \;=\; & -z^{\alpha_2}\, e^{-\delta_2 z^2}\, e^{im_2\phi}\,\Big(\frac{\partial^2}{\partial\rho^2} - \frac{1}{\rho}\frac{\partial}{\partial\rho}\Big)\,\rho^{\beta_2}\, e^{-\delta_2\rho^2} \\
& - z^{\alpha_2}\,\rho^{\beta_2-2}\, e^{-\delta_2(z^2+\rho^2)}\,\frac{\partial^2}{\partial\phi^2}\, e^{im_2\phi} \\
& - \rho^{\beta_2}\, e^{-\delta_2\rho^2}\, e^{im_2\phi}\,\frac{\partial^2}{\partial z^2}\, z^{\alpha_2}\, e^{-\delta_2 z^2} \\
& - i\,\gamma\, z^{\alpha_2}\,\rho^{\beta_2}\, e^{-\delta_2(z^2+\rho^2)}\,\frac{\partial}{\partial\phi}\, e^{im_2\phi} \\
& + \Big(\frac{\gamma^2}{4}\,\rho^2 - \frac{2}{r}\Big)\,\rho^{\beta_2}\, z^{\alpha_2}\, e^{-\delta_2(z^2+\rho^2)}\, e^{im_2\phi}
\end{aligned}
\tag{3.9}
$$

But,

$$
\begin{aligned}
\frac{\partial}{\partial\phi}\,\chi_2 &= im_2\,\chi_2 \\
\frac{\partial^2}{\partial\phi^2}\,\chi_2 &= -m_2^2\,\chi_2 \\
\frac{\partial}{\partial\rho}\,\chi_2 &= \frac{\beta_2}{\rho}\,\chi_2 - 2\rho\delta_2\,\chi_2 \\
\frac{\partial^2}{\partial\rho^2}\,\chi_2 &= \frac{\beta_2}{\rho^2}(\beta_2-1)\,\chi_2 - 4\delta_2\beta_2\,\chi_2 - 2\delta_2\,\chi_2 + 4\rho^2\delta_2^2\,\chi_2 \\
\frac{\partial}{\partial z}\,\chi_2 &= \frac{\alpha_2}{z}\,\chi_2 - 2z\delta_2\,\chi_2 \\
\frac{\partial^2}{\partial z^2}\,\chi_2 &= \frac{\alpha_2}{z^2}(\alpha_2-1)\,\chi_2 - 4\delta_2\alpha_2\,\chi_2 - 2\delta_2\,\chi_2 + 4z^2\delta_2^2\,\chi_2
\end{aligned}
\tag{3.10}
$$

So from equations (3.9) and (3.10), we see that the matrix elements of the Hamiltonian may be reduced to the form

$$
\begin{aligned}
\langle\chi_1|H|\chi_2\rangle \;=\; & (m_2^2-\beta_2^2)\,T_{12}(-2) + (\tfrac{1}{4}\gamma^2-4\delta_2^2)\,T_{12}(2) - \alpha_2(\alpha_2-1)\,R_{12}(-2) \\
& - 4\delta_2^2\,R_{12}(2) + 2\delta_2(2\beta_2+3+2\alpha_2)\,S_{12} - 2P_{12} + \gamma m_2\,S_{12}
\end{aligned}
\tag{3.11}
$$

where

$$
\begin{aligned}
S_{12} &= \langle\chi_1|\chi_2\rangle \\
T_{12}(n) &= \langle\chi_1|\rho^n|\chi_2\rangle \\
R_{12}(n) &= \langle\chi_1|z^n|\chi_2\rangle \\
P_{12} &= \langle\chi_1|r^{-1}|\chi_2\rangle \quad .
\end{aligned}
\tag{3.12}
$$

Note that, in each of the matrix elements, the integral over ϕ is

$$\int_0^{2\pi} e^{i(m_2-m_1)} \, d\phi = 2\pi \, \delta_{m_1,m_2} \quad , \tag{3.13}$$

and so, in order that the total matrix element is non-zero, we must have conservation of the magnetic quantum number. The integral over z, also, gives conservation of parity, as has been seen previously. The first three types of integral in (3.12) are elementary, and may be expressed in the form

$$I_{12}^{p,q} = 2\pi \, \delta_{m_1,m_2} \int_{-\infty}^{\infty} e^{-\Delta z^2} \, z^p \, dz \int_0^{\infty} e^{-\Delta \rho^2} \, \rho^q \, d\rho \tag{3.14}$$

where $\Delta = \delta_1 + \delta_2$ and p and q are integers, and in particular,

$$\begin{aligned} S_{12} &= I_{12}^{A,B+1} \\ T_{12}(n) &= I_{12}^{A,B+n+1} \\ R_{12}(n) &= I_{12}^{A+n,B+1} \end{aligned} \tag{3.15}$$

where $B = \beta_1 + \beta_2$ and $A = \alpha_1 + \alpha_2$ and n is an integer. See Appendix (II) for evaluation of the $I_{12}^{p,q}$.

Angular Dependence of the Wave Functions

In order that the cylindrical wave functions go smoothly into the zero-field case, we must have the correct angular dependence of the wave functions at low fields.

The dependence on ϕ of the pure hydrogenic, zero-field wave functions is $e^{im\phi}$ which is the same as that of the new cylindrical functions. Therefore, the ϕ dependence of the cylindrical basis is already correct.

However, we must also ensure that the wave functions have the correct $\sin\theta$ and $\cos\theta$ dependence. Writing a cylindrical basis function in spherical polar coordinates (r,θ,ϕ), we have

$$\chi = r^{\alpha} \cos^{\alpha}\theta \; r^{\beta} \sin^{\beta}\theta \; e^{-\delta r^2} \; e^{im\phi} \quad . \tag{3.16}$$

The angular dependence of the unperturbed hydrogenic functions is $Y_{\ell m}(\theta,\phi)$. The $\sin\theta$ dependence is $\sin^{|m|}\theta$ and the $\cos\theta$ dependence is

$\cos^N\theta$ where $0 \leq N \leq \ell$ (see Landau and Lifshitz, 1975, p600). So to obtain the correct $\sin\theta$ dependence for low fields, we take

$$\beta = |m|, |m|+1, |m|+2 \quad \ldots \tag{3.17}$$

To obtain the correct $\cos\theta$ dependence, we must have $\alpha \geq 0$. The value of α governs the parity of the state and for each complete wave function, we must have α even or α odd. In order to match the $\cos\theta$ dependence with that of the zero field wave functions, we can build up the following table of parities

Corresponding Zero-field State	$\cos\theta$ Dependence at Zero-field	Parity e = even, o = odd
$1s_o$	1	e
$2s_o$	1	e
$3s_o$	1	e
$2p_{-1}$	1	e
$2p_o$	$\cos\theta$	o
$2p_1$	1	e
$3p_{-1}$	1	e
$3p_o$	$\cos\theta$	o
$3p_1$	1	e
$3d_{-2}$	1	e
$3d_{-1}$	$\cos\theta$	o
$3d_o$	$(1-3\cos^2\theta)$	e
$3d_1$	$\cos\theta$	o
$3d_2$	1	e

Table 3.1

Table to show the parities of states in a magnetic field by looking at their $\cos\theta$ dependence at zero-field.

Evaluating the integrals occurring in the matrix element of the Hamiltonian (i.e. S_{12}, $T_{12}(\pm 2)$ and $R_{12}(\pm 2)$) from equations (3.15), we obtain the results given in tables 3.2 and 3.3, where

$$J(B,\Delta) = \begin{cases} \dfrac{(B-2)!!\sqrt{\pi}}{2^{B+\frac{1}{2}}\,\Delta^{B/2}} & \text{if B is odd} \\ \dfrac{(B/2-1)!}{2\Delta^{B/2}} & \text{if B is even} \end{cases} \qquad (3.18)$$

and

$$K(\alpha_o,\Delta) = \frac{(2\alpha_o - 3)!!\sqrt{\pi}}{2^{\alpha_o}\,\Delta^{\alpha_o-\frac{1}{2}}} \qquad (3.19)$$

with $\alpha_o = \frac{1}{2}(\alpha_1+\alpha_2) = A/2$ and $\Delta = \delta_1+\delta_2$. In these tables, the functions $J(B,\Delta)$ and $K(\alpha_o,\Delta)$ are treated as common factors and the cases B=0,1 and A=0,2 taken as special cases, in order to facilitate computation. To obtain total expressions for $T_{12}(\pm 2)$, $R_{12}(\pm 2)$ and S_{12}, multiply together the two relevant contributions from tables 3.2 and 3.3 and multiply the result by the integral over ϕ, i.e. by $2\pi\,\delta_{m_1,m_2}$.

	B = 0	B = 1	B > 1
S12 R12(-2) R12(2)	$\frac{1}{2\Delta}$	$\frac{\sqrt{\pi}}{4\Delta^{3/2}}$	$\frac{B}{2\Delta}\cdot J(B,\Delta)$
T12(-2)	0	$\frac{\sqrt{\pi}}{2\Delta^{\frac{1}{2}}}$	$J(B,\Delta)$
T12(2)	$\frac{1}{2\Delta^2}$	$\frac{3\sqrt{\pi}}{8\Delta^{5/2}}$	$\frac{B(B+2)}{4\Delta^2}\cdot J(B,\Delta)$

Table 3.2

Integrals over ρ occurring in $\langle\chi_1|H|\chi_2\rangle$. Note that the coefficient of T12(-2) is $(m_2^2 - \beta_2^2)$ which is always zero when B = 0 as $\beta_2 = |m_2|, |m_2+1| \ldots$, so the integral is set to zero in this case.

	A = 0	A = 2	A = 2
R12(-2)	0	$\frac{\sqrt{\pi}}{\Delta^{\frac{1}{2}}}$	$K(\alpha_o,\Delta)$
R12(2)	$\frac{\sqrt{\pi}}{2\Delta^{3/2}}$	$\frac{3\sqrt{\pi}}{4\Delta^{3/2}}$	$\frac{(2\alpha_o+1)(2\alpha_o-1)}{4\Delta^2} \cdot K(\alpha_o,\Delta)$
T12(-2) T12(2) S12	$\frac{\sqrt{\pi}}{\Delta^{\frac{1}{2}}}$	$\frac{\sqrt{\pi}}{2\Delta^{3/2}}$	$\frac{(2\alpha_o-1)}{2\Delta} \cdot K(\alpha_o,\Delta)$

Table 3.3

Integrals over z occurring in $\langle\chi_1|H|\chi_2\rangle$. Note that the coefficient of R12(-2) is zero when A = 0 so the integral is set to zero in this case.

Matrix Element of the Coulomb Term

The matrix element of the Coulomb term, $\frac{1}{r}$, is

$$P_{12} = \langle\chi_1|\frac{1}{r}|\chi_2\rangle \quad . \tag{3.20}$$

Writing P_{12} in spherical polar coordinates, we have

$$P_{12} = \int_0^{2\pi} d\phi \int_{-1}^{1} d(\cos\theta) \int_0^{\infty} r\,(r\cos\theta)^A\,(r\sin\theta)^B\, e^{-\Delta r^2}\, dr \tag{3.21}$$

where $A = \alpha_1 + \alpha_2$ is a non-negative even integer, $B = \beta_1 + \beta_2$ is a non-negative integer, and $\Delta = \delta_1 + \delta_2$. Consider the two cases of odd and even B separately,

Case I - B even

Letting $\mu = \cos\theta$, we can rewrite P_{12} in terms of integrals over r and μ:

$$P_{12} = 2\pi \int_{-1}^{1} d\mu \int_0^{\infty} r^{1+A+B}\, e^{-\Delta r^2}\, (1-\mu^2)^{B/2}\, \mu^A\, dr$$

$$= 2\pi \sum_{p=0}^{B/2} (-1)^p \binom{B/2}{p} \frac{2}{A+2p+1} \left[\frac{(A/2 + B/2)!}{2\Delta^{A/2+B/2+1}}\right] \tag{3.22}$$

Case II - B odd

Writing $\cos\theta$ in terms of $\sin\theta$, we can write the expression for P_{12}:

$$P_{12} = 2\pi \sum_{q=0}^{A/2} (-1)^q \binom{A/2}{q} \int_0^{\pi} \sin^{2q+B+1}\theta \, d\theta \int_0^{\infty} r^{A+B+1} e^{-\Delta r^2} dr \, ,$$

but, (3.23)

$$\int_0^{\pi} \sin^n\theta \, d\theta = \binom{n}{n/2} \frac{\pi}{2^n} \, , \tag{3.24}$$

hence,

$$P_{12} = 2\pi \frac{(A+B)!!\sqrt{\pi}}{2^{c+1}\Delta^{c+\frac{1}{2}}} \left[\sum_{q=0}^{A/2} (-1)^q \binom{A/2}{q} \frac{(2q+B+1)!}{((\frac{2q+B+1}{2})!)^2} \frac{\pi}{2^{2q+B+1}} \right] \tag{3.25}$$

where

$$c = \frac{A + B + 1}{2}$$

So the matrix complete matrix element of the Hamiltonian and the overlap integrals are in computable form. For details of PROGRAM CPOLAR, which solves the eigenvalue equation for this cylindrical basis set, see appendix (I).

§3.4 Estimating Values for the Parameter δ

To ensure accurate low field energies, we choose three values for the parameter δ, namely δ_1, δ_2 and δ_3, to minimize in turn, the zero-field eigenvalues for the n = 1, 2 and 3 levels, n being the principal quantum number. At low fields, the only n = 1 level is the level which corresponds to the zero-field '$1s_o$' state, which is the first even parity state (see Table 3.1). We can approximate the wave function of this '$1s_o$' state, by the first term in the even parity cylindrical basis set, i.e. $e^{-\delta r^2}$. Similarly, the first odd parity state corresponds to the zero-field '$2p_o$' state and its wave function can be approximated by the first term in the odd parity cylindrical basis set, i.e. $ze^{-\delta r^2}$. So now minimizing the energies of the n = 1

and 2 states, the respective approximate low field wave functions for these states are $e^{-\delta_1 r^2}$ and $ze^{-\delta_2 r^2}$. We now have to find a third wave function which is an approximation to an n = 3 state. Now, noting that the second odd parity state (see Table 3.1) corresponds to an n = 3 state, we can approximate the n = 3 wave function by a linear combination of the first two odd parity cylindrical basis functions which is orthonormal to the n = 2 approximate wave function. Such a function can be written (by the Gram-Schmidt orthogonalization process) as

$$\psi_2 = \psi_{20} + a\psi_{10}^{(n)} \tag{3.26}$$

where,

$$\psi_{10} = ze^{-\delta_2 r^2} \tag{3.27}$$

$$\psi_{20} = z\rho e^{-\delta_3 r^2} \quad . \tag{3.28}$$

a is a constant and superscript (n) indicates that the function has been normalised. Applying the Gram-Schmidt procedure, gives

$$\langle\psi_2|\psi_{10}^{(n)}\rangle = \langle\psi_{20}+a\psi_{10}^{(n)}|\psi_{10}^{(n)}\rangle = 0 \quad , \tag{3.29}$$

which implies that

$$a = -\langle\psi_{20}|\psi_{10}^{(n)}\rangle \quad , \tag{3.30}$$

so that

$$\psi_2 = \psi_{20} - \langle\psi_{20}|\psi_{10}^{(n)}\rangle\, \psi_{10}^{(n)} \quad . \tag{3.31}$$

But, on normalising ψ_{10}, we have

$$\psi_{10}^{(n)} = \left\{ \frac{2\Delta_2^{5/2}}{\pi^{3/2}} \right\}^{\frac{1}{2}} ze^{-\delta_2 r^2} \tag{3.32}$$

where $\Delta_2 = 2\delta_2$. Now, letting $\Delta = \delta_2 + \delta_3$, and calculating the matrix element occurring in ψ_2, we obtain

$$\langle\psi_{20}|\psi_{10}^{(n)}\rangle = \left\{ \frac{2\Delta_2^{5/2}}{\pi^{3/2}} \right\}^{\frac{1}{2}} \frac{\pi^2}{4\Delta^3} \quad . \tag{3.33}$$

Substituting this result, and that of equation (3.32) in equation (3.31), we have

$$\psi_2 = z\rho e^{-\delta_3 r^2} - \left\{ \frac{\Delta_2^{5/2}\,\pi^{1/2}}{2\Delta^3} \right\} ze^{-\delta_2 r^2} \tag{3.34}$$

which gives,

$$\psi_2 = \psi_{20} - C\,\psi_{10} \tag{3.35}$$

where,

$$C = \frac{\Delta_2^{5/2}\,\pi^{1/2}}{2\Delta^3} \quad . \tag{3.36}$$

The variational method is used to find the best values for δ_1, δ_2 and δ_3. As discussed in Chapter I, the best value for the energy of any state is the lowest value that can be obtained. So in this case, we have to chose δ_1, δ_2 and δ_3 such that $E_{n=1}$, $E_{n=2}$ and $E_{n=3}$ have minimum values. We can calculate these energies using the Hylleraas-Undheim theorem (also discussed in Chapter I).

(i) Calculation of δ_1 and $E_{n=1}$

By the Hyleraas-Undheim theorem, we have

$$E_{n=1} \leq \frac{\langle e^{-\delta_1 r^2}|H|e^{-\delta_1 r^2}\rangle}{\langle e^{-\delta_1 r^2}|e^{-\delta_1 r^2}\rangle} \tag{3.37}$$

where H is the zero-field Hamiltonian of the hydrogen atom given by

$$H = -\frac{\nabla^2}{2} - \frac{1}{r} \qquad \text{(in atomic units)}. \tag{3.38}$$

Performing the integrations in equation (3.37), and noting that the angular integrations in the numerator and denominator cancel, the following expression is obtained

$$E_{n=1} \leq \frac{3\,\delta_1\,I_2^{(2\delta_1)} - 2\,\delta_1^2\,I_4^{(2\delta_1)} - I_1^{(2\delta_1)}}{I_2^{(2\delta_1)}} \tag{3.39}$$

where

$$I_p^{(a)} = \int_0^\infty e^{-ar^2}\,r^p\,dr \ .$$

Expressions for the integrals $I_p^{(a)}$ are tabulated in Appendix (II). Evaluating the integrals in equation (3.39), we eventually obtain

$$E_{n=1} \leq \frac{3\delta_1}{2} - \frac{2^{3/2}\,\delta_1^{1/2}}{\sqrt{\pi}} \quad . \tag{3.40}$$

The value of δ_1 required to minimize $E_{n=1}$ is given by $\frac{dE_{n=1}}{d\delta_1} = 0$, i.e.

$$\frac{3}{2} - \left(\frac{2}{\pi\delta_1}\right)^{\frac{1}{2}} = 0 \ , \tag{3.41}$$

which gives

$$\delta_1 = \frac{8}{9\pi} = 0.282942 \tag{3.42}$$

and on substituting this value in equation (3.40) we obtain the following value for the minimum energy of the n=1 state :

$$E_{n=1} \leq -0.4244 \text{ a.u.} = -0.8488 \text{ Ry} . \tag{3.43}$$

(ii) Calculation of δ_2 and $E_{n=2}$

The procedure in this case, is analogous to that described in part (i), i.e.

$$E_{n=2} \leq \frac{\langle ze^{-\delta_2 r^2} | H | ze^{-\delta_2 r^2} \rangle}{\langle ze^{-\delta_2 r^2} | ze^{-\delta_2 r^2} \rangle} . \tag{3.44}$$

The zero-field Hamiltonian can be expressed in cylindrical coordinates (ρ, z, ϕ) as

$$H = -\frac{1}{2}\{\frac{\partial^2}{\partial\rho^2} + \frac{1}{\rho}\frac{\partial}{\partial\rho} + \frac{1}{\rho^2}\frac{\partial^2}{\partial\phi^2} + \frac{\partial^2}{\partial z^2}\} - \frac{1}{r} \tag{3.45}$$

where $r^2 = \rho^2 + z^2$. Substituting this expression for the Hamiltonian into equation (3.44), and performing the integrations, we obtain

$$E_{n=2} \leq \frac{1}{I_1^{(2\delta_2)} I_2^{(2\delta_2)}} \{-2\delta_2{}^2 I_2^{(2\delta_2)} I_3^{(2\delta_2)} - 2\delta_2{}^2 I_4^{(2\delta_2)} I_1^{(2\delta_2)} + 5\delta_2 I_2^{(2\delta_2)} I_1^{(2\delta_2)} - \frac{1}{3} I_3^{(2\delta_2)}\} . \tag{3.46}$$

As in part (i), differentiating the resulting expression for $E_{n=2}$ by δ_2, we obtain the following results for δ_2 and $E_{n=2}$:

$$\delta_2 = 0.045270 \tag{3.47}$$

$$E_{n=2} \leq -0.113177 \text{ a.u.} = -0.226354 \text{ Ry} . \tag{3.48}$$

(iii) Calculation of δ_3 and $E_{n=3}$

In this case, the Hylleraas-Undheim theorem gives

$$E_{n=3} \leq \frac{\langle \psi_2 | H | \psi_2 \rangle}{\langle \psi_2 | \psi_2 \rangle} \tag{3.49}$$

where an expression for ψ_2 is given in equation (3.34) and H in equation (3.45). Using equation (3.35), we can write

$$\langle \psi_2 | H | \psi_2 \rangle = \langle \psi_{20} | H | \psi_{20} \rangle + C^2 \langle \psi_{10} | H | \psi_{10} \rangle - C\langle \psi_{10} | H | \psi_{20} \rangle - C\langle \psi_{20} | H | \psi_{10} \rangle . \tag{3.50}$$

Now, we already know that

$$\langle ze^{-\delta_2 r^2}|H|ze^{-\delta_2 r^2}\rangle = -\frac{4\pi}{2}\{\Delta_2{}^2 I_2^{(\Delta_2)} I_3^{(\Delta_2)} + \Delta_2{}^2 I_4^{(\Delta_2)} I_1^{(\Delta_2)} - 5\Delta_2 I_2^{(\Delta_2)} I_1^{(\Delta_2)}\} - \frac{4\pi}{3} I_3^{(\Delta_2)} \quad (3.51)$$

where $\Delta_2 = 2\delta_2$ (cf. equation (3.46)). We also know, from equations (3.46) and (3.48), and using the table of Appendix (II) , that

$$\langle ze^{-\delta_2 r^2}|H|ze^{-\delta_2 r^2}\rangle = -0.113177\,\frac{\pi^{3/2}}{2\Delta_2{}^{5/2}} \quad . \quad (3.52)$$

We can find similar expressions to that of equation (3.52) for the other three matrix elements in equation (3.50):

$$\langle z\rho e^{-\delta_3 r^2}|H|z\rho e^{-\delta_3 r^2}\rangle = -\frac{4\pi}{2}\{I_1^{(\Delta_3)} I_2^{(\Delta_3)} + \Delta_3{}^2 I_2^{(\Delta_3)} I_5^{(\Delta_3)} + \Delta_3{}^2 I_4^{(\Delta_3)} I_3^{(\Delta_3)} - 7\Delta_3 I_2^{(\Delta_3)} I_3^{(\Delta_3)}\} - \frac{8\pi}{15} I_5^{(\Delta_3)} \quad (3.53)$$

$$\langle ze^{-\delta_2 r^2}|H|z\rho e^{-\delta_3 r^2}\rangle = -\frac{4\pi}{2}\{I_2^{(\Delta)} I_0^{(\Delta)} + 2\Delta_3{}^2 I_2^{(\Delta)} I_4^{(\Delta)} - 7\Delta_3 (I_2^{(\Delta)})^2\} - \frac{\pi^2}{2} I_4^{(\Delta)} \quad (3.54)$$

$$\langle z\rho e^{-\delta_3 r^2}|H|ze^{-\delta_2 r^2}\rangle = -\frac{4\pi}{2}\{\Delta_2{}^2 I_4^{(\Delta)} I_2^{(\Delta)} - 5\Delta_2 (I_2^{(\Delta)})^2\} - \frac{\pi^2}{2} I_4^{(\Delta)} \quad (3.55)$$

where $\Delta_3 = 2\delta_3$ and $\Delta = \delta_2 + \delta_3$. Substitution of equations (3.53) - (3.55) into equation (3.50), and also putting in the value for C given in equation (3.36), gives

$$\langle \psi_2|H|\psi_2\rangle = \frac{11\pi^{3/2}}{2\Delta_3{}^{5/2}} - \frac{8\pi}{15\Delta_3{}^3} + \frac{\Delta_2{}^{5/2}\pi^{5/2}}{8\Delta^6}(-0.113177) - \frac{\Delta_2{}^{5/2}\pi^{1/2}}{4\Delta^3} \times \left\{\frac{-3\pi^2}{\Delta^4}(\delta_2{}^2+\delta_3{}^2) + \frac{\pi^2}{2\Delta^3}(5\delta_2+7\delta_3) - \frac{\pi^2}{5\Delta^2} - \frac{3\pi^{5/2}}{4\Delta^{5/2}}\right\} \quad . \quad (3.56)$$

Also, in order to obtain an expression for the minimum upper bound on $E_{n=3}$, we need to calculate $\langle \psi_2|\psi_2\rangle$.

$$\langle \psi_2|\psi_2\rangle = \langle \psi_{20}|\psi_{20}\rangle + C^2\langle \psi_{10}|\psi_{10}\rangle - 2C\langle \psi_{10}|\psi_{20}\rangle$$

$$= \frac{8\pi}{15} I_6^{(\Delta_3)} + C^2\,\frac{4\pi}{3} I_4^{(\Delta_2)} - 2C\,\frac{\pi^2}{4} I_5^{(\Delta)}$$

$$= \frac{\pi^{3/2}}{2\Delta_3{}^{7/2}} - \frac{\Delta_2{}^{5/2}\pi^{5/2}}{8\Delta^6} \quad . \quad (3.57)$$

Substituting the expressions for the matrix elements calculated in equations (3.56) and (3.57) into equation (3.49), and differentiating the resulting expression for $E_{n=3}$ with respect to δ_3 (δ_2 is already known) gives a minimum upper bound for $E_{n=3}$. This expression is complicated in δ_3 and renders the standard variational method of parts (i) and (ii) impossible to use. An alternative method was found using quadratic interpolation to find the minimum. That is, the function $E_{n=3}(\delta_3)$ is approximated by a quadratic polynomial which agrees exactly in function value at a certain number of points. The minimum (or maximum) of the quadratic polynomial passing through the points (x_1,y_1), (x_2,y_2) and (x_3,y_3) is given by $x_1 + \frac{p}{q}$ where,

$$p = (x_2 - x_1)^2(y_3 - y_1) - (x_3 - x_1)^2(y_2 - y_1) \qquad (3.58)$$

$$q = 2\,(x_3 - x_1)(y_2 - y_1) - (x_2 - x_1)(y_3 - y_1) \quad . \qquad (3.59)$$

Provided the minimum (or maximum) lies in the interval $[x_1,x_3]$, we can obtain successive approximations to its true value (Gill and Murray, 1974).

The actual value for δ_3 obtained is 3.74×10^{-3} giving a minimum energy of -0.0165 Ry for the n = 3 state at zero field.

To ensure the correct high field dependence of the wave functions, a fourth value of δ is chosen to give the correct energies as $B \to \infty$. We take $\delta_4 = \frac{\gamma}{2}$, as the term $e^{-\frac{1}{2}\gamma\rho^2}$ is contained in the free Landau functions (Wallis and Bowlden, 1956), which give the correct energies at high fields. Meuller et al, 1975, use this value for their equivalent of δ_4, and show that the correct high field energies are obtained.

To summarize, we ensure accurate low field eigenvalues by choosing δ_1, δ_2 and δ_3 to minimize in turn, the zero field eigenvalues for the n = 1, 2 and 3 levels by using a minimal basis of one, one and two terms respectively (see table 3.4). Table (3.4) also gives the final

zero field results using the full basis - the ground state energy is slightly too high, and remains so at all field strengths, suggesting that it never becomes fully cylindrical. The 6% error at zero field for the n = 3 level could be reduced by using more values of δ, but is sufficiently accurate for our purposes.

n	Exact Energy	Calculated Energy in Minimum Basis	δ	Best Cylindrical Basis Energy
1	-1.000	-0.8488	0.283	-0.982
2	-0.250	-0.2264	0.0453	-0.250
3	-0.111	-0.0165	3.74(-4)	-0.106

Table 3.4

Zero field eigenvalues (Ry) and corresponding values of δ.

§3.5 Solving the Eigenvalue Equation

The equation to be solved in order to evaluate the energies and wave functions is

$$(\{H_{pq}\} - E\{S_{pq}\})\underline{x} = 0 \tag{3.60}$$

(cf. equation (2.28) where,

$$H_{pq} = \sum_i \sum_j C^{(p)}_{\alpha_i,\beta_i,\delta_i} C^{(q)}_{\alpha_j,\beta_j,\delta_j} \langle \chi_i | H | \chi_j \rangle$$

and (3.61)

$$S_{pq} = \sum_i \sum_j C^{(p)}_{\alpha_i,\beta_i,\delta_i} C^{(q)}_{\alpha_j,\beta_j,\delta_j} \langle \chi_i | \chi_j \rangle \quad ,$$

the wave function being defined in equation (3.2) and H being given in equation (3.7). As the size of the basis required in this case is much larger than that required by the basis of hydrogenic states described in Chapter 2, in order to obtain convergence on the eigen-

values (typically the matrices $\{H_{pq}\}$ and $\{S_{pq}\}$ will be of dimension 130 for the cylindrical basis and 12 for the hydrogenic states basis for convergence on the 14 lowest eigenvalues), a different method is used to solve equation (2.15), in order to avoid excessive inversion and manipulation of the larger matrices. Again routines from the NAG library are used and a brief description of the numerical procedures is set out below. Details of the computer program to calculate the eigenvalues and eigenvectors are set out in appendix (I).

Firstly, the problem is reduced to the form

$$P\underline{z} = E\underline{z} \tag{3.62}$$

where P is symmetric, by using Cholesky decomposition of the matrix $\{S_{pq}\}$. For the purpose of this section, we will abbreviate equation (3.60) to

$$(H - ES)\underline{x} = 0 \quad . \tag{3.63}$$

Writing

$$S = LL^T, \tag{3.64}$$

where L is formed using Cholesky factorization of S (Peters and Wilkinson, 1965), equation (3.63) becomes

$$(L^{-1}HL^{-T})(L^T\underline{x}) = E(L^T\underline{x}) \quad . \tag{3.65}$$

Now, $L^{-1}HL^{-T}$ is symmetric and so this reduces immediately to the symmetric problem of equation (3.62), where

$$P = L^{-1}HL^{-T} \tag{3.66}$$

and

$$\underline{z} = L^T\underline{x}. \tag{3.67}$$

The matrix P is then reduced to tridiagonal form with the use of the Householder method described in section §2.4. So the problem then becomes

$$Q\underline{y} = E\underline{y} \tag{3.68}$$

where Q is tridiagonal. The selected eigenvalues, E_i, required can then be calculated by the method of bisection (Wilkinson and Reinsch,

1971, p249). Briefly, a sequence of numbers $a_i(x)$ is defined by

$$a_1(x) = q_1 - x$$
$$a_i(x) = (q_i - x) - \frac{r_i^2}{a_{i-1}(x)} \quad , \quad i = 2, 3 \ldots n \tag{3.69}$$

where $\{q_i : i=1,2 \ldots n\}$ are the diagonal elements and $\{r_i : i=2,3 \ldots n\}$ are the off-diagonal elements of Q. The number of eigenvalues which lie below the value x is equal to the number of negative $a_i(x)$, so by adjusting x, the eigenvalues may be found.

When the required eigenvalues are known, the corresponding eigenvectors can be calculated by inverse iteration. This is described in Wikinson and Reinsch, 1971, p418.

This method of calculating the eigenvalues and eigenvectors of a symmetric tridiagonal matrix P, is more efficient than the QL method used in the case of the hydrogen states basis (see § 2.4), when dealing with large matrices. The primary advantage being that there is no multiplication of large matrices involved, a time consuming process for the computer, requiring much storage space. Obviously, a process which calculates only selected eigenvalues (and corresponding eigenvectors) in the case where they are not all required, must be more economical than a method which calculates all the eigenvalues.

§3.6 Transition Probabilities

The probability that a transition will occur between states m' and m with the emission of one photon of frequency $\omega_{m'm}$, the two states being bound, is (from equation (2.85))

$$A_{m'm} = 2.142020358 \times 10^{10}\ \omega_{m'm}{}^3\ |\langle m'|r_\mu|m\rangle|^2 \quad \text{sec}^{-1} \tag{3.70}$$

in the length formulation, where $\omega_{m'm}$ is given by equation (2.54) and

r_μ by equation (2.91). On evaluation of the matrix element $\langle m'|r_\mu|m\rangle$, we consider the two cases of transitions between states of the same and different parities separately.

(a) Transitions between states of the same parity

The matrix elements are of the form $\langle\chi_j|r_\mu|\chi_k\rangle$ where χ_i and the full wavefunctions are given by equations (3.2), (3.3) and (3.5). For transitions between states of the same parity, $\alpha_j + \alpha_k$ is even.

(i) $\mu = 0$

Now, $r_o = r\cos\theta$. Writing the basis elements χ_i in spherical polar coordinates (r,θ,ϕ) where $z = r\cos\theta$, $\rho = r\sin\theta$, we have

$$\langle\chi_j|r_o|\chi_k\rangle = \int_o^\infty r^{\alpha_j+\alpha_k+\beta_j+\beta_k+3}\, e^{-\Delta r^2}\, dr \int_o^\pi \cos^{\alpha_j+\alpha_k+1}\theta\, \sin^{\beta_j+\beta_k+1}\theta\, d\theta \int_o^{2\pi} e^{i(m_k-m_j)\phi}\, d\phi \qquad (3.71)$$

But the integral over θ reduces to the form

$$\sum_{q=0}^{A/2} (-1)^q \binom{A/2}{q} \int_o^\pi \sin^{1+B+2q}\theta\, \cos\theta\, d\theta \qquad (3.72)$$

with $A = \alpha_j + \alpha_k$ and $B = \beta_j + \beta_k$. Now $\sin^n 0 = \sin^n \pi = 0$ for all n and so this integral is zero for all A and B. So we can deduce from this, that transitions do not occur between states of the same parity and same magnetic quantum number (m).

(ii) $\mu = 1$

Now $r_1 = -\frac{1}{\sqrt{2}}\, r\sin\theta\, e^{i\phi}$, so in this case we can write

$$\langle\chi_j|r_1|\chi_k\rangle = -\frac{1}{\sqrt{2}} \int_o^\infty r^{A+B+3}\, e^{-\Delta r^2}\, dr \int_o^\pi \cos^A\theta\, \sin^{B+2}\theta\, d\theta \int_o^{2\pi} e^{i(m_k-m_j+1)\phi}\, d\phi \qquad (3.73)$$

The integral over r can easily be evaluated using the table in appendix (II) and the integral over θ can easily be reduced to

$$\sum_{q=0}^{\frac{1}{2}(B+2)} (-1)^q \binom{\frac{1}{2}(B+2)}{q} \frac{(2q+A)!}{((\frac{2q+A}{2})!)^2} \frac{\pi}{2^{2q+A}} . \qquad (3.74)$$

The integral over ϕ is zero unless $m_j = m_k + 1$, in which case it is 2π. So in this case we can conclude that transitions between states of the same parity occur if $m_j = m_k + 1$.

(iii) $\mu = -1$

We have, $r_{-1} = \frac{1}{\sqrt{2}} r \sin\theta \, e^{-i\phi}$. This is very similar to the expression for r_1, and so the matrix element can be written

$$\langle \chi_j | r_{-1} | \chi_k \rangle = \frac{1}{\sqrt{2}} \int_0^\infty r^{A+B+3} \, e^{-\Delta r^2} \, dr \int_0^\pi \cos^A\theta \, \sin^{B+2}\theta \, d\theta \int_0^{2\pi} e^{i(m_k - m_j - 1)\phi} \, d\phi \, . \qquad (3.75)$$

The r and θ integrals are exactly the same as those in equation (3.74), and the ϕ integral is zero unless $m_k = m_j + 1$, in which case it is 2π. So, transitions between states of the same parity also occur if $m_k = m_j + 1$.

(b) Transitions between states of different parity

For transitions between states of different parity, we have

$A = \alpha_j + \alpha_k$ odd.

(i) $\mu = 0$

The matrix element of r_o reduces to

$$\langle \chi_j | r_o | \chi_k \rangle = \int_0^\infty r^{A+B+3} \, e^{-\Delta r^2} \, dr \int_0^\pi \cos^{A+1}\theta \, \sin^{B+1}\theta \, d\theta \int_0^{2\pi} e^{i(m_k - m_j)\phi} \, d\phi \, . \qquad (3.76)$$

Again, the integral over r can be evaluated with the aid of the table in appendix (II). The integral over θ reduces to the form

$$\sum_{p=0}^{\frac{1}{2}(B+1)} (-1)^p \binom{\frac{1}{2}(B+1)}{p} \int_0^\pi \cos^{1+A+2p}\theta \, d\theta \qquad (3.77)$$

if B is odd, and

$$\sum_{p=0}^{B/2} (-1)^p \binom{B/2}{p} \int_0^\pi \cos^{1+A+2p}\theta \, \sin\theta \, d\theta \qquad (3.78)$$

if B is even, which can both be evaluated directly. The integral

over ϕ is, as in (a) part (i), $2\pi\delta_{m_j,m_k}$. Therefore, we can deduce, that transitions occur between states of different parity but the same magnetic quantum number.

(ii) $\mu = 1$

The matrix element of r_1 reduces to the expression given by equation (3.75), the only difference being that A is odd and not even. The integral over θ, in particular, is

$$\int_0^{\pi} \cos^A\theta \, \sin^{B+2}\theta \, d\theta \ ,$$

which is always zero for odd A. So transitions do not occur between states of different parity with $m_j = m_k + 1$.

(iii) $\mu = -1$

The integral over θ of the matrix element of r_{-1} is the same as that of r_1, which, as shown in part (ii), is always zero. So transitions also do not occur between states of different parity with $m_k = m_j + 1$.

To summarize, the only allowed transitions are given in table 3.5.

$\Delta\Pi$	Δm
0	1, -1
1, -1	0

Table 3.5

Selection rules for transitions in the cylindrical basis. Π is parity, and m the magnetic quantum number.

The selection rules given in table 3.5 agree with the high field selection rules obtained by Wallis and Bowlden, 1956.

As a further test of this cylindrical basis set model, some transition probabilities are calculated in the dipole velocity approximation and compared with those calculated in the dipole length approximation. In order to find the Einstein A coefficients in the velocity formulation, we need to find $\langle m'|H_{int}|m\rangle$ in terms of $\langle m'|\nabla_\mu|m\rangle$ where H_{int} is given by equation (2.65), and

$$\nabla_{\pm 1} = \mp\frac{1}{\sqrt{2}}\left(\frac{\partial}{\partial x} \pm \frac{\partial}{\partial y}\right) \quad , \quad \nabla_o = \frac{\partial}{\partial z} \quad . \tag{3.79}$$

Now, from equation (2.65), we see that

$$\langle m'|H_{int}|m\rangle = -\frac{ie}{\hbar c}\underline{A}' \cdot \langle m'|\frac{h^2}{\mu}\nabla + i\hbar\omega_L \hat{B} \times \underline{r}|m\rangle \quad . \tag{3.80}$$

Noting that the z component of $\hat{B} \times \underline{r}$ is zero, we can write the z component of the matrix element as $\frac{\hbar^2}{\mu}\langle m'|\frac{\partial}{\partial z}|m\rangle$. So for transitions in which the matrix element of $\nabla_{\pm 1}$ is zero, the expression

$$\langle m'|H_{int}|m\rangle = -\frac{ie}{\hbar c}\underline{A}' \cdot \langle m'|\frac{\hbar^2}{\mu}\nabla|m\rangle \tag{3.81}$$

holds. This expression is the same as the equivalent zero field expression for the transition probability in the dipole velocity approximation (cf. equation (3.70)). So the total transition probability for transitions in which the matrix elements of $\nabla_{\pm 1}$ are zero is

$$A_{m'm} = \frac{4e^2}{3c^3\hbar}\omega_{m'm}\,|\langle m'|\nabla_o|m\rangle|^2 \quad . \tag{3.82}$$

As in the case of the length formulation, we can see, by performing the required differentiation, that the only case where the matrix element of ∇_o is the only non-zero term, is the case where the two states in the transition have different parity. Therefore, this is the only case for which we shall calculate transition probabilities in the velocity formulation.

The expression for the matrix element of ∇_o reduces to

$$\langle \chi_j | \frac{\partial}{\partial z} | \chi_k \rangle = 2\pi \delta_{m_j, m_k} \{ \alpha_2 \int_o^\infty r^{A+B+1} e^{-\Delta r^2} dr \int_o^\pi \sin^{B+1}\theta \cos^{A-1}\theta \, d\theta$$

$$- 2\delta_2 \int_o^\infty r^{A+B+3} e^{-\Delta r^2} dr \int_o^\pi \sin^{B+1}\theta \cos^{A+1}\theta \, d\theta \} \quad (3.83)$$

where the radial integrals can be calculated using the table in appendix (II) and the integrals over θ, using equations (3.77) and (3.78).

The transition probabilities in both the length and velocity formulations, as well as wavelengths and oscillator strengths are calulated by program CPOLAR, details of which are given in Appendix (I).

CHAPTER 4

RESULTS FOR ENERGIES AND TRANSITION PROBABILITIES USING BASES OF HYDROGENIC AND CYLINDRICAL STATES

§4.1 Introduction

In this chapter, the results of the calculations described in chapters 2 and 3 are presented. Results are given for the energy levels of all fourteen states which go to the n = 1, 2 and 3 levels at zero field, for magnetic field strengths in the range $0 \leq \gamma \leq 1.0$ or $0 \leq B \leq 2.35 \times 10^9$ G. Einstein 'A' coefficients and wavelengths for all allowed transitions between the lowest fourteen states are also presented. The main object of this chapter is to compare the results for the energy levels and wavefunctions of hydrogen using the cylindrical and hydrogenic functions and with results obtained by various other authors. It should be noted that in these calculations, and also in those of other authors with whom we compare our results, the accuracy of the energy eigenvalues and wavefunctions obtained is restricted due to the fact that the sets of basis functions used are not complete. The continuum states are not included in the basis sets and so we cannot expect to obtain exact energy eigenvalues. We obtain convergence to three decimal places on the eigenvalues for fields of up to 10^9 G. The calculations involving the basis set of unperturbed hydrogenic functions, have been carried out previously by Brandi, 1975 and Brandi et al, 1976, but as the results for the energy levels of the fourteen lowest states were only presented graphically, and as the results for Einstein 'A' coefficients were incomplete, these results have been recomputed.

§4.2 Convergence of the Energy Eigenvalues

It has already been explained (see chapter 1) that, by the Hylleraas- Undheim theorem, adding more terms to a set of basis functions can only improve the energy eigenvalue and therefore make the wavefunction more accurate. It has also been shown that the exact values of the energies are the lower bounds on these eigenvalues, and so any improvement must be a decrease in energy.

In the case where the set of basis functions consist of unperturbed hydrogenic functions, the eigenvalues converge (to three decimal places) comparatively quickly, as is illustrated in table 4.1. It should be remembered that the selection rules for the coupling of these states are $\Delta\ell = 0, \pm 2$ and $\Delta m = 0$, so only states of like parity and m can 'mix'. In table 4.1, the s, p, d and f states are added in increasing principle quantum number. E_{1s_o} and E_{2p_o} are the energies of the even and odd parity states respectively which converge most quickly, and E_{3d_2} and E_{3p_1} are the energies of the even and odd parity states which converge most slowly.

Table 4.1 shows that convergence to at least 3 decimal places is obtained on the energies of the fourteen lowest states, using a basis of twelve odd and twelve even parity states at $B = 10^7$ G and 22 odd and 22 even parity states at $B = 10^8$ G. At $B \geq 5 \times 10^8$G, the $3d_2$ and $3p_1$ states are not bound in this basis, however, all the bound state energies are converged to 3 decimal places using a basis of 22 odd and 22 even parity states at $B = 5 \times 10^8$ G and $B = 10^9$ G. It is found that if more states are added to this basis in an attempt to improve the eigenvalues even further, singularities occur in the Hamiltonian matrix $\{H_{pq}\}$ and the program (HYDROGN) breaks down. It is also interesting to note that the addition of g states to the basis, has no effect on the energy eigenvalues of the states corresponding to d states at zero field.

B (G)	NS	NP	ND	NF	E_{1s_o}	E_{2p_o}	E_{3d_2}	E_{3p_1}
10^7	6	6	6	6	-0.999991	-0.249946	-0.102116	-0.106209
	7	7	7	7	-0.999991	-0.249946	-0.102116	-0.106209
10^8	10	10	10	10	-0.999096	-0.244765	0.012759	-0.019565
	11	11	11	11	-0.999096	-0.244766	0.012713	-0.019635
5×10^8	10	10	10	10	-0.978008	-0.139991		
	11	11	11	11	-0.978009	-0.140111		
10^9	10	10	10	10	-0.915293	0.169778		
	11	11	11	11	-0.915307	0.169165		

Table 4.1

Convergence of the energy eigenvalues corresponding to the zero field $1s_o$, $3d_2$, $2p_o$ and $3p_1$ states represented by a basis of unperturbed hydrogenic functions. NS, NP, ND, and NF are the numbers of s, p, d and f states respectively included in the basis. Energies are measured in Ry.

The energies given in table 4.1 for the $1s_o$ and $2p_o$ states at $B = 10^7$ and 10^8 G are unchanged from those obtained using a basis of just one s and one p state, i.e. using the zero field wavefunctions for these states. At these fields, the $1s_o$ and $2p_o$ states retain nearly all of their zero field character.

On studying the eigenvectors of these states (which give the coefficients of the basis functions for a normalised wavefunction) it can also be seen that the amount of mixing of states which occurs at these 'low' fields is minimal. However, as the field strength increases, an increasing number of terms is required in the basis set for convergence of the eigenvalues of the lowest fourteen states, and it can be seen, from the eigenvectors for the states at high fields, that very strong mixing of states occurs and at 10^9 G, the higher energy states, e.g. $2p_{-1}$, do not bear much resemblence to their corresponding zero field states.

For the case in which the basis set consists of cylindrically symmetric functions of the type described in chapter 3, convergence is not nearly so rapid. This is basically due to the existence of the three variable parameters (α,β,δ) occurring in the cylindrical basis functions. The lowest even and odd parity states cannot be represented very accurately at low fields by the functions $ze^{-\delta_2 r^2}$ and $e^{-\delta_1 r^2}$ (the lowest terms of the odd and even parity basis sets respectively), at least not as accurately as the lowest even and odd parity states can be represented by the first even and odd parity unperturbed hydrogenic functions. The accurate wavefunctions, even at low fields, are a linear combination of many more terms than in the hydrogenic case.

We conclude then, that the reason for slow convergence of the eigenvalues in this cylindrical basis, is the strong mixing of states even at low fields. Table 4.2 shows the convergence of the energy eigenvalues of the states corresponding to the zero field states $1s_o$, $3d_2$, $2p_o$ and $3p_1$. Again, we have the selection rules $\Delta m = 0$ and $\Delta\pi = 0$ for the coupling of states. It can be seen that convergence to 3 decimal places can be obtained using a basis consisting of 128 terms (for m = 0 states), i.e. with N = 7, for all field strengths up to 10^8 G. N is such that all possible terms with $\alpha \leq N$ and $\beta \leq N$ are included in the basis set; the total number of terms in the basis set will obviously vary with the magnetic quantum number. For field strengths of 5×10^8 G and 10^9 G, the best convergence possible is obtained on all bound states. If N > 7, the program (CPOLAR) breaks down due to the appearance of singularities in the matrices $\{H_{pq}\}$ and $\{S_{pq}\}$. However, it is believed that the eigenvalues obtained for these fields are accurate enough for our purposes.

N	N'	E_{1s_o}	N'	E_{2p_o}	N'	E_{3d_2}	N'	E_{3p_1}
$B = 10^7$ G								
5	72	-0.973916	72	-0.249755	48	-0.100486	60	-0.105630
6	112	-0.981610	84	-0.245607	80	-0.101703	96	-0.106087
7	128	-0.981930	128	-0.249870	96	-0.101867	112	-0.106128
$B = 10^8$ G								
5	72	-0.974129	72	-0.244710	48	0.010397	60	-0.024418
6	112	-0.981472	84	-0.244712	80	0.010381	96	-0.022698
7	128	-0.981907	128	-0.244751	96	0.010380	112	-0.022717

Table 4.2a

Convergence of the energy eigenvalues corresponding to the zero field $1s_o$, $2p_o$, $3d_2$ and $3p_1$ states, represented by a basis of cylindrical functions. N is such that all possible terms with $\alpha \leq N$ and $\beta \leq N$ are included in the wavefunction, and N' is the number of terms in the basis set. Energies are measured in Ry.

N	N'	E_{1s_o}	N'	E_{2p_o}	N'	E_{3p_1}
$B = 5 \times 10^8$ G						
5	72	-0.957080	72	-0.162219	60	0.126399
6	112	-0.963354	84	-0.162225	96	0.126374
7	128	-0.964069	128	-0.162278	112	0.126371
$B = 10^9$ G						
5	72	-0.880895	72	-0.008247		
6	112	-0.892217	84	-0.008254		
7	128	-0.892881	128	-0.008481		

Table 4.2b

Convergence of the energy eigenvalues corresponding to the zero field $1s_o$ $2p_o$ and $3p_1$ states, represented by a basis of cylindrical functions. The $3d_2$ state is not bound at either of these fields and the $3p_1$ state is not bound at 10^9 G. N is such that all possible terms with $\alpha \leq N$ and $\beta \leq N$ are included in the wavefunction, and N' is the number of terms in the basis set. Energies are measured in Ry.

Comparing the results given in tables 4.1 and 4.2, we see that, although the eigenvalues for the cylindrical wavefunctions require many more basis functions than those of the spherical (hydrogenic) wavefunctions, the final converged energy results are lower (and by the Hylleraas-Undheim theorem, better) than those of the hydrogenic case for $B > 10^8$ G. It will be seen, in fact, that this is the case for all the lowest fourteen states (except $1s_o$) suggesting that a basis of cylindrical functions is more accurate than a basis of spherical functions at high fields. These results will be discussed in more detail in section §4.3.

m	Parity e = even o = odd		Labelling of States (in ascending energy)
	h	c	
0	e	e	$1s_o$ $2s_o$ $3s_o$ $3d_o$
0	o	o	$2p_o$ $3p_o$
-1	e	o	$3d_{-1}$
-1	o	e	$2p_{-1}$ $3p_{-1}$
1	e	o	$3d_1$
1	o	e	$2p_1$ $3p_1$
-2	e	e	$3d_{-2}$
2	e	e	$3d_2$

Table 4.3

Table to show the labelling and order of the energy eigenvalues. m is the magnetic quantum number. Parity is also shown for the hydrogenic (h) and cylindrical (c) bases.

At this point, perhaps a mention should be made of the labelling of the states of the hydrogen atom in a magnetic field. We follow

the conventional notation of Brandi, 1975 and label the states in the order given in table 4.3 (the states being labelled in ascending order). This notation does not, however, agree with that of Smith et al, 1973, who interchange the $3s_o$ and $3d_o$ states. Throughout, comparison with the results obtained by Smith et al, 1973, will assume that their states are labelled as in table 4.3.

§4.3 Comparison of the Results for the Energy Eigenvalues

Although, as already described in the previous section, energy eigenvalues are converged to at least three decimal places for fields up to 10^8 G, in both the hydrogenic and cylindrical basis sets, as the field strength increases, an increasing number of basis functions is required, and at $B = 2.35 \times 10^9$ G (i.e. $\gamma = 1$), limitations of time and storage restrict us to only 2 figures for states which go to zero field n = 3 states.

It should be noted that, if the elements of two rows and columns of the matrix H_{pq} (of dimension N) are almost linearly dependent, then this matrix becomes singular, rendering the calculation of a set of N linearly independent eigenvectors impossible. Care should be taken, therefore, to ensure that this case does not occur. In the cylindrical basis, this can be avoided by choosing carefully, values for the parameter δ. The first three values of δ are given in table 3.4 and a fourth value, to ensure correct high field energies is $\frac{\gamma}{2}$. Care should be taken to ensure that $\frac{\gamma}{2}$ is not too close to any of the other three values for δ. If this is the case, then the first value of δ is excluded from the basis set.

Results for fourteen states (which are the lowest lying at low fields) are given as a function of B in the range $10^7 \leq B \leq 10^9$ G in table 4.4, in both the cylindrical and hydrogenic bases, and also

compared graphically in figures 4.1 - 4.9. The zero field ordering is preserved at all fields within the subset of states (π,m_ℓ), but crossings occur between different subsets. At sufficiently high fields, for any state (n,π,m_ℓ), except (1,e,0) the eigenvalue obtained in the cylindrical basis lies lower than that obtained in the hydrogen states basis, but the lowest field at which this occurs is state dependent. The ground state results obtained in the cylindrical basis are anomalous, and within the range of field strengths examined are never better than those obtained in the hydrogen states basis.

It is clearly seen, from both table 4.4 and figures 4.1 - 4.9, that as B increases, so do the energy eigenvalues, in fact at field strengths greater than or equal to $10^8 \times 5$ G, some of the n = 2 and 3 states are no longer bound. The structure of the continuum of a hydrogen atom in a magnetic field is discussed in detail in chapter 1, but it is necessary to point out here that if it contains pure Landau levels, and if the Coulomb force is small compared to the magnetic field, the first of these levels lies at $\frac{1}{2}\hbar\omega_c$ (a.u.), i.e. γ Ry., where ω_c is the cyclotron frequency. This explains why some of the bound states have positive energy.

It is clear from figures 4.1 - 4.9 that the expansion of the wavefunctions in quadratically integrable unperturbed hydrogenic functions breaks down above 10^8 G. By this field strength the atom is needle-shaped (apart from, perhaps, the ground state) and is better described by functions of cylindrical symmetry.

Table 4.4 also gives results of the perturbation calculations of Ruder et al, 1981 at B = 10^7 G. These are in excellent agreement with our results and prove that perturbation theory is still adequate at B = 10^7 G.

State	$B = 10^7$ G			$B = 10^8$ G		$B = 5\times10^8$ G		$B = 10^9$ G	
	c	h	p	c	h	c	h	c	h
$1s_o$	-0.982	-1.000	-1.000	-0.982	-0.999	-0.964	-0.978	-0.893	-0.915
$2s_o$	-0.248	-0.250	-0.250	-0.236	-0.238	-0.082	-0.030	0.130	
$3s_o$	-0.110	-0.111	-0.110	-0.096	-0.094	0.077		0.327	
$2p_{-1}$	-0.254	-0.254	-0.254	-0.282	-0.282	-0.299	-0.249	-0.232	0.155
$2p_o$	-0.250	-0.250	-0.250	-0.245	-0.245	-0.162	-0.140	-0.008	0.170
$2p_1$	-0.246	-0.246	-0.246	-0.197	-0.197	0.126	0.177		
$3p_{-1}$	-0.115	-0.115	-0.115	-0.108	-0.105	0.031		0.216	
$3p_o$	-0.110	-0.111	-0.111	-0.089	-0.088	0.067		0.270	
$3p_1$	-0.106	-0.106	-0.106	-0.023	-0.020				
$3d_{-2}$	-0.119	-0.119	-0.119	-0.160	-0.157	-0.159		-0.069	
$3d_{-1}$	-0.115	-0.115	-0.115	-0.128	-0.127	-0.056		0.098	
$3d_o$	-0.110	-0.110	-0.111	-0.061	-0.057				
$3d_1$	-0.106	-0.107	-0.107	-0.043	-0.042				
$3d_2$	-0.102	-0.102	-0.102	0.010	0.013				

Table 4.4

Energy eigenvalues in Ry of the 14 lowest states at various field strengths using the hydrogenic basis (h), the cylindrical basis (c) and the perturbation theory results of Ruder et al, 1981 (p) at 10^7 G: a blank indicates that the state is no longer bound.

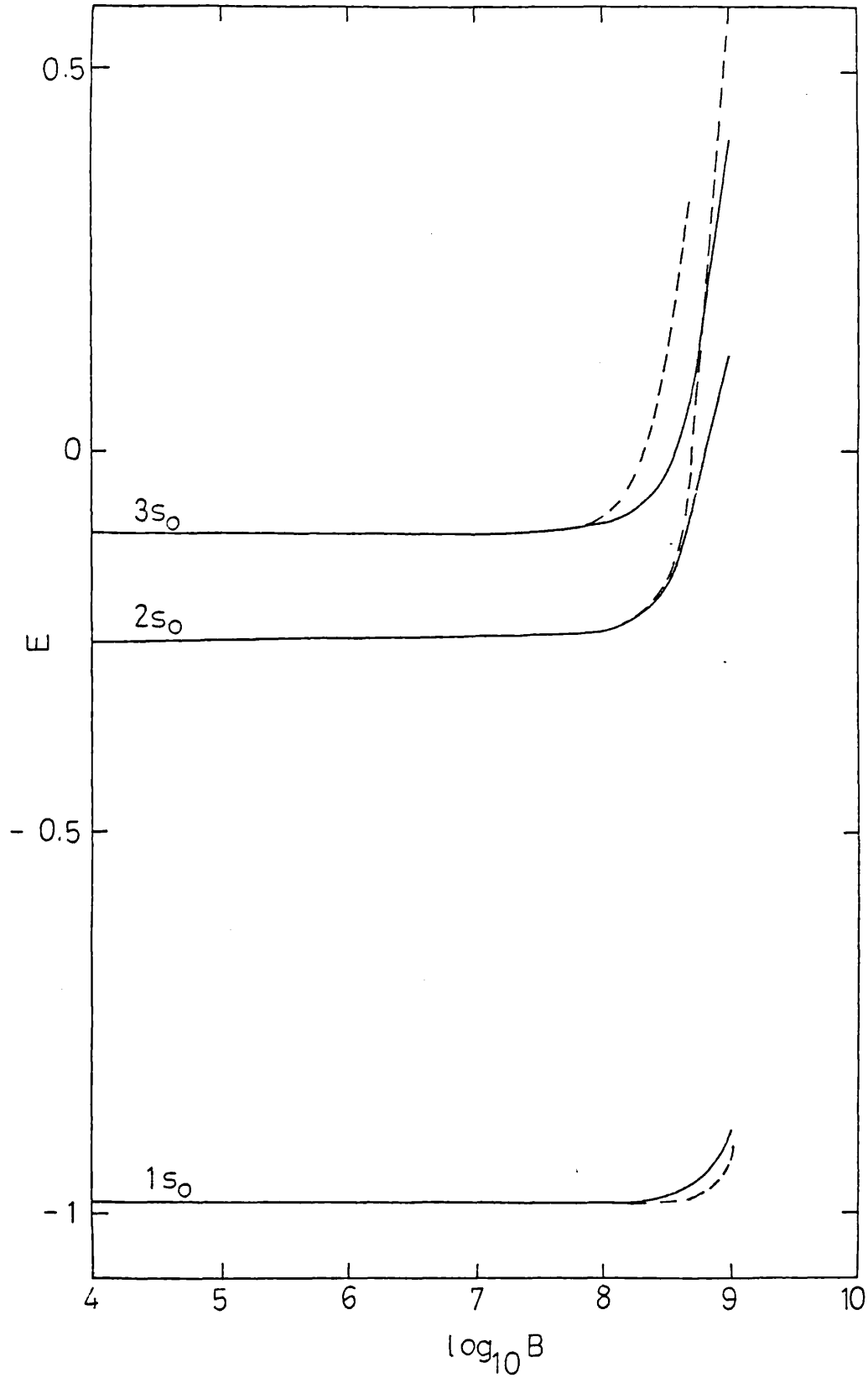

Fig 4.1

Comparison of the "$1s_o$", "$2s_o$" and "$3s_o$" energies in Ry, with increasing field strength B (G) using (i) the hydrogen states basis (broken line) and (ii) the cylindrical basis (solid line).

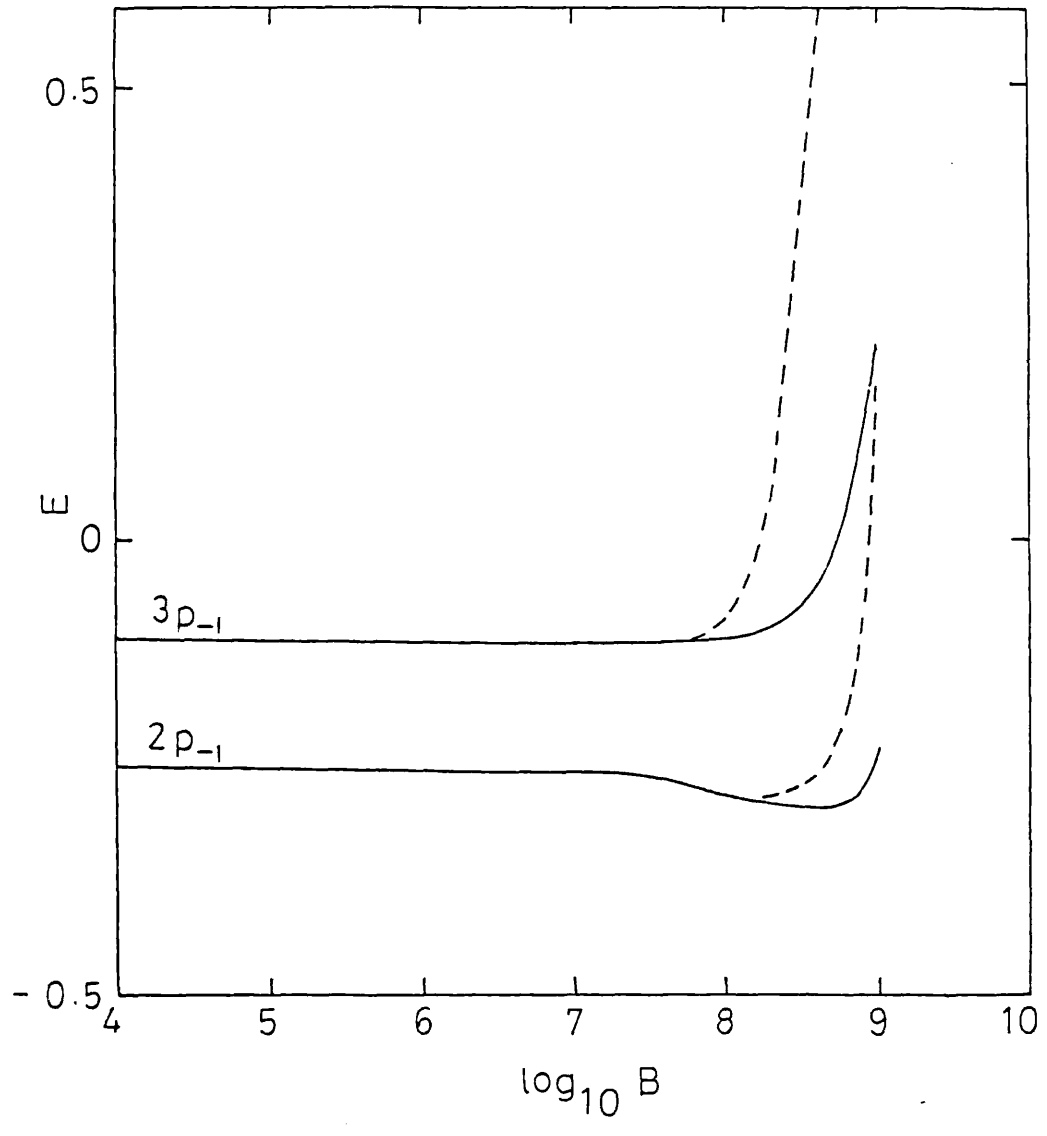

Fig 4.2

Comparison of the "$2p_{-1}$" and "$3p_{-1}$" energies in Ry, with increasing field strength B (G) using (i) the hydrogen states basis (broken line) and (ii) the cylindrical basis (solid line).

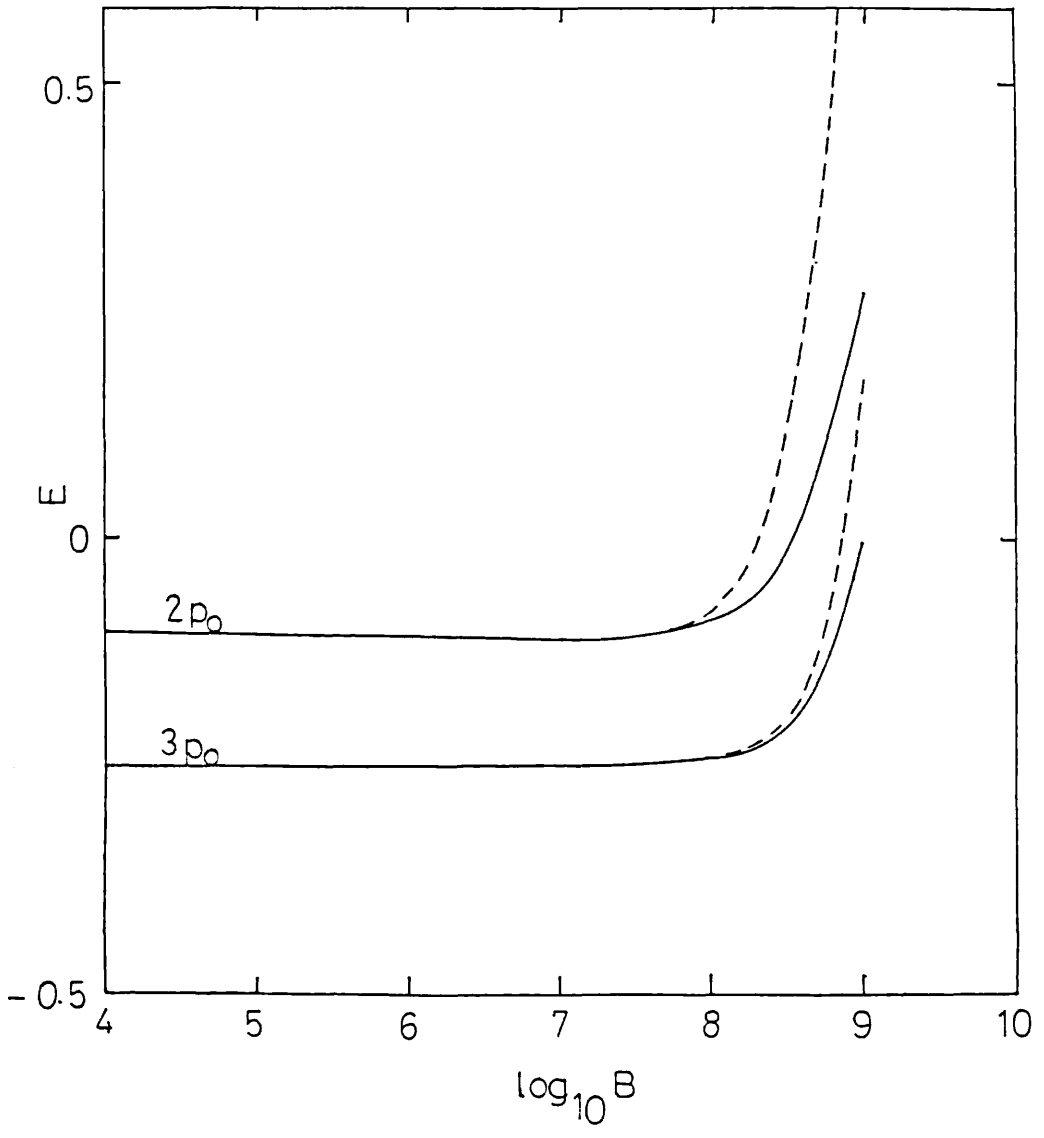

Fig 4.3

Comparison of the "$2p_o$" and "$3p_o$" energies in Ry, with increasing field strength B (G) using (i) the hydrogen states basis (broken line) and (ii) the cylindrical basis (solid line).

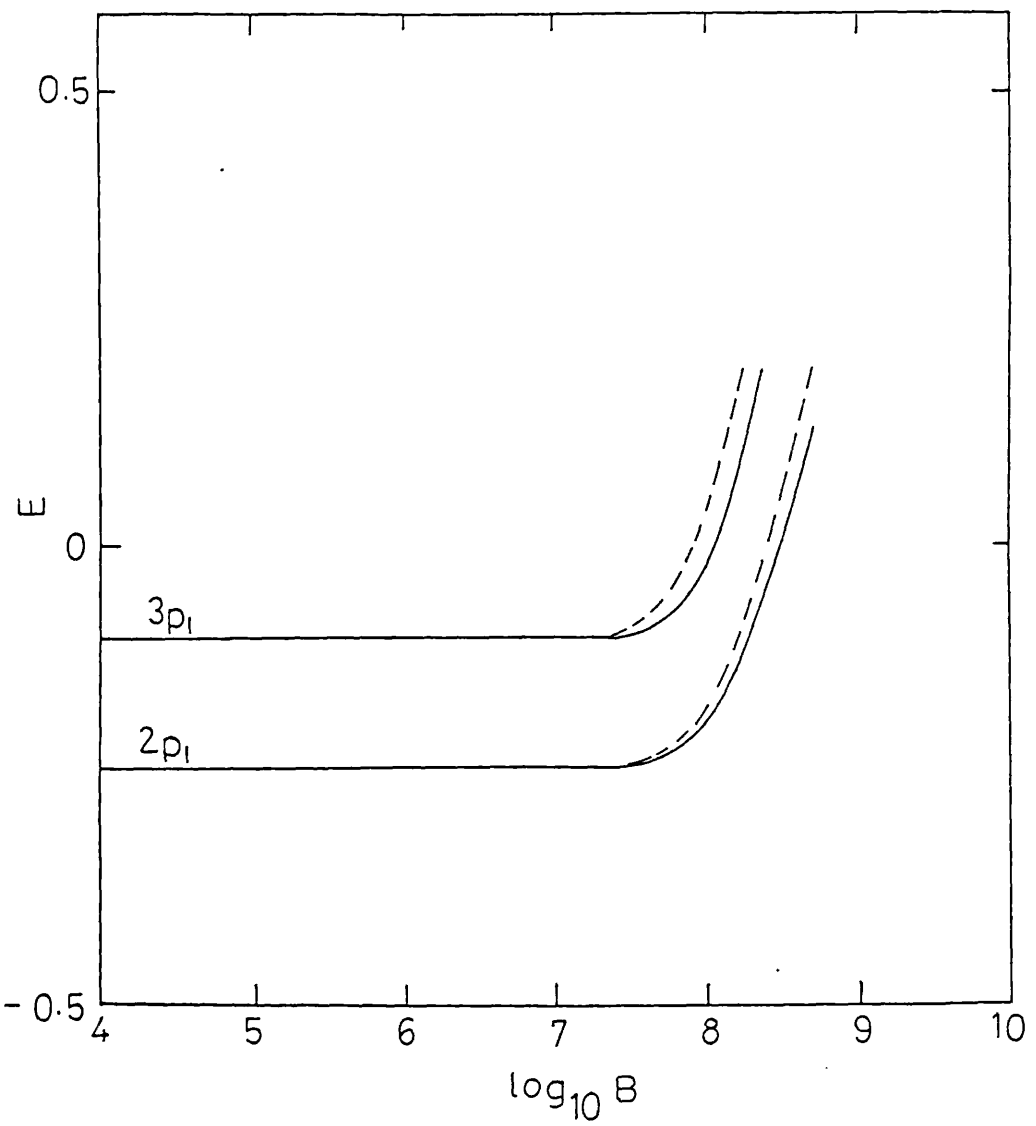

Fig 4.4

Comparison of the "$2p_1$" and "$3p_1$" energies in Ry, with increasing field strength B (G) using (i) the hydrogen states basis (broken line) and (ii) the cylindrical basis (solid line).

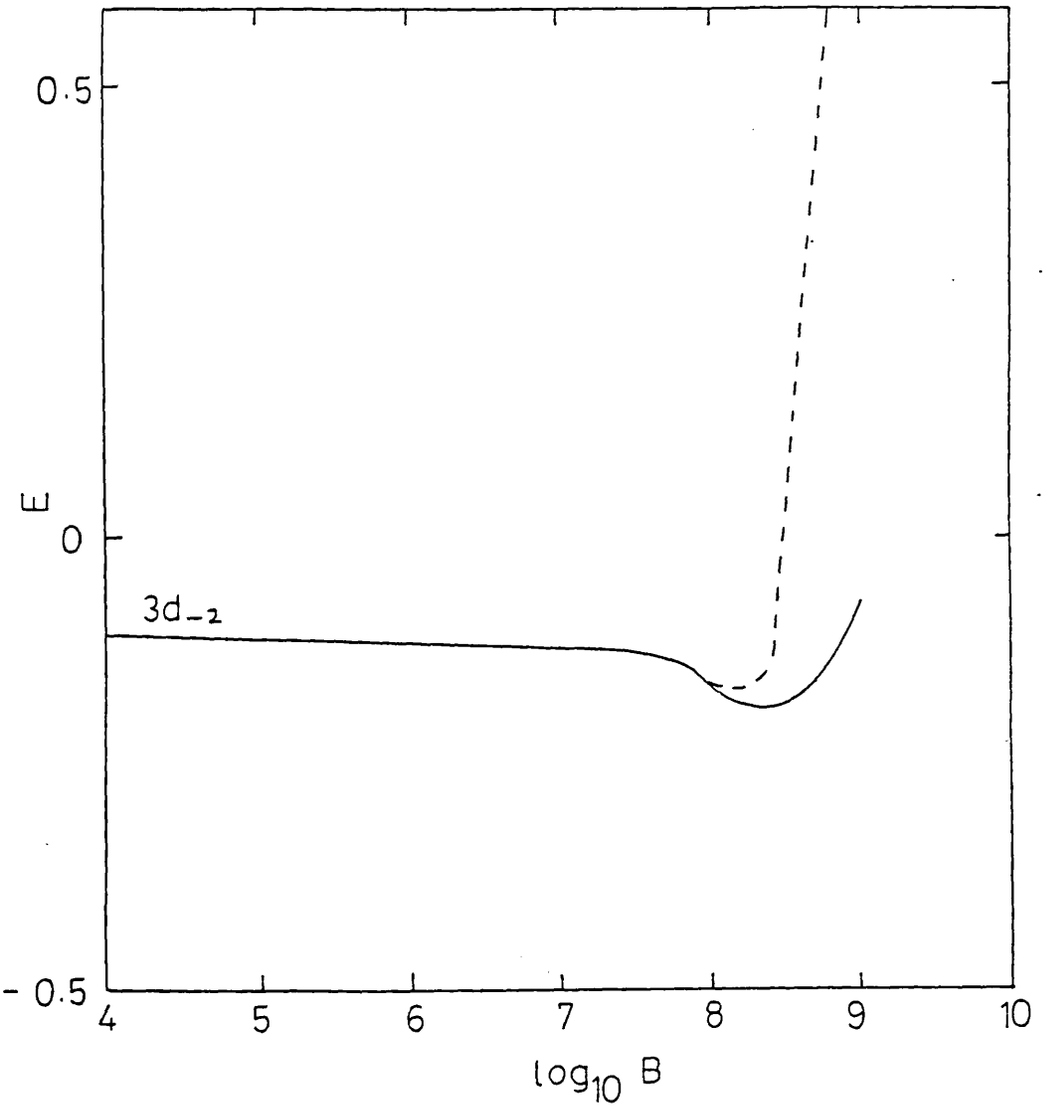

Fig 4.5

Comparison of the "$3d_{-2}$" energies in Ry, with increasing field strength B (G) using (i) the hydrogen states basis (broken line) and (ii) the cylindrical basis (solid line).

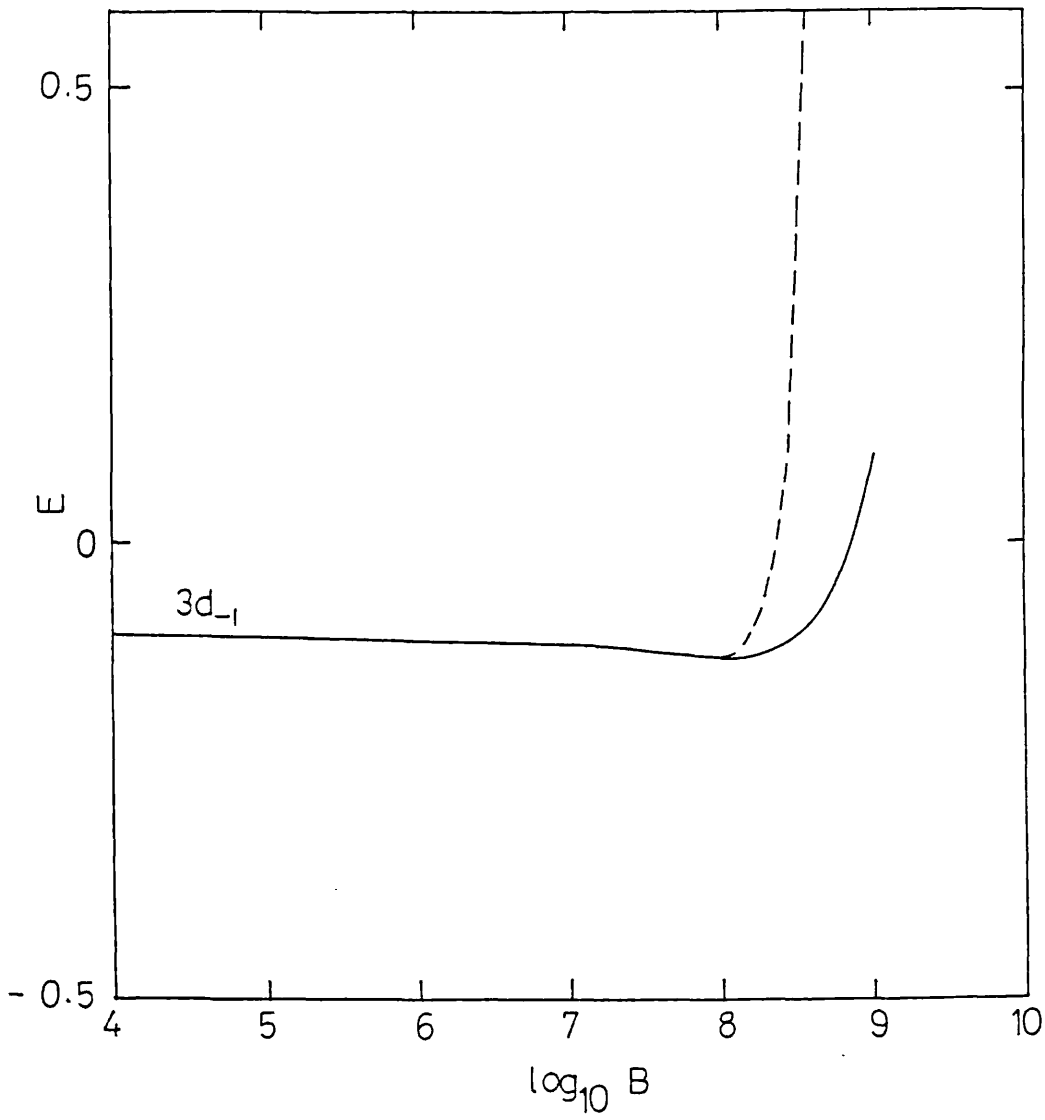

Fig 4.6

Comparison of the "$3d_{-1}$" energies in Ry, with increasing field strength B (G) using (i) the hydrogen states basis (broken line) and (ii) the cylindrical basis (solid line).

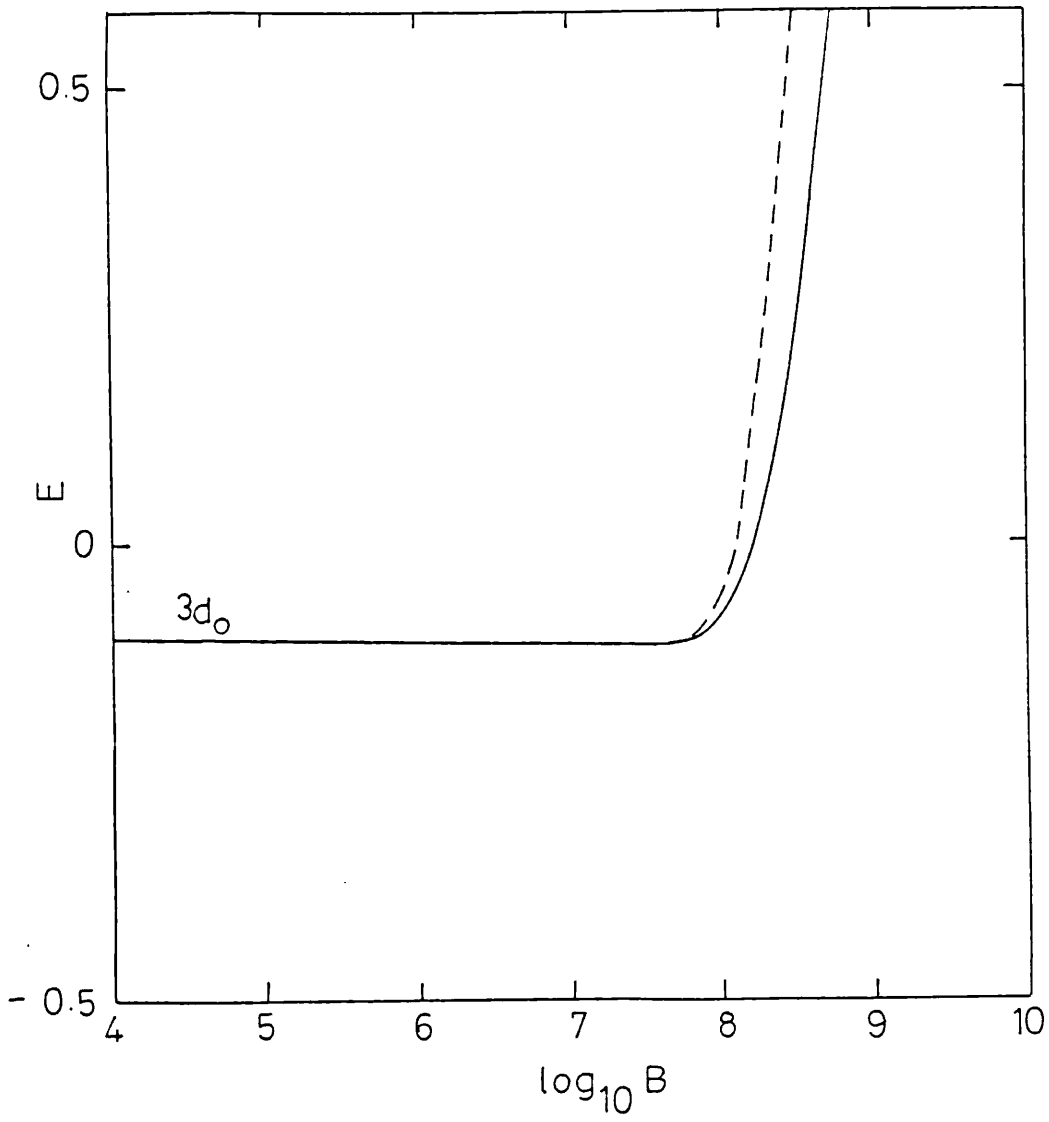

Fig 4.7

Comparison of the "$3d_o$" energies in Ry, with increasing field strength B (G) using (i) the hydrogen states basis (broken line) and (ii) the cylindrical basis (solid line).

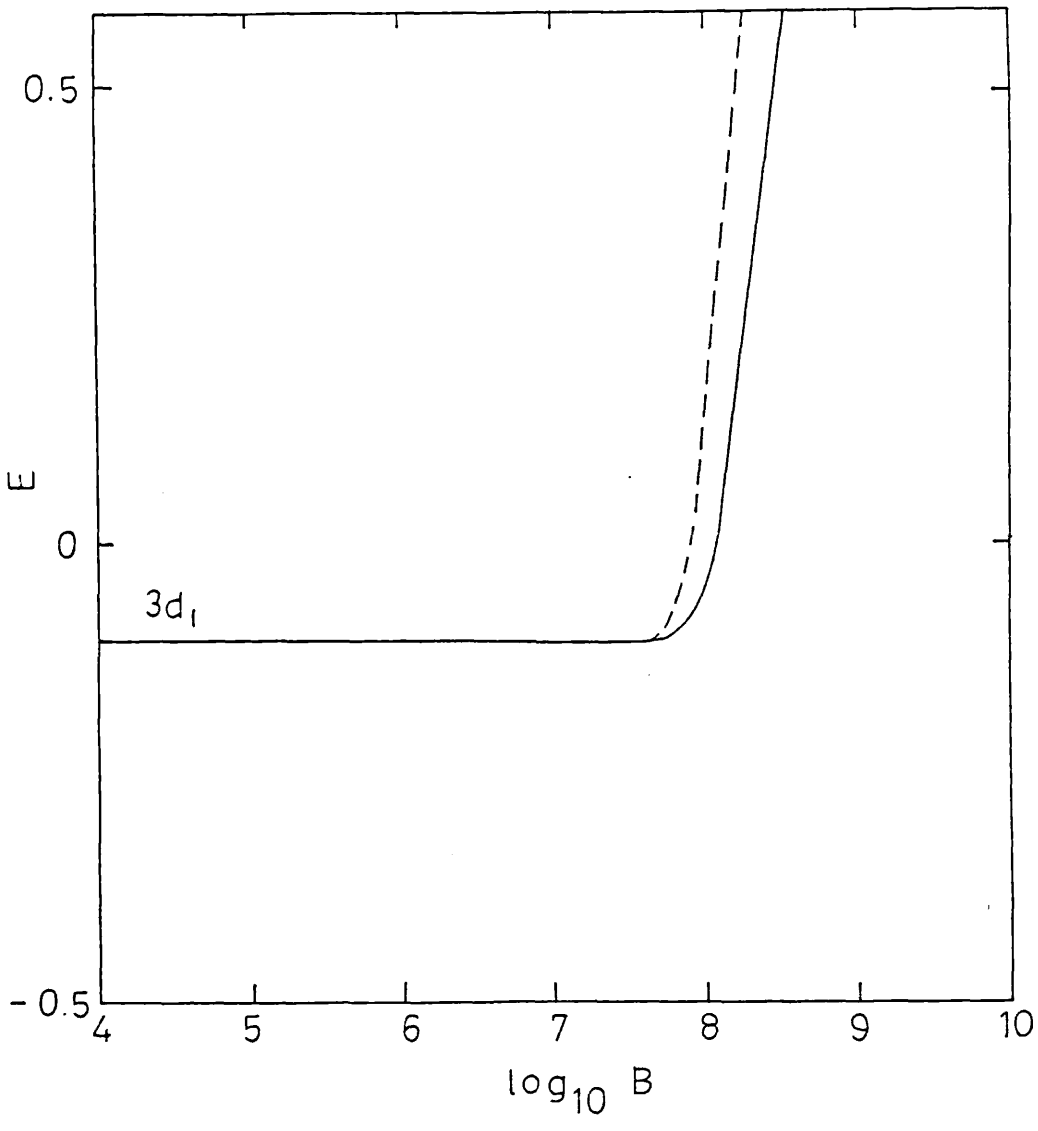

Fig 4.8

Comparison of the "$3d_1$" energies in Ry, with increasing field strength B (G) using (i) the hydrogen states basis (broken line) and (ii) the cylindrical basis (solid line).

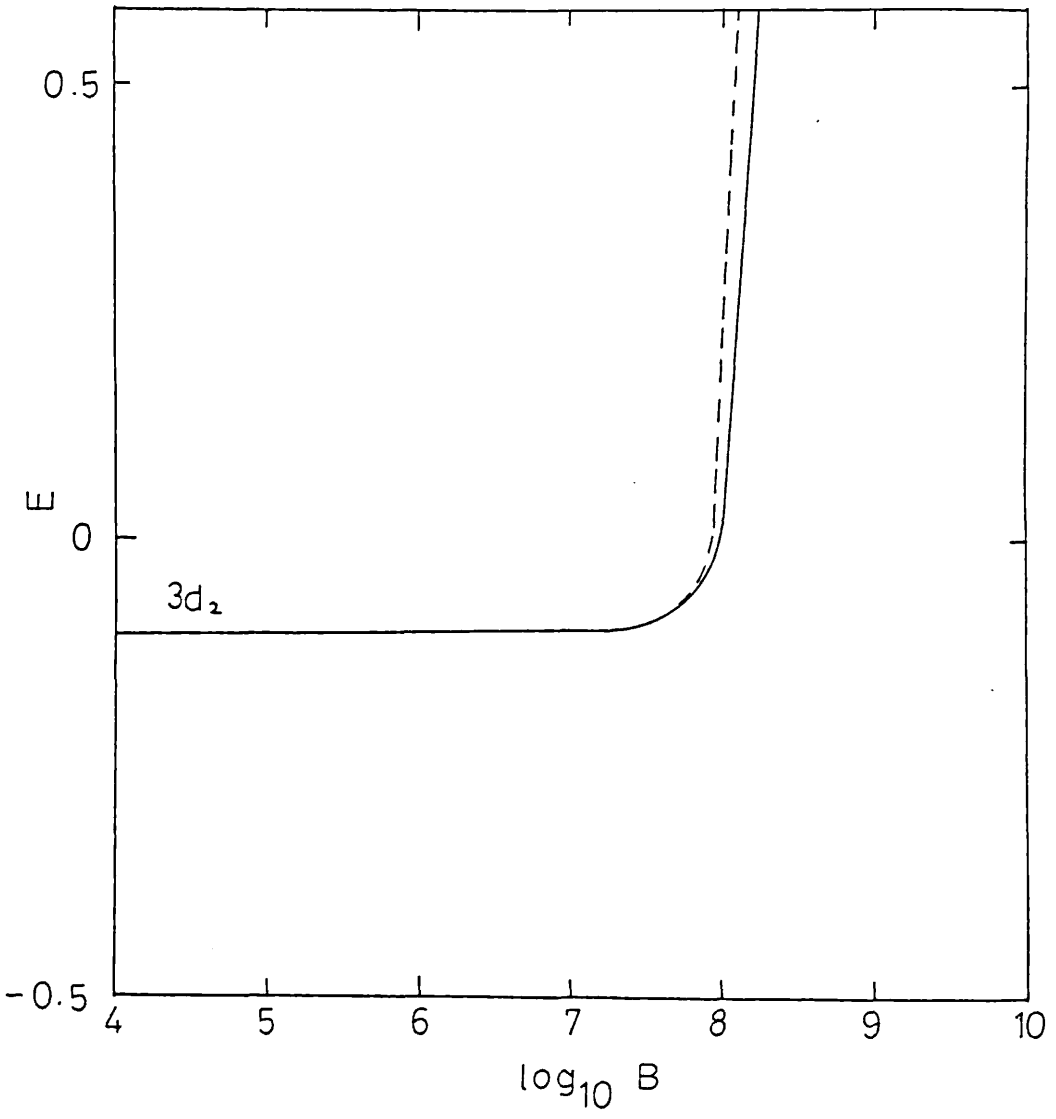

Fig 4.9

Comparison of the "$3d_2$" energies in Ry, with increasing field strength. B (G) using (i) the hydrogen states basis (broken line) and (ii) the cylindrical basis (solid line).

Praddaude, 1972, also used a basis of cylindrical states of the form

$$\chi = z^c \rho^{|m|} e^{-\gamma\rho^2} e^{-2|\varepsilon|^{\frac{1}{2}}r} \sum_{p=0}^{n} L_p^{|m|}(2\gamma\rho^2) \sum_{q=0}^{\infty} \sum_{s=0}^{q} C \rho^{2s} L_{q-s}^{\alpha}(4r|\varepsilon|^{\frac{1}{2}}) \tag{4.1}$$

where $L_a^b(z)$ is the generalized Laguerre polynomial of order a, $c = 0,1, \ldots, m=0,\pm1,\pm2, \ldots, \varepsilon$ is the energy eigenvalue shifted by $\gamma(m + |m| + 2N + 1)$ with $N=0,1, \ldots,$ and $\alpha = 2(C + |m| + 2N) + 1$.

These basis functions are obviously more complex than our previously described cylindrical functions and also have the disadvantage of being non-separable. However, these functions do have the correct behaviour as $r \to 0$ and tend asymptotically to the Landau solutions as $r \to \infty$. As expected, the results of Praddaude, 1972, for the energies of the lowest fourteen states at field strengths of $\gamma = 0.1$ and $\gamma = 1$ (i.e. $B = 2.35 \times 10^8$ and 2.35×10^9 G) are in close agreement with our results, especially for the n = 2 states, and in fact there is no more than 0.02 Ry difference at $\gamma = 0.1$ and 0.03 Ry at $\gamma = 1$, between the two sets of results. Whilst Praddaude's basis is more accurate than ours for some states, the simplicity of our basis set makes it much more attractive for applications e.g. calculating Einstein 'A' coefficients. The results for these energies are given in table 4.5.

Table 4.5 also contains results for calulations carried out by dos Santos and Brandi, 1976, who expand their wavefunctions in a basis of three dimensional harmonic oscillator functions:

$$\chi = \left(\frac{2}{r}\right)^{\frac{1}{2}} \Lambda_n^{\ell+\frac{1}{2}}(r^2)\, Y_{\ell m}(\theta,\phi) \tag{4.2}$$

where

$$\Lambda_a^b(x) = \{\Gamma(b+1) \binom{a+b}{a}\}^{-\frac{1}{2}} e^{-x/2}\, x^{b/2}\, L_a^b(x) \tag{4.3}$$

State	γ = 0.1			γ = 1.0		
	a	b	c	a	b	c
$1s_o$	-0.977	-0.7789	-0.99505	-0.654	-0.6331	-0.66233
$2s_o$	-0.193	-0.1530	-0.19617	0.680	0.7483	0.67897
$3s_o$	-0.039	-0.0397	-0.04986	0.897	1.451	0.86727
$2p_{-1}$	-0.302	-0.2723	-0.30169	0.087	0.920	0.08682
$2p_o$	-0.225	-0.2098	-0.22482	0.480	0.4813	0.47999
$3p_{-1}$	-0.052	-0.0501	-0.06236	0.755	0.8244	0.74889
$3p_o$	-0.022	-0.334	-0.03978	0.825	0.9308	0.81952
$3d_{-2}$	-0.175	-0.1726	-0.17567	0.294	0.2954	0.29389
$3d_{-1}$	-0.114	-0.1138	-0.11562	0.588	0.6024	0.58686

Table 4.5

Comparison of the energy eigenvalues calculated using the cylindrical basis (a) with those obtained by dos Santos and Brandi, 1976 (b) and Praddaude, 1972 (c). The units are Rydbergs.

These wavefunctions give a correct description of the electron in a Coulomb-free field in the plane perpendicular to the magnetic field vector, but restrict the motion parallel to the field. We would therefore expect these functions to give their most accurate description of the wavefunctions at field strengths at which the cyclotron radius is larger than the Bohr radius, i.e. when $\gamma >> 1$. As expected, at the fields $\gamma = 0.1$ and 1, the energies of the lowest fourteen states using this basis expansion, are slightly higher than ours and those of Praddaude, 1972. The agreement between Praddaude and dos Santos and Brandi, in fact, improves with increasing field strength. The agreement is good at $\gamma = 3$.

Other workers who have used this method of expanding the wavefunctions in basis sets include Simola and Virtamo, 1978, who expand their wavefunctions in a basis of pure Landau states - in this method the Coulomb potential is treated as a perturbation and so it can only be expected to be accurate when the magnetic field dominates the Coulomb field, i.e. when $\gamma >> 1$, which is beyond the range of field strengths which we are considering. Edmonds, 1973 expanded his wavefunctions in a basis of Sturmian functions. These have the advantage of forming a complete set (i.e. they also contain continuum functions) although the basis has to be truncated so that the matrices involved in the problem are of finite dimension. His results agree well with those obtained using a basis of hydrogenic states at very low fields (i.e. $B = 10^4$, 3×10^4 G), but the hydrogenic basis is to be preferred since the number of terms required in the wavefunctions (particularly in the states with large n) using the basis of Sturmian functions is large - and indeed becomes larger as the field strength increases. Therefore, it is difficult to obtain accurate energies using this basis set for high fields without using an extremely large basis.

Smith et al, 1973 used a basis set consisting of terms of the form:

$$\psi_m(r) = \sum_{i,\ell} (a_i^{(t)} r^{\ell} + b_i^{(t)} r^{\ell+1}) e^{-\beta_i^{(t)} r} Y_{\ell m}(\theta,\phi). \qquad (4.4)$$

This, like the hydrogenic basis, is spherically symmetric and so cannot, for reasons already discussed, be accurate at $B > 10^8$ G where the atom has cylindrical symmetry. The wave functions go into the exact zero field functions as $B \to 0$, and contain more terms than the hydrogenic basis - therefore we would expect the energies to be slightly lower than those obtained using the hydrogenic basis.

In conclusion, whilst a hydrogenic basis is superior at low field strengths, especially for the ground states, an expansion in functions of cylindrical symmetry is, as expected on physical grounds, to be preferred for $\gamma \geq 0.1$. Such a simple basis set has not previously been used to obtain such accurate energy eigenvalues in the range of field strengths $0.1 \leq \gamma \leq 1$.

§4.4 Transition Probabilities

Transition probabilities for field strengths in the range of interest here, and for transitions between most of the states considered have been given by Brandi et al, 1976, using the basis set of unperturbed hydrogenic functions. The results obtained by Brandi are incomplete, and in the course of confirming their values, we have obtained results for an additional four transitions ($3d_2 \to 2p_1$, $3p_1$ and $3d_{-2} \to 2p_{-1}$, $3p_{-1}$) in this model. These new results are given in table 4.6 for fields of 10^7 and 10^8 G. The results for the weak $3d_2 \to 3p_{\pm 1}$ transitions vary rapidly with increasing field strength.

Smith et al, 1973, whose basis functions have been described in the previous section, have also calculated transition probabilities for the same field strengths, and corrected their results in a later

publication (Smith et al, 1975). The two sets of results are compared by Brandi et al and agree to within 12% at 10^7 G for transitions to $2p_\mu$. However, there are larger discrepancies at this field strength for transitions to $3p_{\pm1}$, for example, the Smith et al results for $3s_o - 3p_{-1}$ is 40% lower than that given by Brandi et al. At 10^8 G the differences are much larger; the two sets of results can differ by about a factor of three, even for strong transitions. For example, for $3d_{-1} - 2p_o$, Smith et al's value is a factor of 3.44 larger than that of Brandi et al. Their results for the $3d_{\pm2} \rightarrow np_{\pm1}$ (n = 2,3) transitions are compared with our new hydrogenic basis values in tables 4.8 and 4.9, and are again as much as a factor of three different at 10^8G.

	B(G)	Present Result	Smith et al	Present Result	Smith et al
		$2p_{-1}$		$2p_1$	
$3d_2$	10^7	-	-	7.160(-1)	6.34(-1)
	10^8	-	-	2.164	7.84(-1)
$3d_{-2}$	10^7	5.961(-1)	6.74(-1)	-	-
	10^8	4.561(-1)	1.33	-	-
		$3p_{-1}$		$3p_1$	
$3d_2$	10^7	-	-	7.317(-5)	8.46(-5)
	10^8	-	-	2.010(-2)	4.41(-2)
$3d_{-2}$	10^7	9.184(-5)	7.87(-5)	-	-
	10^8	8.944(-2)	2.81(-2)	-	-

Table 4.6

Bound-bound transition probabilities for transitions from $3d_2$ and $3d_{-2}$ in 10^8 s^{-1} calculated using a hydrogenic basis and compared with those of Smith et al, 1975.

The results for the cylindrical basis calculated in the dipole length formulation are compared, in tables 4.8 and 4.9 with those obtained by Brandi et al, 1976, and the new hydrogenic basis results given in table 4.6. The results of Brandi et al have been multiplied by a factor of $(\frac{8\pi}{3})$ due to the angular integrations which have been omitted in their analysis and that of Smith et al, 1973, but ensures that the transition probabilities tend to the correct zero-field results (Bethe and Salpeter, 1977). At zero field, the cylindrical results are within 3% of the exact values, and these are given in table 4.7 for both the hydrogenic and cylindrical basis functions.

	(a)	(b)	(c)
1s - 2p	6.17	6.27	6.25
2s - 2p	3.12(-6)	8.46(-11)	0.0
1s - 3p	1.61	1.68	1.64
2s - 3p	2.30(-1)	2.31(-1)	2.20(-1)

Table 4.7

Transition probabilities in 10^8 s^{-1} for B = 0 for transitiitions involving the 2p, 3p, 1s and 2s states using (a) the cylindrical basis and (b) the hydrogenic basis. The true zero-field results given by Bethe and Salpeter, 1977 are in column (c).

	$2p_{-1}$		$2p_{o}$		$2p_{1}$	
	c	h	c	h	c	h
$1s_{o}$	6.06	6.17[1]	6.17	6.27[1]	6.27	6.37[1]
$2s_{o}$	6.94(-5)	1.80(-5)[1]	3.12(-6)	8.46(-11)[1]	1.66(-6)	1.76(-5)[1]
$3d_{-2}$	5.99(-1)	5.96(-1)[2]	-	-	-	-
$3d_{-1}$	3.30(-1)	3.33(-1)[1]	2.99(-1)	3.04(-1)[1]	-	-
$3d_{1}$	-	-	3.59(-1)	3.64(-1)[1]	3.30(-1)	3.33(-1)[1]
$3d_{2}$	-	-	-	-	7.19(-1)[1]	7.16(-1)

Table 4.8a

Transition probabilities in 10^8 s^{-1} for B = 10^7 G, for transitions involving s and d states not higher than the second state for each m, but which are included in the 14 lowest states at zero-field, and the states $2p_{\mu}$, μ = 0, ±1. Results are given using the hydrogen states basis (h) ((1) Brandi et al, 1976, (2) from calculations in chapter 2), and the cylindrical basis (c).

	$3p_{-1}$		$3p_{o}$		$3p_{1}$	
	c	h	c	h	c	h
$1s_{o}$	1.62	1.68[1]	1.61	1.68[1]	1.67	1.72[1]
$2s_{o}$	2.10(-1)	2.13(-1)[1]	2.30(-1)	2.31(-1)[1]	2.53(-1)	2.56(-1)[1]
$3d_{-2}$	8.16(-5)	9.18(-5)[2]	-	-	-	-
$3d_{-1}$	7.11(-13)	1.68(-8)[1]	3.79(-5)	4.94(-5)[1]	-	-
$3d_{1}$	-	-	4.38(-5)	3.15(-5)[1]	7.11(-13)	1.68(-8)[1]
$3d_{2}$	-	-	-	-	8.24(-5)	7.32(-5)[2]

Table 4.8b

Transition probabilities in 10^8 s^{-1} for B = 10^7 G, for transitions involving s and d states not higher than the second state for each m, but which are included in the 14 lowest states at zero-field, and the states $3p_{\mu}$, μ = 0, ±1. Results are given using the hydrogen states basis (h) ((1) Brandi et al, 1976, (2) from calculations in chapter 2), and the cylindrical basis (c).

	$2p_{-1}$		$2p_0$		$2p_1$	
	c	h	c	h	c	h
$1s_0$	5.63	5.69[1]	6.42	6.50[1]	7.94	7.93[1]
$2s_0$	2.11(-2)	1.75(-2)[1]	1.77(-4)	6.50(-5)[1]	1.20(-2)	1.47(-2)[1]
$3d_{-2}$	4.62(-1)	4.56(-1)[2]	-	-	-	-
$3d_{-1}$	4.63(-1)	4.40(-1)[1]	1.97(-1)	1.72(-1)[1]	-	-
$3d_1$	-	-	1.02	8.96(-1)[1]	4.63(-1)	4.41(-1)[1]
$3d_2$	-	-	-	-	2.25	2.16[2]

Table 4.9a

Transition probabilities in 10^8 s^{-1} for B = 10^8 G, for transitions involving s and d states not higher than the second state for each m, but which are included in the 14 lowest states at zero-field, and the states $2p_\mu$, $\mu = 0, \pm 1$. Results are given using the hydrogen states basis (h) ((1) Brandi et al, 1976, (2) from calculations in chapter 2), and the cylindrical basis (c).

	$3p_{-1}$		$3p_{o}$		$3p_{1}$	
	c	h	c	h	c	h
$1s_{o}$	2.14	1.87[1]	1.97	2.06[1]	2.83	2.44[1]
$2s_{o}$	1.92(-1)	2.04(-1)[1]	3.15(-1)	3.53(-1)[1]	8.85(-1)	9.47(-1)[1]
$3d_{-2}$	6.94(-2)	8.94(-2)[2]	-	-	-	-
$3d_{-1}$	5.10(-3)	6.28(-3)[1]	1.46(-2)	1.19(-1)[1]	-	-
$3d_{1}$	-	-	2.13(-2)	1.85(-3)[1]	5.10(-3)	6.28(-3)[1]
$3d_{2}$	-	-	-	-	1.79(-2)	2.01(-2)[2]

Table 4.9b

Transition probabilities in 10^8 s^{-1} for B = 10^8 G, for transitions involving s and d states not higher than the second state for each m, but which are included in the 14 lowest states at zero-field, and the states $3p_{\mu}$, $\mu = 0, \pm 1$. Results are given using the hydrogen states basis (h) ((1) Brandi et al, 1976, (2) from calculations in chapter 2), and the cylindrical basis (c).

	$2p_{-1}$	$2p_0$	$2p_1$	$3p_{-1}$	$3p_0$
$B = 5 \times 10^8$ G					
$1s_0$	5.82	9.47	2.57(+1)	1.03	2.50
$2s_0$	6.18(-1)	1.46(-1)	5.52(-1)	6.99(-2)	7.62(-1)
$3d_{-2}$	3.92(-1)	-	-	1.25(-1)	-
$3d_{-1}$	1.37	9.27(-2)	-	3.47(-1)	2.82(-2)
$B = 10^9$ G					
$1s_0$	5.57	1.33(+1)		7.31(-1)	3.20
$2s_0$	6.75(-1)	7.34(-1)		2.59(-2)	1.04
$3d_{-2}$	3.82(-1)	-		9.44(-2)	-
$3d_{-1}$	2.55	5.73(-2)		6.72(-1)	2.12(-2)
$B = 2.35 \times 10^9$ G ($\gamma = 1.0$)					
$1s_0$	5.51	2.34(+1)		6.38(-1)	4.14
$2s_0$	4.68(-1)	1.71		9.40(-3)	1.22
$3d_{-2}$	3.87(-1)	-		8.06(-2)	-
$3d_{-1}$	5.82	2.90(-2)		1.33	1.02(-2)

Table 4.10

Transition probabilities in 10^8 s^{-1} for $5 \times 10^8 \leq B \leq 2.35 \times 10^9$ G, for transitions involving states not higher than the second state for each parity and m but which are included in the 14 lowest states at zero field using the cylindrical basis. The $2p_1$ state is not bound for $B \geq 10^9$ G.

The present results are generally in good agreement with those of Brandi et al, 1976, at the two field strengths at which detailed comparison is possible;for strong transitions ($A_{mn} \geq 0.1$) the disagreement is less than 4%. However, there are two groups of transitions for which there is strong disagreement.

(i) The very weak transitions $2s_o \rightarrow 2p_o$ and $3d_{\pm1} \rightarrow 3p_{\pm1}$ at 10^7 G where our results are more than three orders of magnitude larger than those of Brandi et al or Smith et al.

(ii) The transitions $3d_{\pm1}$ - $3p_o$ where we agree fairly well with Smith et al (to within 30%) and both of these results are between one and two orders of magnitude different from those of Brandi et al at 10^8 G.

The perturbation theory calculations of Ruder et al, 1981, give results which are in very good agreement with those of the hydrogenic basis for all transitions considered at B = 10^7 G.

There have been no previous published calculations of transition probabilities in the range $10^8 < B < 2.35 \times 10^9$ G, so in table 4.10 we give results at three fields spanning this range. We expect these results to be fairly accurate, since they do not involve the wavefunctions of any states in which our eigenvalues are significantly different from those of Praddaude.

It has been found that the discrepancies occurring in the transition probabilities (and wavelengths) throughout, can be attributed mainly to inaccuracies in the calculation of the energy eigenvalues. The formula for the transition probability in the dipole length formulation (equation (2.85)) contains the factor $\omega_{m'm}^3$ - and so any slight error in the difference between the two energies in the transition will be cubed, and so cause larger differences to occur in the transition probability. This is illustrated in table 4.11 where a few cases in which there are large differences between transition probabilities calculated in the cylindrical and hydrogenic bases, are analysed.

	$E_{m'}$ (Ry)	E_m (Ry)	$\lvert\omega_{m'm}\rvert^3$	$R_{m'm}^2$	$A_{m'm}$ ($10^8 s^{-1}$)
$B=10^7$G					
$2s_o \rightarrow 2p_o$ h	-0.249873	-0.249946	3.890(-13)	1.02	8.46(-11)
$2s_o \rightarrow 2p_o$ c	-0.247532	-0.249870	1.293(-8)	1.13	3.12(-6)
$3p_{-1} \rightarrow 3d_{-1}$ h	-0.114718	-0.115041	3.370(-11)	2.33	1.68(-8)
$3p_{-1} \rightarrow 3d_{-1}$ c	-0.114637	-0.114648	1.331(-15)	2.49	7.11(-13)
$B=10^8$G					
$2s_o \rightarrow 2p_o$ h	-0.238129	-0.244761	2.917(-7)	1.04	6.50(-5)
$2s_o \rightarrow 2p_o$ c	-0.235771	-0.244751	7.242(-7)	1.14	1.77(-4)
$3p_{-1} \rightarrow 3d_{-1}$ h	-0.103987	-0.126589	1.155(-5)	2.54	6.28(-3)
$3p_{-1} \rightarrow 3d_{-1}$ c	-0.107808	-0.128480	8.834(-6)	2.70	5.10(-3)

Table 4.11

Table to illustrate the source of the discrepancies in the transition probabilities ($A_{m'm}$) which occur between using the hydrogenic basis (h) and the cylindrical basis (c). $R_{m'm}$ is the dipole length matrix element.

Table 4.11 illustrates the necessity of accurate eigenvalue calculations, particularly in the $\Delta n = 0$ transitions, in order to obtain correct transition probabilities and wavelengths.

Transition probabilities were also calculated in the dipole velocity approximation for the cylindrical basis wavefunctions (see equation (3.82)), for the transitions where $\Delta m = 0$. These results are compared with those calculated in the length approximation in table 4.12 for field strengths 10^8, 5×10^8 and 10^9 G. The agreement

is very close and confirms the accuracy of the cylindrical wave-functions obtained.

The results for the transition probabilities in the length formulation for two allowed bound-bound transitions at 10^9 G are plotted against field strength in figures 4.10 and 4.11. It has already been shown (see table 4.11) that the variation of transition probability with increasing field strength depends on both the variation of the dipole matrix element and the energy difference, so it is not always a monotonic function. For example, figure 4.11 shows that the $1s_o$-$2p_o$ transition is monotonic, whilst figure 4.10 shows that the $1s_o$-$2p_{-1}$ transition has a minimum. Furthermore, $2p_{-1}$ is only just bound in the hydrogen state basis at 10^9 G (E_h = 0.155 Ry) but is highly bound in the cylindrical basis (E_c = -0.232 Ry) so although the dipole matrix elements are not very different, the transition probabilities differ by about a factor of five. Since E_c is lower, i.e. better, it is likely that the lower value of $A_{m'm}$ is more nearly correct.

In general, for $\Delta n = 0$ transitions $A_{m'm}$ differs little from its zero-field value until $B > 5 \times 10^8$ G when it slowly increases. Transitions between levels which are degenerate in energy at zero field may become relatively strong at fields above 10^9 G, for example, $2s_o$-$2p_o$ has a transition probability increasing by four orders of magnitude between 10^8 and 10^9 G.

	$1s_o$	$2s_o$	$3d_{-1}$	$3d_1$
$B=10^8$G				
$2p_{-1}$			4.63(-1) (4.63(-1))	
$2p_o$	6.42 (6.44	1.73(-4) (1.77(-4))		
$2p_1$				4.63(-1) (4.63(-1)
$3p_{-1}$			5.08(-3) (5.10(-3))	
$3p_o$	1.99 (2.00)	3.14(-1) (3.15(-1))		
$3p_1$				5.08(-3) (5.10(-3))
$B=5\times10^8$G				
$2p_{-1}$			1.37 (1.37)	
$2p_o$	9.45 (9.47)	1.46(-1) (1.46(-1))		
$3p_{-1}$			3.44(-1) (3.47(-1))	
$3p_o$	2.44 (2.50)	7.62(-1) (7.62(-1))		
$B=10^9$G				
$2p_{-1}$			2.55 (2.55)	
$2p_o$	1.32(+1) (1.33(+1))	7.31(-1) (7.34(-1))		
$3p_{-1}$			6.67(-1) (6.72(-1))	
$3p_o$	2.91 (3.20)	1.05 (1.04)		

Table 4.12

Length and velocity values of the transition probability in 10^8 s^{-1} for $\Delta m = 0$ transitions. The length values are shown in brackets.

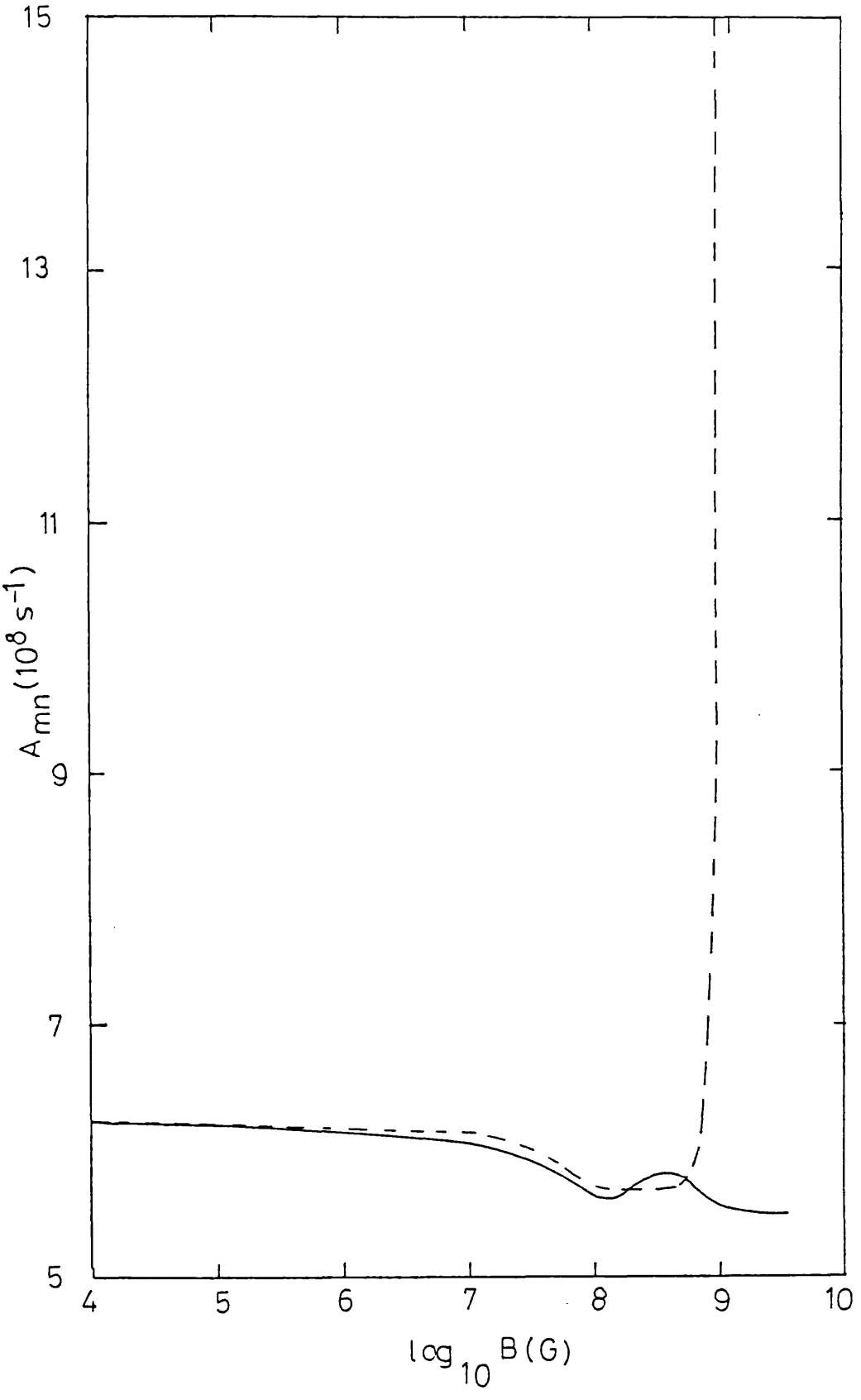

Fig 4.10

Comparison of the $2p_{-1}$-$1s_o$ transition probabilities (in 10^8 s^{-1}) in the dipole length approximation with increasing magnetic field strength B (G) using (i) a basis of hydrogen states (broken line) and (ii) the cylindrical basis (solid line).

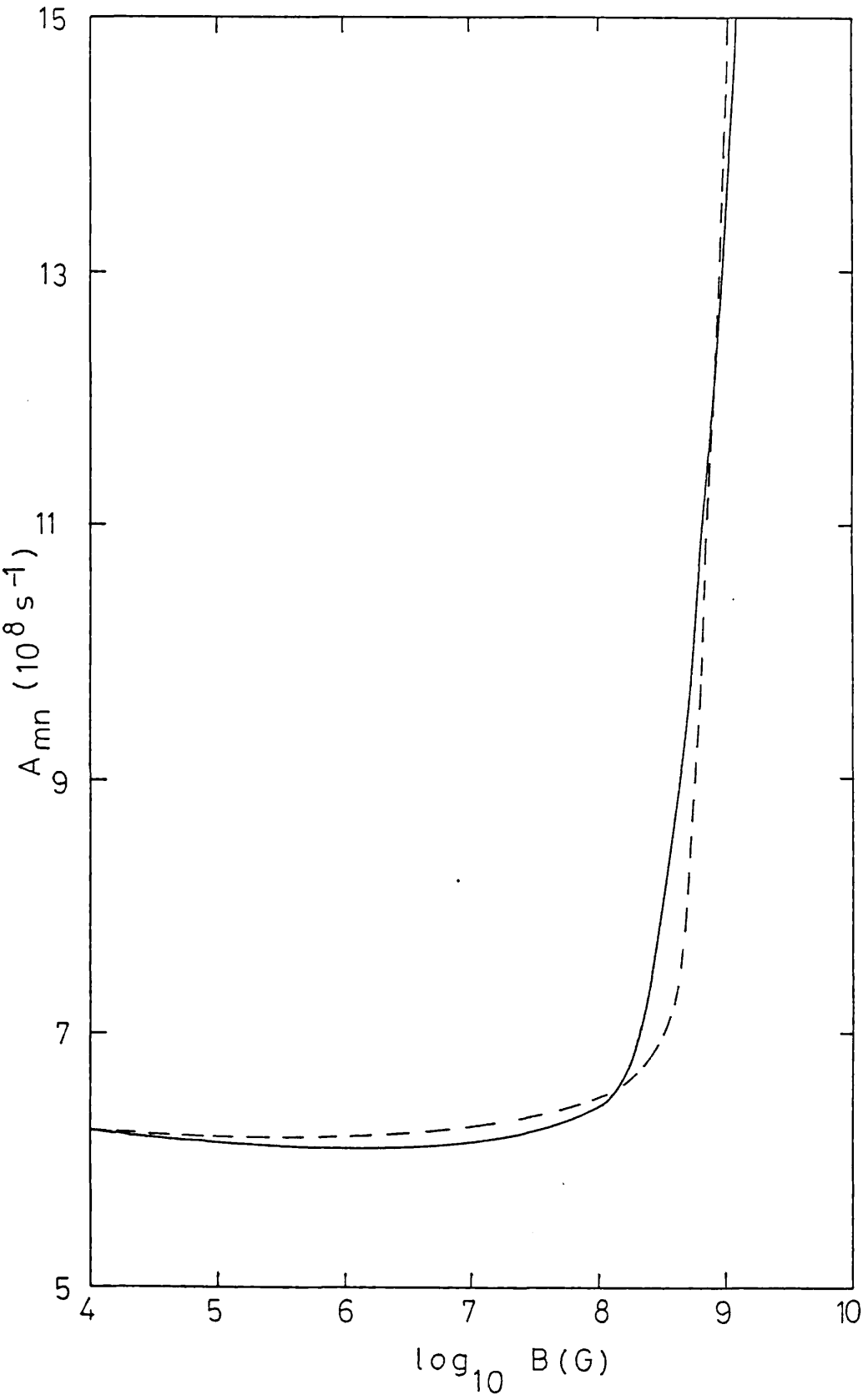

Fig 4.11

Comparison of the $2p_o - 1s_o$ transition probabilities (in 10^8 s^{-1}) in the dipole length approximation with increasing magnetic field strength B (G) using (i) a basis of hydrogen states (broken line) and (ii) the cylindrical basis (solid line).

§4.5 Wavelengths and Oscillator Strengths

Wavelengths are calculated in both the hydrogenic and cylindrical basis sets according to equation (2.111), and a few results are given in table 4.13 for the fields considered here. Table 4.13 emphasizes the importance of accurate eigenvalue calculations in order to determine the correct transition from an observed wavelength. As in the calculation of the $A_{m'm}$, large discrepancies occur in the weak $\Delta n = 0$ transitions where there are also large discrepancies in the values of $E_{m'm}$.

	B(G)	$1s_o$		$2s_o$	
		c	h	c	h
$2p_{-1}$	10^7	1252	1222	138000	213300
	10^8	1303	1271	19590	20660
	5×10^8	1371	1250	4206	4171
	10^9	1379	851.5	2514	-
$2p_o$	10^7	1245	1215	388300	$1.260\ 10^7$
	10^8	1236	1208	101500	137400
	5×10^8	1137	1088	11410	8301
	10^9	1031	840.4	6563	-
$2p_1$	10^7	1238	1208	478600	215200
	10^8	1161	1136	23630	22240
	5×10^8	835.8	789.3	4366	4404
	10^9	-	-	-	-

Table 4.13

Wavelengths in Å calculated in the hydrogenic (h) and cylindrical (c) bases, for transitions from $1s_o$ and $2s_o$ to $2p_{o,\mp1}$ for fields of 10^7, 10^8, 5×10^8 and 10^9 G, accurate to 4 figures.

Oscillator strengths are also easy to calculate from equation (2.113). Here, the results for the oscillator strengths for a few allowed transitions, in the cylindrical and hydrogenic approximations are compared, together with results calculated by Wunner et al, 1981 at B = 10^7 and 10^8 G. Wunner et al, use a polynomial approximation for the dipole matrix element (discussed in §1.2) and table 4.14 demonstrates that their results are in excellent agreement with the hydrogenic basis results. As expected, there are discrepancies between the cylindrical and the two other sets of results at these fields.

	B(G)	$1s_o$			$2s_o$		
		c	h	W	c	h	W
$2p_{-1}$	10^7	0.428	0.414	0.414	5.94(-2)	3.84(-2)	3.86(-2)
	10^8	0.429	0.413	0.392	3.65(-1)	3.51(-1)	3.99(-1)
$2p_o$	10^7	0.430	0.416	0.416	2.11(-2)	6.39(-4)	6.52(-4)
	10^8	0.441	0.427	0.416	8.21(-2)	6.07(-2)	6.52(-2)
$3p_o$	10^7	7.93(-2)	7.95(-2)	7.91(-2)	0.458	0.437	0.425
	10^8	9.22(-2)	8.20(-2)	7.91(-2)	0.542	0.488	0.425

Table 4.14

Oscillator strengths for transitions from $1s_o$ and $2s_o$ to $2p_{o,-1}$ and $3p_o$ at B = 10^7 and 10^8 G in the cylindrical (c) and hydrogenic (h) approximations. Also included are the results of Wunner et al, 1981 (W).

CHAPTER 5

PHOTOIONIZATION CROSS-SECTIONS WHERE THE CONTINUUM CONTAINS PURE LANDAU LEVELS

§5.1 Introduction

This chapter is concerned with the calculation of photoionization cross-sections of atomic hydrogen in a magnetic field, the initial state having cylindrical symmetry and being of the form given by equation (3.2). Throughout this thesis we consider only the dipole approximation. The final state will be that of a free electron in a magnetic field, ie the motion will be confined to the discrete Landau levels in the plane perpendicular to the magnetic field and unrestricted in the field direction (see §1.2). In this chapter we show that, due to the structure of the continuum, the total photoionization cross-sections consist of a series of infinite peaks occurring at the Landau energies (ie $(2\ell + 1)\,\gamma$ Ry where $\ell = 0,1\ldots$). These cross-sections, it will be seen, are very different from the zero field cross-sections in the absence of broadening. However, if broadening, due to the motion of the residual ion, was to be considered (which it is not here), then in the limit as $B \to 0$, it will be seen from presented results, that the cross-section does reduce to the same form as that of the zero field cross-section. It is also shown that the appropriate form of the Wigner threshold law (Wigner, 1948) is satisfied as $B \to 0$.

Although, in reality, the Coulomb attraction of the nucleus modifies the continuum structure, we do not consider the effect in this chapter. Inclusion of a Coulomb force is discussed in chapter 6. It is expected that the pure Landau continuum treatment will be satisfactory when the Coulomb energy $\left|\frac{e^2}{r}\right|$ is small compared with γ, and this is always satisfactory for sufficiently high lying levels, and for all levels when $\gamma \gg 1$.

The wavefunctions of the discrete Landau states can be expressed analytically in cylindrical polar coordinates (Dingle, 1952), and as these functions are separable, then the photoionization cross-sections can also be calculated analytically. A model calculation has previously been performed by Wallis and Bowlden (1956), in which the initial ground state wavefunction takes the simple form

$$\psi_{1s_o} = Ce^{-\delta r^2} .$$

It has already been shown, however, in chapter 3, that a more complete basis set gives more accurate results for the energies and wavefunctions of the initial state, and we would therefore expect the photoionization cross-sections to also be more accurate using the initial state wavefunction given by equation (3.2).

§5.2 Theory

The formula for the photoionization cross-section from an initial state i to a final state f, at zero field, takes the form

$$a_\nu = \frac{4\pi\alpha}{3} \; h\nu \left| \langle \psi_i | \sum_{\mu=-1}^{1} r_\mu | \psi_f \rangle \right|^2 a_o^2 \qquad (5.1)$$

where α is the fine structure constant and $h\nu$ is the photon energy in Rydbergs. In (5.1), we have summed over polarizations and integrated over angles, and this agrees with the expression given by Burke (1976). It is more convenient to write the cross-section in the form

$$a_\nu = 8.56 \times 10^{-19} \; h\nu |R_{if}|^2 \; cm^2 \qquad (5.2)$$

where R_{if} is the matrix element occurring in (5.1).

The structure of this Landau continuum is such that discrete levels occur in the x - y plane, making it necessary to sum over all possible final states, when a magnetic field is switched on. It is then possible for the electron to go into any Landau level which is energetically accessible, up to a maximum at $\ell = \ell_{max}$, say, with excess energy being released in the z- direction, such that energy is conserved overall, ie

$$h\nu = E_I + E_\ell + k_z^2 \,. \qquad (5.3)$$

E_I is the ionization energy of the initial state, E_ℓ the energy of the Landau level, k_z^2 the energy in the z- direction and $h\nu$ the energy of the incident photon.

Now, as we are now summing over final states, it is necessary to multiply the total cross-section by the density per unit volume of the final states, $\rho(E_z)$, where E_z is the 'free energy' released in the z- direction (Powell + Crasemann, 1961, Ch.11). The number of states with energy between E_z and $E_z + dE_z$ is given by $\rho(E_z)\, dE_z$. As we are dealing with a 1-dimensional continuum in the z- direction, the number of such states is the number of points n_z contained in the length element dn_z, where

$$k_z \frac{L_z}{2\pi} = n_z, \qquad (5.4)$$

and L_z is a quantisation length in the z- direction, tending to infinity in the limit. Then we have

$$\rho(E_z)\, dE_z = dn_z = \frac{L_z}{2\pi}\, dk_z \,. \qquad (5.5)$$

We know that $E_z = k_z^2$ and, therefore, $dE_z = 2k_z dk_z$, and so the density of states $\rho(E_z)$ can be written

$$\rho(E_z) = \frac{1}{2k_z}\, \frac{L_z}{2\pi} \,. \qquad (5.6)$$

The expression for the total photoionization cross-section now becomes

$$a_\nu = 8.56 \times 10^{-19}\, h\nu \sum_{\ell=0}^{\ell_{max}} |R_{if}|^2\, \frac{L_z}{4\pi k_z} \qquad (5.7)$$

where the final state wavefunction is dependent on ℓ, and a sum over magnetic sub-levels is implied. The perturbation of the bound states by the magnetic field is fully accounted for, if the wavefunction of the initial state is taken to have the cylindrical form discussed in chapter 3, ie

$$\psi_j^{(m,\pi)} = \sum_{\alpha,\beta,\delta} C_{\alpha\beta\delta}^{(j)}\, \chi_{\alpha\beta\delta}^{(m,\pi)}(\underline{r}) \qquad (5.8)$$

where

$$\chi^{(m,\pi)}_{\alpha\beta\delta}(\underline{r}) = z^{\alpha}\,\rho^{\beta}\,e^{-\delta r^2}\,e^{im\phi} \quad . \qquad (5.9)$$

In chapter 3 it was discovered that, in order to obtain convergence to 4 figures on the energy eigenvalues of 14 low lying states, it was necessary to use a large basis, containing up to 128 terms. However, as we are here only considering photoionization from the ground and $2p_o$ states, and to avoid computational problems occurring in the calculation of $|R_{if}|^2$ through the multiplication of very large numbers by very small numbers, the size of the basis can be reduced such that only those basis elements with large coefficients remain. The Hamiltonian has to be re-diagonalized in this new basis, and this reduction has no effect on the calculated energies of the lowest lying level of each parity. Details of the new basis are given in table 5.1

B(G)	α max	β max	δ's included in basis
10^7	7	7	δ_1, δ_2
10^8	7	7	δ_1, δ_2, δ_3
5×10^8	7	7	δ_1, δ_2, δ_3
10^9	7	7	δ_2, δ_3

Table 5.1

Terms included in the wavefunctions of the lowest even and odd parity states. All possible integer α and β up to α max and β max, respectively are included and $\delta_1 = 0.283$, $\delta_2 = 0.0453$, $\delta_3 = \gamma/2$. (Reasons for the choice of values for δ are given by §3.4)

The wavefunctions of the final states, ie those corresponding to the Landau levels, are given by the solutions of the Schrodinger equation for a free electron in a magnetic field, ie

$$\frac{1}{\rho}\frac{\partial}{\partial\rho}\left(\rho\frac{\partial\psi_\ell}{\partial\rho}\right) + \left(E'_\ell - \frac{m_f^2}{\rho^2} - \frac{\gamma^2\rho^2}{4}\right)\psi_\ell = 0 \qquad (5.10)$$

where $E'_\ell = E_\ell - m_f\,\gamma$ (Ry) and m_f is the magnetic quantum number of this free

state. This equation has been solved by Dingle (1952) and the final solutions are shown to be of the form

$$\psi^{(\ell)}_{k_z,m_f}(\underline{r}) = \rho^{-1}\, g^{(\ell)}_{m_f}(\rho)\, e^{ik_z z}\, e^{im_f\phi} \tag{5.11}$$

where

$$g^{(\ell)}_{m_f}(\rho) = \sigma^{\frac{1}{2}(|m_f|+1)}\, e^{-\sigma/2}\, (-1)^{m_f} \frac{|m_f|!\,\ell!}{((\ell+|m_f|)!)^2}\, L^{|m_f|}_{\ell+|m_f|}(\sigma)\,. \tag{5.12}$$

$L^b_a(x)$ is the associated Laguerre polynomial defined by

$$L^b_a(x) = (-1)^b \frac{a!}{(a-b)!}\, e^x\, x^{-b}\, \frac{d^{a-b}}{dx^{a-b}}\, (e^{-x}x^a) \tag{5.13}$$

and $\sigma = \gamma\rho^2/2$. Now in order to find the correct normalized solutions, we must have

$$\int \psi^{(\ell)}_{k_z,m_f}(\underline{r})^*\, \psi^{(\ell)}_{k_z',m_f}(\underline{r})\, \rho\, d\rho d\phi dz = \delta_{k_z,k_z'} \tag{5.14}$$

where the particle is confined to a large length L_z in the z direction (Schiff, 1968, p.54 and Kelly, 1963). Now

$$\int \psi^{(\ell)}_{k_z,m_f}(\underline{r})^*\, \psi^{(\ell)}_{k_z',m_f}(\underline{r})\, \rho\, d\rho d\phi dz = \int_0^\infty \rho^{-1}(g^{(\ell)}_{m_f}(\rho))^2\, d\rho \times \int_0^{2\pi} d\phi \int_{-\frac{1}{2}L_z}^{\frac{1}{2}L_z} e^{iz(k_z'-k_z)}\, dz\,. \tag{5.15}$$

The integral over ϕ is obviously 2π, and the integral over z is $L_z\delta_{k_z',k_z}$. The radial normalization has been carried out by Wallis and Bowlden (1956), and the complete normalized wavefunction of the free state may now be written as

$$\psi^{(\ell)}_{k_z,m_f}(\underline{r}) = \frac{1}{(2\pi L_z)^{\frac{1}{2}}} \left(\frac{\gamma\,\ell!}{((\ell+|m_f|)!)^3}\right)^{\frac{1}{2}} \sigma^{|m_f|/2} e^{-\sigma/2} \times L^{|m_f|}_{\ell+|m_f|}(\sigma)\,. \tag{5.16}$$

The energy eigenvalues corresponding to these wavefunctions are also calculated by Dingle (1956) and are given by

$$E_\ell = \gamma(2\ell + m_f + |m_f| + 1) + k_z^2 \quad \text{Ry.} \tag{5.17}$$

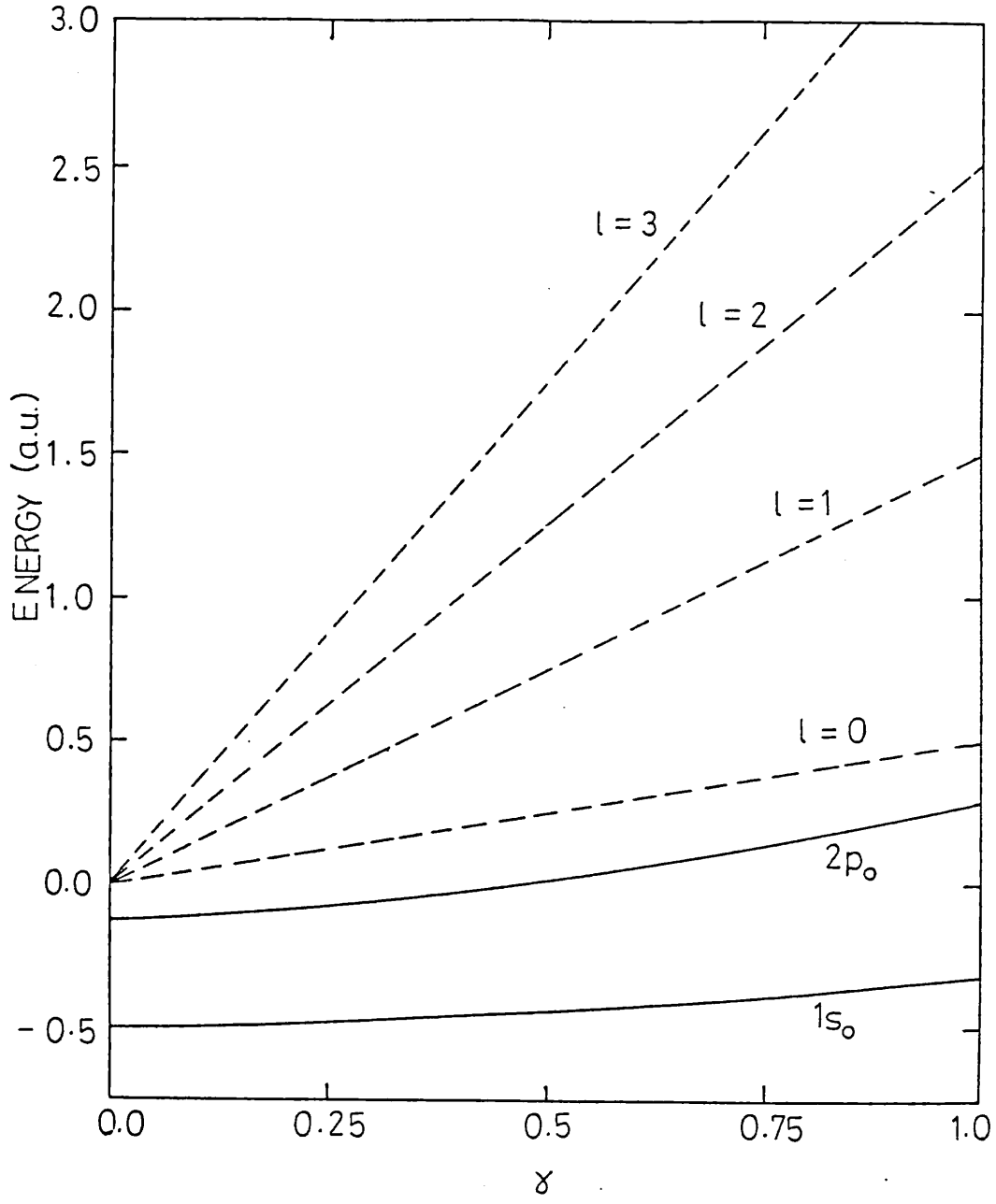

Fig 5.1

The behaviour of the lowest odd ("$2p_o$") and even ("$1s_o$") bound levels and the lowest few discrete levels of the continuum are shown (schematically) as a function of the magnetic field strength γ , ignoring Coulomb effects on the continuum and spin splittings.

The variation of the Landau energies and the energies of the $1s_o$ and $2p_o$ bound states with magnetic field strength is shown in fig. 5.1.

§5.3 Evaluation of $|R_{if}|^2$

An expression for the total photoionization cross-section is given by equation (5.7) and in this section we evaluate the $|R_{if}|^2$. It is first necessary to calculate the matrix element $\langle \chi_i | \sum_\mu r_\mu | \psi^{(\ell)}_{k_z, m_f} \rangle$ where χ_i is given by equation (3.5) and $\psi^{(\ell)}_{k_z, m_f}$ by equation (5.11). There are three cases:

(i) $\mu = -1$

Here we have

$$\langle \chi_i | r_{-1} | \psi^{(\ell)}_{k_z, m_f} \rangle = C_0 \frac{1}{\sqrt{2}} \int \rho^\beta z^\alpha e^{-\delta r^2} e^{im_i\phi} \rho e^{-i\phi} \times e^{-\sigma/2} \sigma^{|m_f|/2} L^{|m_f|}_{\ell+|m_f|}(\sigma) e^{im_f\phi} e^{ik_z z} \rho \, d\rho \, d\phi \, dz \tag{5.18}$$

where

$$C_0^2 = \frac{\gamma \ell!}{2\pi L_z ((\ell+|m_f|)!)^3} \tag{5.19}$$

(a) Integral over ϕ

This gives

$$\int_0^{2\pi} e^{i\phi(m_f - m_i - 1)} \, d\phi = 2\pi\delta(m_f - m_i - 1). \tag{5.20}$$

Therefore, in order that the matrix elements of r_{-1} be non-zero, we must have $m_f = m_i + 1$.

(b) Integral over z

The z integral may be expressed as

$$Z(\alpha, \delta, k_z) = \int_{-\infty}^{\infty} z^\alpha e^{-\delta z^2} e^{ik_z z} \, dz \, . \tag{5.21}$$

This integral is complex, the real part of which is zero if α is odd and the imaginary part is zero if α is even, as the integrand is an even function in both cases. The integral may be written in terms of Hermite

polynomials for odd or even α :

$$Z(\alpha,\delta,k_z) = \frac{(-1)^{\alpha/2}}{2^{\alpha/2}\,\delta^{\frac{1}{2}(\alpha+1)}}\; e^{-k_z^2/4\delta}\; He_\alpha\left(\frac{k_z}{(2\delta)^{\frac{1}{2}}}\right) \tag{5.22}$$

(Bateman Manuscript Project, 1954). $He_n(x)$ is the Hermite polynomial defined by

$$He_n(x) = (-1)^n\, e^{\frac{1}{2}x^2}\, \frac{d^n}{dx^n}\; (e^{-\frac{1}{2}x^2}) \,. \tag{5.23}$$

So equation (5.22) reduces to

$$Z(\alpha,\delta,k_z) = \frac{(-1)^{3\alpha/2}\sqrt{\pi}}{2^{\alpha/2}\,\delta^{\frac{1}{2}(\alpha+1)}}\; \frac{d^\alpha}{dx^\alpha}(e^{-x^2/2}) \tag{5.24}$$

with

$$x = \frac{k_z}{(2\delta)^{\frac{1}{2}}} \tag{5.25}$$

(c) Integral over ρ

The integral over ρ may be written

$$\mathcal{R}\,(\beta,m_f,\delta,\gamma) = \int_0^\infty \rho^{\beta+2}\; e^{-\delta\rho^2}\; \sigma^{m/2}\; e^{-\sigma/2}\; L_{\ell+m}^{m}(\sigma)\; d\rho \tag{5.26}$$

with $m = |m_f|$. Writing this integral in terms of σ , making use of the fact that $\rho\, d\rho = \frac{d\sigma}{\gamma}$, we have

$$\mathcal{R}\,(\beta,m_f,\delta,\gamma) = \frac{2^{\frac{1}{2}(\beta+1)}}{\gamma^{\frac{1}{2}(\beta+3)}} \int_0^\infty \sigma^{\frac{1}{2}(\beta+1+m)}\; e^{-\Delta\sigma}\; L_{\ell+m}^{m}(\sigma)\; d\sigma \tag{5.27}$$

where

$$\Delta = \frac{2}{\gamma}\,(\delta + \frac{\gamma}{4}). \tag{5.28}$$

Using the series expansion for the Laguerre polynomial given by equation (5.13), we obtain

$$\mathcal{R}\,(\beta,m_f,\delta,\gamma) = A \sum_{p=0}^{\ell} \frac{(-1)^{\ell-p}}{(\ell-p)!} \binom{\ell+m}{p} \int_0^\infty \sigma^{a-p}\; e^{-\Delta\sigma}\; d\sigma \tag{5.29}$$

where $$a = \tfrac{1}{2}(\beta + 1 + m + \ell) \tag{5.30}$$

and $$A = \frac{2^{\frac{1}{2}(\rho+1)}}{\gamma^{\frac{1}{2}(\beta+3)}} (-1)^m \Gamma(\ell+m+1) . \tag{5.31}$$

Therefore, the integral over ρ may be expressed as

$$\mathcal{R}(\beta, m_f, \delta, \gamma) = A \sum_{p=0}^{\ell} \frac{(-1)^{\ell-p}}{(\ell-p)!} \binom{\ell+m}{p} \frac{\Gamma(a-p+1)}{\Delta^{a-p+1}} . \tag{5.32}$$

(ii) $\mu = 0$

In this case the matrix element may be written

$$\langle \chi_i | r_o | \psi^{(\ell)}_{k_z, m_f} \rangle = C_0 \int \rho^{\beta} z^{\alpha} e^{-\delta r^2} e^{-im_i\phi} z \sigma^{m/2} L^m_{\ell+m}(\sigma) \times e^{-\sigma/2} e^{im_f\phi} e^{ik_z z} \rho \, d\rho \, d\phi \, dz . \tag{5.33}$$

(a) Integral over ϕ

This gives

$$\int_0^{2\pi} e^{i\phi(m_f-m_i)} \, d\phi = 2\pi \delta(m_f-m_i). \tag{5.34}$$

Therefore, in order that the matrix elements of r_o be non-zero, we must have $m_f = m_i$.

(b) Integral over z

Using the same notation as in (i) part (b), the z integral may be written

$$Z(\alpha+1, \delta, k_z) = \int_{-\infty}^{\infty} z^{\alpha+1} e^{-\delta z^2} e^{ik_z z} \, dz . \tag{5.35}$$

Again, this integral is complex, the real part being zero if $(\alpha + 1)$ is odd and the imaginary part being zero if $(\alpha + 1)$ is even. An expression for Z is given by equation (5.22).

(c) Integral over ρ

Using the same notation as in (i) part (c), the integral over ρ may be written

$$\mathcal{R}(\beta-1, m_f, \delta, \gamma) = \int_0^{\infty} \rho^{\beta+1} e^{-\delta\rho^2} \sigma^{m/2} e^{-\sigma/2} L^m_{\ell+m}(\sigma) \, d\rho \tag{5.36}$$

and $\mathcal{R}$ is given by equation (5.26).

(iii) $\mu = 1$

The matrix element, in this case, may be written

$$\langle \chi_i | r_1 | \psi^{(\ell)}_{k_z, m_f} \rangle = \frac{C_0}{\sqrt{2}} \int \rho^{\beta} z^{\alpha} e^{-\delta r^2} e^{-im_i\phi} \rho e^{i\phi} \sigma^{m/2} e^{-\sigma/2} L^{m}_{\ell+m}(\sigma) e^{im_f\phi} e^{ik_z z} \rho \, d\rho dz d\phi . \tag{5.37}$$

It is clearly seen, that the integrals over ρ and z for this case are exactly the same as for case (i), ie $\mu = -1$. The integral over ϕ gives

$$\int_0^{2\pi} e^{i\phi(m_f+1-m_i)} \, d\phi = 2\pi \delta(m_f - m_i + 1) . \tag{5.38}$$

Therefore, for the matrix elements of r_1 to be non-zero, we must have $m_f = m_i - 1$.

The total expression for $|R_{if}|^2$ can now be written

$$|R_{if}|^2 = 4\pi^2 C_0^2 \left| \sum_{\mu=-1}^{1} \frac{1}{2^{|\mu|}} \left\{ \sum_{\alpha\beta\delta} C_{\alpha\beta\delta} \mathcal{R}(\beta + |\mu| - 1, m_f, \delta, \gamma) \times Z(\alpha - |\mu| + 1, \delta, k_z) \right\} \right|^2 \tag{5.39}$$

It has now been shown that all the integrals occurring in a_ν, when the continuum contains pure Landau levels only, can be evaluated analytically, and computation of these cross-sections is carried out by program QMAT, details of which are given in appendix (I).

§5.4 Threshold Behaviour

The total photoionization cross section from an initial bound state (π, m) will include contributions from the transitions to final states $(\bar{\pi}, m)$, $(\pi, m-1)$ and $(\pi, m+1)$ (see section §3.6), corresponding to $\mu = 0, 1$ and -1 respectively, where π and $\bar{\pi}$ are opposite parities. We first consider the dependence of a_ν on k_z from the $\mu = 0$ contribution. It has already been shown that

$$a_\nu^{(\bar{\pi}, m)} = \sum_{\ell=0}^{\ell_{max}} D_1 \left[Z(\alpha+1, \delta, k_z) \right]^2 \rho(E_z) \tag{5.40}$$

where D_1 is independent of k_z and the dependence of the density of states on k_z is $\frac{1}{k_z}$. An expression for $Z(\alpha + 1, \delta, k_z)$ is given by equation (5.24).

Expanding the Hermite polynomials in these expressions (see table (III.1) of appendix (III)), we obtain

$$Z(\alpha+1, \delta, k_z) = C_1 (b_1 k_z + b_3 k_z^3 + \ldots . b_{\alpha+1} k_z^{\alpha+1}) e^{-k_z^2/4\delta} \quad (5.41)$$

if α is even, ie if the initial state has even parity, and

$$Z(\alpha+1, \delta, k_z) = C_1 (b_o + b_2 k_z^2 + \ldots . + b_{\alpha+1} k_z^{\alpha+1}) e^{-k_z^2/4\delta} \quad (5.42)$$

if α is odd, ie if the initial state has odd parity, and C_1 is also independent of k_z. As threshold is reached, k_z becomes increasingly small, and in this region only the term in the smallest power of k_z occurring in a_ν is significant, all higher terms can be neglected. We therefore have, near threshold

$$a_\nu^{(\bar{\pi}, m)} \sim \sum_{\ell=0}^{\ell_{max}} A_1 k_z \quad (5.43)$$

if α is even and

$$a_\nu^{(\bar{\pi}, m)} \sim \sum_{\ell=0}^{\ell_{max}} \frac{B_1}{k_z} \quad (5.44)$$

if α is odd.

Now, considering the dependence on k_z from the contributions arising from the transitions to $(\pi, m \pm 1)$ we have

$$a_\nu^{(\pi, m\pm1)} = \sum_{\ell=0}^{\ell_{max}} D_2 [Z(\alpha, \delta, k_z)]^2 \rho(E_z) \quad (5.45)$$

where D_2 is independent of k_z. Again, expanding the expressions for $Z(\alpha, \delta, k_z)$ when α is even and odd in terms of k_z, we obtain

$$Z(\alpha, \delta, k_z) = C_2(a_o + a_2 k_z^2 + \ldots . a_\alpha k_z^\alpha) e^{-k_z^2/4\delta} \quad (5.46)$$

if α is even, and

$$Z(\alpha, \delta, k_z) = C_2(a_1 k_z + a_3 k_z^3 + \ldots . a_\alpha k_z^\alpha) e^{-k_z^2/4\delta} \quad (5.47)$$

if α is odd. Taking only the terms in the lowest powers of z in the expressions for $Z(\alpha, \delta, k_z)$, we have

$$a_\nu^{(\pi, m\pm1)} \sim \sum_{\ell=0}^{\ell_{max}} \frac{A_2}{k_z} \quad (5.48)$$

if α is even and

$$a_{\nu}^{(\pi, m\pm1)} \sim \sum_{\ell=0}^{\ell_{max}} B_2 k_z \qquad (5.49)$$

if α is odd.

As $B \to 0$, the fact that ℓ_{max} becomes very large, and that the distance between the Landau levels becomes very small, must be taken into consideration. As $B \to 0$ the zero field limit is reached where the Landau levels are infinitely close together, forming a continuum, and the 1st Landau level tending to zero energy. This enables the sum over Landau levels to be replaced by an integral over all energies up to $E_{\ell_{max}}$ in the limit as $B \to 0$. For example, the contribution to the total photoionization cross section from the transition to the $(\bar{\pi}, m)$ state from an odd parity bound state, becomes

$$a_{\nu}^{(\bar{\pi}, m)} \sim B_1 \int_{E_o}^{E_{\ell_{max}}} \frac{1}{k_z} dE_z = 2B_1 \int_0^{k_z} dk_z = 2B_1 k_z \qquad (5.50)$$

where E_i is the energy of the Landau level corresponding to $\ell = i$. In this case, the dependence of $a_{\nu}^{(\bar{\pi}, m)}$ on k_z is k_z. The dependence of Z and the photoionization cross section contributions for both the limiting case and a finite magnetic field, on k_z, for all allowed transitions are summarized in Table (5.2). The dependence of the final state on z is $e^{ik_z z}$ (= $\cos k_z z + i \sin k_z z$). If the final state has odd parity, then only the term $\cos k_z z$ contributes towards the cross section and if the final state has even parity, then only the $i \sin k_z z$ term contributes.

Initial State		Final State		Dependence of Z on k_z	Dependence of a_ν on k_z for finite B	Dependence of a_ν on k_z for $B \to 0$
Parity	m_i	Parity	m_f			
even	m	odd	m	k_z	k_z	k_z^3
even	m	even	$m \pm 1$	1	k_z^{-1}	k_z
odd	m	odd	$m \pm 1$	k_z	k_z	k_z^3
odd	m	even	m	1	k_z^{-1}	k_z

Table (5.2)

The dependence of Z and the contributions to the total photoionization cross-section on k_z at threshold for all allowed transitions.

At zero magnetic field, the Wigner Law (Wigner, 1948) is satisfied,

$$a_\nu \sim k^{2\ell_o+1}$$

where ℓ_o is the angular momentum quantum number of the free state. For a transition from an odd parity bound state, the total final state must be a sum of s,d..... ℓ_o^{max} states, where ℓ_o^{max} is the highest allowed value for ℓ_o, and so

$$a_\nu \sim a_1 k + a_2 k^5 + \ldots\ldots$$

At threshold, the term in k is dominant. As there is always a contribution to the total cross-section from an s-wave, the dependence of a_ν on k at threshold must be k. For a transition from an even parity bound state, by a similar argument there must always be a contribution from a p-wave and so the dependence of a_ν on k at threshold must be k^3.

Considering now, the case where the magnetic field is switched on, it is observed that the only dependence of the cross-section on the magnetic field strength occurs in the contribution to the matrix element from the integral over ρ, the formula for which is given by equation (5.32). This dependence near threshold, ie considering only the contribution from

the first Landau level in which $\ell = 0$, is of the form $e^{-\gamma\rho^2/4}\gamma^{m/2}$, m being the magnetic quantum number of the final state. Therefore, as $B \to 0$, the contributions to the total cross-section from transitions to final states with m = 0 can be regarded as negligible. Only the case m = 0 is not directly dependent on γ. This is not surprising as it is only the m = 0 states which occur at zero field.

It can now be seen that, using the results given in table (5.2), since there is at most only one contribution from the transition to the final state with m = 0, then if this is an odd parity state, the dependence of a_ν on k_z is k_z^3 and if it is an even parity state, the dependence is k_z. This is in accordance with the Wigner Law and also agrees with the results obtained by Blumberg et al 1979.

From table (5.2) it can also be seen that, for a finite field strength B, since we are summing over m in the total photoionization cross-section, there is always at least one contribution whose dependence on k_z is k_z^{-1}. If the incident energy $h\nu$ is such that

$$h\nu = E_1 + E_\ell$$

for some ℓ, then there will always be a contribution to the cross-section from the transition to the final state with energy E_ℓ, with no energy released in the z direction, ie $k_z^2 = 0$. Therefore, for such incident energies, the total photoionization cross-section will always be infinite at this energy in the absence of broadening. These infinities occur because, in using the Landau model, we have separated out the z-motion and represented it by a plane wave. This is, of course, unsatisfactory when $k_z^2 \to 0$, even in the Coulomb-modified case discussed in chapter 6, and we should, in principle, replace the plane wave.

$$e^{ik_z z} = \sum_{p=o}^{\infty} i^p (2p + 1)\, j_p (k_z z)\, P_p (\cos\theta) \qquad (5.51)$$

by a distorted wave with $j_p (k_z z)$ replaced by

$$\chi_p(k_z z) = j_p (k_z z) + (-1)^p \tan\delta_p (k_z^2)\, y_p (k_z z) \qquad (5.52)$$

Here, $\delta_p(k_z^2)$ is the phase shift produced by the potential which may be taken to be short range. Consequently, by the effective range expansion

$$\lim_{k_z^2 \to 0} \delta_p(k_z^2) \sim k_z^{2p+1} + O(k_z^{2p+2}) \quad . \tag{5.53}$$

we have

$$\tan \delta_p(k_z^2)\, y_p(k_z z) \sim k_z^p \tag{5.54}$$

and the threshold dependence is readily seen to be unaffected on replacing the result in equation (5.51) with that given by equation (5.52), provided the potential is short range in the z- direction (Wunner et al, 1981 a).

§5.5 Results

The total photoionization cross-sections and the contributions from each of the possible Landau levels given in the form

$$S_\nu^{(\ell, m_f)} = \frac{1}{k_z} |\langle \Psi_i | \sum_{\mu=-1}^{1} r_\mu | \Psi_{k_z, m_f}^{(\ell)} \rangle|^2 \tag{5.55}$$

are calculated by program QMAT, details of which are given in Appendix (I). Results for photoionization from the bound states "$1s_o$" and "$2p_o$" to the continuum states with energy up to 8 Ry are given in tables 5.3 - 5.10 and the total cross-sections plotted in figures 5.2 - 5.9. It is observed from these results, that the total photoionization cross-section has an infinite peak corresponding to the energy of each discrete Landau level. It is clear, from table 5.2, that this is to be expected in the absence of broadening, due to the dominance of the contribution(s) whose dependence on k_z is as k_z^{-1} at each threshold (ie when $k_z \to 0$). As the energies of the Landau levels corresponding to all states of the same ℓ and with $m_f \leq 0$ are degenerate, and the energies of the levels (ℓ, m_f) where $m_f > 0$ are equal to those of the levels $(\ell + m_f, m)$ where $m = 0, -1, -2 \ldots$, it follows (from the results given in table 5.2) that there is always an infinite contribution to the total photoionization

cross-section at the thresholds which correspond to the Landau energies. In practice, however, these peaks would be finite and broadened due to the motion of the residual ion and other effects discussed in §5.4 (Blumberg et al, 1979).

It is seen from figures 5.2 - 5.9, that the cross-sections, away from the resonances, are very much smaller than the corresponding field-free cross-sections. In fact the field-free case is not marked on some of the figures, indicating that it lies beyond the scale of the graph. However, at $B = 10^7$G, for example, we are only dealing with a very narrow range of energies (from threshold up to about 0.5 eV), and it can be seen that, taking the very large difference in the energy scales into consideration, the $1s_o$ and $2p_o$ cross-sections become closer to the field free cross-section with decreasing B. For comparison, the zero field cross-sections, as computed by Burgess (1964) are given in table 5.11 along with the corresponding energies in Z^2 Ry for the 4 field strengths which are considered here. We would expect that, if broadening were considered, the field-free case would be reached in the limit as $B \rightarrow 0$. If an average smooth curve were to be drawn such that the actual cross-section consisted of a series of (both finite and infinite) peaks superimposed on this smooth curve, then it would be seen that the initial gradient of this curve would increase with decreasing field strength. In the limit as $B \rightarrow 0$ we would expect the initial gradient to become infinitely large as in the zero field case. This is illustrated schematically in figure 5.10.

Another feature of these cross-sections, is that apart from the infinite resonances occurring at the Landau energies, there are also secondary maxima appearing in some cases. These are due to maxima occurring in some individual contributions. However, it is not necessarily true that a maximum in one contribution will cause a maximum to occur in the total cross-section. For example,

E_f (γ Ry)	$S_\nu^{(0,-1)}$	$S_\nu^{(1,-1)}$	$S_\nu^{(2,-1)}$	$S_\nu^{(3,-1)}$	$S_\nu^{(0,0)}$	$S_\nu^{(1,0)}$	$S_\nu^{(2,0)}$	$S_\nu^{(3,0)}$	$S_\nu^{(0,1)}$	$S_\nu^{(1,1)}$	$S_\nu^{(2,1)}$	a_ν
1.0	0	-	-	-	∞	-	-	-	-	-	-	∞
1.2	1.739(-1)	-	-	-	1.330(2)	-	-	-	-	-	-	2.904(1)
1.4	2.417(-1)	-	-	-	8.978(1)	-	-	-	-	-	-	1.970(1)
1.6	2.909(-1)	-	-	-	6.997(1)	-	-	-	-	-	-	1.543(1)
1.8	3.302(-1)	-	-	-	5.782(1)	-	-	-	-	-	-	1.281(1)
2.0	3.628(-1)	-	-	-	4.931(1)	-	-	-	-	-	-	1.098(1)
2.2	3.906(-1)	-	-	-	4.291(1)	-	-	-	-	-	-	9.604
2.4	4.146(-1)	-	-	-	3.784(1)	-	-	-	-	-	-	8.514
2.6	4.356(-1)	-	-	-	3.370(1)	-	-	-	-	-	-	7.622
2.8	4.541(-1)	-	-	-	3.024(1)	-	-	-	-	-	-	6.875
2.99	4.697(-1)	-	-	-	2.742(1)	-	-	-	-	-	-	6.266
3.0	4.705(-1)	0	-	-	2.728(1)	∞	-	-	0	-	-	∞
3.2	4.850(-1)	2.890(-1)	-	-	2.473(1)	1.127(2)	-	-	1.739(-1)	-	-	3.119(1)
3.4	4.978(-1)	4.017(-1)	-	-	2.249(1)	7.612(1)	-	-	2.417(-1)	-	-	2.256(1)
3.6	5.092(-1)	4.836(-1)	-	-	2.051(1)	5.936(1)	-	-	2.909(-1)	-	-	1.841(1)
3.8	5.193(-1)	5.489(-1)	-	-	1.875(1)	4.908(1)	-	-	3.302(-1)	-	-	1.576(1)
4.0	5.283(-1)	6.032(-1)	-	-	1.717(1)	4.189(1)	-	-	3.628(-1)	-	-	1.383(1)
4.2	5.363(-1)	6.496(-1)	-	-	1.575(1)	3.647(1)	-	-	3.906(-1)	-	-	1.232(1)
4.4	5.432(-1)	6.896(-1)	-	-	1.446(1)	3.219(1)	-	-	4.146(-1)	-	-	1.110(1)
4.6	5.494(-1)	7.247(-1)	-	-	1.330(1)	2.869(1)	-	-	4.356(-1)	-	-	1.007(1)

Table 5.3 a

E_f (γ Ry)	$S_\nu^{(0,-1)}$	$S_\nu^{(1,-1)}$	$S_\nu^{(2,-1)}$	$S_\nu^{(3,-1)}$	$S_\nu^{(0,0)}$	$S_\nu^{(1,0)}$	$S_\nu^{(2,0)}$	$S_\nu^{(3,0)}$	$S_\nu^{(0,1)}$	$S_\nu^{(1,1)}$	$S_\nu^{(2,1)}$	a_ν
4.8	5.547(-1)	7.555(-1)	-	-	1.223(1)	2.576(1)	-	-	4.541(-1)	-	-	9.194
4.99	5.591(-1)	7.815(-1)	-	-	1.131(1)	2.337(1)	-	-	4.697(-1)	-	-	8.464
5.0	5.593(-1)	7.828(-1)	0	-	1.126(1)	2.326(1)	∞	-	4.705(-1)	0	-	∞
5.2	5.632(-1)	8.070(-1)	3.603(-1)	-	1.037(1)	2.109(1)	9.563(1)	-	4.849(-1)	2.890(-1)	-	3.016(1)
5.4	5.665(-1)	8.285(-1)	5.009(-1)	-	9.549	1.920(1)	6.465(1)	-	4.978(-1)	4.017(-1)	-	2.246(1)
5.6	5.693(-1)	8.476(-1)	6.031(-1)	-	8.796	1.752(1)	5.045(1)	-	5.092(-1)	4.836(-1)	-	1.868(1)
5.8	5.715(-1)	8.645(-1)	6.846(-1)	-	8.102	1.603(1)	4.174(1)	-	5.193(-1)	5.489(-1)	-	1.622(1)
6.0	5.732(-1)	8.796(-1)	7.524(-1)	-	7.461	1.470(1)	3.564(1)	-	5.283(-1)	6.032(-1)	-	1.441(1)
6.2	5.745(-1)	8.929(-1)	8.103(-1)	-	6.869	1.349(1)	3.105(1)	-	5.363(-1)	6.496(-1)	-	1.297(1)
6.4	5.753(-1)	9.047(-1)	8.604(-1)	-	6.322	1.240(1)	2.743(1)	-	5.432(-1)	6.896(-1)	-	1.179(1)
6.6	5.758(-1)	9.150(-1)	9.042(-1)	-	5.815	1.141(1)	2.446(1)	-	5.494(-1)	7.247(-1)	-	1.079(1)
6.8	5.758(-1)	9.240(-1)	9.428(-1)	-	5.346	1.051(1)	2.198(1)	-	5.547(-1)	7.555(-1)	-	9.920
6.99	5.756(-1)	9.314(-1)	9.754(-1)	-	4.932	9.722	1.996(1)	-	5.591(-1)	7.815(-1)	-	9.195
7.0	5.756(-1)	9.318(-1)	9.770(-1)	0	4.911	9.682	1.986	∞	5.593(-1)	7.828(-1)	0	∞
7.2	5.750(-1)	9.384(-1)	1.007	3.993(-1)	4.508	8.925	1.802(1)	8.131(1)	5.632(-1)	8.070(-1)	3.603(-1)	2.818(1)
7.4	5.741(-1)	9.441(-1)	1.034	5.552(-1)	4.134	8.229	1.642(1)	5.501(1)	5.665(-1)	8.285(-1)	5.009(-1)	2.137(1)
7.6	5.729(-1)	9.488(-1)	1.058	6.690(-1)	3.379	7.589	1.500(1)	4.295(1)	5.693(-1)	8.476(-1)	6.031(-1)	1.801(1)
7.8	5.715(-1)	9.526(-1)	1.080	7.590(-1)	3.465	6.998	1.373(1)	3.555(1)	5.715(-1)	8.645(-1)	6.846(-1)	1.580(1)
8.0	5.698(-1)	9.556(-1)	1.099	8.344(-1)	3.167	6.453	1.260(1)	3.038(1)	5.732(-1)	8.796(-1)	7.524(-1)	1.415(1)

Table 5.3 b

Total photoionization cross-sections (a_ν) in 10^{-18} cm^2 for transitions from the bound state $2p_0$ to the pure Landau continuum at $B = 10^7$G. The energy of the final state is E_f (γ Ry), where $\gamma = 4.25 \times 10^{-3}$, and the contribution $S_\nu^{(\ell,m)}$ is given by eq.(5.51).

E_f (γ Ry)	$S_\nu^{(0,-1)}$	$S_\nu^{(1,-1)}$	$S_\nu^{(2,-1)}$	$S_\nu^{(3,-1)}$	$S_\nu^{(0,0)}$	$S_\nu^{(1,0)}$	$S_\nu^{(2,0)}$	$S_\nu^{(3,0)}$	$S_\nu^{(0,1)}$	$S_\nu^{(1,1)}$	$S_\nu^{(2,1)}$	a_ν
1.0	∞	-	-	-	0	-	-	-	-	-	-	∞
1.2	1.245(-2)	-	-	-	4.385(-3)	-	-	-	-	-	-	1.422(-2)
1.4	8.767(-3)	-	-	-	6.196(-3)	-	-	-	-	-	-	1.265(-2)
1.6	7.129(-3)	-	-	-	7.581(-3)	-	-	-	-	-	-	1.245(-2)
1.8	6.149(-3)	-	-	-	8.744(-3)	-	-	-	-	-	-	1.262(-2)
2.0	5.477(-3)	-	-	-	9.766(-3)	-	-	-	-	-	-	1.292(-2)
2.2	4.980(-3)	-	-	-	1.069(-2)	-	-	-	-	-	-	1.329(-2)
2.4	4.591(-3)	-	-	-	1.153(-2)	-	-	-	-	-	-	1.369(-2)
2.6	4.277(-3)	-	-	-	1.231(-2)	-	-	-	-	-	-	1.410(-2)
2.8	4.016(-3)	-	-	-	1.304(-2)	-	-	-	-	-	-	1.451(-2)
2.99	3.805(-3)	-	-	-	1.369(-2)	-	-	-	-	-	-	1.490(-2)
3.0	3.795(-3)	∞	-	-	1.372(-2)	0	-	-	∞	-	-	∞
3.2	3.603(-3)	2.944(-2)	-	-	1.437(-2)	4.252(-3)	-	-	1.245(-2)	-	-	5.463(-2)
3.4	3.436(-3)	2.072(-2)	-	-	1.499(-2)	6.007(-3)	-	-	8.767(-3)	-	-	4.599(-2)
3.6	3.288(-3)	1.685(-2)	-	-	1.558(-2)	7.350(-3)	-	-	7.129(-3)	-	-	4.284(-2)
3.8	3.155(-3)	1.453(-2)	-	-	1.614(-2)	8.479(-3)	-	-	6.149(-3)	-	-	4.139(-2)
4.0	3.036(-3)	1.294(-2)	-	-	1.668(-2)	9.469(-3)	-	-	5.477(-3)	-	-	4.070(-2)
4.2	2.927(-3)	1.176(-2)	-	-	1.719(-2)	1.036(-2)	-	-	4.980(-3)	-	-	4.041(-2)
4.4	2.828(-3)	1.084(-2)	-	-	1.769(-2)	1.118(-2)	-	-	4.591(-3)	-	-	4.037(-2)
4.6	2.737(-3)	1.009(-2)	-	-	1.817(-2)	1.194(-2)	-	-	4.277(-3)	-	-	4.048(-2)

Table 5.4 a

E_f (γ Ry)	$S_\nu^{(0,-1)}$	$S_\nu^{(1,-1)}$	$S_\nu^{(2,-1)}$	$S_\nu^{(3,-1)}$	$S_\nu^{(0,0)}$	$S_\nu^{(1,0)}$	$S_\nu^{(2,0)}$	$S_\nu^{(3,0)}$	$S_\nu^{(0,1)}$	$S_\nu^{(1,1)}$	$S_\nu^{(2,1)}$	a_ν
4.8	2.654(-3)	9.475(-3)	-	-	1.864(-2)	1.264(-2)	-	-	4.016(-3)	-	-	4.069(-2)
4.99	2.580(-3)	8.974(-3)	-	-	1.906(-2)	1.328(-2)	-	-	3.805(-3)	-	-	4.096(-2)
5.0	2.576(-3)	8.950(-3)	∞	-	1.908(-2)	1.331(-2)	0	-	3.795(-3)	∞	-	∞
5.2	2.504(-3)	8.496(-3)	4.962(-2)	-	1.952(-2)	1.394(-2)	4.098(-3)	-	3.603(-3)	2.944(-2)	-	1.128(-1)
5.4	2.436(-3)	8.099(-3)	3.492(-2)	-	1.994(-2)	1.454(-2)	5.791(-3)	-	3.436(-3)	2.072(-2)	-	9.452(-2)
5.6	2.373(-3)	7.748(-3)	2.839(-2)	-	2.034(-2)	1.511(-2)	7.086(-3)	-	3.288(-3)	1.685(-2)	-	8.711(-2)
5.8	2.313(-3)	7.433(-3)	2.447(-2)	-	2.074(-2)	1.565(-2)	8.175(-3)	-	3.155(-3)	1.453(-2)	-	8.312(-2)
6.0	2.257(-3)	7.150(-3)	2.179(-2)	-	2.112(-2)	1.618(-2)	9.131(-3)	-	3.036(-3)	1.294(-2)	-	8.071(-2)
6.2	2.205(-3)	6.893(-3)	1.980(-2)	-	2.149(-2)	1.668(-2)	9.991(-3)	-	2.927(-3)	1.176(-2)	-	7.919(-2)
6.4	2.155(-3)	6.658(-3)	1.825(-2)	-	2.185(-2)	1.716(-2)	1.078(-2)	-	2.828(-3)	1.084(-2)	-	7.820(-2)
6.6	2.107(-3)	6.443(-3)	1.699(-2)	-	2.221(-2)	1.763(-2)	1.151(-2)	-	2.737(-3)	1.009(-2)	-	7.757(-2)
6.8	2.062(-3)	6.244(-3)	1.595(-2)	-	2.255(-2)	1.808(-2)	1.219(-2)	-	2.654(-3)	9.475(-3)	-	7.719(-2)
6.99	2.021(-3)	6.068(-3)	1.510(-2)	-	2.286(-2)	1.849(-2)	1.281(-2)	-	2.580(-3)	8.974(-3)	-	7.699(-2)
7.0	2.019(-3)	6.059(-3)	1.506(-2)	∞	2.288(-2)	1.852(-2)	1.284(-2)	0	2.576(-3)	8.950(-3)	∞	∞
7.2	1.978(-3)	5.888(-3)	1.429(-2)	7.161(-2)	2.320(-2)	1.894(-2)	1.345(-2)	3.932(-3)	2.504(-3)	8.496(-3)	4.962(-3)	1.854(-1)
7.4	1.939(-3)	5.727(-3)	1.362(-2)	5.040(-2)	2.352(-2)	1.935(-2)	1.402(-2)	5.556(-3)	2.436(-3)	8.099(-3)	3.492(-2)	1.558(-1)
7.6	1.902(-3)	5.577(-3)	1.303(-2)	4.096(-2)	2.382(-2)	1.974(-2)	1.458(-2)	6.800(-3)	2.373(-3)	7.748(-3)	2.839(-2)	1.432(-1)
7.8	1.866(-3)	5.436(-3)	1.250(-2)	3.530(-2)	2.412(-2)	2.012(-2)	1.510(-2)	7.845(-3)	2.313(-3)	7.433(-3)	2.447(-2)	1.360(-1)
8.0	1.832(-3)	5.303(-3)	1.202(-2)	3.143(-2)	2.441(-2)	2.050(-2)	1.561(-2)	8.763(-3)	2.257(-3)	7.150(-3)	2.179(-2)	1.314(-1)

Table 5.4 b

Total photoionization cross-sections (a_ν) in 10^{-18} cm^2 for transitions from the bound state $1s_0$ to the pure Landau continuum at B = 10^7G. The energy of the final state is E_f (γ Ry) where $\gamma = 4.25 \times 10^{-3}$, and the contribution $S^{(\ell,m)}$ is given by eq.(5.51).

E_f (γ Ry)	$S_\nu^{(0,-1)}$	$S_\nu^{(1,-1)}$	$S_\nu^{(2,-1)}$	$S_\nu^{(3,-1)}$	$S_\nu^{(0,0)}$	$S_\nu^{(1,0)}$	$S_\nu^{(2,0)}$	$S_\nu^{(3,0)}$	$S_\nu^{(0,1)}$	$S_\nu^{(1,1)}$	$S_\nu^{(2,1)}$	a_ν
1.0	0	-	-	-	∞	-	-	-	-	-	-	∞
1.2	1.168(1)	-	-	-	1.470(2)	-	-	-	-	-	-	4.019(1)
1.4	1.354(1)	-	-	-	5.726(1)	-	-	-	-	-	-	1.845(1)
1.6	1.365(1)	-	-	-	2.366(1)	-	-	-	-	-	-	9.990
1.8	1.302(1)	-	-	-	9.027	-	-	-	-	-	-	6.065
2.0	1.208(1)	-	-	-	2.726	-	-	-	-	-	-	4.179
2.2	1.102(1)	-	-	-	4.090(-1)	-	-	-	-	-	-	3.309
2.4	9.947	-	-	-	1.612(-2)	-	-	-	-	-	-	2.958
2.6	8.923	-	-	-	5.060(-1)	-	-	-	-	-	-	2.868
2.8	7.972	-	-	-	1.339	-	-	-	-	-	-	2.900
2.99	7.145	-	-	-	2.195	-	-	-	-	-	-	2.974
3.0	7.104	0	-	-	2.240	∞	-	-	0	-	-	∞
3.2	6.322	3.902	-	-	3.071	3.622(1)	-	-	1.168(1)	-	-	1.995(1)
3.4	5.622	4.691	-	-	3.776	1.632(1)	-	-	1.354(1)	-	-	1.465(1)
3.6	4.998	4.902	-	-	4.337	8.151	-	-	1.365(1)	-	-	1.227(1)
3.8	4.445	4.846	-	-	4.757	4.079	-	-	1.302(1)	-	-	1.084(1)
4.0	3.956	4.653	-	-	5.051	1.935	-	-	1.208(1)	-	-	9.828
4.2	3.523	4.392	-	-	5.235	8.141	-	-	1.102(1)	-	-	9.054
4.4	3.140	4.099	-	-	5.329	2.651(-1)	-	-	9.947	-	-	8.422
4.6	2.802	3.797	-	-	5.348	4.172(-2)	-	-	8.923	-	-	7.884

Table 5.5 a

E_f (γ Ry)	$S_\nu^{(0,-1)}$	$S_\nu^{(1,-1)}$	$S_\nu^{(2,-1)}$	$S_\nu^{(3,-1)}$	$S_\nu^{(0,0)}$	$S_\nu^{(1,0)}$	$S_\nu^{(2,0)}$	$S_\nu^{(3,0)}$	$S_\nu^{(0,1)}$	$S_\nu^{(1,1)}$	$S_\nu^{(2,1)}$	a_ν
4.8	2.503	3.499	-	-	5.307	2.180(-3)	-	-	7.972	-	-	7.411
4.99	2.251	3.227	-	-	5.226	5.812(-2)	-	-	7.145	-	-	7.006
5.0	2.239	3.213	0	-	5.221	6.264(-1)	∞	-	7.104	0	-	∞
5.2	2.004	2.942	1.358	-	5.099	1.729(-1)	1.161(1)	-	6.322	3.902	-	1.333(1)
5.4	1.797	2.689	1.676	-	4.950	3.028(-1)	5.738	-	5.622	4.691	-	1.115(1)
5.6	1.612	2.455	1.796	-	4.782	4.349(-1)	3.190	-	4.998	4.902	-	9.993
5.8	1.449	2.239	1.820	-	4.601	5.589(-1)	1.820	-	4.445	4.846	-	9.163
6.0	1.303	2.041	1.791	-	4.412	6.698(-1)	1.028	-	3.956	4.653	-	8.497
6.2	1.174	1.860	1.731	-	4.218	7.650(-1)	5.578(-1)	-	3.523	4.392	-	7.931
6.4	1.058	1.695	1.653	-	4.023	8.442(-1)	2.810(-1)	-	3.140	4.099	-	7.432
6.6	9.549(-1)	1.545	1.565	-	3.829	9.077(-1)	1.237(-1)	-	2.802	3.797	-	6.984
6.8	8.628(-1)	1.408	1.474	-	3.637	9.566(-1)	4.152(-2)	-	2.503	3.499	-	6.575
6.99	7.843(-1)	1.290	1.386	-	3.458	9.908(-1)	7.366(-3)	-	2.251	3.227	-	6.216
7.0	7.804(-1)	1.284	1.382	0	3.449	9.923(-1)	6.424(-3)	∞	2.239	3.213	0	∞
7.2	7.066(-1)	1.172	1.291	5.194(-1)	3.267	1.016	5.546(-4)	4.456	2.004	2.942	1.358	8.836
7.4	6.405(-1)	1.069	1.203	6.534(-1)	3.090	1.030	1.228(-2)	2.348	1.797	2.689	1.676	7.763
7.6	5.811(-1)	9.766(-1)	1.119	7.136(-1)	2.920	1.035	3.399(-2)	1.398	1.612	2.455	1.796	7.118
7.8	5.278(-1)	8.924(-1)	1.039	7.363(-1)	2.756	1.032	6.074(-2)	8.611(-1)	1.449	2.239	1.820	6.620
8.0	4.799(-1)	8.160(-1)	9.635(-1)	7.370(-1)	2.600	1.023	8.932(-2)	5.329(-1)	1.303	2.041	1.791	6.199

Table 5.5 b

Total photoionization cross-sections (a_ν) in 10^{-18} cm^2 for transitions from the bound state $2p_o$ to the pure Landau continuum at $B = 10^8$G. The energy of the final state is $E_f(\gamma$ Ry) where $\gamma = 4.25 \times 10^{-2}$ and the contribution $S_\nu^{(\ell,m)}$ is given by eq.(5.51).

E_f (γ Ry)	$S_\nu^{(0,-1)}$	$S_\nu^{(1,-1)}$	$S_\nu^{(2,-1)}$	$S_\nu^{(3,-1)}$	$S_\nu^{(0,0)}$	$S_\nu^{(1,0)}$	$S_\nu^{(2,0)}$	$S_\nu^{(3,0)}$	$S_\nu^{(0,1)}$	$S_\nu^{(1,1)}$	$S_\nu^{(2,1)}$	a_ν
1.0	∞	-	-	-	0	-	-	-	-	-	-	∞
1.2	5.156(-1)	-	-	-	1.038(-1)	-	-	-	-	-	-	5.476(-1)
1.4	3.580(-1)	-	-	-	1.673(-1)	-	-	-	-	-	-	4.683(-1)
1.6	2.819(-1)	-	-	-	2.145(-1)	-	-	-	-	-	-	4.461(-1)
1.8	2.324(-1)	-	-	-	2.460(-1)	-	-	-	-	-	-	4.335(-1)
2.0	1.964(-1)	-	-	-	2.645(-1)	-	-	-	-	-	-	4.209(-1)
2.2	1.686(-1)	-	-	-	2.730(-1)	-	-	-	-	-	-	4.065(-1)
2.4	1.465(-1)	-	-	-	2.749(-1)	-	-	-	-	-	-	3.910(-1)
2.6	1.286(-1)	-	-	-	2.726(-1)	-	-	-	-	-	-	3.752(-1)
2.8	1.141(-1)	-	-	-	2.681(-1)	-	-	-	-	-	-	3.602(-1)
2.99	1.026(-1)	-	-	-	2.631(-1)	-	-	-	-	-	-	3.472(-1)
3.0	1.021(-1)	∞	-	-	2.628(-1)	0	-	-	∞	-	-	∞
3.2	9.215(-2)	6.235(-1)	-	-	2.576(-1)	9.715(-2)	-	-	5.156(-1)	-	-	1.518
3.4	8.387(-2)	3.944(-1)	-	-	2.529(-1)	1.262(-1)	-	-	3.580(-1)	-	-	1.172
3.6	7.692(-2)	3.023(-1)	-	-	2.490(-1)	1.395(-1)	-	-	2.819(-1)	-	-	1.020
3.8	7.105(-2)	2.536(-1)	-	-	2.458(-1)	1.447(-1)	-	-	2.324(-1)	-	-	9.276(-1)
4.0	6.604(-2)	2.237(-1)	-	-	2.434(-1)	1.458(-1)	-	-	1.964(-1)	-	-	8.633(-1)
4.2	6.172(-2)	2.029(-1)	-	-	2.416(-1)	1.453(-1)	-	-	1.686(-1)	-	-	8.147(-1)
4.4	5.797(-2)	1.867(-1)	-	-	2.402(-1)	1.447(-1)	-	-	1.465(-1)	-	-	7.766(-1)
4.6	5.466(-2)	1.729(-1)	-	-	2.391(-1)	1.448(-1)	-	-	1.286(-1)	-	-	7.460(-1)

Table 5.6 a

E_f (γ Ry)	$S_\nu^{(0,-1)}$	$S_\nu^{(1,-1)}$	$S_\nu^{(2,-1)}$	$S_\nu^{(3,-1)}$	$S_\nu^{(0,0)}$	$S_\nu^{(1,0)}$	$S_\nu^{(2,0)}$	$S_\nu^{(3,0)}$	$S_\nu^{(0,1)}$	$S_\nu^{(1,1)}$	$S_\nu^{(2,1)}$	a_ν
4.8	5.171(-2)	1.604(-1)	-	-	2.380(-1)	1.458(-1)	-	-	1.141(-1)	-	-	7.209(-1)
4.99	4.917(-2)	1.492(-1)	-	-	2.369(-1)	1.479(-1)	-	-	1.026(-1)	-	-	7.010(-1)
5.0	4.905(-2)	1.486(-1)	∞	-	2.368(-1)	1.480(-1)	0	-	1.021(-1)	∞	-	∞
5.2	4.661(-2)	1.373(-1)	6.404(-1)	-	2.354(-1)	1.512(-1)	1.832(-2)	-	9.215(-2)	6.235(-1)	-	2.003
5.4	4.434(-2)	1.264(-1)	4.362(-1)	-	2.337(-1)	1.552(-1)	5.605(-2)	-	8.387(-2)	3.944(-1)	-	1.587
5.6	4.222(-2)	1.161(-1)	3.487(-1)	-	2.316(-1)	1.598(-1)	9.367(-2)	-	7.692(-2)	3.023(-1)	-	1.432
5.8	4.022(-2)	1.063(-1)	2.980(-1)	-	2.289(-1)	1.645(-1)	1.206(-1)	-	7.105(-2)	2.536(-1)	-	1.350
6.0	3.830(-2)	9.714(-2)	2.635(-1)	-	2.259(-1)	1.692(-1)	1.348(-1)	-	6.604(-2)	2.237(-1)	-	1.290
6.2	3.646(-2)	8.866(-2)	2.374(-1)	-	2.223(-1)	1.735(-1)	1.382(-1)	-	6.172(-2)	2.029(-1)	-	1.238
6.4	3.469(-2)	8.089(-2)	2.160(-1)	-	2.183(-1)	1.771(-1)	1.346(-1)	-	5.797(-2)	1.867(-1)	-	1.188
6.6	3.297(-2)	7.384(-2)	1.975(-1)	-	2.139(-1)	1.799(-1)	1.271(-1)	-	5.466(-2)	1.729(-1)	-	1.138
6.8	3.131(-2)	6.750(-2)	1.810(-1)	-	2.092(-1)	1.817(-1)	1.183(-1)	-	5.171(-2)	1.604(-1)	-	1.089
6.99	2.977(-2)	6.211(-2)	1.666(-1)	-	2.044(-1)	1.824(-1)	1.103(-1)	-	4.917(-2)	1.492(-1)	-	1.045
7.0	2.969(-2)	6.184(-2)	1.659(-1)	∞	2.042(-1)	1.824(-1)	1.099(-1)	0	4.905(-2)	1.486(-1)	∞	∞
7.2	2.812(-2)	5.682(-2)	1.520(-1)	5.077(-1)	1.989(-1)	1.820(-1)	1.027(-1)	7.224(-3)	4.661(-2)	1.373(-1)	6.404(-1)	2.271
7.4	2.660(-2)	5.239(-2)	1.391(-1)	3.359(-1)	1.935(-1)	1.804(-1)	9.721(-2)	4.139(-2)	4.434(-2)	1.264(-1)	4.362(-1)	1.858
7.6	2.513(-2)	4.850(-2)	1.273(-1)	2.562(-1)	1.880(-1)	1.778(-1)	9.348(-2)	8.111(-2)	4.222(-2)	1.161(-1)	3.487(-1)	1.681
7.8	2.372(-2)	4.510(-2)	1.165(-1)	2.074(-1)	1.825(-1)	1.742(-1)	9.143(-2)	1.096(-1)	4.022(-2)	1.063(-1)	2.980(-1)	1.568
8.0	2.236(-2)	4.214(-2)	1.066(-1)	1.738(-1)	1.770(-1)	1.697(-1)	9.089(-2)	1.222(-1)	3.830(-2)	9.714(-2)	2.635(-1)	1.475

Table 5.6 b

Total photoionization cross sections (a_ν) in 10^{-18} cm^2 for transitions from the bound state $1s_o$ to the pure Landau continuum at B = 10^8G. The energy of the final state is E_f (γ Ry) where $\gamma = 4.25 \times 10^{-2}$ and the contribution $S_\nu^{(\ell,m)}$ is given by eq. (5.51)

E_f (γ Ry)	$S_\nu^{(0,-1)}$	$S_\nu^{(1,-1)}$	$S_\nu^{(2,-1)}$	$S_\nu^{(3,-1)}$	$S_\nu^{(0,0)}$	$S_\nu^{(1,0)}$	$S_\nu^{(2,0)}$	$S_\nu^{(3,0)}$	$S_\nu^{(0,1)}$	$S_\nu^{(1,1)}$	$S_\nu^{(2,1)}$	a_ν
1.0	0	-	-	-	∞	-	-	-	-	-	-	∞
1.2	8.068	-	-	-	1.082(1)	-	-	-	-	-	-	6.750
1.4	6.341	-	-	-	3.606(-2)	-	-	-	-	-	-	2.511
1.6	4.495	-	-	-	2.203	-	-	-	-	-	-	2.882
1.8	3.124	-	-	-	3.702	-	-	-	-	-	-	3.185
2.0	2.179	-	-	-	3.998	-	-	-	-	-	-	3.108
2.2	1.537	-	-	-	3.702	-	-	-	-	-	-	2.827
2.4	1.099	-	-	-	3.212	-	-	-	-	-	-	2.483
2.6	7.960(-1)	-	-	-	2.707	-	-	-	-	-	-	2.145
2.8	5.832(-1)	-	-	-	2.250	-	-	-	-	-	-	1.838
2.99	4.382(-1)	-	-	-	1.874	-	-	-	-	-	-	1.580
3.0	4.318(-1)	0	-	-	1.856	∞	-	-	0	-	-	∞
3.2	3.228(-1)	2.498(-1)	-	-	1.523	6.360(-1)	-	-	8.068	-	-	7.793
3.4	2.435(-1)	2.501(-1)	-	-	1.245	1.188(-1)	-	-	6.341	-	-	6.214
3.6	1.854(-1)	2.205(-1)	-	-	1.014	1.107(-2)	-	-	4.495	-	-	4.707
3.8	1.424(-1)	1.861(-1)	-	-	8.235(-1)	1.159(-3)	-	-	3.124	-	-	3.553
4.0	1.104(-1)	1.541(-1)	-	-	6.678(-1)	1.369(-2)	-	-	2.179	-	-	2.710
4.2	8.632(-2)	1.266(-1)	-	-	5.416(-1)	2.768(-2)	-	-	1.537	-	-	2.096
4.4	6.812(-2)	1.036(-1)	-	-	4.399(-1)	3.810(-2)	-	-	1.099	-	-	1.644
4.6	5.423(-2)	8.478(-2)	-	-	3.586(-1)	4.458(-2)	-	-	7.960(-1)	-	-	1.307

Table 5.7 a

E_f (γ Ry)	$S_\nu^{(0,-1)}$	$S_\nu^{(1,-1)}$	$S_\nu^{(2,-1)}$	$S_\nu^{(3,-1)}$	$S_\nu^{(0,0)}$	$S_\nu^{(1,0)}$	$S_\nu^{(2,0)}$	$S_\nu^{(3,0)}$	$S_\nu^{(0,1)}$	$S_\nu^{(1,1)}$	$S_\nu^{(2,1)}$	a_ν
4.8	4.354(-2)	6.948(-2)	-	-	2.939(-1)	4.787(-2)	-	-	5.832(-1)	-	-	1.051
4.99	3.559(-2)	5.764(-2)	-	-	2.447(-1)	4.882(-2)	-	-	4.382(-1)	-	-	8.642(-1)
5.0	3.522(-2)	5.708(-2)	0	-	2.424(-1)	4.882(-2)	∞	-	4.318(-1)	0	-	∞
5.2	2.869(-2)	4.705(-2)	2.477(-2)	-	2.014(-1)	4.811(-2)	8.272(-2)	-	3.228(-1)	2.498(-1)	-	1.092
5.4	2.352(-2)	3.892(-2)	2.779(-2)	-	1.687(-1)	4.626(-2)	2.621(-2)	-	2.435(-1)	2.501(-1)	-	9.257(-1)
5.6	1.939(-2)	3.232(-2)	2.680(-2)	-	1.424(-1)	4.365(-2)	7.895(-3)	-	1.854(-1)	2.205(-1)	-	7.859(-1)
5.8	1.606(-2)	2.694(-2)	2.445(-2)	-	1.211(-1)	4.058(-2)	1.858(-3)	-	1.424(-1)	1.861(-1)	-	6.687(-1)
6.0	1.336(-2)	2.255(-2)	2.178(-2)	-	1.038(-1)	3.728(-2)	1.813(-4)	-	1.104(-1)	1.541(-1)	-	5.706(-1)
6.2	1.115(-2)	1.894(-2)	1.920(-2)	-	8.940(-2)	3.392(-2)	4.375(-5)	-	8.632(-2)	1.266(-1)	-	4.888(-1)
6.4	9.339(-3)	1.597(-2)	1.687(-2)	-	7.740(-2)	3.063(-2)	4.435(-4)	-	6.812(-2)	1.036(-1)	-	4.204(-1)
6.6	7.842(-3)	1.351(-2)	1.479(-2)	-	6.725(-2)	2.751(-2)	1.029(-3)	-	5.423(-2)	8.478(-2)	-	3.633(-1)
6.8	6.602(-3)	1.147(-2)	1.297(-2)	-	5.860(-2)	2.462(-2)	1.665(-3)	-	4.354(-2)	6.948(-2)	-	3.152(-1)
6.99	5.620(-3)	9.847(-3)	1.143(-2)	-	5.148(-2)	2.211(-2)	2.253(-3)	-	3.559(-2)	5.764(-2)	-	2.766(-1)
7.0	5.573(-3)	9.769(-3)	1.135(-2)	0	5.113(-2)	2.199(-2)	2.282(-3)	∞	3.522(-2)	5.708(-2)	0	∞
7.2	4.716(-3)	8.344(-3)	9.931(-3)	4.370(-3)	4.465(-2)	1.962(-2)	2.831(-3)	1.683(-2)	2.869(-2)	4.705(-2)	2.477(-2)	3.071(-1)
7.4	4.001(-3)	7.148(-3)	8.675(-3)	5.154(-3)	3.900(-2)	1.752(-2)	3.274(-3)	6.718(-3)	2.352(-2)	3.892(-2)	2.779(-2)	2.701(-1)
7.6	3.405(-3)	6.140(-3)	7.568(-3)	5.231(-3)	3.406(-2)	1.567(-2)	3.587(-3)	2.928(-3)	1.939(-2)	3.232(-2)	2.680(-2)	2.392(-1)
7.8	2.906(-3)	5.289(-3)	6.596(-3)	5.023(-3)	2.973(-2)	1.404(-2)	3.763(-3)	1.286(-3)	1.606(-2)	2.694(-2)	2.445(-2)	2.122(-1)
8.0	2.489(-3)	4.567(-3)	5.746(-3)	4.704(-3)	2.594(-2)	1.261(-2)	3.812(-3)	5.270(-4)	1.336(-2)	2.255(-2)	2.178(-2)	1.884(-1)

Table 5.7 b

Photoionization cross sections (a_ν) in 10^{-18} cm^2 for transitions from the bound state $2p_o$ to the pure Landau continuum at $B = 5 \times 10^8$G. The energy of the final state is E_f (γ Ry) where $\gamma = 2.13 \times 10^{-1}$ and the contribution $S_\nu^{(\ell,m)}$ is given by eq. (5.51).

E_f (γ Ry)	$S_\nu^{(0,-1)}$	$S_\nu^{(1,-1)}$	$S_\nu^{(2,-1)}$	$S_\nu^{(3,-1)}$	$S_\nu^{(0,0)}$	$S_\nu^{(1,0)}$	$S_\nu^{(2,0)}$	$S_\nu^{(3,0)}$	$S_\nu^{(0,1)}$	$S_\nu^{(1,1)}$	$S_\nu^{(2,1)}$	a_ν
1.0	∞	-	-	-	0	-	-	-	-	-	-	∞
1.2	1.071	-	-	-	5.324	-	-	-	-	-	-	1.674
1.4	6.385(-1)	-	-	-	6.401(-1)	-	-	-	-	-	-	1.381
1.6	4.448(-1)	-	-	-	6.233(-1)	-	-	-	-	-	-	1.193
1.8	3.282(-1)	-	-	-	5.692(-1)	-	-	-	-	-	-	1.035
2.0	2.488(-1)	-	-	-	5.146(-1)	-	-	-	-	-	-	9.079(-1)
2.2	1.919(-1)	-	-	-	4.693(-1)	-	-	-	-	-	-	8.104(-1)
2.4	1.501(-1)	-	-	-	4.324(-1)	-	-	-	-	-	-	7.352(-1)
2.6	1.191(-1)	-	-	-	4.002(-1)	-	-	-	-	-	-	6.744(-1)
2.8	9.596(-2)	-	-	-	3.695(-1)	-	-	-	-	-	-	6.215(-1)
2.99	7.923(-2)	-	-	-	3.401(-1)	-	-	-	-	-	-	5.743(-1)
3.0	7.846(-2)	∞	-	-	3.385(-1)	0	-	-	∞	-	-	∞
3.2	6.507(-2)	4.745(-1)	-	-	3.068(-1)	8.970(-2)	-	-	1.071	-	-	2.826
3.4	5.465(-2)	2.837(-1)	-	-	2.789(-1)	1.540(-1)	-	-	6.385(-1)	-	-	2.030
3.6	4.638(-2)	1.911(-1)	-	-	2.439(-1)	1.449(-1)	-	-	4.448(-1)	-	-	1.586
3.8	3.968(-2)	1.398(-1)	-	-	2.149(-1)	1.138(-1)	-	-	3.282(-1)	-	-	1.269
4.0	3.414(-2)	1.097(-1)	-	-	1.887(-1)	8.967(-2)	-	-	2.488(-1)	-	-	1.042
4.2	2.948(-2)	9.056(-2)	-	-	1.656(-1)	7.783(-2)	-	-	1.919(-1)	-	-	8.830(-1)
4.4	2.551(-2)	7.715(-2)	-	-	1.459(-1)	7.553(-2)	-	-	1.501(-1)	-	-	7.712(-1)
4.6	2.208(-2)	6.662(-2)	-	-	1.294(-1)	7.878(-2)	-	-	1.191(-1)	-	-	6.917(-1)

Table 5.8 a

E_f (γ Ry)	$S_\nu^{(0,-1)}$	$S_\nu^{(1,-1)}$	$S_\nu^{(2,-1)}$	$S_\nu^{(3,-1)}$	$S_\nu^{(0,0)}$	$S_\nu^{(1,0)}$	$S_\nu^{(2,0)}$	$S_\nu^{(3,0)}$	$S_\nu^{(0,1)}$	$S_\nu^{(1,1)}$	$S_\nu^{(2,1)}$	a_ν
4.8	1.912(-2)	5.758(-2)	-	-	1.157(-1)	8.393(-2)	-	-	9.596(-2)	-	-	6.325(-1)
4.99	1.667(-2)	4.986(-2)	-	-	1.049(-1)	8.785(-2)	-	-	7.923(-2)	-	-	5.869(-1)
5.0	1.655(-2)	4.947(-2)	∞	-	1.044(-1)	8.799(-2)	0	-	7.846(-2)	∞	-	∞
5.2	1.432(-2)	4.212(-2)	1.920(-1)	-	9.510(-2)	8.902(-2)	2.651(-2)	-	6.507(-2)	4.745(-1)	-	1.770
5.4	1.240(-2)	3.555(-2)	1.195(-1)	-	8.737(-2)	8.633(-2)	2.677(-2)	-	5.465(-2)	2.837(-1)	-	1.277
5.6	1.073(-2)	2.980(-2)	8.748(-2)	-	8.083(-2)	8.030(-2)	2.525(-2)	-	4.638(-2)	1.911(-1)	-	1.018
5.8	9.307(-3)	2.490(-2)	6.907(-2)	-	7.515(-2)	7.202(-2)	2.555(-2)	-	3.968(-2)	1.398(-1)	-	8.569(-1)
6.0	8.087(-3)	2.083(-2)	5.676(-2)	-	7.008(-2)	6.275(-2)	2.769(-2)	-	3.414(-2)	1.097(-1)	-	7.479(-1)
6.2	7.048(-3)	1.751(-2)	4.754(-2)	-	6.541(-2)	5.360(-2)	3.067(-2)	-	2.948(-2)	9.056(-2)	-	6.679(-1)
6.4	6.164(-3)	1.485(-2)	4.007(-2)	-	6.099(-2)	4.535(-2)	3.327(-2)	-	2.551(-2)	7.715(-2)	-	6.038(-1)
6.6	5.415(-3)	1.274(-2)	3.378(-2)	-	5.673(-2)	3.840(-2)	3.454(-2)	-	2.208(-2)	6.662(-2)	-	5.479(-1)
6.8	4.780(-3)	1.108(-2)	2.843(-2)	-	5.259(-2)	3.287(-2)	3.404(-2)	-	1.912(-2)	5.758(-2)	-	4.962(-1)
6.99	4.267(-3)	9.836(-3)	2.412(-2)	-	4.874(-2)	2.886(-2)	3.204(-2)	-	1.667(-2)	4.986(-2)	-	4.498(-1)
7.0	4.242(-3)	9.778(-3)	2.391(-2)	∞	4.854(-2)	2.868(-2)	3.190(-2)	0	1.655(-2)	4.947(-2)	∞	∞
7.2	3.785(-3)	8.749(-3)	2.015(-2)	8.938(-2)	4.459(-2)	2.565(-2)	2.862(-2)	7.674(-3)	1.432(-2)	4.212(-2)	1.920(-1)	1.019
7.4	3.395(-3)	7.925(-3)	1.708(-2)	5.784(-2)	4.076(-2)	2.358(-2)	2.486(-2)	7.785(-3)	1.240(-2)	3.555(-2)	1.195(-1)	7.619(-1)
7.6	3.062(-3)	7.251(-3)	1.460(-2)	4.409(-2)	3.709(-2)	2.223(-2)	2.115(-2)	8.653(-3)	1.073(-2)	2.980(-2)	8.748(-2)	6.321(-1)
7.8	2.775(-3)	6.685(-3)	1.264(-2)	3.559(-2)	3.361(-2)	2.143(-2)	1.790(-2)	1.018(-2)	9.307(-3)	2.490(-2)	6.907(-2)	5.481(-1)
8.0	2.526(-3)	6.194(-3)	1.109(-2)	2.935(-2)	3.036(-2)	2.099(-2)	1.529(-2)	1.178(-2)	8.087(-3)	2.083(-2)	5.676(-2)	4.866(-1)

Table 5,8 b

Photoionization cross sections (a_ν) in 10^{-18} cm^2 for transitions from the bound state $1s_o$ to the pure Landau continuum at $B = 5 \times 10^8$G. The energy of the final state is E_f (γ Ry) where $\gamma = 2.13 \times 10^{-1}$ and the contribution $S_\nu^{(\ell,m)}$ is given by eq. (5.51).

E_f (γ Ry)	$S_\nu^{(0,-1)}$	$S_\nu^{(1,-1)}$	$S_\nu^{(2,-1)}$	$S_\nu^{(3,-1)}$	$S_\nu^{(0,0)}$	$S_\nu^{(1,0)}$	$S_\nu^{(2,0)}$	$S_\nu^{(3,0)}$	$S_\nu^{(0,1)}$	$S_\nu^{(1,1)}$	$S_\nu^{(2,1)}$	a_ν
1.0	0	-	-	-	∞	-	-	-	-	-	-	∞
1.2	3.576	-	-	-	3.437(-1)	-	-	-	-	-	-	1.741
1.4	2.125	-	-	-	1.925	-	-	-	-	-	-	2.094
1.6	1.210	-	-	-	2.759	-	-	-	-	-	-	2.342
1.8	7.076(-1)	-	-	-	2.323	-	-	-	-	-	-	2.009
2.0	4.291(-1)	-	-	-	1.738	-	-	-	-	-	-	1.594
2.2	2.686(-1)	-	-	-	1.273	-	-	-	-	-	-	1.246
2.4	1.726(-1)	-	-	-	9.322(-1)	-	-	-	-	-	-	9.736(-1)
2.6	1.134(-1)	-	-	-	6.832(-1)	-	-	-	-	-	-	7.601(-1)
2.8	7.610(-2)	-	-	-	4.992(-1)	-	-	-	-	-	-	5.908(-1)
2.99	5.305(-2)	-	-	-	3.688(-1)	-	-	-	-	-	-	4.624(-1)
3.0	5.207(-2)	0	-	-	3.629(-1)	∞	-	-	0	-	-	∞
3.2	3.633(-2)	3.643(-2)	-	-	2.629(-1)	6.191(-2)	-	-	3.576	-	-	4.659
3.4	2.584(-2)	3.328(-2)	-	-	1.904(-1)	3.949(-3)	-	-	2.125	-	-	2.962
3.6	1.871(-2)	2.697(-2)	-	-	1.385(-1)	1.760(-4)	-	-	1.210	-	-	1.838
3.8	1.379(-2)	2.123(-2)	-	-	1.018(-1)	2.073(-3)	-	-	7.076(-1)	-	-	1.178
4.0	1.031(-2)	1.662(-2)	-	-	7.592(-2)	3.922(-3)	-	-	4.291(-1)	-	-	7.844(-1)
4.2	7.821(-3)	1.301(-2)	-	-	5.766(-2)	5.547(-3)	-	-	2.686(-1)	-	-	5.419(-1)
4.4	6.002(-3)	1.020(-2)	-	-	4.466(-2)	6.897(-3)	-	-	1.726(-1)	-	-	3.869(-1)
4.6	4.652(-3)	8.003(-3)	-	-	3.530(-2)	7.741(-3)	-	-	1.134(-1)	-	-	2.845(-1)

Table 5.9 a

E_f (γ Ry)	$S_\nu^{(0,-1)}$	$S_\nu^{(1,-1)}$	$S_\nu^{(2,-1)}$	$S_\nu^{(3,-1)}$	$S_\nu^{(0,0)}$	$S_\nu^{(1,0)}$	$S_\nu^{(2,0)}$	$S_\nu^{(3,0)}$	$S_\nu^{(0,1)}$	$S_\nu^{(1,1)}$	$S_\nu^{(2,1)}$	a_ν
4.8	3.636(-3)	6.294(-3)	-	-	2.842(-2)	7.930(-3)	-	-	7.610(-2)	-	-	2.148(-1)
4.99	2.896(-3)	5.025(-3)	-	-	2.349(-2)	7.544(-3)	-	-	5.305(-2)	-	-	1.678(-1)
5.0	2.863(-3)	4.967(-3)	0	-	2.326(-2)	7.511(-3)	∞	-	5.207(-2)	0	-	∞
5.2	2.267(-3)	3.938(-3)	2.413(-3)	-	1.929(-2)	6.680(-3)	6.521(-3)	-	3.633(-2)	3.643(-2)	-	2.165(-1)
5.4	1.806(-3)	3.142(-3)	2.530(-3)	-	1.615(-2)	5.675(-3)	1.094(-3)	-	2.584(-2)	3.328(-2)	-	1.767(-1)
5.6	1.445(-3)	2.525(-3)	2.301(-3)	-	1.362(-2)	4.685(-3)	2.493(-4)	-	1.871(-2)	2.697(-2)	-	1.443(-1)
5.8	1.162(-3)	2.045(-3)	2.036(-3)	-	1.153(-2)	3.822(-3)	8.593(-5)	-	1.379(-2)	2.123(-2)	-	1.181(-1)
6.0	9.385(-4)	1.669(-3)	1.792(-3)	-	9.782(-3)	3.127(-3)	1.298(-5)	-	1.031(-2)	1.662(-2)	-	9.702(-2)
6.2	7.613(-4)	1.373(-3)	1.565(-3)	-	8.299(-3)	2.597(-3)	1.135(-5)	-	7.821(-3)	1.301(-2)	-	8.027(-2)
6.4	6.203(-4)	1.137(-3)	1.352(-3)	-	7.033(-3)	2.206(-3)	1.112(-4)	-	6.002(-3)	1.020(-2)	-	6.700(-2)
6.6	5.078(-4)	9.470(-4)	1.153(-3)	-	5.947(-3)	1.924(-3)	2.693(-4)	-	4.652(-3)	8.003(-3)	-	5.642(-2)
6.8	4.176(-4)	7.929(-4)	9.737(-4)	-	5.016(-3)	1.721(-3)	4.046(-4)	-	3.636(-3)	6.294(-3)	-	4.782(-2)
6.99	3.484(-4)	6.726(-4)	8.250(-4)	-	4.255(-3)	1.578(-3)	4.649(-4)	-	2.896(-3)	5.025(-3)	-	4.101(-2)
7.0	3.451(-4)	6.668(-4)	8.177(-4)	0	4.218(-3)	1.572(-3)	4.660(-4)	∞	2.863(-3)	4.967(-3)	0	∞
7.2	2.867(-4)	5.627(-4)	6.862(-4)	3.419(-4)	3.537(-3)	1.457(-3)	4.529(-4)	1.194(-3)	2.267(-3)	3.938(-3)	2.413(-3)	4.506(-2)
7.4	2.393(-4)	4.762(-4)	5.776(-4)	3.845(-4)	2.958(-3)	1.362(-3)	3.940(-4)	2.400(-4)	1.806(-3)	3.142(-3)	2.530(-3)	3.812(-2)
7.6	2.009(-4)	4.039(-4)	4.893(-4)	3.737(-4)	2.468(-3)	1.276(-3)	3.215(-4)	1.070(-4)	1.445(-3)	2.525(-3)	2.301(-3)	3.305(-2)
7.8	1.695(-4)	3.432(-4)	4.178(-4)	3.539(-4)	2.056(-3)	1.194(-3)	2.566(-4)	8.677(-5)	1.162(-3)	2.045(-3)	2.036(-3)	2.882(-2)
8.0	1.438(-4)	2.921(-4)	3.597(-4)	3.314(-4)	1.710(-3)	1.110(-3)	2.081(-4)	5.409(-5)	9.385(-4)	1.669(-3)	1.792(-3)	2.514(-2)

Table 5.9 b

Total photoionization cross-sections (a_ν) in 10^{-18} cm^2 for transitions from the bound state $2p_o$ to the pure Landau continuum at B = 10^9G. The energy of the final state is E_f (γ Ry) where $\gamma = 4.25 \times 10^{-1}$ and the contribution $S^{(\ell,m)}$ is given by eq. (5.51).

E_f (γ Ry)	$S_\nu^{(0,-1)}$	$S_\nu^{(1,-1)}$	$S_\nu^{(2,-1)}$	$S_\nu^{(3,-1)}$	$S_\nu^{(0,0)}$	$S_\nu^{(1,0)}$	$S_\nu^{(2,0)}$	$S_\nu^{(3,0)}$	$S_\nu^{(0,1)}$	$S_\nu^{(1,1)}$	$S_\nu^{(2,1)}$	a_ν
1.0	∞	-	-	-	0	-	-	-	-	-	-	∞
1.2	7.824(-1)	-	-	-	7.127(-1)	-	-	-	-	-	-	1.796
1.4	4.168(-1)	-	-	-	6.717(-1)	-	-	-	-	-	-	1.387
1.6	2.588(-1)	-	-	-	4.946(-1)	-	-	-	-	-	-	1.015
1.8	1.716(-1)	-	-	-	3.922(-1)	-	-	-	-	-	-	8.005(-1)
2.0	1.187(-1)	-	-	-	3.486(-1)	-	-	-	-	-	-	6.975(-1)
2.2	8.491(-2)	-	-	-	3.237(-1)	-	-	-	-	-	-	6.396(-1)
2.4	6.242(-2)	-	-	-	2.941(-1)	-	-	-	-	-	-	5.840(-1)
2.6	4.697(-2)	-	-	-	2.536(-1)	-	-	-	-	-	-	5.142(-1)
2.8	3.601(-2)	-	-	-	2.068(-1)	-	-	-	-	-	-	4.332(-1)
2.99	2.837(-2)	-	-	-	1.635(-1)	-	-	-	-	-	-	3.556(-1)
3.0	2.802(-2)	∞	-	-	1.614(-1)	0	-	-	∞	-	-	∞
3.2	2.205(-2)	1.519(-1)	-	-	1.227(-1)	7.166(-2)	-	-	7.824(-1)	-	-	2.220
3.4	1.751(-2)	8.513(-2)	-	-	9.296(-2)	6.415(-2)	-	-	4.168(-1)	-	-	1.355
3.6	1.399(-2)	5.720(-2)	-	-	7.163(-2)	2.890(-2)	-	-	2.588(-1)	-	-	8.934(-1)
3.8	1.125(-2)	4.226(-2)	-	-	5.713(-2)	1.975(-2)	-	-	1.716(-1)	-	-	6.485(-1)
4.0	9.084(-3)	3.256(-2)	-	-	4.764(-2)	2.502(-2)	-	-	1.187(-1)	-	-	5.176(-1)
4.2	7.370(-3)	2.540(-2)	-	-	4.157(-2)	3.613(-2)	-	-	8.491(-2)	-	-	4.481(-1)
4.4	6.007(-3)	1.983(-2)	-	-	3.770(-2)	4.467(-2)	-	-	6.242(-2)	-	-	4.038(-1)
4.6	4.920(-3)	1.547(-2)	-	-	3.513(-2)	4.544(-2)	-	-	4.697(-2)	-	-	3.609(-1)

Table 5.10 a

E_f (γ Ry)	$S_\nu^{(0,-1)}$	$S_\nu^{(1,-1)}$	$S_\nu^{(2,-1)}$	$S_\nu^{(3,-1)}$	$S_\nu^{(0,0)}$	$S_\nu^{(1,0)}$	$S_\nu^{(2,0)}$	$S_\nu^{(3,0)}$	$S_\nu^{(0,1)}$	$S_\nu^{(1,1)}$	$S_\nu^{(2,1)}$	a_ν
4.8	4.050(-3)	1.213(-2)	-	-	3.324(-2)	3.903(-2)	-	-	3.601(-2)	-	-	3.127(-1)
4.99	3.385(-3)	9.725(-3)	-	-	3.166(-2)	2.986(-2)	-	-	2.837(-2)	-	-	2.659(-1)
5.0	3.353(-3)	9.616(-3)	∞	-	3.158(-2)	2.936(-2)	0	-	2.802(-2)	∞	-	∞
5.2	2.793(-3)	7.743(-3)	4.291(-2)	-	2.989(-2)	2.013(-2)	1.560(-2)	-	2.205(-2)	1.519(-1)	-	7.788(-1)
5.4	2.340(-3)	6.350(-3)	2.449(-2)	-	2.801(-2)	1.318(-2)	1.226(-2)	-	1.751(-2)	8.513(-2)	-	5.168(-1)
5.6	1.974(-3)	5.305(-3)	1.724(-2)	-	2.590(-2)	8.728(-3)	3.224(-3)	-	1.399(-2)	5.720(-2)	-	3.745(-1)
5.8	1.676(-3)	4.506(-3)	1.361(-2)	-	2.358(-2)	6.244(-3)	1.828(-3)	-	1.125(-2)	4.226(-2)	-	3.019(-1)
6.0	1.432(-3)	3.876(-3)	1.114(-2)	-	2.113(-2)	5.083(-3)	3.810(-3)	-	9.084(-3)	3.256(-2)	-	2.599(-1)
6.2	1.231(-3)	3.365(-3)	9.073(-3)	-	1.863(-2)	4.770(-3)	7.897(-3)	-	7.370(-3)	2.540(-2)	-	2.349(-1)
6.4	1.065(-3)	2.936(-3)	7.268(-3)	-	1.618(-2)	5.007(-3)	1.147(-2)	-	6.007(-3)	1.983(-2)	-	2.159(-1)
6.6	9.266(-4)	2.567(-3)	5.753(-3)	-	1.384(-2)	5.592(-3)	1.227(-2)	-	4.920(-3)	1.547(-2)	-	1.943(-1)
6.8	8.108(-4)	2.244(-3)	4.554(-3)	-	1.169(-2)	6.358(-3)	1.037(-2)	-	4.050(-3)	1.213(-2)	-	1.692(-1)
6.99	7.176(-4)	1.971(-3)	3.690(-3)	-	9.842(-3)	7.106(-3)	7.457(-3)	-	3.385(-3)	9.725(-3)	-	1.453(-1)
7.0	7.131(-4)	1.957(-3)	3.651(-3)	∞	9.751(-3)	7.144(-3)	7.301(-3)	0	3.353(-3)	9.616(-3)	∞	∞
7.2	6.301(-4)	1.702(-3)	2.995(-3)	1.565(-2)	8.053(-3)	7.810(-3)	4.492(-3)	4.638(-3)	2.793(-3)	7.743(-3)	4.291(-2)	3.366(-1)
7.4	5.591(-4)	1.475(-3)	2.526(-3)	9.113(-3)	6.596(-3)	8.249(-3)	2.556(-3)	3.224(-3)	2.340(-3)	6.350(-3)	2.449(-2)	2.334(-1)
7.6	4.980(-4)	1.274(-3)	2.191(-3)	6.622(-3)	5.369(-3)	8.403(-3)	1.470(-3)	5.718(-4)	1.974(-3)	5.305(-3)	1.724(-2)	1.798(-1)
7.8	4.450(-4)	1.096(-3)	1.946(-3)	5.431(-3)	4.355(-3)	8.260(-3)	9.687(-4)	3.106(-4)	1.676(-3)	4.506(-3)	1.361(-2)	1.536(-1)
8.0	3.988(-4)	9.417(-4)	1.759(-3)	4.601(-3)	3.528(-3)	7.850(-3)	8.177(-4)	1.005(-3)	1.432(-3)	3.876(-3)	1.114(-2)	1.373(-1)

Table 5.10 b

Total photoionization cross-sections (a_ν) in 10^{-18}cm^2 for transitions from the bound state $1s_o$ to the pure Landau continuum at $B = 10^9$G. The energy of the final state is E_f (γ Ry) where $\gamma = 4.25 \times 10^{-1}$ and the contribution $S^{(\ell,m)}$ is given by eq. (5.51).

Energy of final State in a.u.	Energy of Final State in γ Ry				Photoionization Cross Sections from "$1s_o$" ($10^{-18}cm^2$)	Photoionization Cross Sections from "$2p_o$" ($10^{-18}cm^2$)
	$B = 10^7G$	$B = 10^8G$	$B = 5 \times 10^8G$	$B = 10^9G$		
0	0	0	0	0	6.30	1.35(1)
0.005	2.35	0.24	0.047	0.024	6.22	1.33(1)
0.010	4.70	0.47	0.094	0.047	6.14	1.31(1)
0.020	9.40	0.94	0.188	0.094	5.98	1.28(1)
0.040	18.80	1.88	0.376	0.19	5.68	1.20(1)
0.080	37.61	3.76	0.752	0.38	5.13	1.07(1)
0.160	75.21	7.52	1.50	0.75	4.23	8.57
0.320	150.43	15.04	3.01	1.50	2.98	5.72
0.640	300.86	30.09	6.02	3.01	1.63	2.86
1.280	601.71	60.17	12.03	6.02	6.40(-1)	9.72(-1)
2.560	1203.42	120.34	48.14	12.03	1.74(-1)	2.14(-1)

Table 5.11

Zero-field photoionization cross-sections from $1s_o$ and $2p_o$, as calculated by Burgess, 1964 for various final state energies. The energies of the final states are given in a.u., and in units of γ Ry for the field strengths 10^7, 10^8, 5×10^8 and 10^9G.

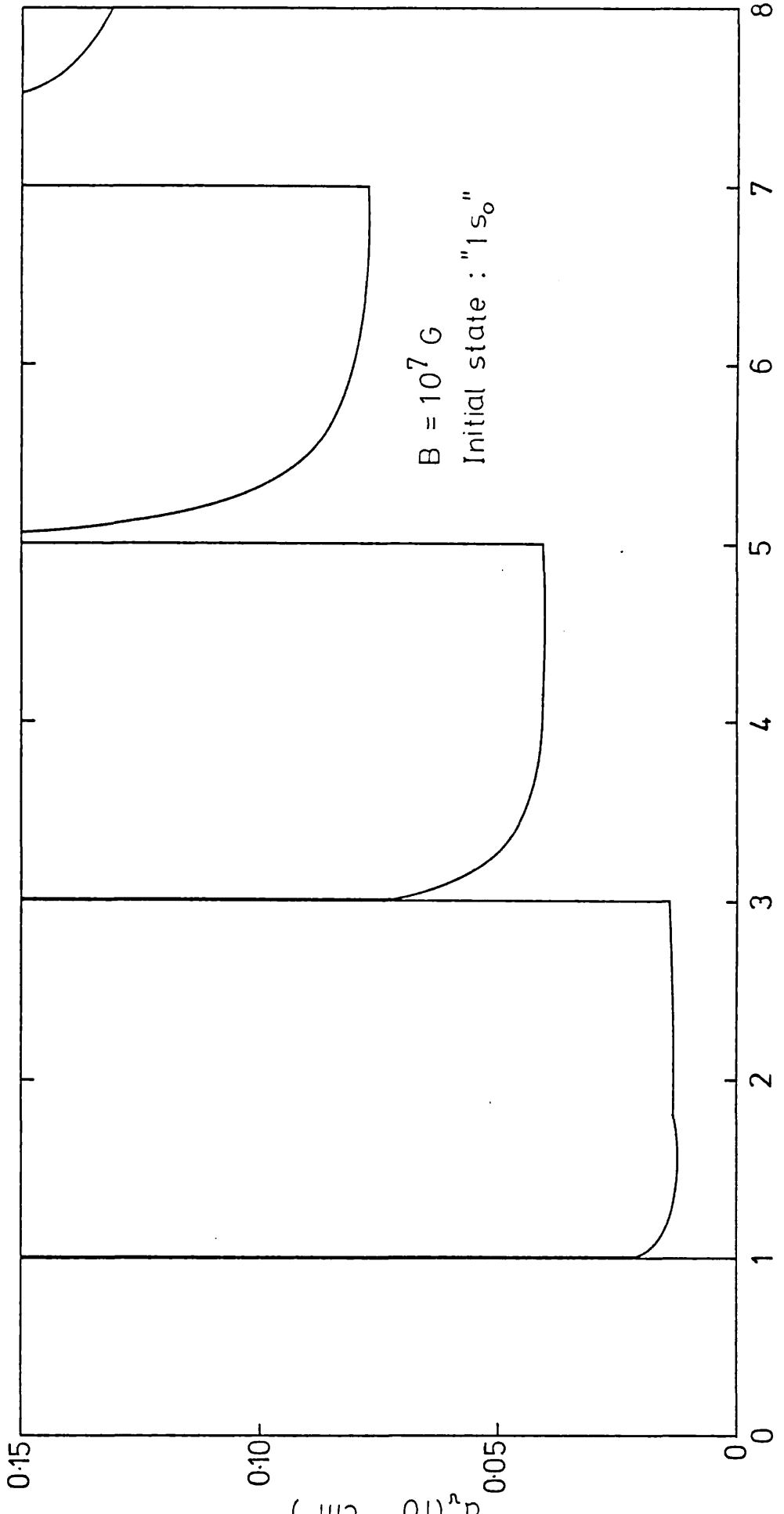
0·15
0·10
0·05
0
$\sigma_\gamma (10^{-18}$ cm^2)
0
1
2
3
4
5
6
7
8
ENERGY (δry)
B = 10^7 G
Initial state : "$1s_o$"

Fig 5.2

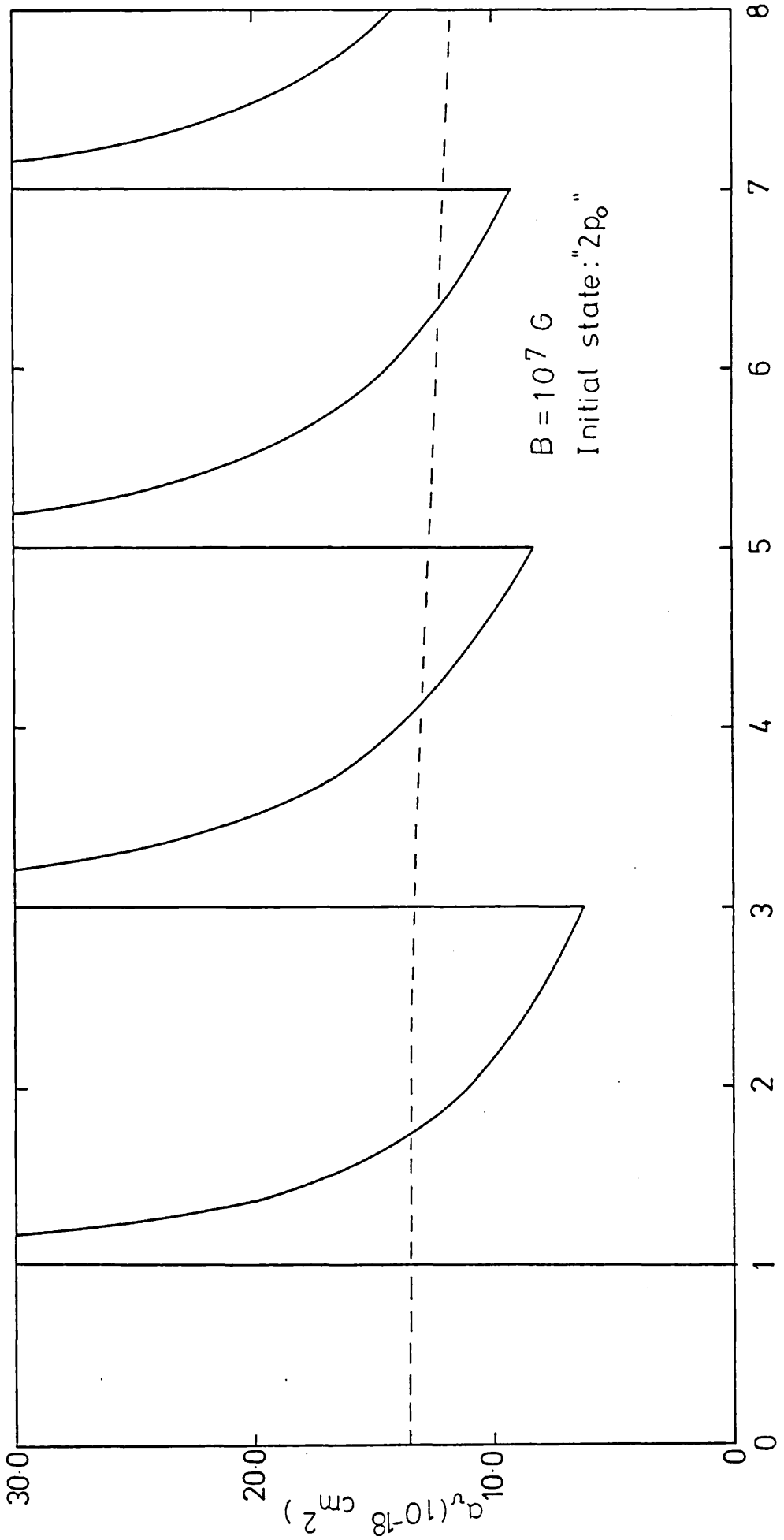
B = 10^7 G
Initial state: "2p0"
ENERGY (x ry)
0
1
2
3
4
5
6
7
8
0
10·0
20·0
30·0
σν (10^-18 cm^2)

Fig 5.3

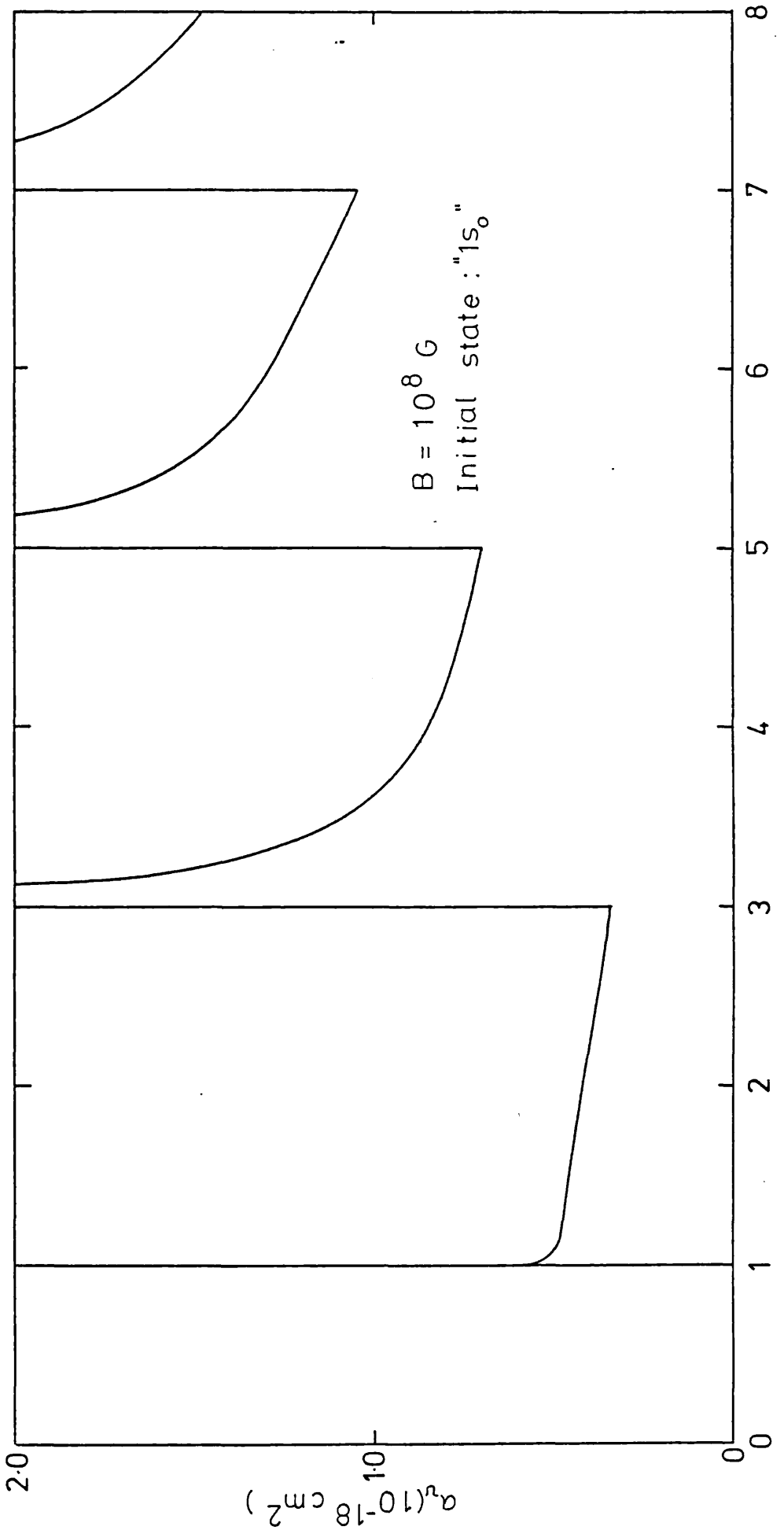
$B = 10^8$ G
Initial state : "$1s_o$"
$a_u(10^{-18}\ cm^2)$
2·0
1·0
0
0
1
2
3
4
5
6
7
8
ENERGY (Ry)

Fig 5.4

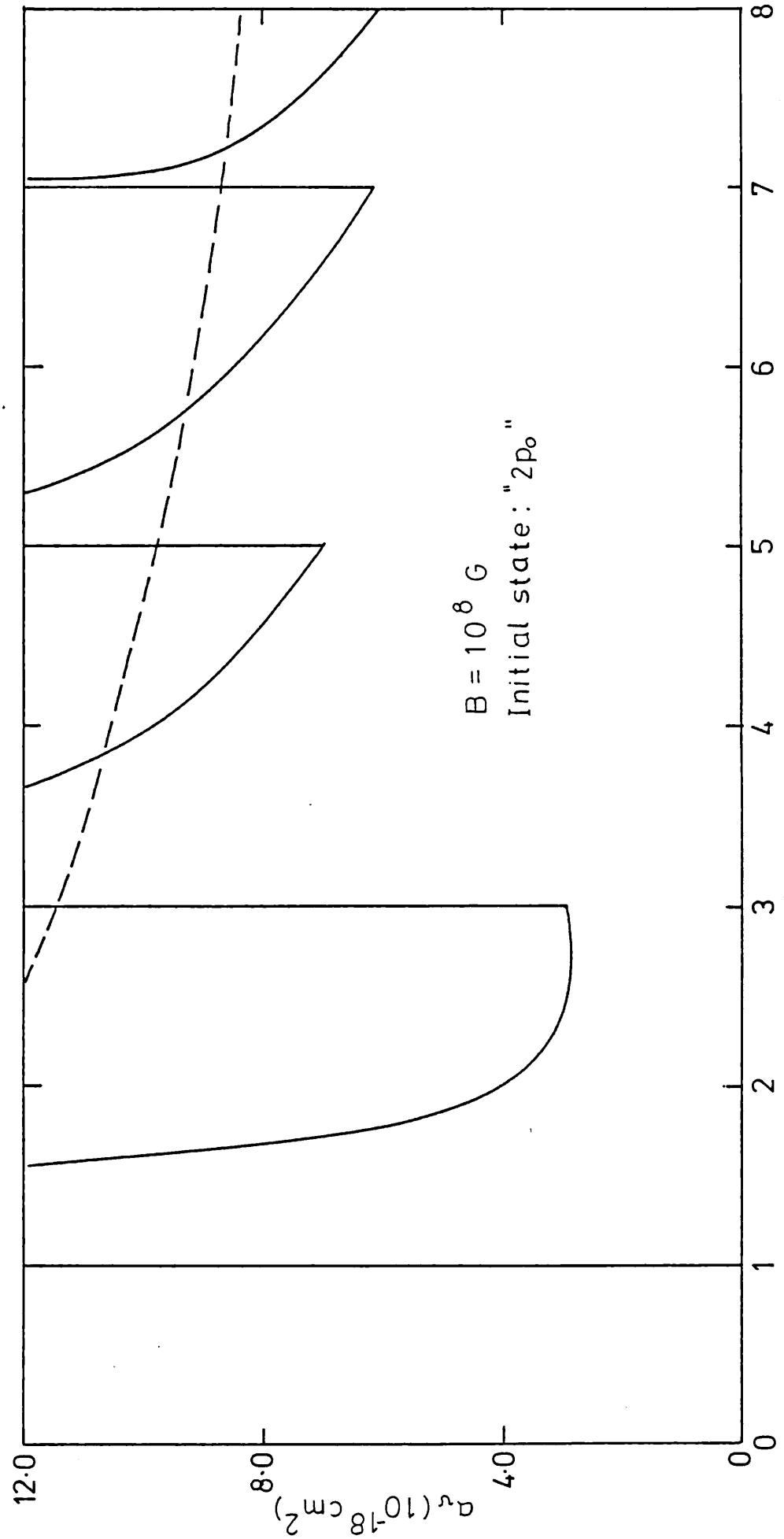
12·0
8·0
4·0
0
a_ν (10^{-18} cm^2)
0
1
2
3
4
5
6
7
8
ENERGY (Ry)
B = 10^8 G
Initial state: "$2p_o$"

Fig 5.5

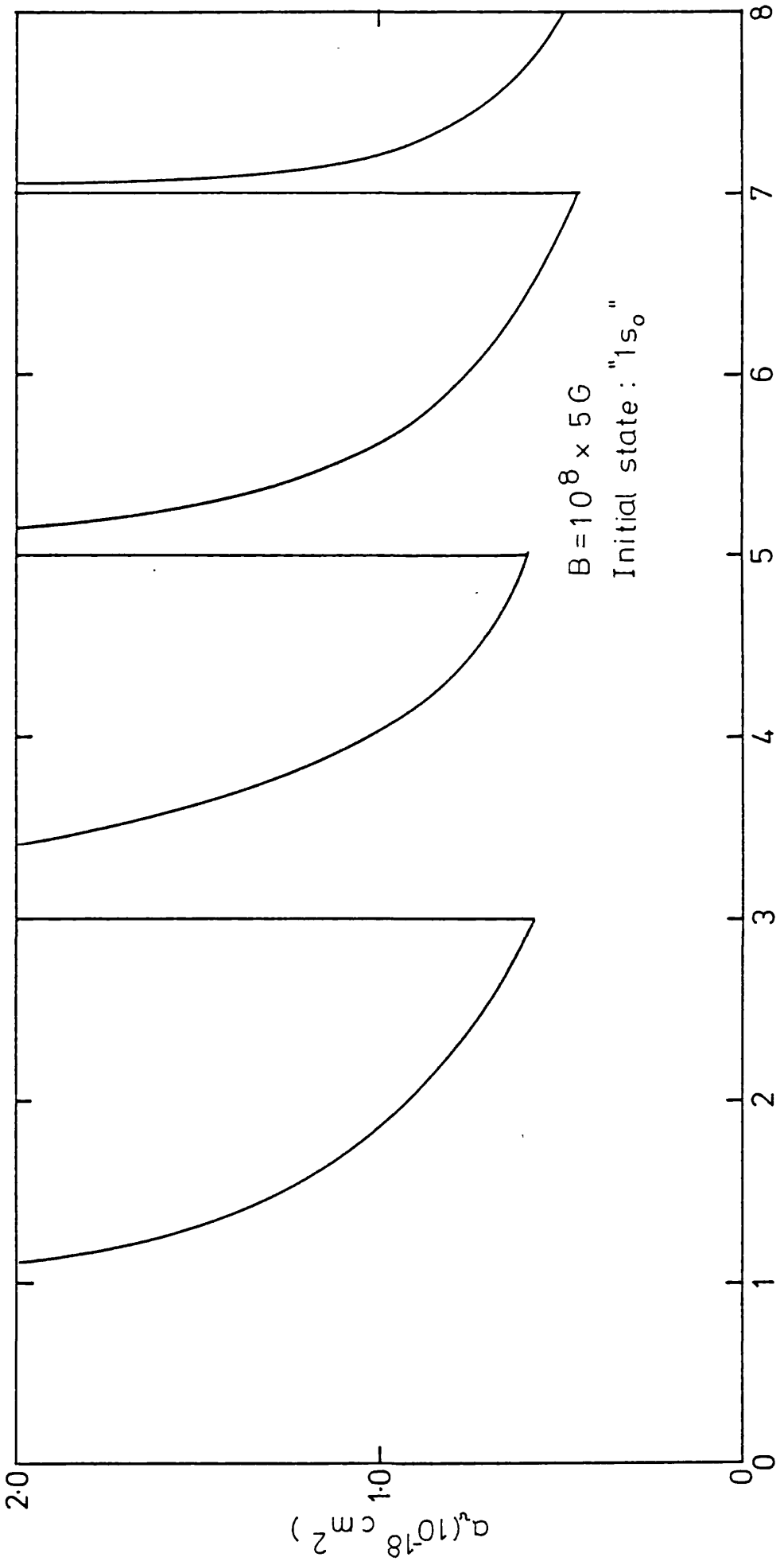
$B = 10^8 \times 5$ G
Initial state : "$1s_o$"
$\alpha_2 (10^{-18}$ cm^2)
2·0
1·0
0
0
1
2
3
4
5
6
7
8
ENERGY (Ry)

Fig 5.6

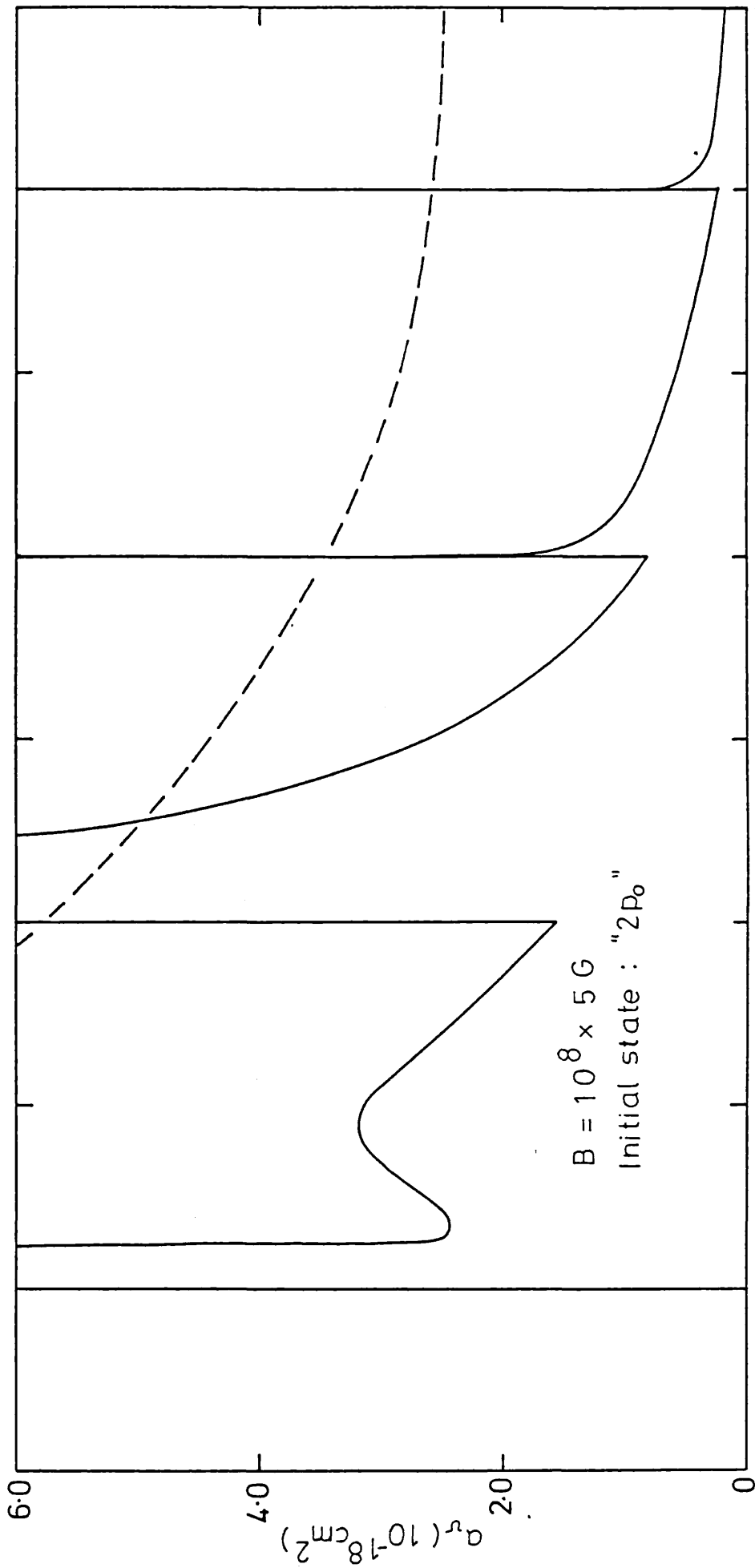
$B = 10^8 \times 5$ G
Initial state : "$2p_o$"
Q_r (10^{-18} cm^2)
0·9
0·7
4·0
2·0
0
1
2
3
4
5
6
7
8
ENERGY (× ry)

Fig 5.7

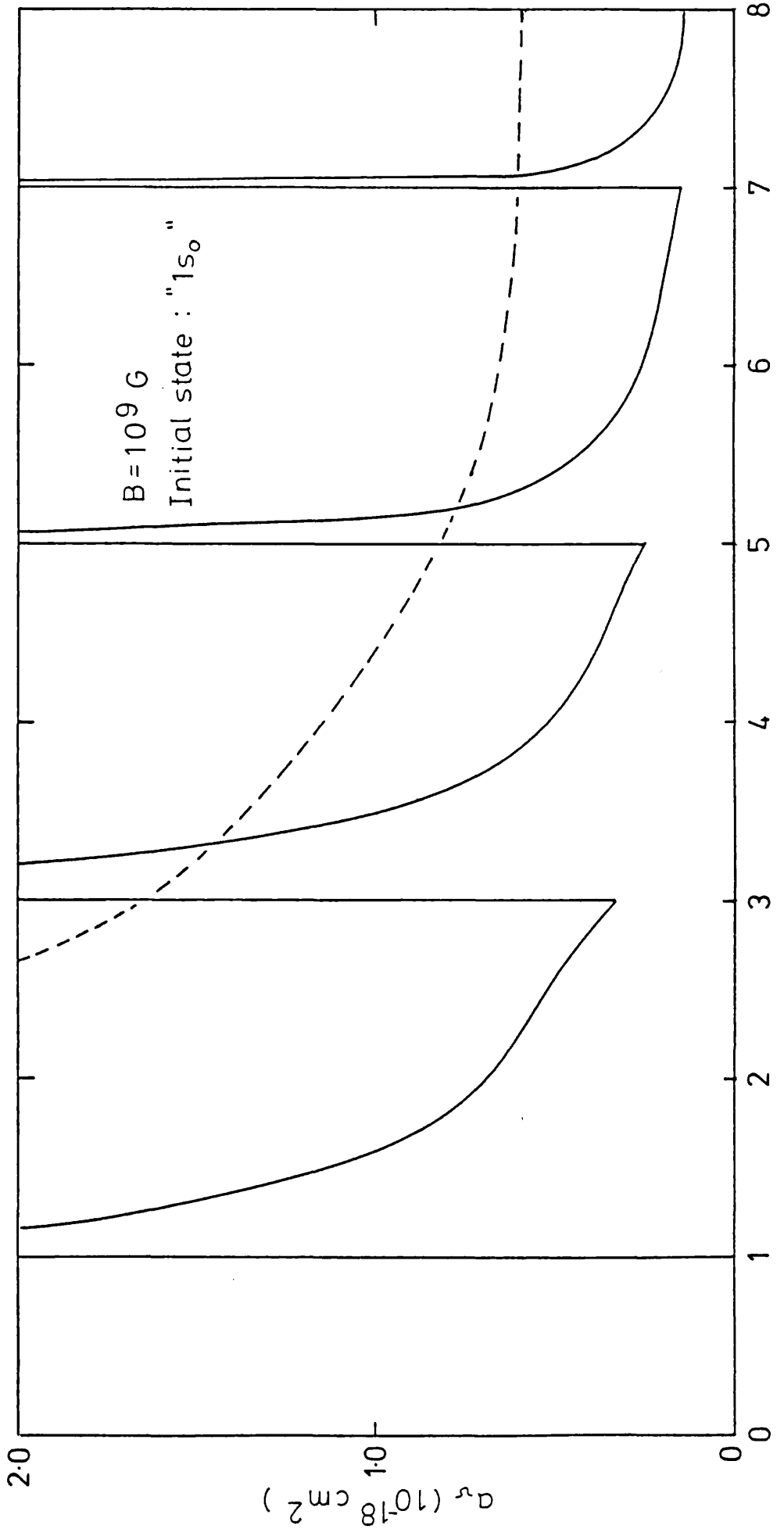
B=10^9 G
Initial state : "1s_o"
2·0
1·0
0
0
1
2
3
4
5
6
7
8
ENERGY (Ry)
a_s (10^-18 cm^2)

Fig 5.8

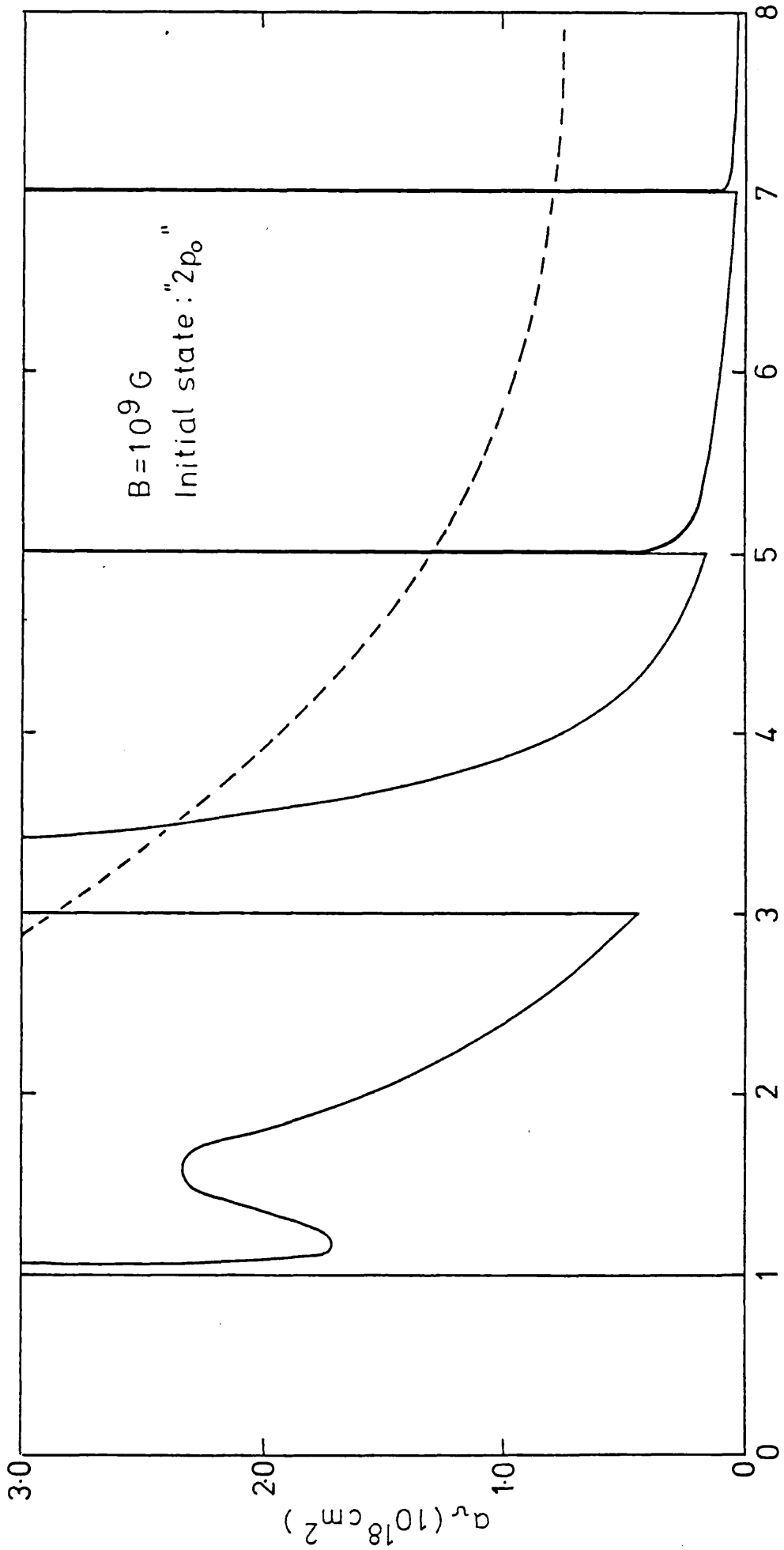
B=10^9 G
Initial state: "2p_o"
3·0
2·0
1·0
0
0
1
2
3
4
5
6
7
8
ENERGY (γry)
a_γ (10^18 cm^2)

Fig 5.9

Figure 5.2

The photoionization cross-section ($10^{-18}cm^2$) from "$1s_o$" to the Landau continuum at $B = 10^7G$.

Figure 5.3

The photoionization cross-section ($10^{-18}cm^2$) from "$2p_o$" to the Landau continuum at $B = 10^7G$.

The zero field cross-section is given by the broken line.

Figure 5.4

The photoionization cross-section ($10^{-18}cm^2$) from "$1s_o$" to the Landau continuum at $B = 10^8G$.

Figure 5.5

The photoionization cross-section ($10^{-18}cm^2$) from "$2p_o$" to the Landau continuum at $B = 10^8G$.

The zero field cross-section is given by the broken line.

Figure 5.6

The photoionization cross-section ($10^{-18}cm^2$) from "$1s_o$" to the Landau continuum at $B = 5 \times 10^8G$.

Figure 5.7

The photoionization cross-section ($10^{-18}cm^2$) from "$2p_o$" to the Landau continuum at $B = 5 \times 10^8G$.

The zero field cross-section is given by the broken line.

Figure 5.8

The photoionization cross-section ($10^{-18}cm^2$) from "$1s_o$" to the Landau continuum at $B = 10^9G$.

The zero field cross-section is given by the broken line.

Figure 5.9

The photoionization cross-section ($10^{-18}cm^2$) from "$2p_o$" to the Landau continuum at $B = 10^9G$.

The zero field cross-section is given by the broken line.

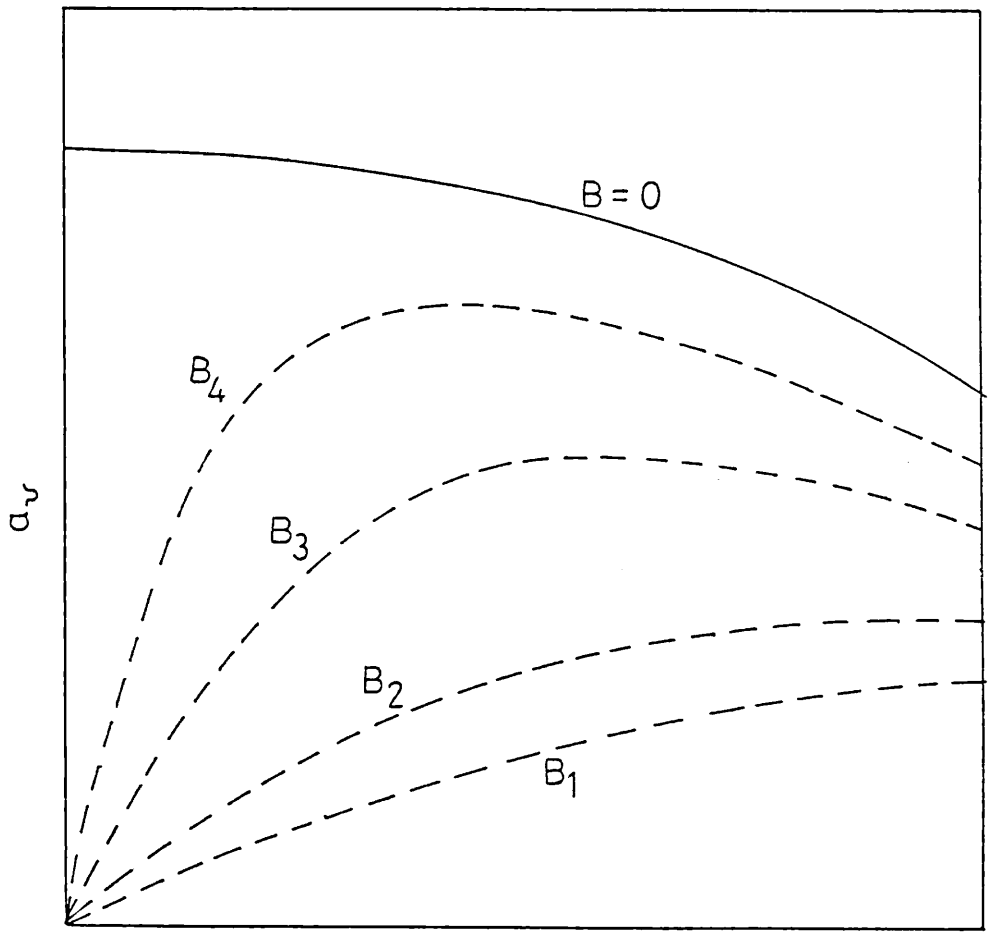

Fig 5.10

Schematic diagram to show how the "average" smooth curve superimposed on the photoionization cross-sections, tends to the zero field limit. $B_1 < B_2 < B_3 < B_4$.

at B = 10^8G, for photoionization from the "$1s_o$" state, the contribution from the (2,0) state has a maximum between the Landau energies 5γ and 7γ Ry, however, a_ν is monotonic and decreasing in this region (figure 5.4). A secondary maximum can occur if the terms corresponding to a particular Landau level have a maximum between two Landau energies and if these terms contribute significantly to the total cross-section. For example, the case where there are only two contributions to the total cross-section from the Landau levels (0,-1) and (0,0) at B = 10^9G for photoionization from the "$1s_o$" state. Here, a maximum occurs between the 2 Landau energies at γ Ry and 3γ Ry (figure 5.8), caused by a maximum occurring in the contribution from the state (0,0). It is shown in section §5.6 how these secondary maxima arise for a Landau continuum function and very simple model functions for the bound states. The actual location and shape of the secondary maxima depend, in a sensitive manner, on the details of the wavefunctions.

§5.6 Secondary Maxima in a_ν

In this model

$$a_\nu \propto \frac{h\nu}{k_z} \sum_{\ell} |R(\beta', m_f, \delta, \gamma)\ Z(\alpha', \delta, k_z)\ d_{\alpha\beta\delta}|^2 \qquad (5.56)$$

and $$\alpha' = \begin{cases} \alpha+1 \\ \alpha \end{cases} \quad \beta' = \begin{cases} \beta-1 \\ \beta \end{cases} \text{ when } \Delta m = \begin{cases} 0 \\ \pm 1 \end{cases} \qquad (5.57)$$

We are interested in the variation with $h\nu$ in the energy range $I_x + E_\ell \leq h\nu$, where I_x is the ionization potential, and we write $h\nu = I_x + E_\ell + k_z^2$. The $h\nu$ dependence of a_ν is obtained by considering

$$a_\nu^{(\ell)}(E) = \frac{AE}{(E-X)^{\frac{1}{2}}}\ Z(\alpha', \delta, (E-X)^{\frac{1}{2}})^2 \qquad (5.58)$$

where $a_\nu^{(\ell)}$ is the contribution from the ℓ'th Landau level, $h\nu$ has been replaced by E, $X = I_x + E_\ell$ and A is independent of E. We illustrate the behaviour of $a_\nu^{(\ell)}(E)$ by considering only simple bound state wave functions of the form

$$|1s_o\rangle = N_1 e^{-\delta r^2}$$

$$|2p_o\rangle = N_2 z e^{-\delta r^2} \qquad (5.59)$$

There are four cases to consider:

Case I: $m_f = 0$, initial state has even parity, ie is $|1s_o\rangle$

$$a_\nu^{(\ell)}(E) = \frac{AE}{(E - X)^{\frac{1}{2}}} Z(1, \delta, (E - X)^{\frac{1}{2}})^2. \qquad (5.60)$$

Thus

$$a_\nu^{(\ell)}(E) = A'E (E - X)^{\frac{1}{2}} e^{-(E-X)/2\delta} \qquad (5.61)$$

where A' is also independent of E. Now differentiating $a_\nu^{(\ell)}(E)$ with respect to E, we find that there are two stationary points occurring at

$$E = \tfrac{1}{2}\{(3\delta + X) \pm \sqrt{9\delta^2 + X^2 - 2\delta X}\} \qquad (5.62)$$

providing $(9\delta^2 + X^2 - 2\delta X) > 0$. From Table 3 it can be seen that the dependence of a_ν on k_z in the region $k_z^2 \sim 0$, for this case, is as k_z. Therefore, close to the Landau energy E_ℓ, $a_\nu^{(\ell)}$ is an increasing function, and so the first stationary point will be a maximum and the second a minimum. If $(9\delta^2 + X^2 - 2\delta X) \neq 0$, then $a_\nu^{(\ell)}(E)$ is a monotonic increasing function (in this simple approximation).

Case II: $m_f = \pm 1$, initial state has even parity,

$$a_\nu^{(\ell)}(E) = \frac{AE}{(E - X)^{\frac{1}{2}}} [Z(0, \delta, (E - X)^{\frac{1}{2}})]^2 \qquad (5.63)$$

Thus

$$a_\nu^{(\ell)}(E) = A''E (E - X)^{-\frac{1}{2}} e^{-(E-X)/2\delta} \qquad (5.64)$$

Again, differentiating $a_\nu^{(\ell)}(E)$ with respect to E, we find that there are two stationary points occurring at

$$E = \tfrac{1}{2}\{(X - \delta) \pm \sqrt{X^2 + \delta^2 - 6\delta X}\} \qquad (5.65)$$

providing $(X^2 - \delta^2 - 6\delta X) > 0$. From Table 3, it can be seen that, close to the Landau energy, the dependence of $a_\nu^{(\ell)}$ on k_z is k_z^{-1} and therefore the function is decreasing with increasing k_z in this region.

The first stationary point will then be a minimum and the second a maximum. If $(X^2 - \delta^2 - 6\delta X) \not> 0$, then $a_\upsilon^{(\ell)}$ will be a monotonic decreasing function.

Case III: $m_f = \pm 1$, initial state has odd parity, ie is $2p_o$

$$a_\upsilon^{(\ell)}(E) = \frac{AE}{(E-X)^{\frac{1}{2}}}\left[Z(1, \delta, (E-X)^{\frac{1}{2}})\right]^2 \qquad (5.66)$$

This expression is exactly the same as that given by (5.60) and so the stationary points are given by (5.62). From Table 3 it is seen that the behaviour close to the Landau energy is the same as that of Case I and so, as in Case I, the first stationary point is a maximum and the second a minimum and $a_\upsilon^{(\ell)}$ is a monotonic increasing function if the stationary points do not exist.

Case IV: $m_f = 0$, initial state has odd parity.

In this case

$$a_\upsilon^{(\ell)}(E) = \frac{AE}{(E-X)^{\frac{1}{2}}}\left[1 - \frac{1}{\delta}(E-X) + \frac{1}{4\delta^2}(E-X)^2\right] e^{-(E-X)/2\delta} \qquad (5.67)$$

so again a_υ decreases immediately above a threshold. We can write

$$a_\upsilon^{(\ell)}(E) = \frac{A}{2\delta}\,\frac{e^{-y}}{y}\,(a_o y^3 + a_1 y^2 + a_2 y + a_3) \qquad (5.68)$$

with $y = (E-X)/2\delta$. The behaviour is complicated, and one or more turning points may occur. If there are two positive roots of the cubic, then a secondary maximum occurs. The overall result, however, is that found in cases II and IV, that secondary maxima can occur both for odd and even parity initial states.

CHAPTER 6

Photoionization Cross-Sections Where The Continuum Is Modified By The Coulomb Attraction Of The Nucleus

§6.1 Introduction

For fields in which the magnetic field strength does not entirely dominate the Coulomb attraction of the nucleus, it is shown, in this chapter, that the Coulomb force has a significant effect on the structure of the continuum and that this, in turn, has a significant effect on the photoionization cross-sections. The inclusion of the Coulomb term in the calculation of the continuum wavefunctions, however, renders the Schrodinger equation,

$$H \psi^{(\ell)}_{k_z,m} = E_\ell \psi^{(\ell)}_{k_z,m} \qquad (6.1)$$

inseparable, and so some approximation must be made in order to overcome this problem. We follow Starace (1973) and Rau (1979) in supposing that the main effect of the Coulomb interaction is to restrict the continuum electrons' motion perpendicular to the field lines, which is uncoupled from the motion along the field lines. This approximation is excellent at low fields, and gives the observed $1.5\hbar\omega_c$ splitting of the embedded levels near the ionization threshold (Garton and Tomkins, 1969).

It is found that the Coulomb modified continuum wavefunctions remain unchanged in their z and ϕ dependence but that their radial dependence is no longer analytic, being calculated in numerical form. The method used in calculating these wavefunctions and their corresponding energies is described in detail in section §6.2 and results are presented graphically for a few of the radial functions.

The photoionization cross-sections are calculated in a very similar way to those of the pure Landau case in §6.3. The only difference being in the evaluation of the ρ integral occurring in the expression for $|R_{if}|^2$. It is shown that within this model the same threshold law holds as for the

pure Landau case despite the inclusion of a radial Coulomb attraction, since, in the present Coulomb-modified model, the only k_z^2 dependence of the dipole matrix element arises from the motion along the field. In practice, the reservations outlined in §5.4 may modify this result. Detailed results are tabulated for the cross-sections and their individual contributions and the total cross-sections are also plotted in figures (6.15)-(6.22).

§6.2 Calculation of the Free Wavefunctions

6.2.1 Basic Method

The wavefunctions and energies of the continuum states, ie those corresponding to the Coulomb-modified Landau levels, are given by the solutions of the Schrodinger equation

$$\left\{ -\frac{\partial^2}{\partial\rho^2} - \frac{1}{\rho}\frac{\partial}{\partial\rho} - \frac{1}{\rho^2}\frac{\partial^2}{\partial\phi^2} - \frac{\partial^2}{\partial z^2} + \frac{\gamma}{i}\frac{\partial}{\partial\phi} + \frac{\gamma^2\rho^2}{4} - \frac{2\alpha_0}{r} \right\} \psi^{(l)}_{k_z,m}(\underline{r}) = E^{(l)}\psi^{(l)}_{k_z,m}(\underline{r}) \quad (6.2)$$

where α_0 is the residual charge on the ion. The continuum functions may be written in the form

$$\psi^{(l)}_{k_z,m}(\underline{r}) = C\,\rho^{-\frac{1}{2}} f^{(l)}(\rho,z)\, e^{im\phi} \quad (6.3)$$

so that f satisfies

$$\left\{ -\frac{\partial^2}{\partial\rho^2} - \frac{\partial^2}{\partial z^2} + \left(V(\rho,z) - E_1^{(l)} \right) \right\} f^{(l)}(\rho,z) = 0 \quad (6.4)$$

with $E_1^{(l)} = E^{(l)} - m\gamma$ (6.5)

and $$V(\rho,z) = \frac{m^2-\frac{1}{4}}{\rho^2} + \frac{\gamma^2\rho^2}{4} - \frac{2\alpha_0}{r}\,. \quad (6.6)$$

Now, in order that equation (6.4) be separable, and that a solution $f^{(l)}(\rho,z)$ be found, it is convenient to approximate the Coulomb term by $\frac{2\alpha_0}{\rho}$, ie we put z = 0 in the Coulomb interaction. A full discussion of this approximation is given by Starace (1973) and Rau (1979). We can now write $V(\rho,z) = V(\rho)$ and the equation becomes separable so that writing

$$f^{(l)}(\rho,z) = u_l(\rho)\,Z(z) \quad (6.7)$$

we have the following equations for u and Z:

$$\frac{d^2}{dz^2} Z(z) = h_\ell(\rho)\, Z(z) \tag{6.8}$$

and $$\left\{\frac{d^2}{d\rho^2} + V_1(\rho)\right\} u_\ell(\rho) = 0 . \tag{6.9}$$

In equation (6.8) we have written

$$h_\ell(\rho) = -\frac{\partial^2}{\partial\rho^2} + V(\rho) - E_1^{(\ell)} \tag{6.10}$$

and in (6.9) we write

$$V_1(\rho) = E_1^{(\ell)} - V(\rho) . \tag{6.11}$$

Solving equation (6.8) we find that $Z(z)$ is of the form

$$Z(z) = Ae^{ik_z z} \tag{6.12}$$

where A is constant with respect to z.

Solving equation (6.9), however, is not nearly so simple. This equation is an eigenvalue equation having eigenvalues $E_1^{(\ell)}$ with the boundary conditions that the wavefunctions vanish at $\rho = 0$ and ∞

ie $$u_\ell(0) = u_\ell(\infty) = 0. \tag{6.13}$$

The solutions, are, of course, the Landau functions given by equation (5.16) if $\alpha_o = 0$, the Schrodinger equation reducing to the form of equation (5.10) in this case.

Starace (1973) and Rau (1979) used a JWKB approximation to $u_\ell(\rho)$ but for our purposes this is unnecessary. As the integrals occurring in the photoionization cross-section must be evaluated numerically, it is more convenient to find an exact numerical solution for $u_\ell(\rho)$ from equation (6.9). It can be shown that these numerical solutions reduce to the pure Landau solutions in the case $\alpha_o = 0$. Equation (6.9) can be rewritten as a system of first order, ordinary differential equations:

$$\left.\begin{aligned} u_1'(\rho) &= u_2(\rho) \\ u_2'(\rho) &= -V_1(E_1, \rho)\, u_1(\rho) \end{aligned}\right) \tag{6.14}$$

where $u_1(\rho) = u(\rho)$, primes denote differentiation with respect to ρ, and the boundary conditions are given by (6.13).

Basically, the method used in solving (6.14) is to integrate outwards from $\rho = 0$ and inwards from some large value of ρ, say $\rho = R$, using a Runge-Kutta technique (Mayers, 1962) with initial estimates for the eigenvalue and boundary conditions on $u_2(\rho)$. The solutions are then matched at some point between 0 and R, a second approximation to the eigenvalue and boundary conditions on $u_2(\rho)$ are found such that $u_1(\rho)$ and its first derivative are continuous at the matching point, and the process is then repeated with the new estimated values for E_1, $u_2(0)$ and $u_2(R)$ (Hartree, 1955).

The matching point is denoted by ρ_o, the outward solution (ie that found between 0 and ρ_o) by $u_{1(out)}$ and the inward solution (ie that found between R and ρ_o) by $u_{1(in)}$. Now $u_{1(out)}$ and $u_{1(in)}$ are arbitrary to the extent of a multiplying constant, and so we can write

$$\left.\begin{aligned} u_{1(out)} &= AU_{1(out)} \\ u_{1(in)} &= BU_{1(in)} \end{aligned}\right\} \qquad (6.15)$$

The total wavefunction $u_1(\rho)$ must be normalized, ie

$$\int_0^{\rho_o} \left[u_{1(out)}(\rho) \right]^2 d\rho + \int_{\rho_o}^{R} \left[u_{1(in)}(\rho) \right]^2 d\rho = 1. \qquad (6.16)$$

Also, the following condition must be satisfied in order that the function be continuous and have continuous gradient at the matching point:

$$\frac{u'_{1(out)}(\rho_o)}{u_{1(out)}(\rho_o)} = \frac{u'_{1(in)}(\rho_o)}{u_{1(in)}(\rho_o)} \qquad (6.17)$$

A and B are chosen such that the inward and outward solutions meet at ρ_o, ie such that $u_{1(out)}(\rho_o) = u_{1(in)}(\rho_o)$ and also such that the normalizing condition is satisfied, ie

$$B = A \frac{U_{1(out)}(\rho_o)}{U_{1(in)}(\rho_o)} \qquad (6.18)$$

and

$$A^2 \int_0^{\rho_o} \left[U_{1(out)}(\rho) \right]^2 d\rho + B^2 \int_{\rho_o}^{R} \left[U_{1(in)}(\rho) \right]^2 d\rho = 1. \quad (6.19)$$

We now define N as

$$N = \left\{ \int_0^{\rho_o} \left[\frac{U_{1(out)}(\rho)}{U_{1(out)}(\rho_o)} \right]^2 d\rho + \int_{\rho_o}^{R} \left[\frac{U_{1(in)}(\rho)}{U_{1(in)}(\rho_o)} \right]^2 d\rho \right\}^{-\frac{1}{2}} \quad (6.20)$$

and from equations (6.18) - (6.20) we obtain

$$A = \frac{N}{U_{1(out)}(\rho_o)} \quad (6.21)a$$

and

$$B = \frac{N}{U_{1(in)}(\rho_o)} . \quad (6.21)b$$

Now Hartree, 1955 considers a similar problem and obtains the following expression for the new approximation for the eigenvalue such that the matching condition at ρ_o (ie equation (6.18)) is satisfied. Let the eigenvalue E_1 be changed by an amount ΔE_1, so that the new eigenvalue is $E_1 + \Delta E_1$ (ΔE_1 can, of course, be positive or negative), then from Hartree, 1955

$$\left[\frac{u_{1(in)}}{u_{1(in)}} - \frac{u_{1(out)}}{u_{1(out)}} \right]_{\rho=\rho_o} = \left[\frac{\int_0^{\rho_o} (u_{1(out)}(\rho))^2 d\rho}{(u_{1(out)}(\rho_o))^2} + \frac{\int_{\rho_o}^{R} (u_{1(in)}(\rho))^2 d\rho}{(u_{1(in)}(\rho_o))^2} \right] \Delta E_1 \quad (6.22)$$

ie

$$\Delta E_1 = N^2 \left[\frac{u'_{1(in)}}{u_{1(in)}} - \frac{u'_{1(out)}}{u_{1(out)}} \right]_{\rho = \rho_o} . \quad (6.23)$$

In order to choose successive approximations for the gradient at 0 and R (ie to obtain boundary conditions on $u_2(\rho)$), we consider

$$u_{2(in)}(R) = u'_{1(in)}(R) = B U'_{1(in)}(R) \quad (6.24)$$

Now we choose a first approximation for $u'_{1(in)}(R)$ as being unity (this is not necessarily a good approximation), and this leads us to choose, as a second approximation for $u'_{1(in)}(R)$,

$$u_{2(in)}(R) = B = \frac{N}{U_{1(in)}(\rho o)} \quad . \tag{6.25}$$

Similarly, we can choose as a second approximation for $u_{2(out)}(0)$, after an initial approximation of 1,

$$u_{2(out)}(0) = A = \frac{N}{U_{1(out)}(\rho o)} \tag{6.26}$$

To summarize, after the first trial integration with eigenvalue E_1 and boundary conditions

$$u_1(0) = u_1(R) = 0$$

and $$u_2(0) = u_2(R) = 1$$

in the limit as $R \to \infty$, the resulting function $u_1(\rho)$ contains a mismatch at ρo. In order to attempt to obtain a function which is continuous and has continuous first derivative at ρo, we take a second approximation to the eigenvalue, $E_1 + \Delta E_1$, and choose new boundary conditions

$$u_1(0) = u_1(R) = 0$$

and $$u_2(0) = A \ , \quad u_2(R) = B \quad .$$

We continue to take successive approximations in this way until convergence on the eigenvalue is obtained and the inward and outward functions $u_{1(in)}$ and $u_{1(out)}$ and their first derivatives, are equal at ρo.

The numerical integrations (both inward and outward) are actually carried out using Merson's method, a variation on the standard Runge-Kutta method (Lambert, 1973, Ch.4). The variation involves altering the steplength at each calculation in order to keep the solution within given error bounds. This method is carried out in the NAG library subroutine D02ABF. The integrals involved in the calculation of N (equation (6.20)) are also calculated numerically by the method described by Gill and Miller,1972, using the NAG library subroutine D01GAF .

The program which calculates these continuum functions is WFCOUL and is described in more detail in Appendix (I).

6.2.2. Starting the Outward Integration

As $V_l(\rho)$ has a singularity at $\rho = 0$, an approximation for $u_l(\rho)$ using a series expansion must be found in this region. The Schrödinger equation can be rewritten

$$\rho^2 \frac{d^2 u_l}{d\rho^2} + \left\{ E_l \rho^2 + 2\alpha_o \rho - (m^2 - 1/4) \right\} u_l = 0 \qquad (6.27)$$

ie
$$\rho^2 \frac{d^2 u_l}{d\rho^2} + r(\rho)\, u_l = 0 \qquad (6.28)$$

where
$$r(\rho) = \sum_{p=0}^{2} r_p \rho^p \qquad (6.29)$$

with
$$\left.\begin{aligned} r_o &= -m^2 + 1/4 \\ r_1 &= 2\alpha_o \\ r_2 &= E_l . \end{aligned}\right\} \qquad (6.30)$$

Now writing u_l as a series in ρ, we have

$$u_l = \sum_{n=0}^{\infty} a_n \rho^{n+s} . \qquad (6.31)$$

On substituting equation (6.31) into equation (6.28), it is seen that

$$\sum_{n=0}^{\infty} a_n (s+n)(s+n-1) \rho^n + \sum_{p=0}^{2} \sum_{n=0}^{\infty} a_n r_p \rho^{n+p} = 0 . \qquad (6.32)$$

Matching the coefficients of the powers of ρ in the two series in the above expression, we obtain the following conditions which must be satisfied:

(i) for the coefficient of ρ^o : $a_o s(s-1) + a_o r_o = 0$

(ii) for the coefficient of ρ^1 : $a_1(s-1)s + a_1 r_o + a_o r_1 = 0$

(iii) for the coefficient of ρ^k $(k \geq 2)$:

$$a_k(s + k)(s + k - 1) + a_k r_o + a_{k-1} r_1 + a_{k-2} r_2 = 0 .$$

Now condition (i) gives

$$r_o = -s(s-1) \qquad (6.33)$$

ie
$$s = \tfrac{1}{2} \pm m . \qquad (6.34)$$

The regular solution for $u_l(\rho)$ is obtained when s is given its highest value, ie when

$$s = \tfrac{1}{2} + |m| . \qquad (6.35)$$

Solving the equations in a_1, a_2..... successively, substituting in this value for s, the following results for a_1, a_2 and a_3 are obtained. As we are only considering this series expansion as a solution close to $\rho = 0$, we neglect terms of order ρ^4 and higher.

$$a_1 = -\frac{2\alpha_o}{1+2|m|}\, a_o = b_1 a_o \qquad (6.36)a$$

$$a_2 = \frac{(4\alpha_o^2 - E_1(1+2|m|))}{4(1+2|m|)(1+|m|)}\, a_o = b_2 a_o \qquad (6.36)b$$

$$a_3 = \frac{(\alpha_o E_1 (6|m|+5) - 4\alpha_o^3)}{6(1+2|m|)(1+|m|)(3+2|m|)}\, a_o = b_3 a_o \,. \qquad (6.36)c$$

We now have the solution

$$u_1(\rho) = A\rho^{|m|+\frac{1}{2}} (1+b_1\rho + b_2\rho^2 + b_3\rho^3) + O(\rho^4) \qquad (6.37)$$

where A is a constant (in fact the same constant given by equation (6.21)a).

It is interesting to note here, that if no Coulomb term is included in the Hamiltonian when calculating this final state function (ie when $\alpha_o = 0$), then b_1 and b_3 are both zero and so the terms in $\rho^{|m|+3/2}$ and $\rho^{|m|+7/2}$ are not included in this series expansion for the wavefunctions near the origin. As the behaviour of the wavefunction near the origin determines the nature of the function elsewhere, the two cases $\alpha_o = 0$ and 1 (ie the pure Landau and Coulomb-modified cases respectively) must produce wavefunctions of a different character. This emphasizes the importance of including the effect of the Coulomb force of the nucleus in calculating the free wavefunctions. It will be seen later, in fact, that these wavefunctions (with the Coulomb term included) are not only different from the pure Landau levels, but also have very different energy eigenvalues for the field strengths which are considered here. The structure of the Coulomb-modified continuum is discussed in more detail below.

To ensure that equation (6.37) gives an accurate description of the wavefunction in the region $\rho = 0$, it is necessary that the second difference

of $u_1(\rho)$ agrees with $u_1''(\rho)$ to reasonable accuracy. It is found that evaluation of $u_1(\rho)$ at the three points 0.09, 0.1 and 0.11, gives agreement to two decimal places for $B \leq 10^9$G. This is illustrated for the Coulomb-modified case in table 6.1 and for the pure Landau case in table 6.2, both for $B = 10^7$ and 10^9G, when $|m| = 1$. It is expected that the results are in equally good agreement for intermediate field strengths and energies and also for other values of m. A further check is that by running the code with $\alpha_o = 0$, the numerical solution is identical to six figures with the analytic Landau solution.

B (G)	E_1 (γ Ry)	ρ	$u(\rho)$	$\frac{\delta^2 u(0.1)}{(\delta\rho)^2}$	$u''(0.1)$
10^7	3.72	0.09	0.0286556		
		0.1	0.0337824	3.208	3.207
		0.11	0.0392300		
	6.31	0.09	0.0286553		
		0.1	0.0337820	3.208	3.206
		0.11	0.0392290		
	20	0.09	0.0286538		
		0.1	0.0337798	3.206	3.205
		0.11	0.0392263		
10^9	2.14	0.09	0.0286322		
		0.1	0.0337487	3.180	3.179
		0.11	0.0391832		
	4.36	0.09	0.0286075		
		0.1	0.0337132	3.150	3.149
		0.11	0.0391339		
	20	0.09	0.028434		
		0.1	0.0334631	2.940	2.939
		0.11	0.0387865		

Table 6.1

Table to illustrate the agreement between $\frac{\delta^2 u}{(\delta\rho)^2}$ and u'' at $\rho = 0.1$ for the field strengths $B = 10^7$ and 10^9G and energies up to 20 γRy. $\alpha_o = 1$, ie the Coulomb-modified case is considered and $|m| = 1$.

B (G)	E_l (γ Ry)	ρ	$u(\rho)$	$\frac{\delta^2 u(0.1)}{(\delta\rho)^2}$	$u''(0.1)$
10^7	2	0.09	0.0269998		
		0.1	0.0316224	2.373	2.371
		0.11	0.0364824		
	4	0.09	0.0269995		
		0.1	0.0316221	2.366	2.371
		0.11	0.0364819		
	20	0.09	0.0269977		
		0.1	0.0316194	2.370	2.369
		0.11	0.0364782		
10^9	2	0.09	0.0269767		
		0.1	0.0315891	2.344	2.342
		0.11	0.0364359		
	4	0.09	0.0269535		
		0.1	0.0315555	2.314	2.313
		0.11	0.0363890		
	20	0.09	0.0267674		
		0.1	0.0312864	2.079	2.077
		0.11	0.0360133		

Table 6.2

Table to illustrate the agreement between $\frac{\delta^2 u}{(\delta\rho)^2}$ and u'' at $\rho = 0.1$ when $\delta\rho = 0.01$ for field strengths $B = 10^7$ and 10^9G and energies up to 20 γRy. $\alpha_o = 0$, ie the pure Landau case is considered.

6.2.3 Starting the Inward Integration

The inward integration is started in a region where $|u_1(\rho)|$ is small and $u_1(\rho)$ is slowly tending to zero. Assume that $V_1(E_1, \rho)$ does not vary rapidly in this region, then an approximate solution can be given by

$$u_1(\rho) \sim V_1^{-1/4} \left[Ce^{\int V_1^{\frac{1}{2}} d\rho} + De^{-\int V_1^{\frac{1}{2}} d\rho} \right] , \qquad (6.38)$$

and we require the solution which tends to zero as ρ increases. Its values at three points, equally spaced in ρ, will be approximately in geometric progression. Consider the values of u_1 at $R + \delta\rho$, R and $R - \delta\rho$, and let the solutions here be

$$\left.\begin{aligned} u_1(R + \delta\rho) &= \frac{c}{1+x} \\ u_1(R) &= c \\ u_1(R - \delta\rho) &= c(1+x) \end{aligned}\right\} \qquad (6.39)$$

(Hartree, 1955) where c is a constant. We can write

$$u_1''(R) = \frac{\delta^2 u_1}{(\delta\rho)^2} + O\left(\frac{\delta^4 u_1}{(\delta\rho)^4}\right) \qquad (6.40)$$

(Froberg, 1965) and so

$$\delta^2 u_1 = (\delta\rho)^2 c V_1(E_1, R) + O(\delta\rho)^4, \qquad (6.41)$$

$$\text{but } \delta^2 u_1 = c(1+x) - 2c + \frac{c}{1+x} = \frac{cx^2}{1+x} \qquad (6.42)$$

(the second finite difference) and so we can write

$$x = \tfrac{1}{2}\left[(\delta\rho)^2 V_1 + \sqrt{\left((\delta\rho)^4 V_1^2 + 4(\delta\rho)^2 V_1 \right)} \right] \qquad (6.43)$$

where $V_1 = V_1(E_1, R)$. We can now obtain values for $u_1(R \pm \delta\rho)$ and $u_1(R)$ (to within an arbitrary multiplying constant). Table (6.3) shows that there is very good agreement between $u''(R)$ and $\frac{\delta^2 u(R)}{(\delta\rho)^2}$ for the field strengths which are considered here when $|m| = 1$, if R is taken to be a sufficient distance from the classical limit of the wavefunction. We illustrate here, only the Coulomb-modified case and only the lowest (estimated) energy eigenvalue E_1, for each of four field strengths.

Again, it is expected that results for other values of E_1 and m are in equally good agreement, as long as R is large enough.

B (G)	E_1 (γ Ry)	ρ_2	R	$\delta\rho$	$V_1(R)$	$u_1''(R)$ (= V(R)u(R))	x	$\frac{\delta^2 u(R)}{(\delta\rho)^2} = \frac{cx^2}{1+x}$
10^7	3.72	91.2	119.5	0.5	0.032111	0.032111c	0.093702	0.032111c
10^8	3.03	22.0	29.5	0.5	0.197965	0.197965c	0.248584	0.197965c
5×10^8	3.64	9.3	12.5	0.5	0.838160	0.838160c	0.574362	0.838160c
10^9	2.14	5.3	7.5	0.5	1.381664	1.381664c	0.785280	1.381664c

Table (6.3)

Table to show the agreement in the inward integration between u'' and $\frac{\delta^2 u}{(\delta\rho)^2}$, for B = 10^7, 10^8, 5×10^8, 10^9G at a point R where $R > \rho_2$. The agreement is shown for just the wavefunction corresponding to the lowest eigenvalue E_1 and for $|m| = 1$.

6.2.4. Estimating the Energy Eigenvalues of the Continuum States

In order to find solutions for $u_2(\rho)$ by the method described in §6.2, it is necessary to first obtain good estimates for the corresponding energy eigenvalues. It has been shown by Kemble, 1958 and others, that if the wavefunctions are calculated according to the WKB approximation, then, even though the WKB wavefunctions are quantum-mechanical, their corresponding eigenvalues can be calculated by the semi-classical Bohr-Sommerfeld quantisation condition

$$\int_{\rho_2}^{\rho_1} \left\{ V_2(E_1, \rho) \right\}^{\frac{1}{2}} d\rho = (\ell + \tfrac{1}{2})\pi, \quad \ell = 0,1..... \qquad (6.44)$$

where $V_2(\rho_1) = V_2(\rho_2) = 0$, (6.45)

(ie ρ_1 and ρ_2 are the classical turning points) and

$$V_2(\rho) = E_1 - V(\rho) - \frac{1}{4\rho^2} \quad . \qquad (6.46)$$

Although the eigenvalues calculated by this method will not be the exact eigenvalues corresponding to the wavefunctions calculated by the method described in §6.2, they will provide a good first approximation, as we would expect these wavefunctions to be of a similar form to those calculated using the WKB approximation. These approximate eigenvalues are calculated from equation (6.44), evaluating the integral numerically by the method described by Patterson (Froberg, 1965) using subroutine D01ACF from the NAG library, increasing the energy until ℓ has increased from k to k+1 where k is an integer. Results are shown in tables 6.4 - 6.7 for the energies which lie in the continuum for various integer values of ℓ with $|m| = 1$. The spacings between the levels are also given in these tables.

Starace, 1973, calculated these energies and energy spacings for hydrogen by a similar method, but for low field strengths (of the order of 10^4 and 10^5G). The energies and energy spacings in this case, were calculated by differentiating equation (6.44) - it is expected that these results are accurate for low fields, as the wavefunction with the lowest

energy in the continuum has a large value of ℓ (ℓ_{min} = 69 for $B = 10^4$G). It is seen from tables 6.4 - 6.7, that as the field strength increases, the value of ℓ_{min} decreases. In this respect, the structure of the continuum differs greatly from the pure Landau continuum, as the lowest Landau function, regardless of field strength, always has ℓ_{min} = 0 (Dingle, 1952). Indeed, as expected, the deviation becomes greater as the field strength decreases. For the higher field strengths which are considered here, it is believed that, due to the small values of ℓ involved, it is better to calculate the energy spacings directly.

It was also pointed out by Starace, 1973, that at the low fields which he considers, near threshold, the energy spacing is approximately 3 γ Ry, decreasing to 2 γ Ry in the limit as $E_1 \to \infty$ (ie in the Landau limit). This 3 γ Ry spacing at low fields was first observed experimentally by Garton and Tomkins (1969) in their work on the principal series of BaI. This result can be clearly seen from the spacings given in tables 6.4 - 6.7, where energies are given until the spacing is as low as 2.1 γ Ry, ie the Landau limit is almost reached where the spacing is 2 γ Ry. The presence of the Coulomb force, it is shown, has the effect of increasing the level spacings to a maximum of about 3 γ Ry and this is illustrated in figure 6.1. It is clear from these results, that the Coulomb field is certainly non-negligible in the range of field strengths which we are studying. In fact at $B = 10^7$G, the whole structure of the continuum will be completely different, with the lowest wavefunction having principle quantum number ℓ = 7. For this reason, it is also expected that results for the photoionization cross-sections are different when the Coulomb force is included in the system.

ρ_1	ρ_2	ℓ	$E_1^{(\ell)}$ (γ Ry)	Energy Spacing (γRy)
0.498	91.186	7	2.717	
				2.60
0.497	101.347	8	5.309	
				2.48
0.495	110.634	9	7.789	
				2.40
0.494	119.215	10	10.190	
				2.34
0.493	127.219	11	12.534	
				2.30
0.492	134.740	12	14.834	
				2.26
0.491	141.852	13	17.100	
				2.24
0.490	148.612	14	19.338	
				2.22
0.489	155.065	15	21.551	
				2.20
0.487	161.251	16	23.750	
				2.18
0.486	167.197	17	25.931	
				2.16
0.485	172.929	18	28.097	
				2.16
0.484	178.469	19	30.252	
				2.14
0.483	183.835	20	32.396	
				2.14
0.482	189.041	21	34.531	
				2.12
0.481	194.101	22	36.657	
				2.12
0.480	199.027	23	38.776	
				2.12
0.480	203.828	24	40.889	
				2.10
0.479	208.514	25	42.996	
				2.10
0.478	213.093	26	45.097	
		⋮		⋮
		∞		2.00

Table 6.4

The energies $E_1^{(\ell)} = E^{(\ell)}$-m and energy spacings (in γ Ry) of the modified Landau levels for $|m| = 1$ at $B = 10^7$G calculated using the Bohr-Sommerfeld quantization condition. The values of ℓ, and the classical turning points are also given. The levels for $\ell < 7$ do not exist.

ρ_1	ρ_2	ℓ	E_1 (γ Ry)	Energy Spacing (γ Ry)
0.485	21.951	3	2.033	
				2.40
0.474	26.029	4	4.435	
				2.28
0.465	29.552	5	6.725	
				2.22
0.456	32.688	6	8.949	
				2.18
0.448	35.541	7	11.131	
				2.16
0.441	38.172	8	13.283	
				2.14
0.434	40.628	9	15.414	
				2.12
0.428	42.937	10	17.527	
				2.10
0.422	45.124	11	19.627	
		⋮		⋮
		∞		2.00

Table 6.5

The energies $E_1^{(\ell)} = E^{(\ell)}$-m and energy spacings (in γ Ry) of the modified Landau levels for $|m| = 1$ at $B = 10^8$G calculated using the Bohr-Sommerfeld quantization condition. The values of ℓ and the classical turning points are also given. The levels $\ell = 0,1,2$ do not exist.

ρ_1	ρ_2	ℓ	E_1(γ Ry)	Energy Spacing (γ Ry)
0.429	9.300	2	2.643	2.22
0.400	11.190	3	4.857	2.14
0.378	12.799	4	7.006	2.12
0.360	14.223	5	9.120	2.10
0.345	15.513	6	11.211	2.08
0.332	16.700	7	13.286	⋮
		⋮		⋮
		∞		2.00

Table 6.6

The energies $E_1^{(\ell)} = E^{(\ell)}$-m and energy spacings (in γ Ry) of the modified Landau levels for $|m| = 1$ at $B = 5 \times 10^8$G calculated using the Bohr-Sommerfeld quantization condition. The values of ℓ and the classical turning points are also given. The $\ell = 0$ and 1 levels are missing.

ρ_1	ρ_2	ℓ	E_1(γ Ry)	Energy Spacing (γ Ry)
0.420	5.265	1	1.140	2.22
0.372	6.856	2	3.363	2.14
0.340	8.139	3	5.503	2.10
0.317	9.242	4	7.604	2.08
0.298	10.224	5	9.680	2.06
0.283	11.117	6	11.743	2.06
0.270	11.943	7	13.794	⋮
		⋮		⋮
		∞		2.00

Table 6.7

The energies $E_1^{(\ell)} = E^{(\ell)}$-m and energy spacings (in γ Ry) of the modified Landau levels for $|m| = 1$ at $B = 10^9$G calculated using the Bohr-Sommerfeld quantization condition. The values of ℓ and the classical turning points are also given. Note that at this high field only $\ell = 0$ is missing.

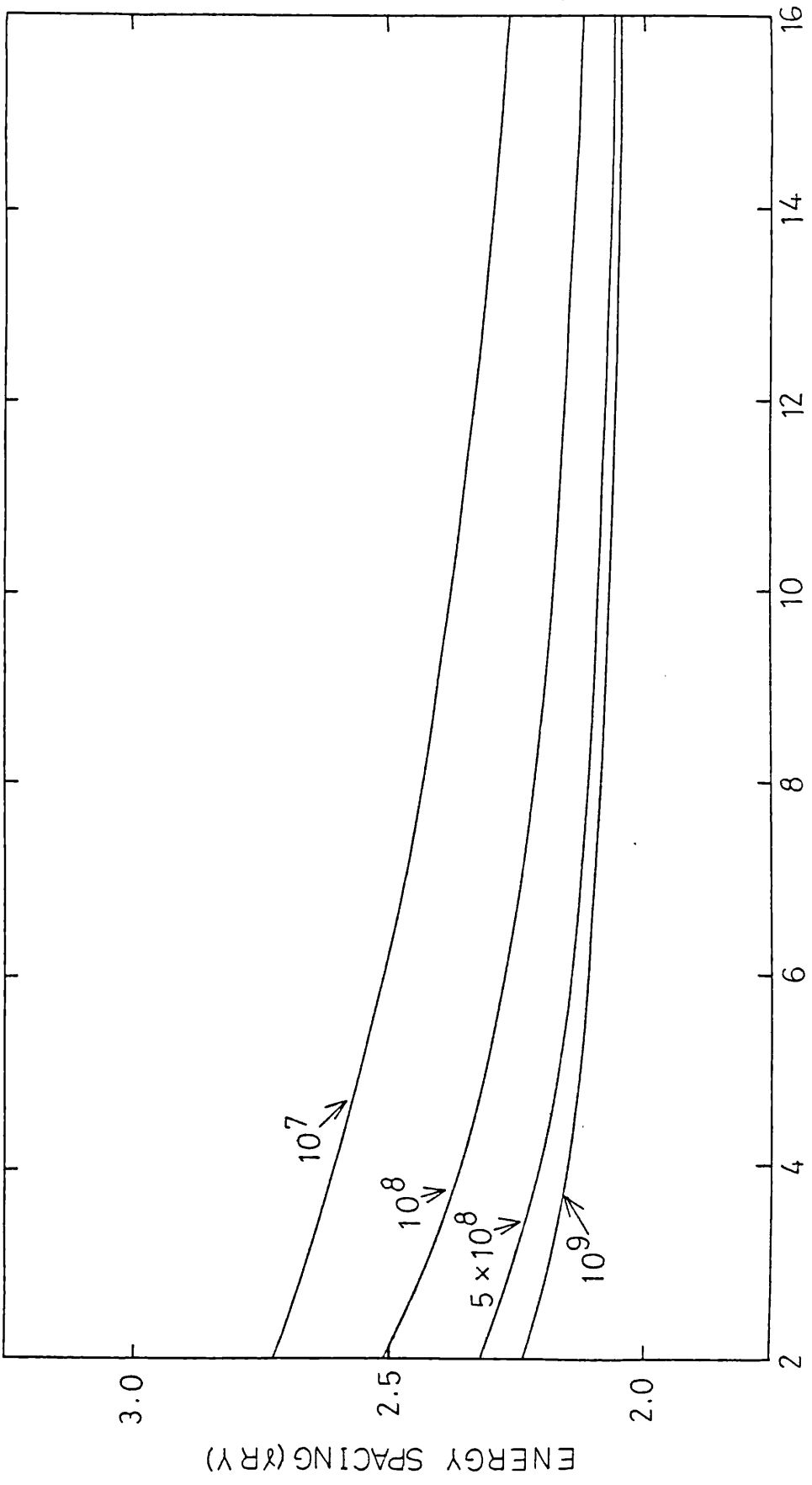
ENERGY SPACING (γRY)
3.0
2.5
2.0
2
4
6
8
10
12
14
16
ENERGY (γRY)
10^7
10^8
5×10^8
10^9

Fig 6.1

Figure 6.1

Energy spacing in γ Ry of the discrete levels in the Coulomb modified continuum in the interval $[2,16]$ γ Ry for $B = 10^7$, 10^8, 5×10^8 and 10^9 G.

6.2.5. Results for Energies and Wavefunctions

Having calculated good initial estimates for the energy eigenvalues, the function $u_\ell(\rho)$ can then be calculated by the method described in §6.2.

In computing these functions, we obtain agreement at the matching point to 4 figures in $u_\ell(\rho)$ and its first derivative. Table (6.8) gives the final results for the energies of all the continuum states which lie below 8 γ Ry at B = 10^7, 10^8, 5 x 10^8 and 10^9G for m = 0, $\pm$ 1.

At B = 10^7G the lowest six Landau levels disappear, and the lowest surviving continuum discrete state is ℓ = 6, m = 1 at 1.961 γ Ry, while for m = 0 or m = -1 the lowest state has ℓ = 7.

At the highest field strength considered (10^9G) there are discrete states corresponding to each of the Landau levels for m = 1, and for all except ℓ = 0 for m = -1, while they begin at ℓ = 2 for m = 0. The lowest level shifts in energy from γ to 0.67γRy.

Table (6.8) also gives the energies of the (ℓ, m) discrete Landau levels in the absence of any Coulomb attraction (given by equation (5.17)). We see that the energy shifts can be very large when γ is small: for example, for the lowest level at 10^7G, the shift is more than 13γRy. However, for 10^9G, the lowest level has a shift of only about 2.3γRy, and similar shifts persist to very high ℓ. The spacing of the unperturbed levels is fairly close to the semi-classical value

$$\Delta E_{\ell,\ell+1} = 3\gamma^2 \text{Ry} \qquad (6.47)$$

given by Starace (1973), however, this value refers to E = 0 and not to the actual levels.

B(G)	ℓ	$E_{m=-1}$	$E^L_{m=-1}$	$E_{m=0}$	$E^L_{m=0}$	$E_{m=1}$	$E^L_{m=1}$
10^7	6	-		-		1.96090	15
	7	2.72564	15	1.02009	15	4.72564	17
	8	5.31670	17	3.79300	17	7.31670	19
	9	7.79648	19	6.39200	19	-	
10^8	2	-		-		1.41470	9
	3	2.0488	7	0.54390	7	4.04888	11
	4	4.45037	9	3.20969	9	6.45037	13
	5	6.73956	11	5.63640	11	-	
	6	-		7.94700	13	-	
5×10^8	1	0.30852	3	-		2.30852	5
	2	2.66137	5	1.56361	5	4.66137	7
	3	4.87242	7	3.98075	7	6.872	9
	4	7.02042	9	6.23796	9	-	
10^9	0	-		-		0.67461	3
	1	1.16075	3	-		3.16075	5
	2	3.37873	5	2.52522	5	5.37873	7
	3	5.51588	7	4.81222	7	7.51588	9
	4	7.61436	9	6.99740	9	-	

Table 6.8

Energy eigenvalues of the discrete states in the Coulomb-modified continuum (E) and the pure Landau continuum (E^L) in γ Ry, for those states which lie in the region [0,8] γ Ry in the Coulomb-modified continuum.

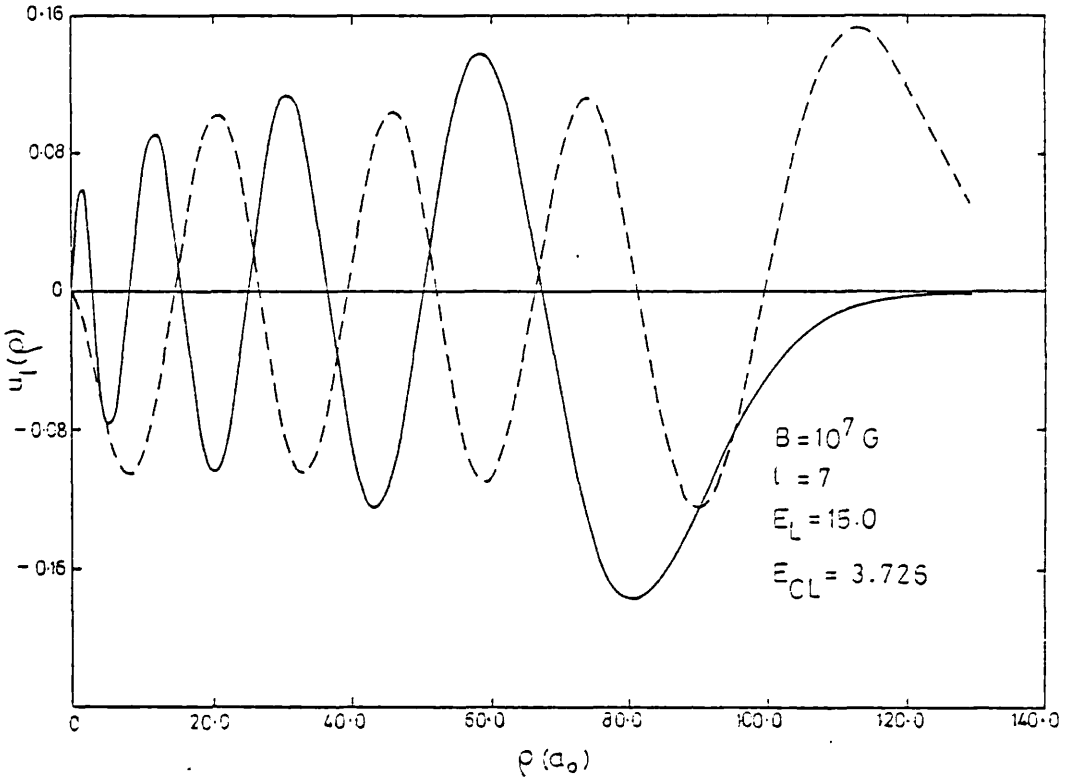
0·16
0·08
0
-0·08
-0·16
$\eta_l(\rho)$
B = 10^7 G
l = 7
E_L = 15·0
E_{CL} = 3.725
0
20·0
40·0
60·0
80·0
100·0
120·0
140·0
ρ (a_o)

Fig. 6.2

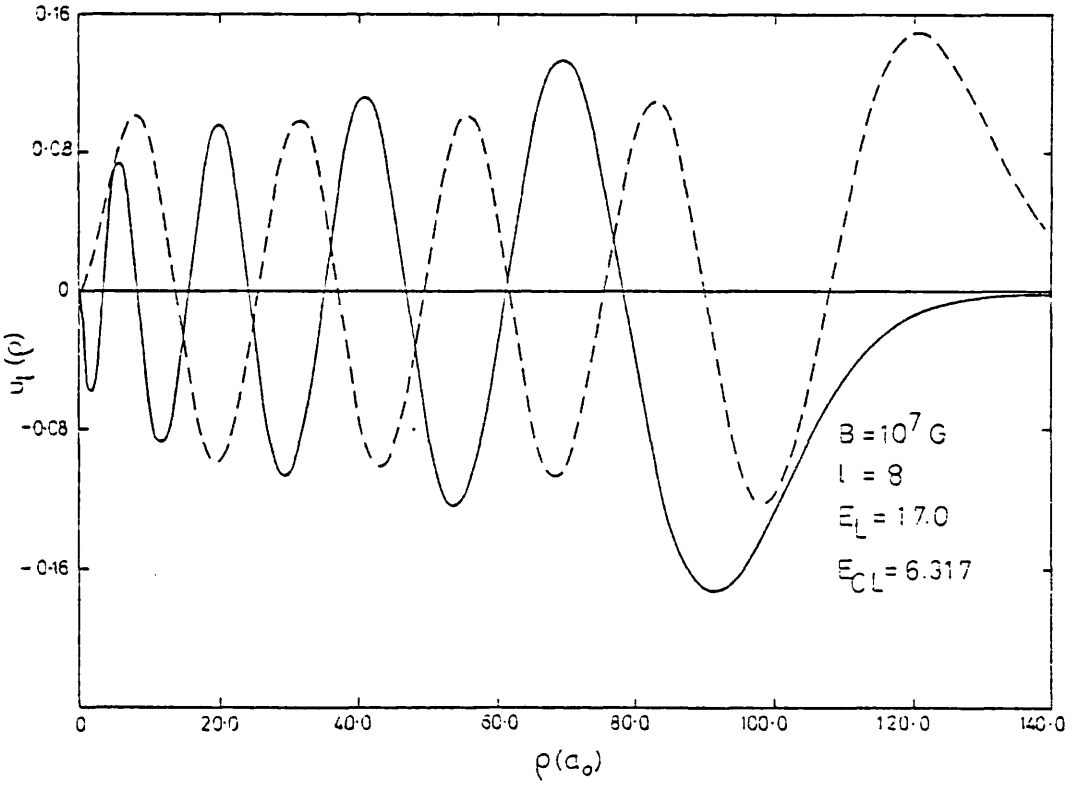
0·16
0·08
0
-0·08
-0·16
$\eta_l(\rho)$
B = 10^7 G
l = 8
E_L = 17.0
E_{CL} = 6.317
0
20·0
40·0
60·0
80·0
100·0
120·0
140·0
$\rho(a_o)$

Fig. 6.3

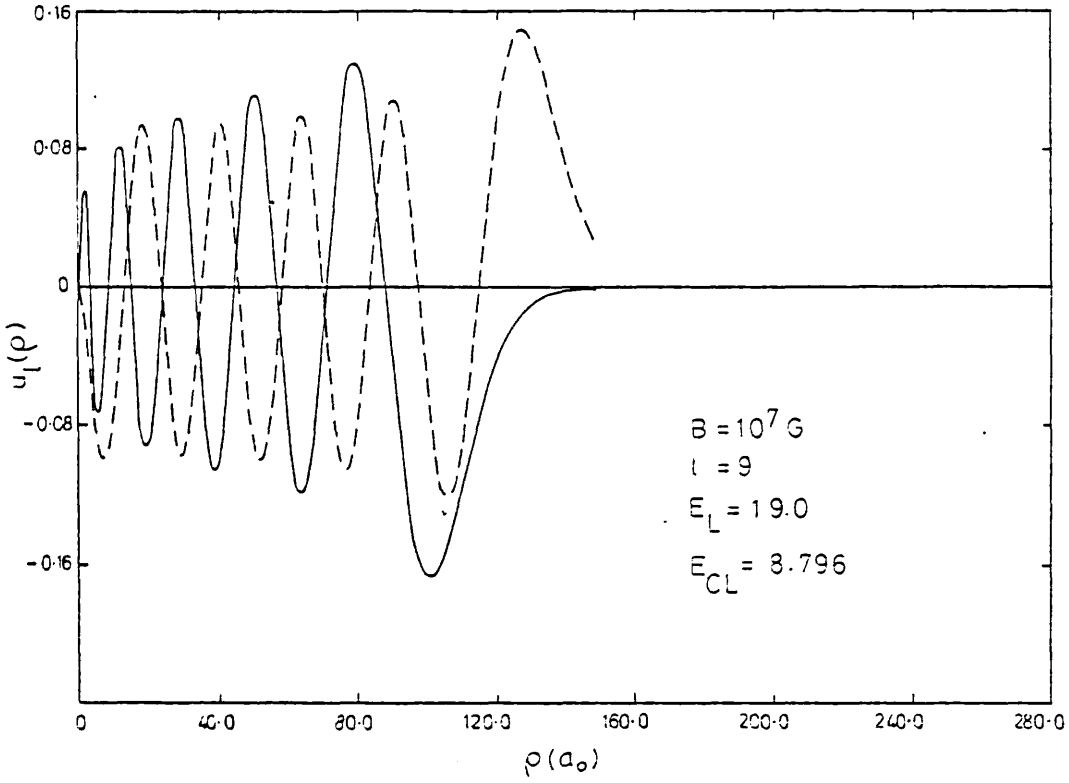
0·16
0·08
0
-0·08
-0·16
$u_l(\rho)$
B = 10^7 G
l = 9
E_L = 19.0
E_{CL} = 8.796
0
40·0
80·0
120·0
160·0
200·0
240·0
280·0
$\rho(a_o)$

Fig. 6.4

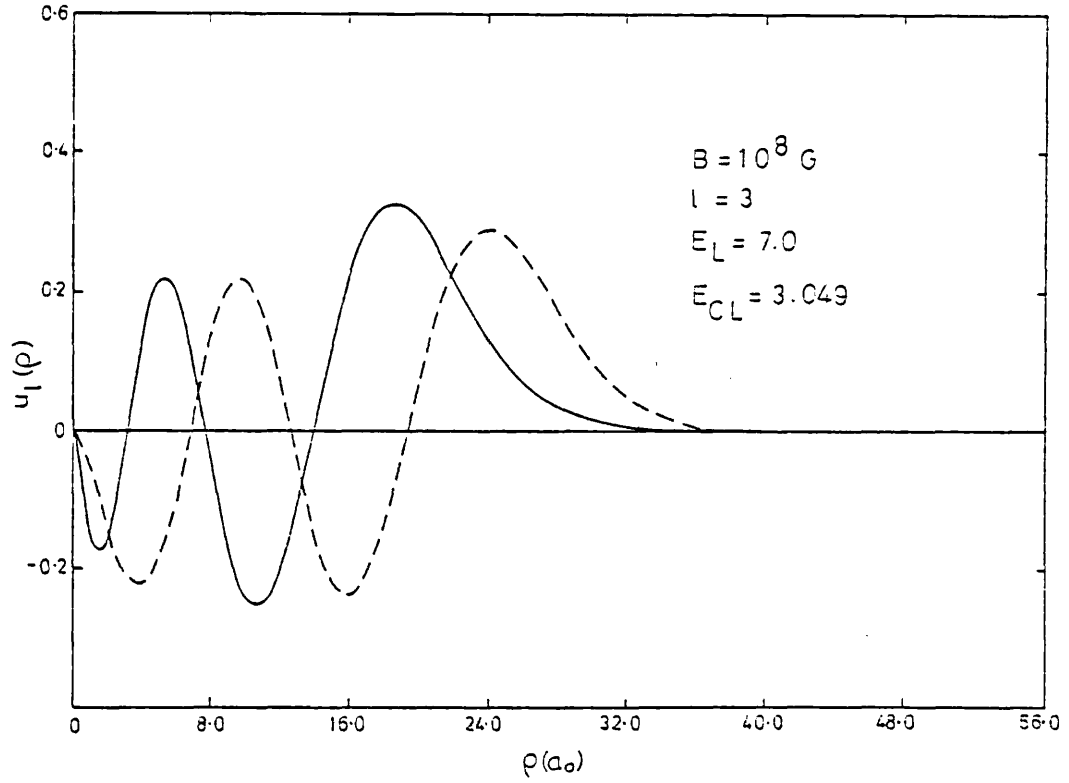
0·6
0·4
0·2
0
-0·2
$u_l(\rho)$
B = 10^8 G
l = 3
E_L = 7.0
E_{CL} = 3.049
0
8·0
16·0
24·0
32·0
40·0
48·0
56·0
$\rho(a_o)$

Fig. 6.5

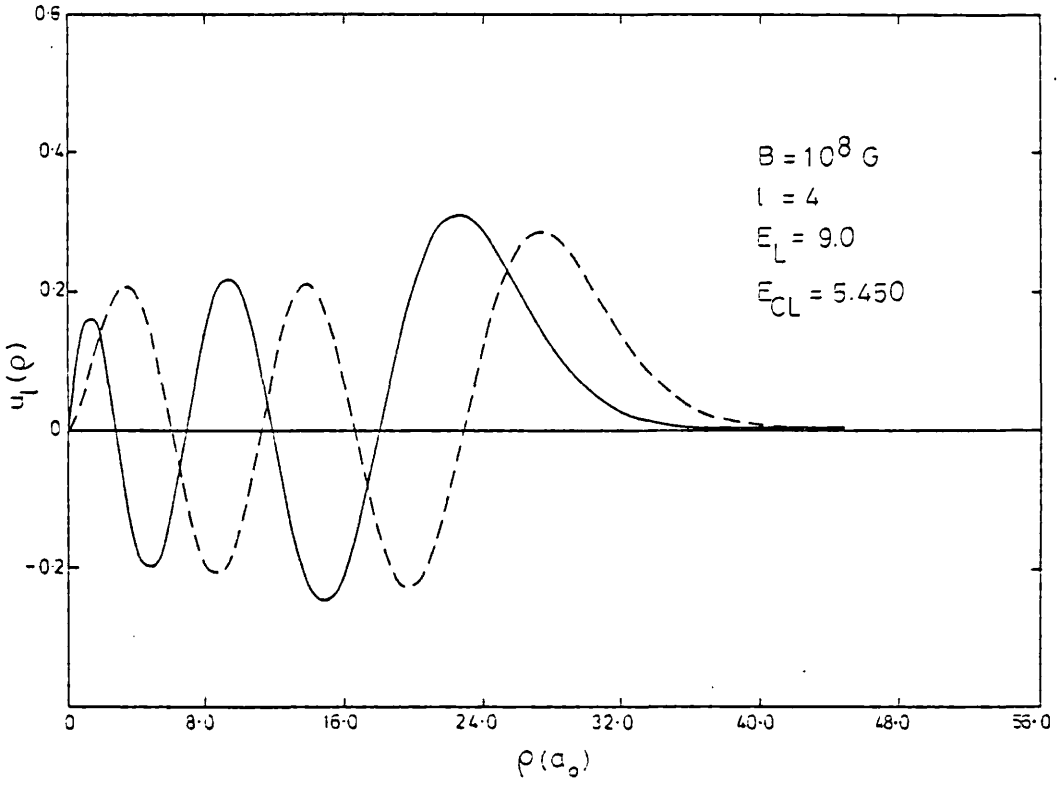
0·6
0·4
0·2
0
-0·2
$u_l(\rho)$
$B = 10^8$ G
l = 4
E_L = 9.0
E_{CL} = 5.450
0
8·0
16·0
24·0
32·0
40·0
48·0
56·0
$\rho(a_o)$

Fig. 6.6

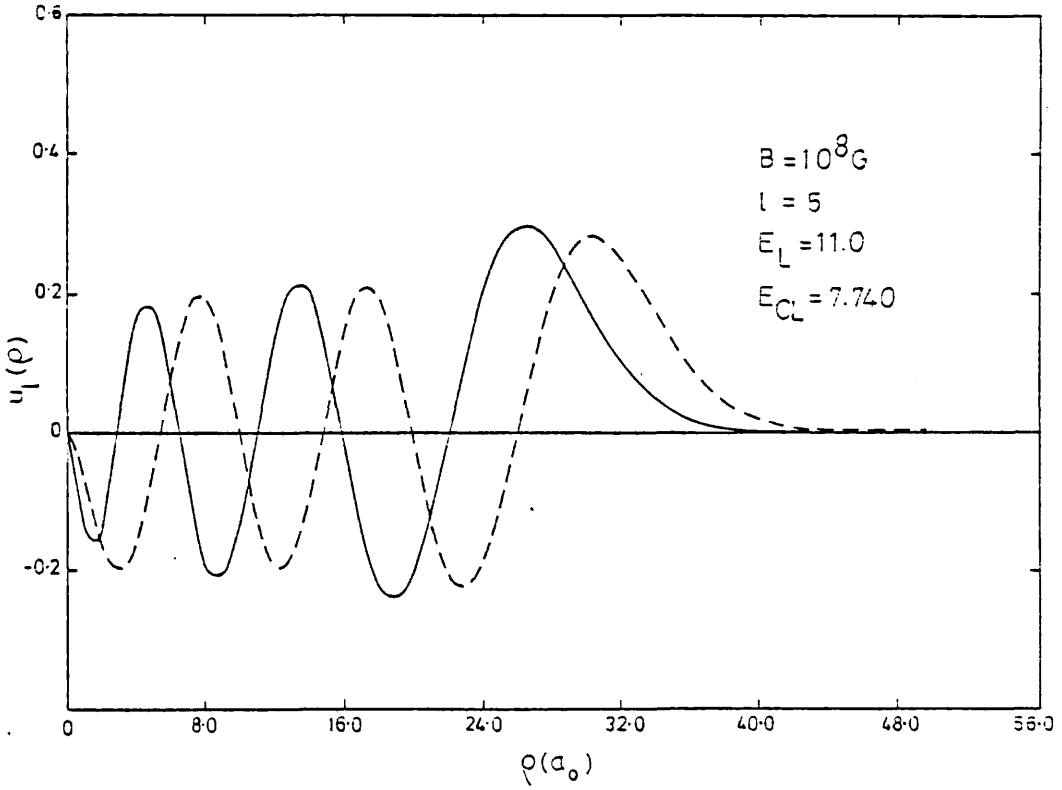
0·6
0·4
0·2
0
-0·2
$u_l(\rho)$
$B = 10^8$G
l = 5
E_L =11.0
E_{CL} = 7.740
0
8·0
16·0
24·0
32·0
40·0
48·0
56·0
$\rho(a_o)$

Fig. 6.7

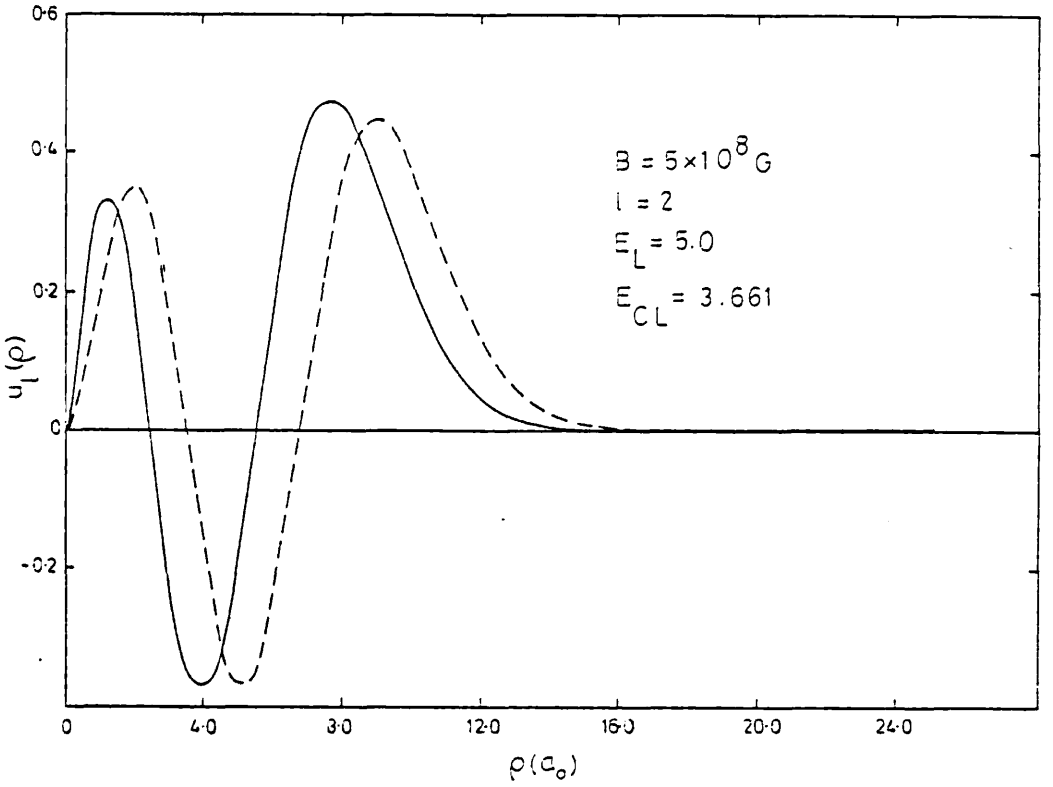
0·6
0·4
0·2
0
-0·2
$u_l(\rho)$
B = 5×10^8 G
l = 2
E_L = 5.0
E_{CL} = 3.661
0
4·0
8·0
12·0
16·0
20·0
24·0
$\rho(a_o)$

Fig. 5.8

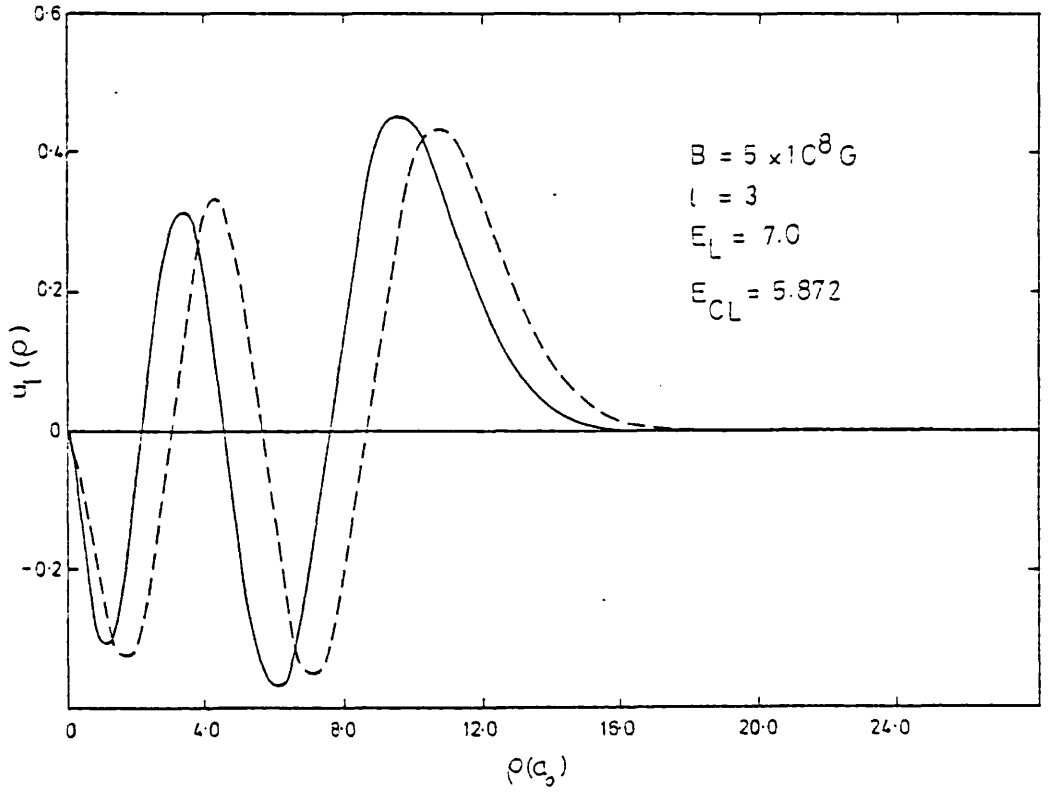
0·6
0·4
0·2
0
-0·2
$u_l(\rho)$
B = 5 ×10^8 G
l = 3
E_L = 7.0
E_{CL} = 5.872
0
4·0
8·0
12·0
16·0
20·0
24·0
$\rho(a_o)$

Fig. 5.9

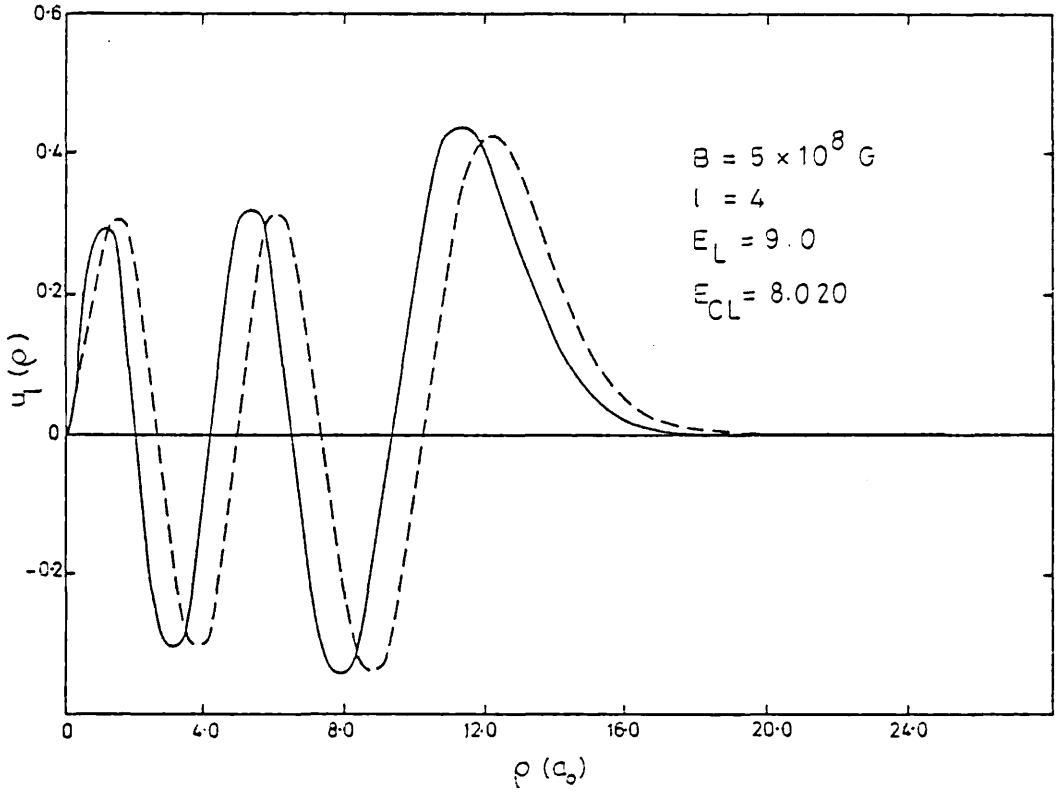

Fig. 6.10

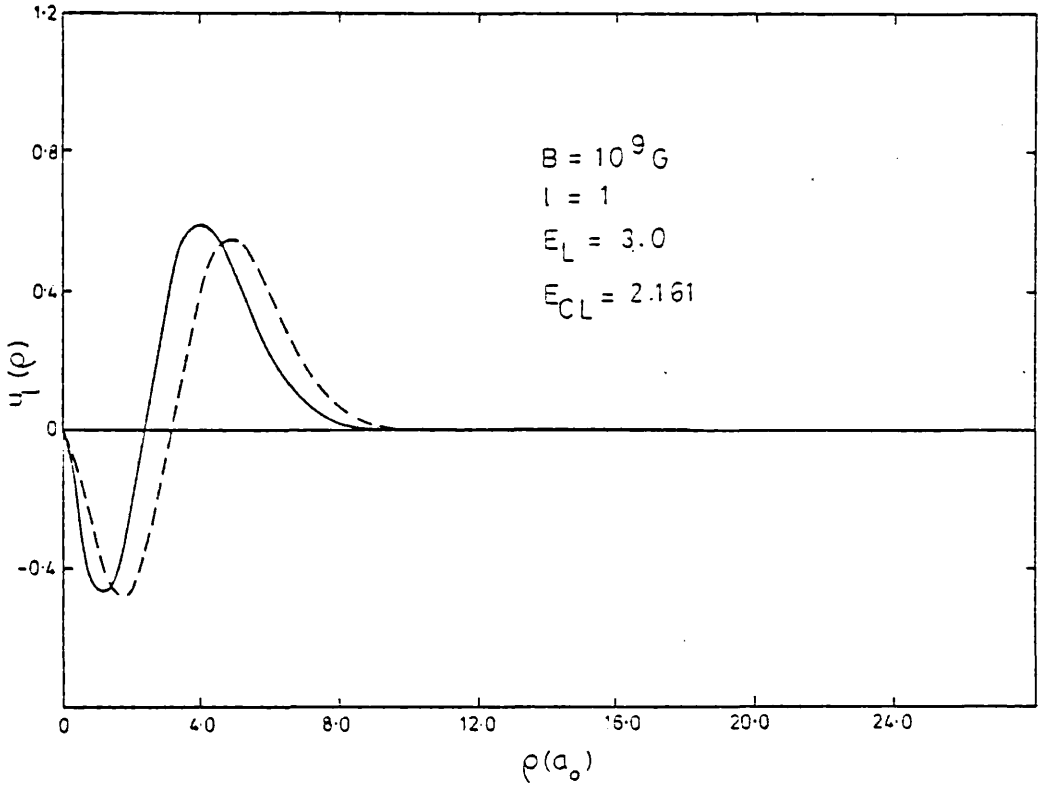

Fig. 6.11

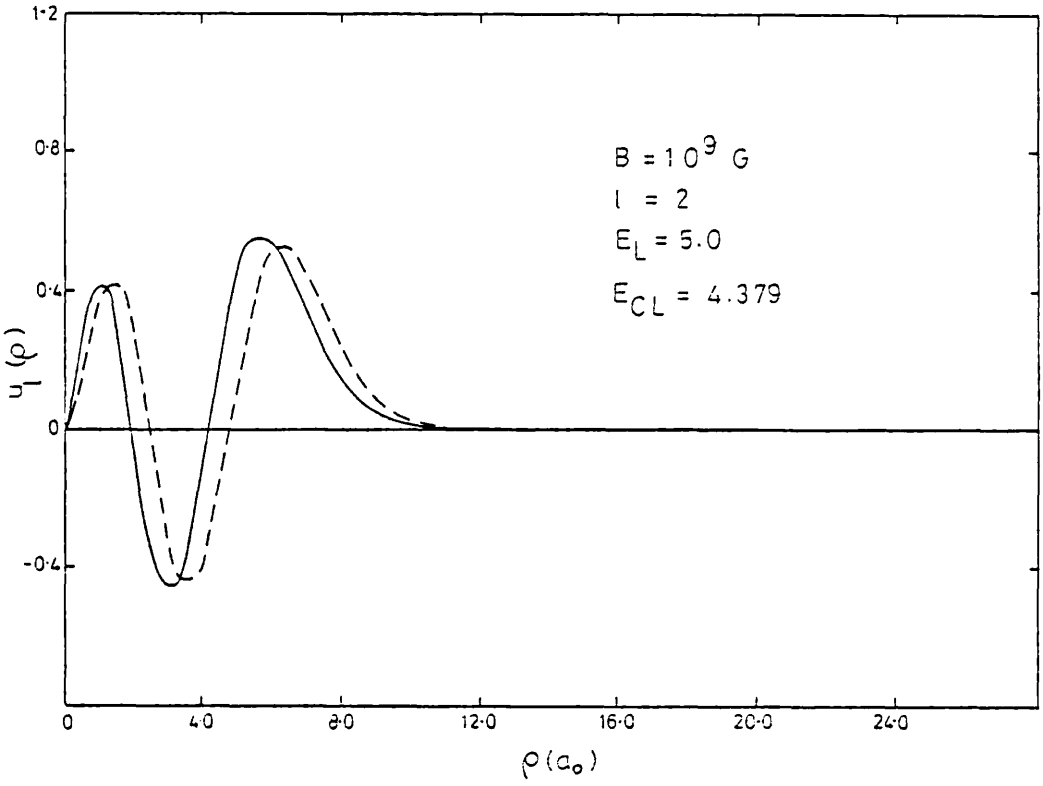

Fig. 6.12

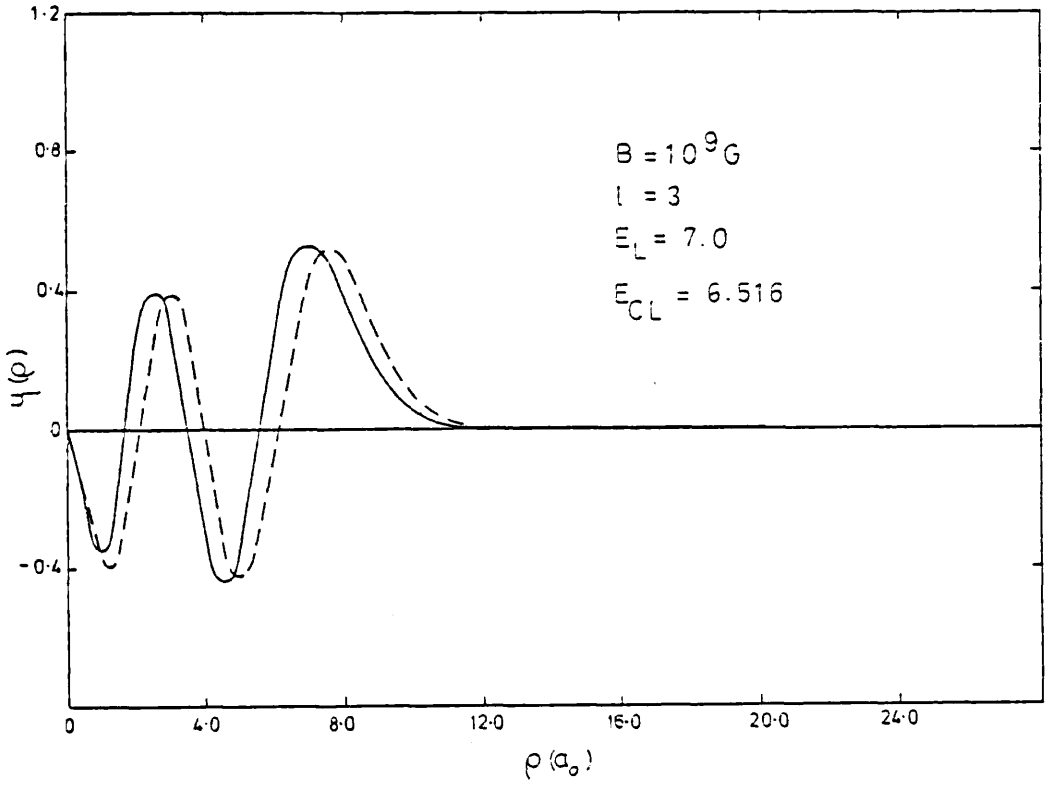

Fig. 6.13

Figure 6.2

Continuum radial functions $u_{\ell}(\rho)$ at $B = 10^7 G$, with $m_f = -1$ and $\ell = 7$ in the Landau (broken line) and Coulomb modified (continuous line) cases, where the energies of the states are E_L and E_{CL} Ry respectively.

Figure 6.3

Continuum radial functions $u_{\ell}(\rho)$ at $B = 10^7 G$, with $m_f = -1$ and $\ell = 8$ in the Landau (broken line) and Coulomb modified (continuous line) cases, where the energies of the states are E_L and E_{CL} Ry respectively.

Figure 6.4

Continuum radial functions $u_{\ell}(\rho)$ at $B = 10^7 G$, with $m_f = -1$ and $\ell = 9$ in the Landau (broken line) and Coulomb modified (continuous line) cases, where the energies of the states are E_L and E_{CL} Ry respectively.

Figure 6.5

Continuum radial functions $u_{\ell}(\rho)$ at $B = 10^8 G$, with $m_f = -1$ and $\ell = 9$ in the Landau (broken line) and Coulomb modified (continuous line) cases, where the energies of the states are E_L and E_{CL} Ry respectively.

Figure 6.6

Continuum radial functions $u_{\ell}(\rho)$ at $B = 10^8 G$, with $m_f = -1$ and $\ell = 4$ in the Landau (broken line) and Coulomb modified (continuous line) cases, where the energies of the states are E_L and E_{CL} Ry respectively.

Figure 6.7

Continuum radial functions $u_{\ell}(\rho)$ at $B = 10^7 G$, with $m_f = -1$ and $\ell = 5$ in the Landau (broken line) and Coulomb modified (continuous line) cases, where the energies of the states are E_L and E_{CL} Ry respectively.

Figure 6.8

Continuum radial functions $u_{\ell}(\rho)$ at $B = 5 \times 10^8 G$, with $m_f = -1$ and $\ell = 2$ in the Landau (broken line) and Coulomb modified (continuous line) cases, where the energies of the states are E_L and E_{CL} Ry respectively.

Figure 6.9

Continuum radial functions $u_{\ell}(\rho)$ at $B = 5 \times 10^8 G$, with $m_f = -1$ and $\ell = 3$ in the Landau (broken line) and Coulomb modified (continuous line) cases, where the energies of the states are E_L and E_{CL} Ry respectively.

Figure 6.10

Continuum radial functions $u_{\ell}(\rho)$ at $B = 5 \times 10^8 G$, with $m_f = -1$ and $\ell = 4$ in the Landau (broken line) and Coulomb modified (continuous line) cases, where the energies of the states are E_L and E_{CL} Ry respectively.

Figure 6.11

Continuum radial functions $u_{\ell}(\rho)$ at $B = 10^9 G$, with $m_f = -1$ and $\ell = 1$ in the Landau (broken line) and Coulomb modified (continuous line) cases, where the energies of the states are $E_{\perp}$ and $E_{C\perp}$ γ Ry respectively.

Figure 6.12

Continuum radial functions $u_{\ell}(\rho)$ at $B = 10^9 G$, with $m_f = -1$ and $\ell = 2$ in the Landau (broken line) and Coulomb modified (continuous line) cases, where the energies of the states are $E_{\perp}$ and $E_{C\perp}$ γ Ry respectively.

Figure 6.13

Continuum radial functions $u_{\ell}(\rho)$ at $B = 10^9 G$, with $m_f = -1$ and $\ell = 3$ in the Landau (broken line) and Coulomb modified (continuous line) cases, where the energies of the states are $E_{\perp}$ and $E_{C\perp}$ γ Ry respectively.

It is also interesting to note that there is no longer any degeneracy in the energy levels, ie the degeneracy is lifted by the Coulomb field, whereas for the bound states it is broken by the magnetic field. This results in different sets of energy levels for each m which must cause a significant change in the photoionization cross-sections from the pure Landau case.

The label ℓ is, both in the Landau and Coulomb-modified case, the principal quantum number and gives the number of nodes in the radial wavefunction (Powell and Crasemann, p.135). Some of the Coulomb-modified, radial continuum wavefunctions $u_\ell(\rho)$, for m = -1 are plotted with the corresponding Landau wavefunctions of the same principal quantum number for various field strengths in figures 6.2 - 6.13. As predicted, these 2 sets of wavefunctions are very different in a region where the Coulomb field is not of negligible strength compared to the magnetic field, for instance at $B = 10^7$G, the wavefunctions corresponding to the ℓ = 7, 8 and 9 states have opposite sign near the origin and are almost exactly out of phase in the region $[\rho_1, \rho_2]$. At $B = 10^9$G however, where the Coulomb field becomes less important, the two sets of wavefunctions for the ℓ = 1, 2 and 3 states are more similar and certainly have closer corresponding energies. In each case, it can be seen that the Coulomb attraction draws the electron to smaller ρ as expected. Similar behaviour is predicted for other values of m.

§6.3 Photoionization Cross Sections

We are now in a position to calculate the photoionization cross-section using the Coulomb modified continuum wavefunctions given by

$$\psi^{(\ell)}_{k_z,m}(\underline{r}) = C\,\rho^{-\frac{1}{2}}\,u_\ell(\rho)\,e^{ik_z z}\,e^{im\phi} \qquad (6.48)$$

where C is a normalizing constant and $u_\ell(\rho)$ is defined numerically at a number of points in the interval $[0,R]$. The formula for evaluation of

the photoionization cross-section is given by equation (5.7) with the exception that the sum over ℓ will start from ℓ_{min} and not 0, as the principle quantum number of the state of lowest energy in the continuum may be positive (as explained in 6.2.4).

Writing $C^2 = \frac{N^2}{2\pi L_z}$, where N is the normalization constant such that

$$N^2 \int u_\ell(\rho)^* u_\ell(\rho)\, d\rho = 1, \tag{6.49}$$

then we obtain the following expression for the matrix element $|R_{if}|^2$:

$$|R_{if}|^2 = \frac{N^2}{2\pi L_z} \Big| \sum_{\alpha,\beta,\delta} C_{\alpha\beta\delta} \int \rho^\beta z^\alpha e^{-\delta r^2} e^{im_i\phi} \sum_{\mu=-1}^{1} r_\mu \rho^{-\frac{1}{2}} u_\ell(\rho) \times e^{im_f\phi} e^{ik_z z} \rho\, d\rho d\phi dz \Big|^2 \frac{L_z}{4\pi k_z} . \tag{6.50}$$

This can be reduced to the form

$$|R_{if}|^2 = \frac{N^2}{4k_z} \Big| \sum_{\alpha,\beta,\delta} C_{\alpha\beta\delta} \times R'(\beta,\delta) \times Z(\alpha,\delta,k_z) \Big|^2 \tag{6.51}$$

if $\Delta m = \pm 1$ and

$$|R_{if}|^2 = \frac{N^2}{2k_z} \Big| \sum_{\alpha,\beta,\delta} C_{\alpha\beta\delta} \times R'(\beta-1,\delta) \times Z(\alpha+1,\delta,k_z) \Big|^2 \tag{6.52}$$

if $\Delta m = 0$, where $Z(\alpha, \delta, k_z)$ is defined by equation (5.24) and $R'(\beta,\delta)$ is given by

$$R'(\beta,\delta) = \int_0^\infty \rho^{\beta+3/2} e^{-\delta\rho^2} u_\ell(\rho)\, d\rho . \tag{6.53}$$

The dependence of the total photoionization cross-section on k_z, within this model, is exactly the same as that for the pure Landau case. For this reason, the behaviour of the cross-section near to the threshold energies, also remains unchanged (see section §5.4). As there is no longer any degeneracy in the continuum energy levels, there will now be some finite, as well as infinite, peaks occurring in the total cross-section due to the contributions from the terms whose k_z dependence at threhold is as k_z (table (5.2)). This is apparent from the results plotted in figures (6.15) - (6.22).

The initial bound state wavefunctions "$1s_o$" and "$2p_o$" used in these calculations are exactly the same as those used to obtain the results of Chapter 5, and are given by table (5.1).

Total photoionization cross-sections and the contributions from each of the possible (Coulomb-modified) continuum levels given by $S_{\nu}^{(\ell,m_f)}$ (equation (5.1)), are calculated by program QMAT1, details of which are given in appendix (I). Results for the total cross-sections from the bound "$1s_o$" and "$2p_o$" states are tabulated in tables 6.9 - 6.12 for B = 10^7, 10^8, 5 x 10^8 and 10^9G, with the energy of the final state in the range $\nu \leq E_f \leq 8\nu$ Ry. The contributions to the total cross-sections from the $m_f = 0, \pm 1$ continua for B = 10^7 and 10^9G are also given in tables 6.13 - 6.18. For the same reason as in the pure Landau continuum (Chapter 5), the total photoionization cross section is much smaller than the field-free cross section within 10 ν Ry above the threshold energy. In addition, for all field strengths studied here, the total photoionization cross sections are also smaller than those calculated with the Landau continuum. This is due to the difference in the nature of the final state wavefunctions in the two cases. It can be seen from figures 6.2 - 6.13, that in the case of the Landau continuum, the radial wavefunctions are almost entirely confined to the classically allowed region $\rho_1 \leq \rho \leq \rho_2$ where ρ_1 and ρ_2 are the roots of $V_1(\rho) = 0$. However, the Coulomb attraction draws the electron to smaller ρ, with the result that there is considerable oscillation in the region of overlap with the bound state. Consequently, the radial matrix element will tend to be much smaller in the Coulomb modified case. At 10^9G however, there is little difference in the wavefunctions other than a drawing in of the modified function by about $1a_o$. The difference in the results for the radial part of $|R_{if}|^2$ is illustrated in figure 6.14, where ρ is plotted against the function $u_1(\rho)\ \rho^{3/2} e^{-\delta\rho^2}$ (ie the radial integrand of R_{if} when $\beta = 1$ and $\ell = 1$) for the Landau and Coulomb modified cases at B = 10^9G and with $m_f = -1$. It is clearly seen that when the integral of the function between 0 and ∞ is calculated, the result will be much smaller for the Coulomb modified case than for the Landau case.

It is found that for high field strengths and large ℓ, the Landau model is in good accord with the Coulomb modified model, in the sense that

giving both cases the same threshold, the values of the $\ell = \ell_1$ contribution in each model agree well away from threshold. This is illustrated in figure 6.25 for the m = -1 contribution to the photoionization of the "$2p_o$" bound state at 10^9G. However, because of the large shift in the thresholds, and the change in threshold behaviour (see section §5.4), the overall cross-section is very different in the two models. As expected, the Coulomb-modified cross-sections are much smaller, especially at low fields. For this case ($2p_o \rightarrow$ m = -1) the cross-section shows a series of finite peaks or resonances at each discrete state energy, but decreases monotonically between peaks. For photon energies in the range $E(\ell_1, m) < h\nu < E(\ell_1+1, m)$ the dominant contribution comes from $\ell = \ell_1$, those for $\ell < \ell_1$ being small. The results are similar for all $\Delta m = \pm 1$ transitions, but for photoionization from "$1s_o$" the threshold peaks are infinitely high in this model (figure 6.23).

The cross-section for $\Delta m = 0$ transitions is shown for the same two cases in figures 6.25 and 6.26. Here the infinite peaks occur for "$2p_o$", but the cross-sections are no longer necessarily monotonic decreasing between peaks. It is shown in section §5.6, how this maximum arises for a Landau continuum function and very simple model wavefunctions for the bound states. The actual location and shape of the secondary maxima depend, in a sensitive manner, on the details of the wavefunctions.

The total photoionization cross sections from the "$1s_o$" and "$2p_o$" states at B = 10^7G are given in figures 6.15 and 6.16 respectively. The "$1s_o$" cross section above the lowest ($\ell = 7$, $m_f = 0$) threshold is very small, but above the first $m_f = 1$ threshold is characterized by two series ($m_f = \pm 1$) of narrow resonances. These are small features, probably unobservable, at higher $m_f = 0$ thresholds. The cross-section, away from the resonances, is very much smaller than the field free cross-section in this narrow range of photon energies (from threshold to 0.5eV). The "$2p_o$" cross section has a rather different structure. It is zero below

the lowest (ℓ = 7, m_f = 0) threshold, where there is a strong resonance peak, and this series of resonances at each successive m_f = 0 threshold is the dominating feature. Between these resonances there are discontinuities at the $m_f = \pm 1$ thresholds, and for $\ell > 3$ the cross section tends to rise almost monotonically between resonances. For sufficiently large ℓ (not shown) it eventually starts to decrease, and finally goes over to the Landau value.

At B = 10^8G, the $1s_o$ cross section (fig.6.17) has a slightly more complex behaviour. There is a peak after the first (3,0) level and the total cross-section is not necessarily monotonic, decreasing between the threshold peaks. There is a tendency for it to increase soon after the m_f = 0 peaks, which are again very small. As at B = 10^7G, the cross-section eventually starts to decrease for some ℓ and again goes over to the Landau limit. The $2p_o$ cross-section (fig.6.18) is different in character from the B = 10^7G case, in that, in general, it is seen to be decreasing from about 3 γ Ry, which is what we would expect for the higher field strength. Also, the peaks corresponding to the $m_f = \pm 1$ continuum states are now much larger. No secondary maxima occur in this cross-section, but it is not monotonic decreasing between the levels (3,0) and (2,1).

The $1s_o$ cross-section at B = 5 x 10^8G (fig.6.19) is now seen to be decreasing, in general, from about 2.5 γ Ry. The first continuum level is no longer an m_f = 0 level, but an m_f = -1 level where there is an infinite peak. The threshold peaks become smaller with increasing energy and are probably undetectable after about 5 γ Ry (when broadening is included) and secondary maxima occur at about 3.8, 6.2, and 7.6 γ Ry, with a stationary point also at about 5.2 γ Ry. The $2p_o$ cross-section at this field strength (fig. 6.20) has a dominant resonance corresponding to the (1,1) continuum level and from there, rapidly decreases with increasing energy. There is also a fairly wide resonance, though not so high as the (1,1) resonance, at the (1,-1) level and no secondary maxima are seen in this cross-section.

At 10^9G, the "$1s_o$" cross-section (shown in fig 6.21) shows a broad resonance at the threshold of the lowest ($\ell = 0$, $m = 1$) discrete level, and narrow resonances at all the higher $m = 1$ and $m = -1$ thresholds. In general it decreases quite smoothly between the resonances, except for a weak secondary maximum when $E = h\nu - I_x$ lies between 6 γ and 7 γ Ry. On these $m_f = \pm 1$ contributions, is superimposed the $m_f = 0$ contribution, which shows broad peaks above each $m_f = 0$ threshold. These peaks have widths of the order of 0.5 γ Ry ($\gamma = 0.43$) so should be readily resolved, while apart from the ($\ell = 0$, $m_f = 1$) case the other peaks may be too narrow to detect. The "$2p_o$" cross-section (fig 6.22) has a broad feature at the lowest ($\ell = 0$, $m_f = 1$) threshold with a secondary ($m_f = -1$) peak on its shoulder and the same pattern is followed at each higher $m_f = 1$ threshold with the secondary $m_f = -1$ peak becoming relatively weaker. The $m_f = 0$ thresholds now show very strong resonances which become increasingly narrow as ℓ increases. No non-threshold secondary maxima are seen.

In general, it is seen from the results given by figs 6.15 - 6.22, that the overall behaviour of the cross-sections, is, as in the Landau continuum case, that illustrated by fig 5.10, although (as already discussed) the cross-sections in this case, are much smaller.

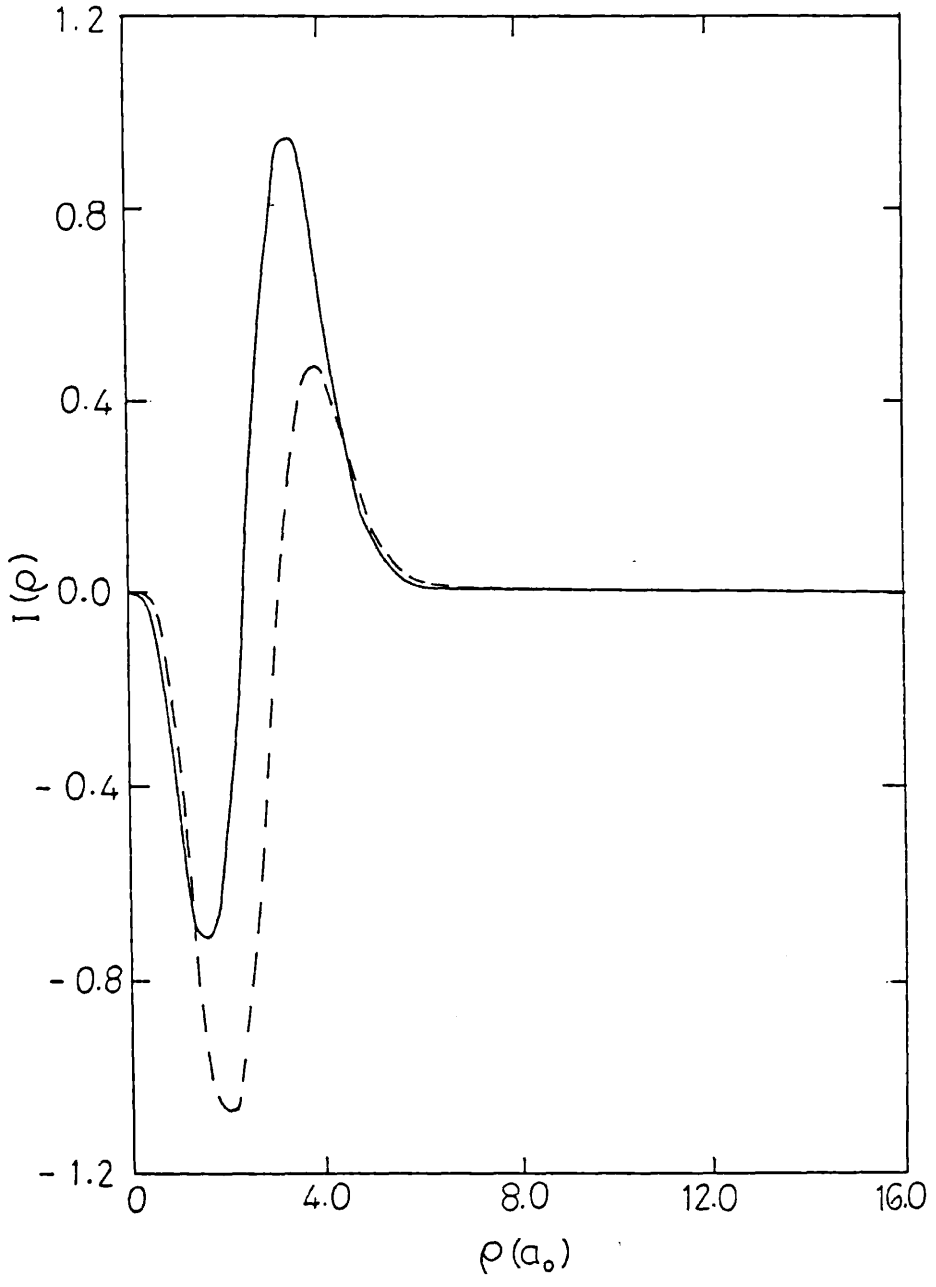

Fig 6.14

The function $I(\rho) = u_1^{m=-1}(\rho)\ \rho^{3/2}\ e^{-\delta\rho^2}$ plotted against ρ . The function $u_1^{m=-1}(\rho)$ is the radial part of the continuum state wavefunction for the Landau continuum (broken line) and the Coulomb modified continuum (continuous line).

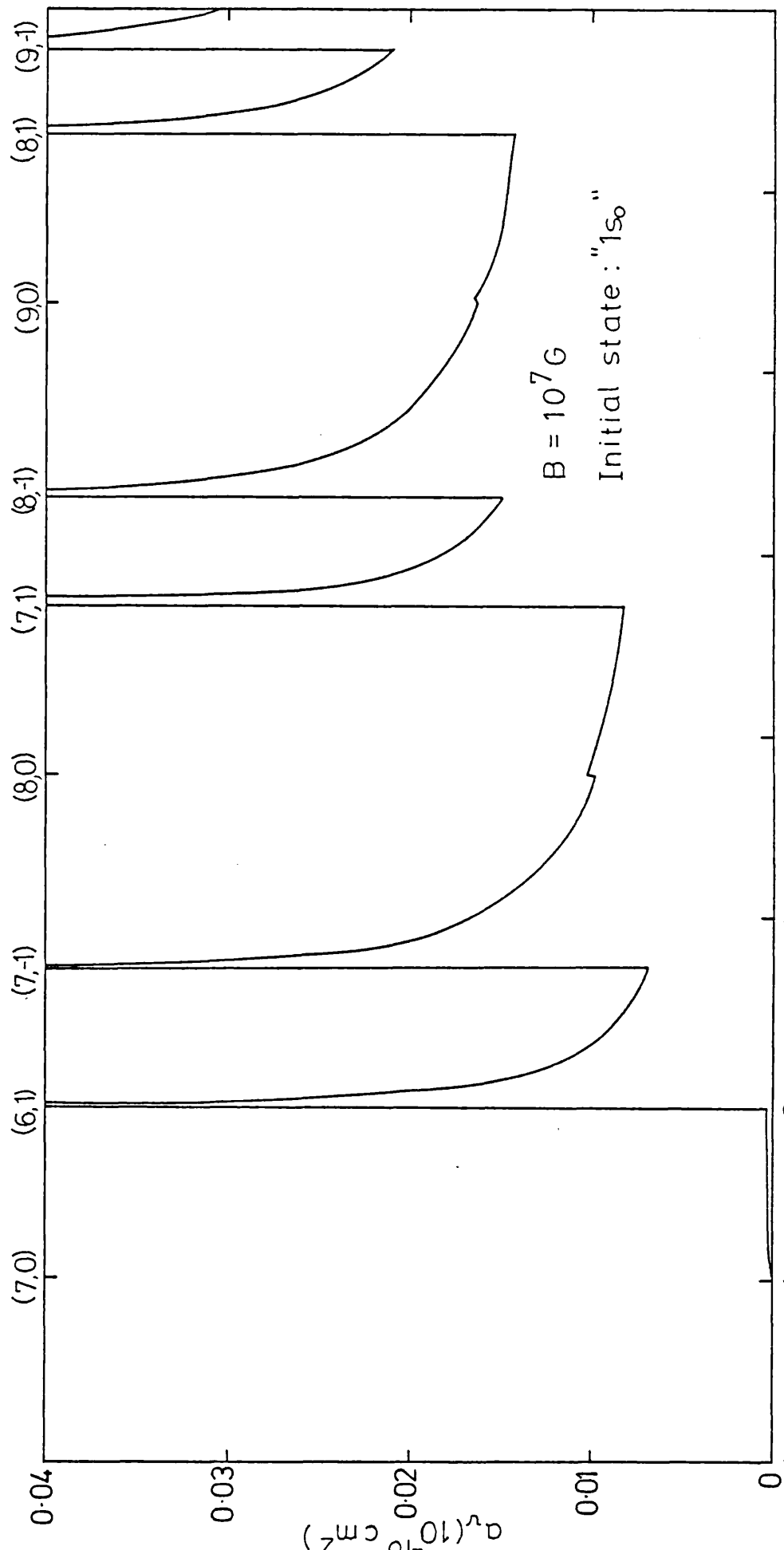
(7,0)
(6,1)
(7,-1)
(8,0)
(7,1)
(8,-1)
(9,0)
(8,1)
(9,-1)
B = 10^7 G
Initial state : "1s0"
0·04
0·03
0·02
0·01
0
0
1
2
3
4
5
6
7
8
ENERGY (⅄ry)
$a_\nu(10^{-18}\ cm^2)$

Fig 6.15

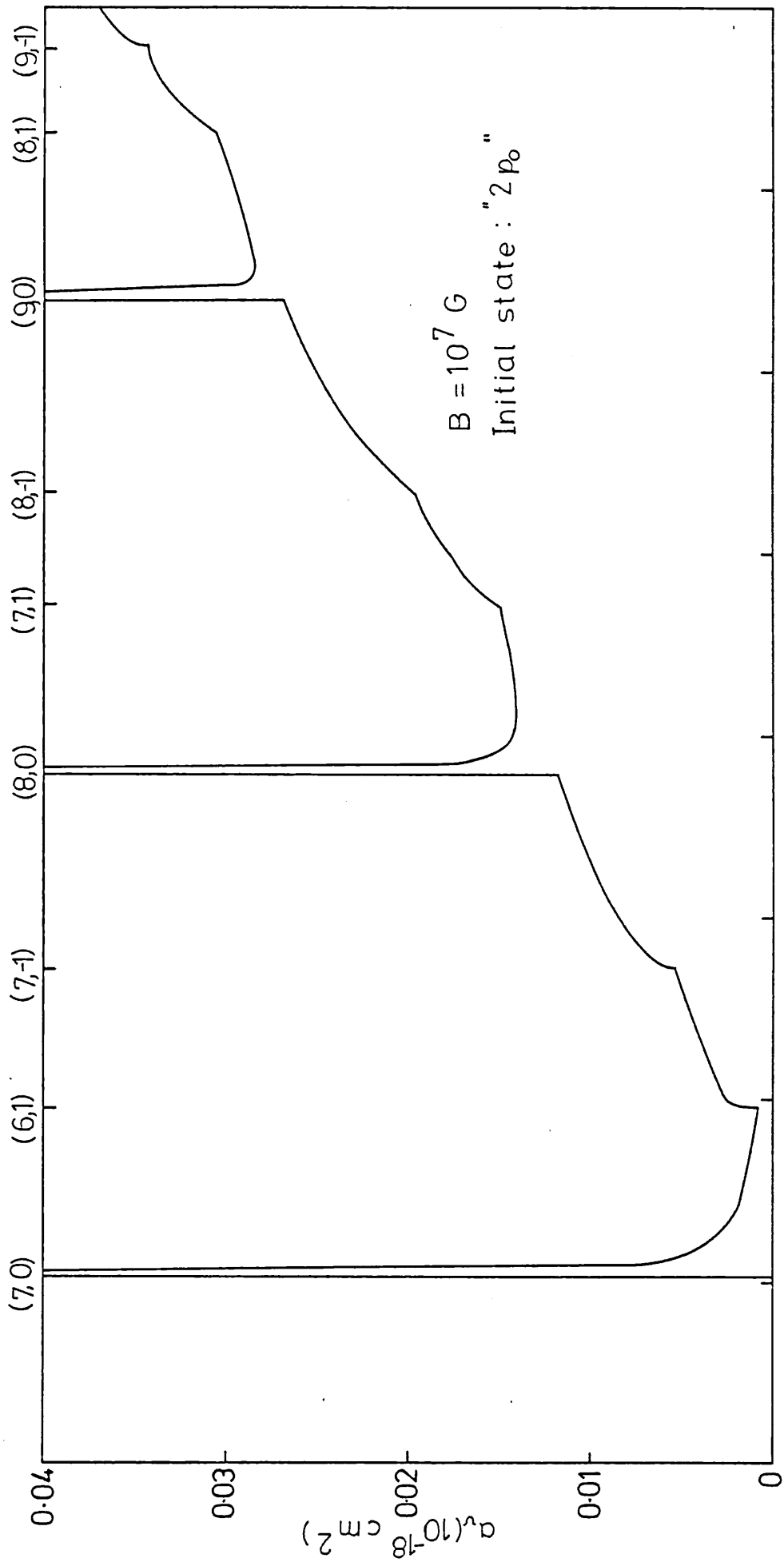
(7,0)
(6,1)
(7,-1)
(8,0)
(7,1)
(8,-1)
(9,0)
(8,1)
(9,-1)
B = 10^7 G
Initial state : "2p_o"
0·04
0·03
0·02
0·01
0
0
1
2
3
4
5
6
7
8
ENERGY (Ry)
σ_v(10^-18 cm^2)

Fig 6.16

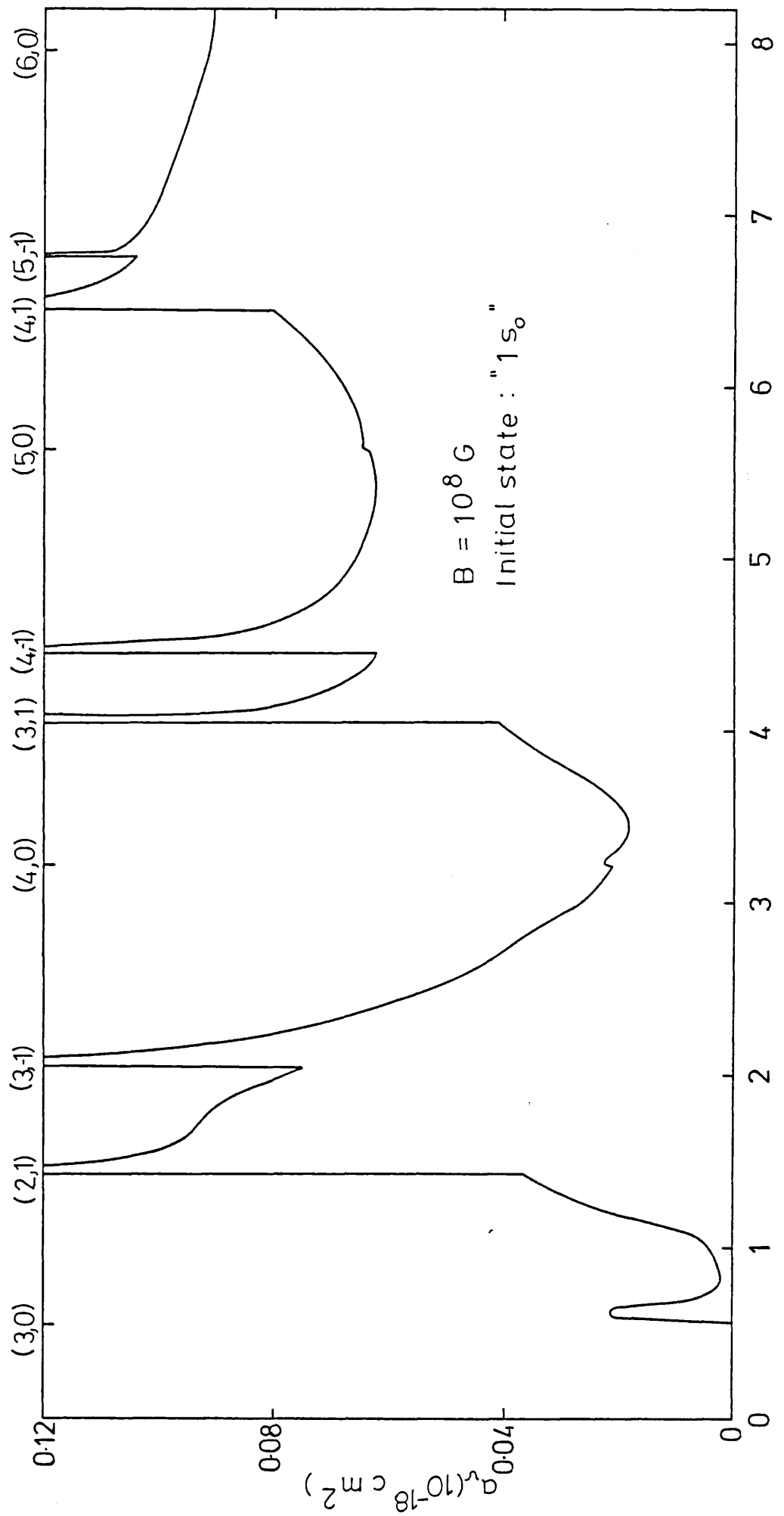
(3,0)
(2,1)
(3,-1)
(4,0)
(3,1)
(4,-1)
(5,0)
(4,1)
(5,-1)
(6,0)
B = 10^8 G
Initial state : "1 s_o"
0·12
0·08
0·04
0
Q_ς(10^-18 c m^2)
0
1
2
3
4
5
6
7
8
ENERGY (Ry)

Fig 6.17

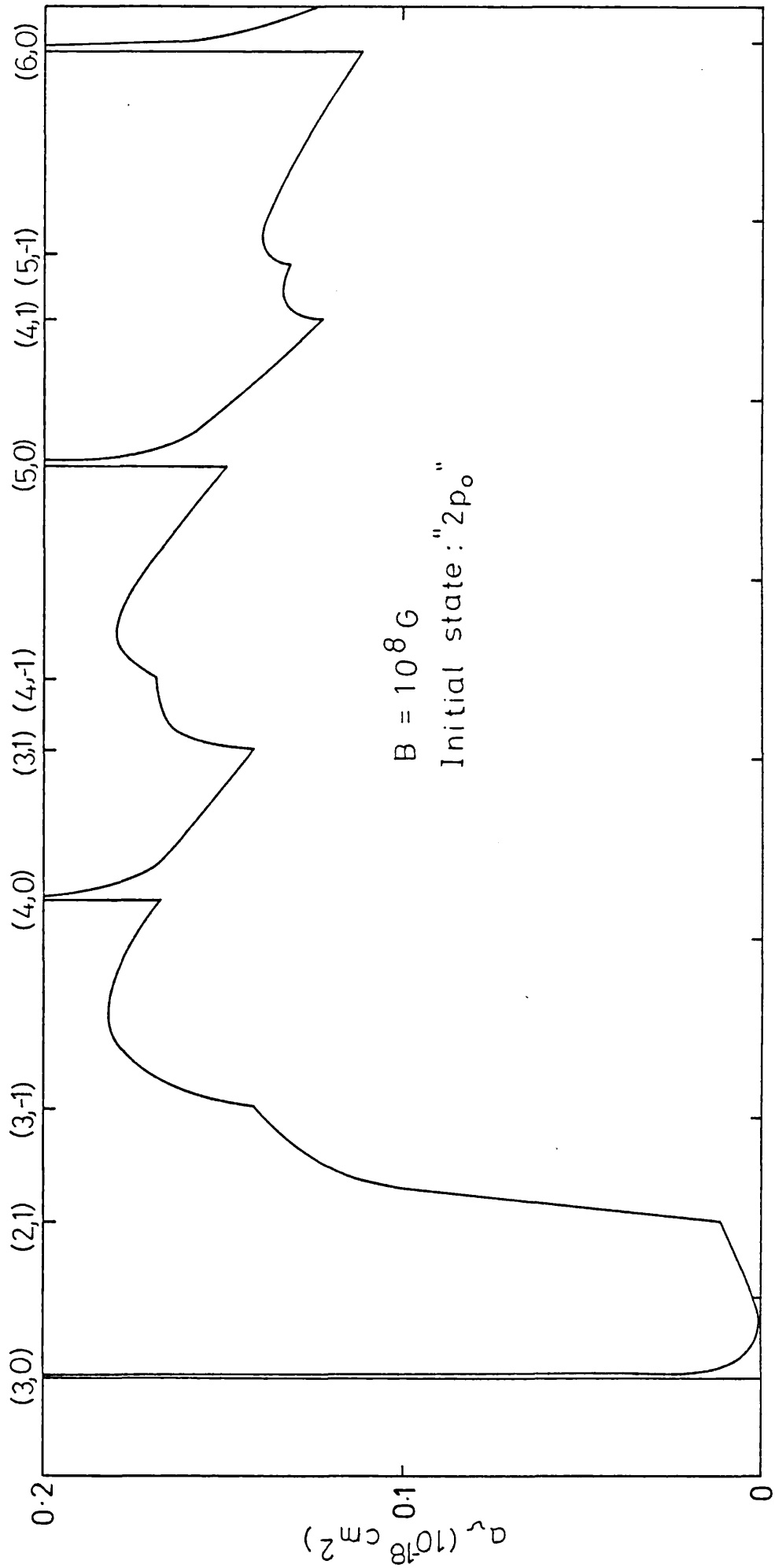
(3,0)
(2,1)
(3,-1)
(4,0)
(3,1)
(4,-1)
(5,0)
(4,1)
(5,-1)
(6,0)
0·2
0·1
0
σ_ν (10^{-18} cm^2)
0
1
2
3
4
5
6
7
8
ENERGY (Ry)
B = 10^8 G
Initial state: "$2p_o$"

Fig 6.18

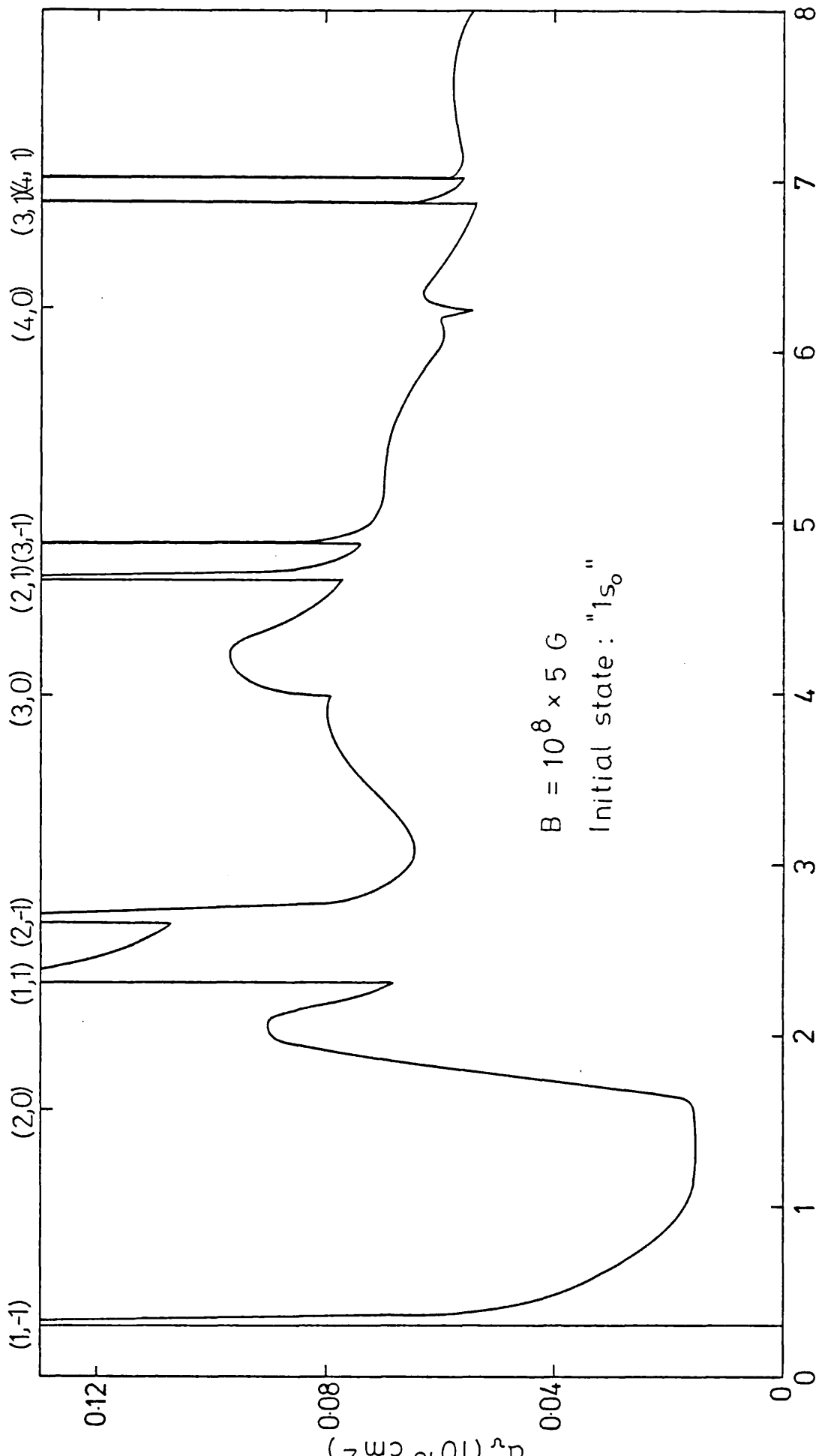
(1,-1)
(2,0)
(1,1)
(2,-1)
(3,0)
(2,1)(3,-1)
(4,0)
(3,1)(4,1)
0·12
0·08
0·04
0
Q_γ (10^{-18} cm 2)
B = 10^8 x 5 G
Initial state : "$1s_0$"
0
1
2
3
4
5
6
7
8
ENERGY (X ry)

Fig 6.19

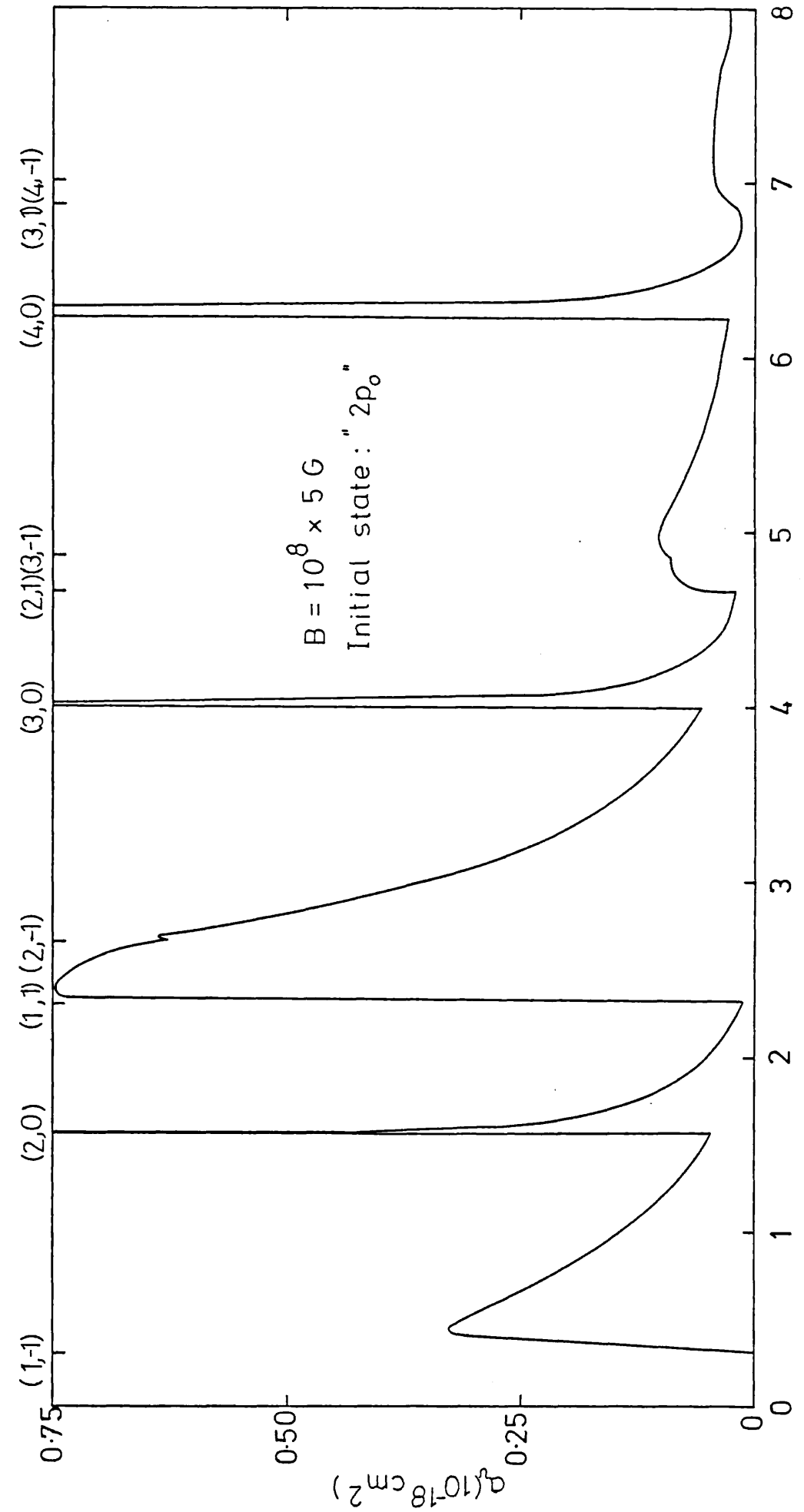
(1,-1)
(2,0)
(1,1) (2,-1)
(3,0)
(2,1)(3,-1)
(4,0)
(3,1)(4,-1)
B = 10^8 x 5 G
Initial state : "2p_o"
0·75
0·50
0·25
0
q(10^-18 cm^2)
0
1
2
3
4
5
6
7
8
ENERGY (Ry)

Fig 6.20

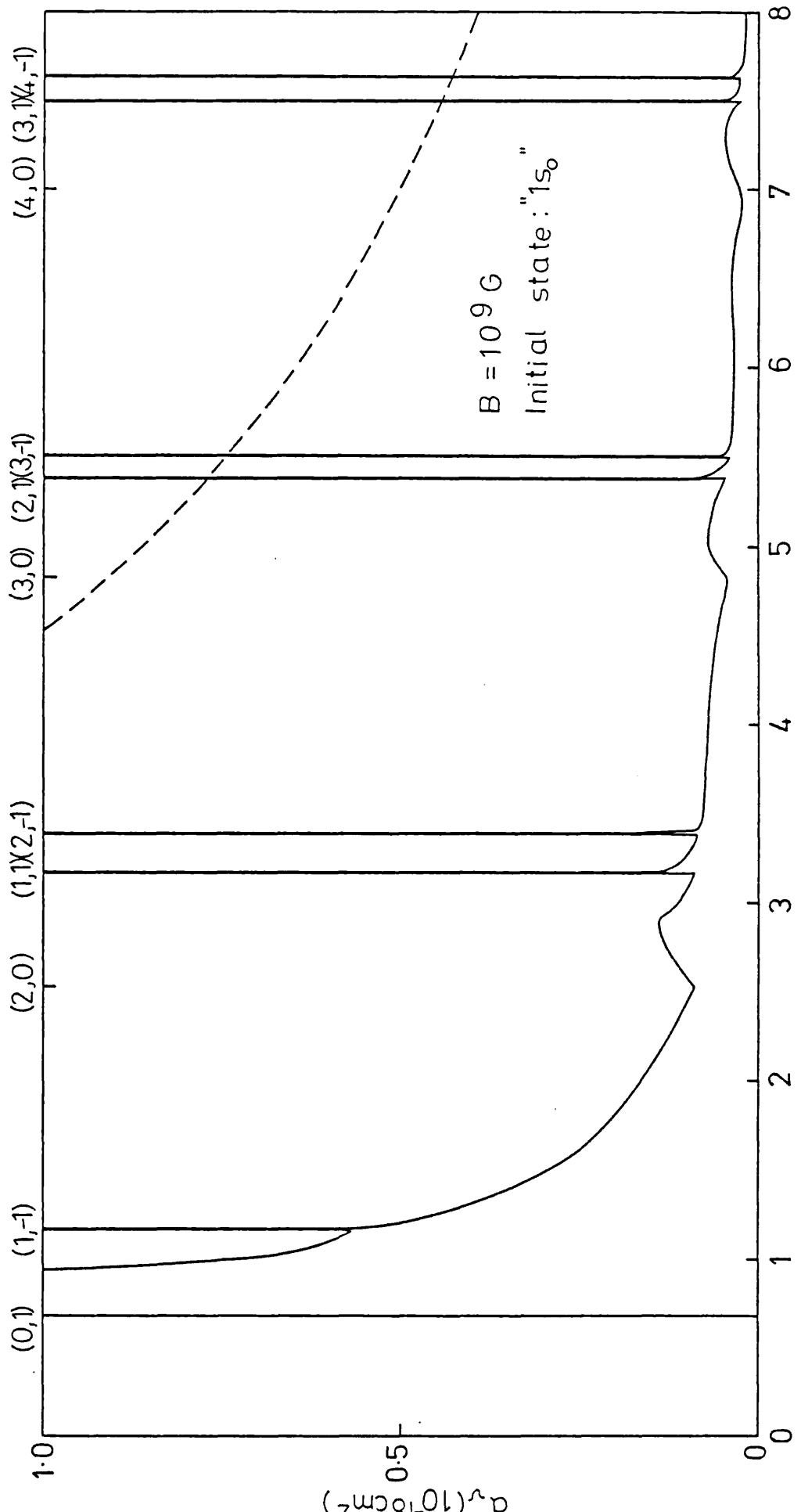
(0,1)
(1,-1)
(2,0)
(1,1)(2,-1)
(3,0)
(2,1)(3,-1)
(4,0)
(3,1)(4,-1)
B = 10^9 G
Initial state: "1s0"
1·0
0·5
0
$\alpha_\nu(10^{-18}cm^2)$
0
1
2
3
4
5
6
7
8
ENERGY (δ ry)

Fig 6.21

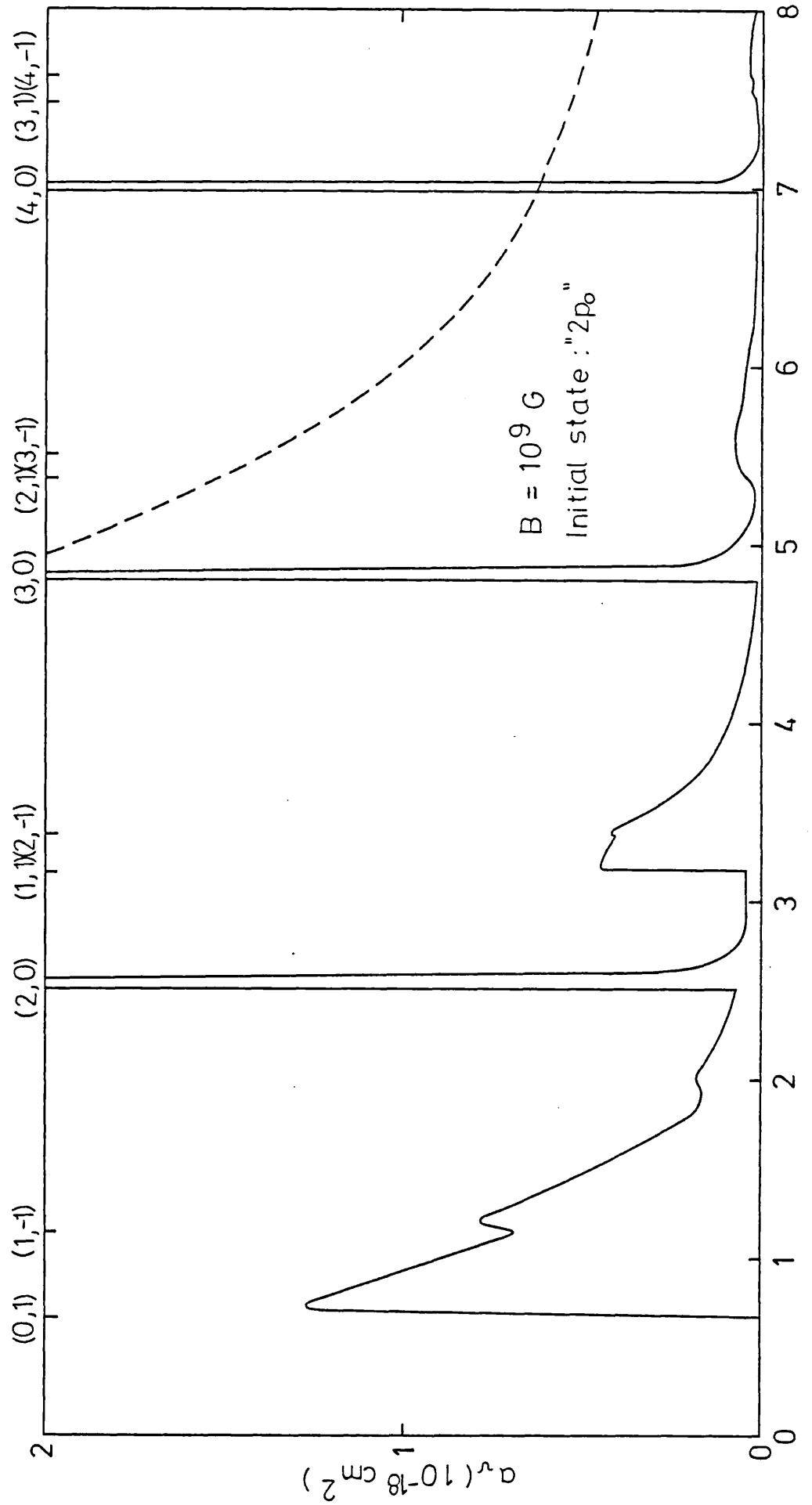
(0,1)
(1,-1)
(2,0)
(1,1)(2,-1)
(3,0)
(2,1)(3,-1)
(4,0)
(3,1)(4,-1)
B = 10^9 G
Initial state : "2p0"
σ_γ (10^-18 cm^2)
ENERGY (χ ry)
0
1
2
3
4
5
6
7
8

Fig 6.22

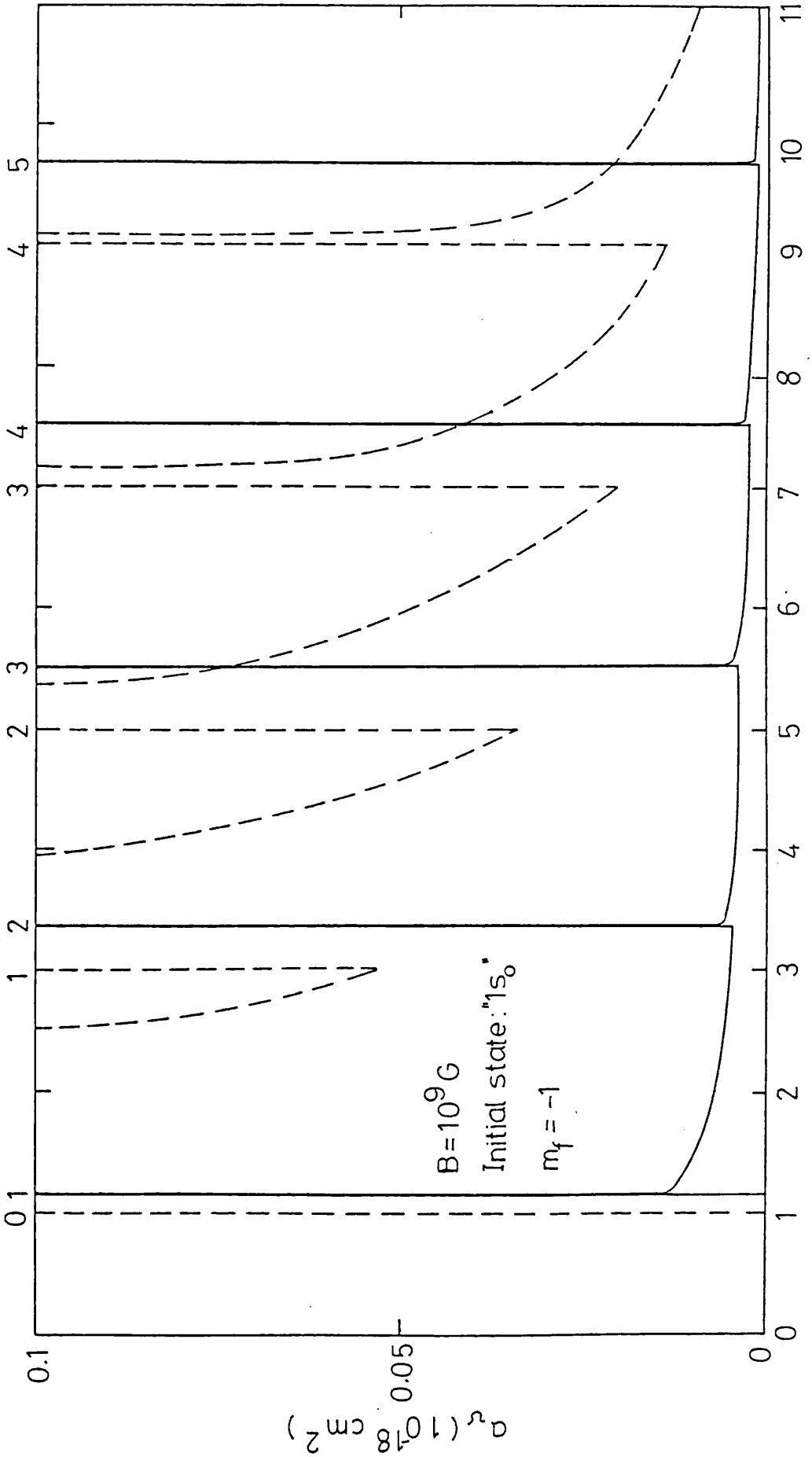
σ_γ (10^{-18} cm^2)
0.1
0.05
0
0 1 2 3 4 5 6 7 8 9 10 11
ENERGY (γ ry)
0 1 2 3 4 5
B=10^9G
Initial state: ^1s_o
$m_f = -1$

Fig 6.23

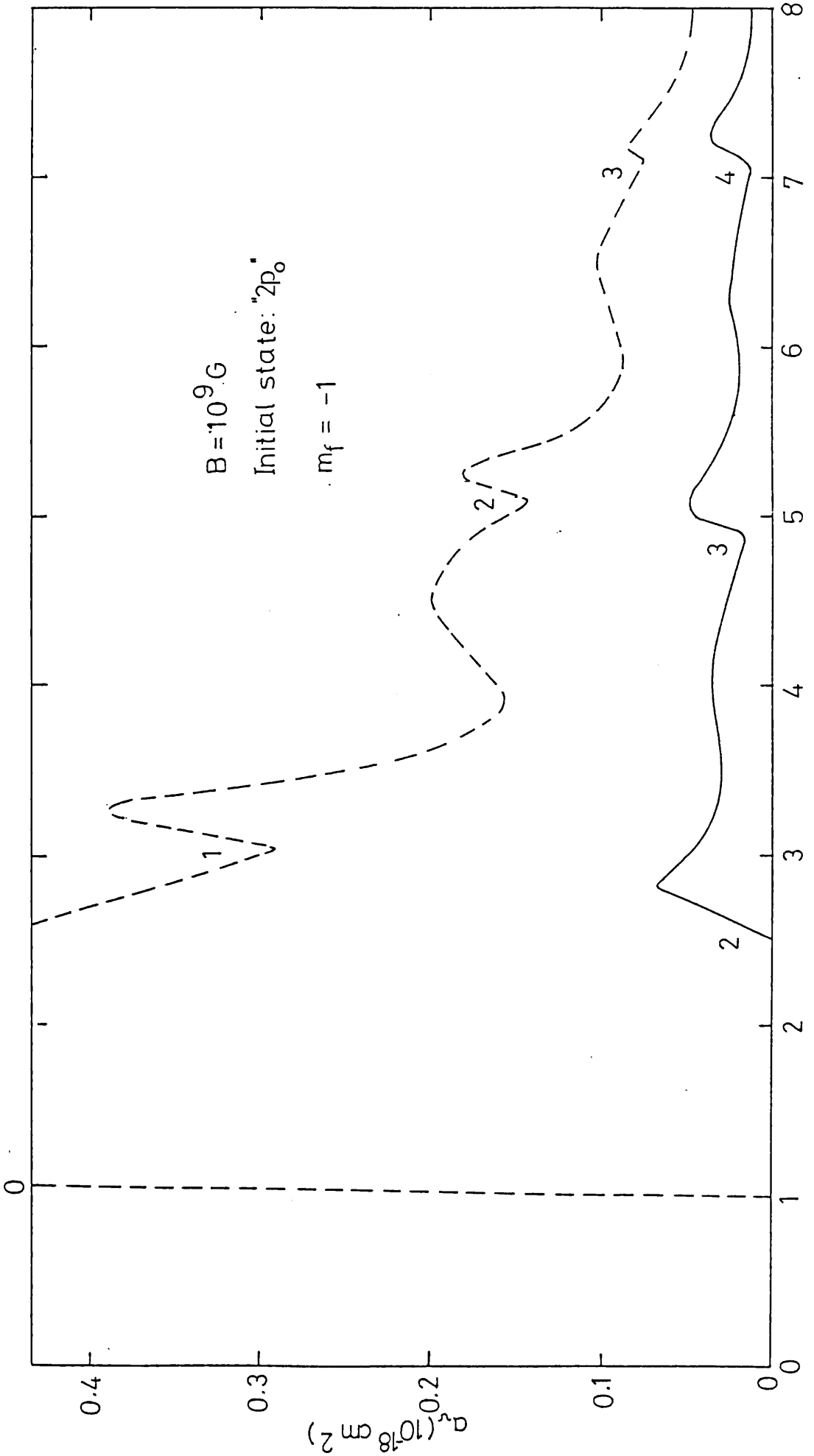
B=10^9 G
Initial state: "2p_o"
m_f = -1
1
2
3
2
3
4
0
0.1
0.2
0.3
0.4
0
1
2
3
4
5
6
7
8
ENERGY (δ ry)
σ_ς(10^-18 cm^2)

Fig 6.24

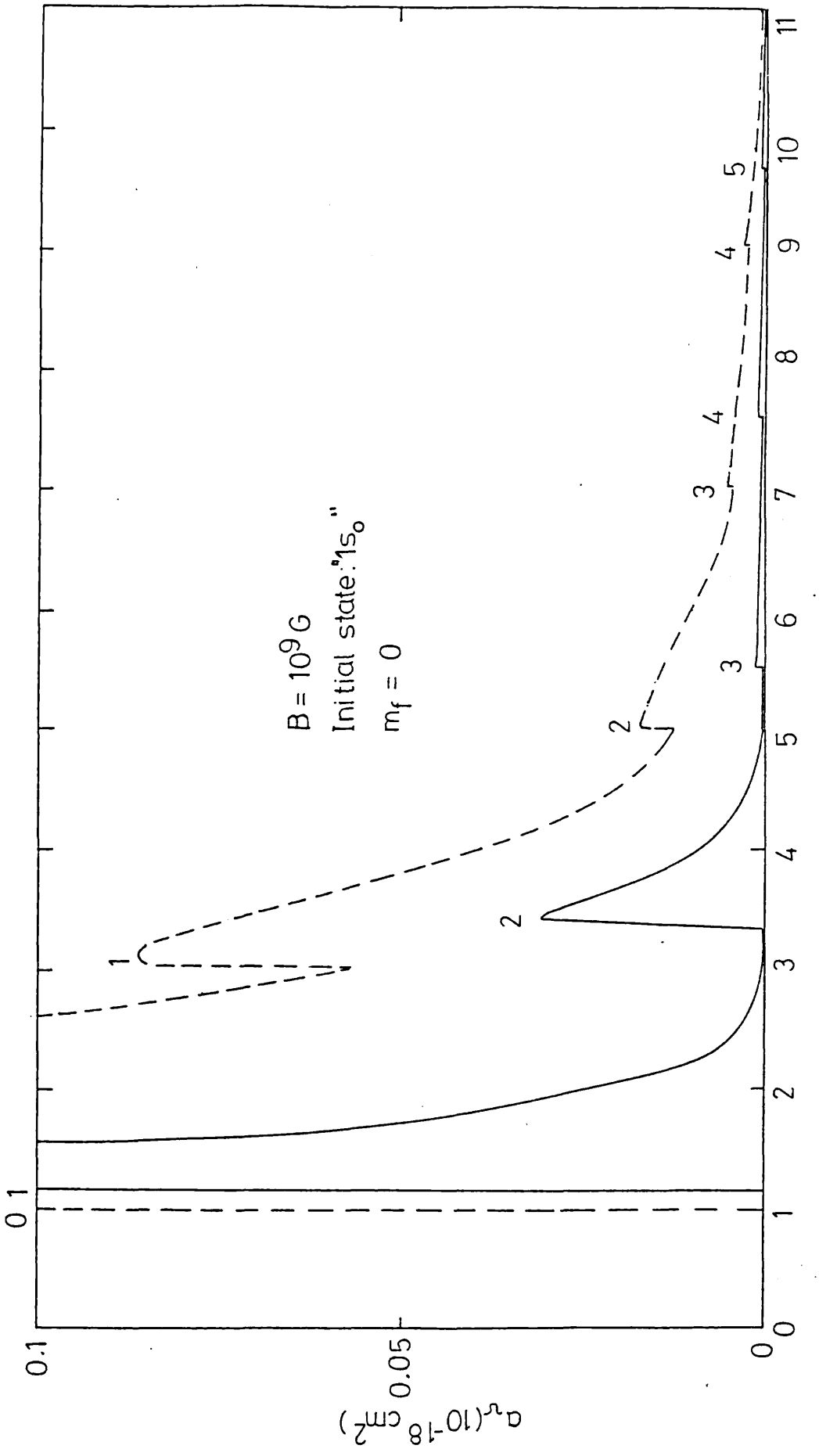
$B = 10^9$ G
Initial state: ^1s_o
$m_f = 0$
$\alpha_\gamma (10^{-18}$ cm$^2)$
0.1
0.05
0
0 1
0 1 2 3 4 5 6 7 8 9 10 11
ENERGY (X ry)
1
2
2
3
3
4
4
5

Fig 6.25

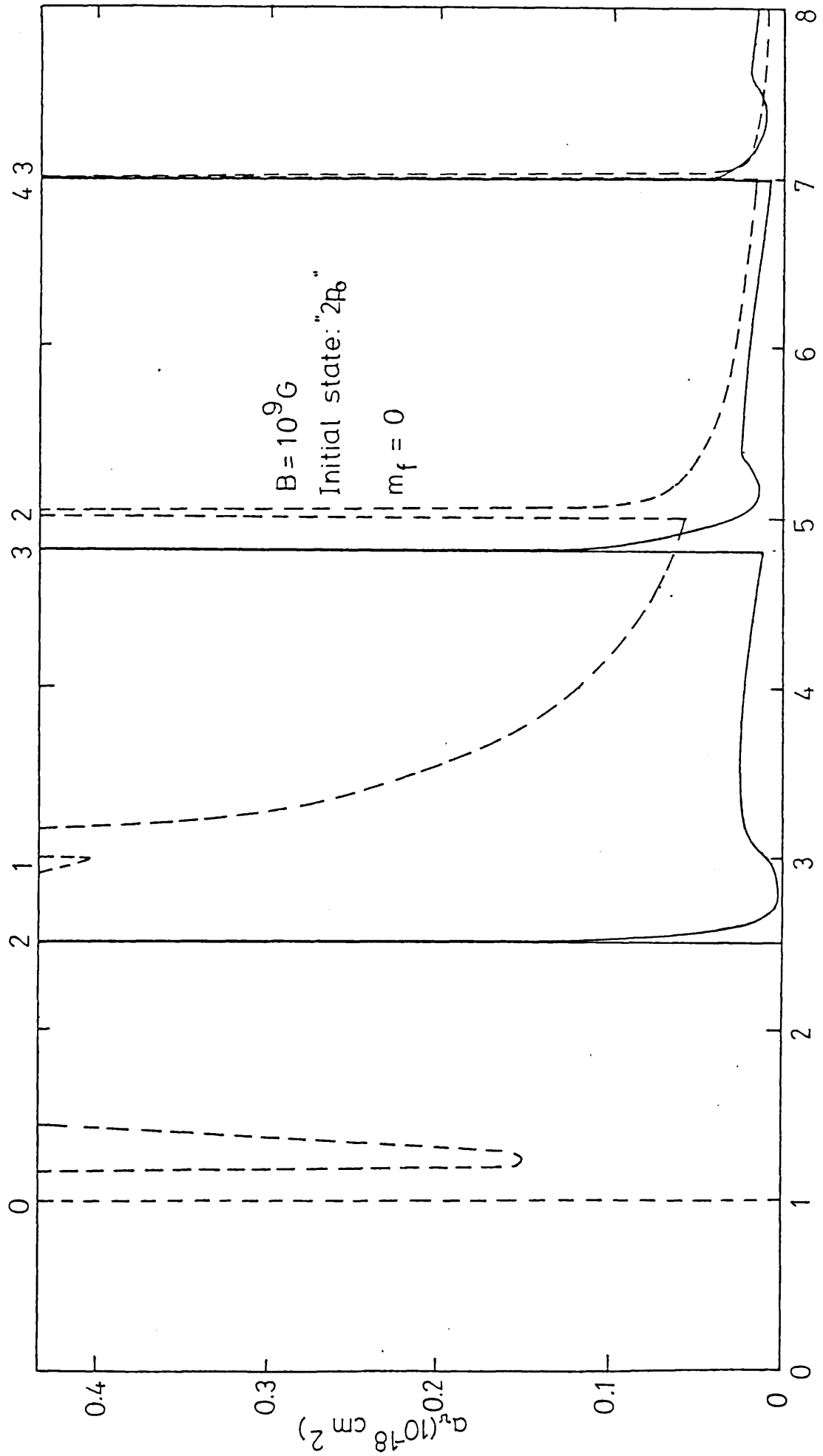
$B = 10^9 G$
Initial state: "$2p_0$"
$m_f = 0$
$\alpha_\epsilon (10^{-18}$ cm $^2)$
0.4
0.3
0.2
0.1
0
0 1 2 3 4 5 6 7 8
ENERGY (χ ry)

Fig 6.26

Figure 6.15

The photoionization cross-section ($10^{-18}cm^2$) from "$1s_o$" to the Coulomb modified continuum at $B = 10^7G$. The corresponding (ℓ,m) are given by the peaks and the energy is measured in units of γ Ry above the field dependent ionization threshold.

Figure 6.16

The photoionization cross-section ($10^{-18}cm^2$) from "$2p_o$" to the Coulomb modified continuum at $B = 10^7G$. The corresponding (ℓ,m) are given by the peaks and the energy is measured in units of γ Ry above the field dependent ionization threshold.

Figure 6.17

The photoionization cross-section ($10^{-18}cm^2$) from "$1s_o$" to the Coulomb modified continuum at $B = 10^8G$. The corresponding (ℓ,m) are given by the peaks and the energy is measured in units of γ Ry above the field dependent ionization threshold.

Figure 6.18

The photoionization cross-section ($10^{-18}cm^2$) from "$2p_o$" to the Coulomb modified continuum at $B = 10^8G$. The corresponding (ℓ,m) are given by the peaks and the energy is measured in units of γ Ry above the field dependent ionization threshold.

Figure 6.19

The photoionization cross-section ($10^{-18}cm^2$) from "$1s_o$" to the Coulomb modified continuum at $B = 5 \times 10^8G$. The corresponding (ℓ,m) are given by the peaks and the energy is measured in units of γ Ry above the field dependent ionization threshold.

Figure 6.20

The photoionization cross-section ($10^{-18}cm^2$) from "$2p_o$" to the Coulomb modified continuum at $B = 5 \times 10^8G$. The corresponding (ℓ,m) are given by the peaks and the energy is measured in units of γ Ry above the field dependent ionization threshold.

Figure 6.21

The photoionization cross-section ($10^{-18}cm^2$) from "$1s_o$" to the Coulomb modified continuum at $B = 10^9G$. The corresponding (ℓ,m) are given by the peaks and the energy is measured in units of γ Ry above the field dependent ionization threshold.
The zero field cross-section is given by the broken line.

Figure 6.22

The photoionization cross-section ($10^{-18}cm^2$) from "$2p_o$" to the Coulomb modified continuum at $B = 10^9G$. The corresponding (ℓ,m) are given by the peaks and the energy is measured in units of γ Ry above the field dependent ionization threshold.
The zero field cross-section is given by the broken line.

Figure 6.23

The photoionization cross-sections ($10^{-18}cm^2$) from "$1s_o$" to the $m_f = -1$ continuum at $B = 10^9G$ in the Landau (broken line) and Coulomb modified (continuous line) cases. The numbers by the peaks indicate the corresponding principle quantum number (ℓ) and the energy is measured in units of γ Ry above the field dependent ionization threshold.

Figure 6.24

The photoionization cross-sections ($10^{-18}cm^2$) from "$2p_o$" to the $m_f = -1$ continuum at $B = 10^9G$ in the Landau (broken line) and Coulomb modified (continuous line) cases. The numbers by the peaks indicate the corresponding principle quantum number (ℓ) and the energy is measured in units of γ Ry above the field dependent ionization threshold.

Figure 6.25

The photoionization cross-sections ($10^{-18}cm^2$) from "$1s_o$" to the $m_f = 0$ continuum at $B = 10^9G$ in the Landau (broken line) and Coulomb modified (continuous line) cases. The numbers by the peaks indicate the corresponding principle quantum number (ℓ) and the energy is measured in units of γ Ry above the field dependent ionization threshold.

Figure 6.26

The photoionization cross-sections ($10^{-18}cm^2$) from "$2p_o$" to the $m_f = 0$ continuum at $B = 10^9G$ in the Landau (broken line) and Coulomb modified (continuous line) cases. The numbers by the peaks indicate the corresponding principle quantum number (ℓ) and the energy is measured in units of γ Ry above the field dependent ionization threshold.

Energy of the Final State in Ry	Total Photoionization Cross Section from "$1s_o$" State in $10^{-18}cm^2$	Total Photoionization Cross Section from the "$2p_o$" State in $10^{-18}cm^2$
1.02009 (7,0)	0	∞
1.021	1.268(-5)	5.378(-2)
1.2	1.774(-4)	3.403(-3)
1.4	2.565(-4)	2.041(-3)
1.6	3.152(-4)	1.428(-3)
1.8	3.637(-4)	1.055(-3)
1.96	3.976(-4)	8.421(-4)
1.96090 (6,1)	∞	8.410(-4)
1.961	5.517(-1)	9.008(-4)
2.0	2.830(-2)	1.978(-3)
2.2	1.175(-2)	3.498(-3)
2.4	8.844(-3)	4.339(-3)
2.6	7.460(-3)	4.979(-3)
2.72	6.914(-3)	5.307(-3)
2.72564 (7,-1)	∞	5.322(-3)
2.726	2.851(-1)	5.410(-3)
2.8	2.599(-2)	6.763(-3)
3.0	1.615(-2)	8.355(-3)
3.2	1.332(-2)	9.485(-3)
3.4	1.176(-2)	1.042(-2)

Table 6.9a

Energy of the Final State in Y Ry	Total Photoionization Cross Section from "$1s_o$" State in $10^{-18}cm^2$	Total Photoionization Cross Section from the "$2p_o$" State in $10^{-18}cm^2$
3.6	1.073(-2)	1.122(-2)
3.79	9.997(-3)	1.191(-2)
3.79300 (8,0)	9.987(-3)	∞
3.794	9.996(-3)	3.944(-2)
4.0	9.548(-3)	1.422(-2)
4.2	9.139(-3)	1.417(-2)
4.4	8.796(-3)	1.440(-2)
4.6	8.505(-3)	1.471(-2)
4.72	8.350(-3)	1.491(-2)
4.72564 (7,1)	∞	1.492(-2)
4.726	2.889(-1)	1.501(-2)
4.8	2.779(-2)	1.633(-2)
5.0	1.823(-2)	1.784(-2)
5.2	1.561(-2)	1.891(-2)
5.31	1.476(-2)	1.943(-2)
5.31670 (8,-1)	∞	1.946(-2)
5.317	3.148(-1)	1.952(-2)
5.4	3.223(-2)	2.092(-2)
5.6	2.307(-2)	2.262(-2)
5.8	2.010(-2)	2.393(-2)

Table 6.9b

Energy of the Final State in Ry	Total Photoionization Cross Section from "$1s_o$" State in 10^{-18} cm^2	Total Photoionization Cross Section from The "$2p_o$" State in 10^{-18} cm^2
6.0	1.838(-2)	2.505(-2)
6.2	1.719(-2)	2.604(-2)
6.39	1.633(-2)	2.690(-2)
6.39200 (9,0)	1.632(-2)	∞
6.393	1.633(-2)	4.048(-2)
6.4	1.632(-2)	3.171(-2)
6.6	1.574(-2)	2.853(-2)
6.8	1.521(-2)	2.896(-2)
2.0	1.476(-2)	2.951(-2)
7.2	1.437(-2)	3.006(-2)
7.31	1.418(-2)	3.036(-2)
7.31670 (8,1)	∞	3.038(-2)
7.317	3.168(-1)	3.045(-2)
7.4	3.221(-2)	3.174(-2)
7.6	2.360(-2)	3.320(-2)
7.79	2.112(-2)	3.426(-2)
7.79648 (9,-1)	∞	3.429(-2)
7.797	2.480(-1)	3.437(-2)
7.8	1.082(-1)	3.450(-2)
8.0	3.108(-2)	3.672(-2)

Table 6.9c

Total photoionization cross-sections for transitions from the bound states "$1s_o$" and "$2p_o$" to the Coulomb-modified continuum at B = 10^7G. (ℓ,m) is given when the final state energy corresponds to the energy of a discrete level in the continuum.

Energy of the Final State in γ Ry	Total Photoionization Cross Section from "$1s_o$" State in $10^{-18}cm^2$	Total photoionization Cross Section from The "$2p_o$" State in $10^{-18}cm^2$
0.54390 (3,0)	0	∞
0.544	1.447(-3)	5.003(-1)
0.6	2.072(-2)	1.160(-2)
0.8	2.098(-3)	1.534(-5)
1.0	4.237(-3)	2.984(-3)
1.2	2.074(-2)	7.305(-3)
1.41	3.654(-2)	1.123(-2)
1.41470 (2,1)	∞	1.131(-2)
1.415	7.115(-1)	1.517(-2)
1.6	9.623(-2)	9.986(-2)
1.8	9.059(-2)	1.264(-1)
2.0	7.790(-2)	1.389(-1)
2.04888 (3,-1)	∞	1.407(-1)
2.049	9.110(-1)	1.415(-1)
2.2	8.890(-2)	1.693(-1)
2.4	6.528(-2)	1.793(-1)
2.6	4.848(-2)	1.815(-1)
2.8	3.618(-2)	1.794(-1)
3.0	2.762(-2)	1.746(-1)
3.2	2.200(-2)	1.680(-1)

Table 6.10a

Energy of the Final State in Ry	Total Photoionization Cross Section from "$1s_o$" State in $10^{-18}cm^2$	Total Photoionization Cross Section from The "$2p_o$" State in $10^{-18}cm^2$
3.20969 (4,0)	2.178(-2)	∞
3.21	2.244(-2)	2.077(-1)
3.4	1.896(-2)	1.667(-1)
3.6	2.026(-2)	1.601(-1)
3.8	2.971(-2)	1.522(-1)
4.0	3.857(-2)	1.435(-1)
4.04888 (3,1)	∞	1.413(-1)
4.049	9.286(-2)	1.568(-1)
4.2	7.205(-2)	1.660(-1)
4.4	6.348(-2)	1.684(-1)
4.45037 (4,-1)	∞	1.679(-1)
4.451	3.923(-1)	1.689(-1)
4.6	8.242(-2)	1.791(-1)
4.8	7.157(-2)	1.783(-1)
5.0	6.624(-2)	1.733(-1)
5.2	6.361(-2)	1.664(-1)
5.4	6.290(-2)	1.585(-1)
5.6	6.352(-2)	1.500(-1)
5.63640 (5,0)	6.373(-2)	∞
5.637	6.412(-2)	3.926(-1)

Table 6.10b

Energy of the Final State in ϒ Ry	Total Photoionization Cross Section from "$1s_o$" State in 10^{-18} cm^2	Total Photoionization Cross Section from The "$2p_o$" State in 10^{-18} cm^2
5.8	6.5361(-2)	1.600(-1)
6.0	6.745(-2)	1.469(-1)
6.2	7.302(-2)	1.359(-1)
6.4	7.833(-2)	1.257(-1)
6.45037 (4,1)	∞	1.232(-1)
6.451	4.338(-1)	1.244(-1)
6.5	1.225(-1)	1.312(-1)
6.7	1.053(-1)	1.323(-1)
6.73956 (5,-1)	∞	1.316(-1)
6.74	1.507(-1)	1.322(-1)
6.8	1.066(-1)	1.371(-1)
7.0	1.019(-1)	1.375(-1)
7.2	9.940(-2)	1.337(-1)
7.4	9.706(-2)	1.283(-1)
7.6	9.481(-2)	1.221(-1)
7.8	9.267(-2)	1.157(-1)
7.94	9.122(-2)	1.111(-1)
7.94700 (6,0)	9.115(-2)	∞
7.948	9.115(-2)	4.727(-1)
8.0	9.079(-2)	1.595(-1)
8.2	9.103(-2)	1.255(-1)

Table 6.10c

Total photoionization cross-sections for transitions from the bound states "$1s_o$" and "$2p_o$" to the Coulomb-modified continuum at B = 10^8G. (ℓ,m) is given when the final state energy corresponds to the energy of a discrete level in the continuum.

Energy of the Final State in Ry	Total Photoionization Cross Section from "$1s_o$" State in $10^{-18}cm^2$	Total Photoionization Cross Section from The "$2p_o$" State in $10^{-18}cm^2$
0.308520 (1,-1)	∞	0
0.309	4.9241(-1)	2.537(-2)
0.4	4.975(-2)	2.720(-1)
0.6	3.237(-2)	2.786(-1)
0.8	2.288(-2)	2.095(-1)
1.0	1.795(-2)	1.461(-1)
1.2	1.601(-2)	9.925(-2)
1.4	1.570(-2)	6.681(-2)
1.56	1.596(-2)	4.856(-2)
1.56361 (2,0)	1.596(-2)	∞
1.564	1.610(-2)	2.424
1.6	1.608(-2)	2.927(-1)
1.8	5.948(-2)	1.065(-1)
2.0	8.983(-2)	5.091(-2)
2.2	7.938(-2)	2.284(-2)
2.3	6.889(-2)	1.506(-2)
2.30852 (1,1)	∞	1.454(-2)
2.309	7.638(-1)	8.723(-2)
2.4	1.288(-1)	7.500(-1)
2.6	8.924(-2)	6.931(-1)
2.66137 (2,-1)	∞	6.276(-1)

Table 6.11a

Energy of the Final State in Ry	Total Photoionization Cross Section from "$1s_o$" State in $10^{-18}cm^2$	Total Photoionization Cross Section from The "$2p_o$" State in $10^{-18}cm^2$
2.662	2.183(-1)	6.311(-1)
2.8	7.430(-2)	5.266(-1)
3.0	6.483(-2)	3.605(-1)
3.2	6.578(-2)	2.424(-1)
3.4	7.092(-2)	1.642(-1)
3.6	7.634(-2)	1.131(-1)
3.8	7.946(-2)	7.958(-2)
3.98	7.926(-2)	5.921(-2)
3.98075 (3,0)	7.926(-2)	∞
3.981	8.034(-2)	6.674
4.0	8.838(-2)	7.352(-1)
4.2	9.722(-2)	9.901(-2)
4.4	8.898(-2)	3.932(-2)
4.6	7.899(-2)	2.542(-2)
4.66137 (2,1)	∞	2.375(-2)
4.662	2.511(-1)	3.042(-2)
4.8	7.770(-2)	9.024(-2)
4.87	7.403(-2)	9.136(-2)
4.87242 (3,-1)	∞	9.132(-2)
4.873	1.019(-1)	9.277(-2)
5.0	7.213(-2)	1.013(-1)

Table 6.11b

Energy of the Final State in Ry	Total Photoionization Cross Section from "$1s_o$" State in $10^{-18}cm^2$	Total Photoionization Cross Section from The "$2p_o$" State in $10^{-18}cm^2$
5.2	6.999(-2)	8.703(-2)
5.4	6.940(-2)	7.055(-2)
5.6	6.790(-2)	5.659(-2)
5.8	6.476(-2)	4.561(-2)
6.0	6.024(-2)	3.720(-2)
6.2	6.024(-2)	3.079(-2)
6.23796 (4,0)	5.404(-2)	∞
6.238	5.433(-2)	17.922
6.4	6.231(-2)	1.106(-1)
6.6	5.843(-2)	2.957(-2)
6.8	5.526(-2)	1.907(-2)
6.87242 (3,1)	∞	1.853(-2)
6.873	8.861(-2)	2.051(-2)
7.0	5.608(-2)	4.018(-2)
7.02042 (4,-1)	∞	4.078(-2)
7.021	5.960(-2)	4.154(-2)
7.2	5.670(-2)	4.913(-2)
7.4	5.761(-2)	4.409(-2)
7.6	5.779(-2)	3.765(-2)
7.8	5.686(-2)	3.185(-2)
8.0	5.495(-2)	2.708(-2)

Table 6.11c

Total photoionization cross-sections for transitions from the bound states "$1s_o$" and "$2p_o$" to the Coulomb-modified continuum at $B = 5 \times 10^8$G. (ℓ,m) is given when the final state energy corresponds to the energy of a discrete level in the continuum.

Energy of the Final State in ϒ Ry	Total Photoionization Cross Section from "$1s_o$" State in $10^{-18}cm^2$	Total Photoionization Cross Section from The "$2p_o$" State in $10^{-18}cm^2$
0.674613 (0,1)	∞	0
0.675	3.027(1)	9.448(-2)
0.8	1.478	1.093
1.0	7.441(-1)	9.028(-1)
1.1	5.884(-1)	7.573(-1)
1.16075 (1,-1)	∞	6.763(-1)
1.161	6.245(-1)	6.905(-1)
1.2	4.928(-1)	7.776(-1)
1.4	3.477(-1)	5.729(-1)
1.6	2.586(-1)	3.797(-1)
1.8	1.994(-1)	2.554(-1)
2.0	1.578(-1)	1.762(-1)
2.2	1.271(-1)	1.244(-1)
2.4	1.036(-1)	8.958(-2)
2.52	9.193(-2)	7.423(-2)
2.52522 (2,0)	9.147(-2)	∞
2.526	9.177(-2)	9.443
2.6	1.054(-1)	4.703(-1)
2.8	1.353(-1)	5.261(-2)
3.0	1.118(-1)	4.748(-2)
3.16	9.061(-2)	5.107(-2)
3.16075 (1,1)	∞	5.107(-2)

Table 6.12a

Energy of the Final State in ϒ Ry	Total Photoionization Cross Section from "$1s_o$" State in $10^{-18}cm^2$	Total Photoionization Cross Section from The "$2p_o$" State in $10^{-18}cm^2$
3.161	2.618(-1)	9.014(-2)
3.2	1.067(-1)	4.461(-1)
3.37	8.799(-2)	4.208(-1)
3.37873 (2,-1)	∞	4.119(-1)
3.379	8.975(-2)	4.138(-1)
3.4	8.648(-2)	4.078(-1)
3.6	7.835(-2)	2.445(-1)
3.8	7.590(-2)	1.420(-1)
4.0	7.434(-2)	8.718(-2)
4.2	7.048(-2)	5.712(-2)
4.4	6.372(-2)	3.965(-2)
4.6	5.514(-2)	2.886(-2)
4.8	4.581(-2)	2.186(-2)
4.81222 (3,0)	4.581(-2)	∞
4.813	4.578(-2)	7.632
5.0	6.980(-2)	3.946(-2)
5.2	6.585(-2)	1.926(-2)
5.37	4.920(-2)	2.701(-2)
5.37873 (2,1)	∞	2.719(-2)
5.379	5.180(-2)	3.072(-2)
5.4	4.774(-2)	5.581(-2)
5.51	4.161(-2)	7.018(-2)

Table 6.12b

Energy of the Final State in γ Ry	Total Photoionization Cross Section from "$1s_o$" State in $10^{-18}cm^2$	Total Photoionization Cross Section from The "$2p_o$" State in $10^{-18}cm^2$
5.51588 (3,-1)	∞	6.997(-2)
5.516	4.185(-2)	7.049(-2)
5.6	3.836(-2)	7.379(-2)
5.8	3.593(-2)	5.488(-2)
6.0	3.744(-2)	3.936(-2)
6.2	3.959(-2)	2.905(-2)
6.4	3.985(-2)	2.216(-2)
6.6	3.749(-2)	1.733(-2)
6.8	3.326(-2)	1.378(-2)
6.99	2.868(-2)	1.119(-2)
6.99740 (4,0)	2.851(-2)	∞
6.998	2.852(-2)	6.929
7.0	2.848(-2)	3.250
7.2	4.619(-2)	1.793(-2)
7.4	4.178(-2)	1.390(-2)
7.51	3.432(-2)	1.853(-2)
7.51588 (3,1)	∞	1.868(-2)
7.516	3.459(-2)	1.940(-2)
7.61	2.914(-2)	3.312(-2)
7.61436 (4,-1)	∞	3.319(-2)
7.615	2.917(-2)	3.379(-2)
7.8	2.412(-2)	3.383(-2)
8.0	2.337(-2)	2.576(-2)

Table 6.12c

Total photoionization cross-sections for transitions from the bound states "$1s_o$" and "$2p_o$" to the Coulomb-modified continuum at $B = 10^9$G (ℓ,m) is given when the final state energy corresponds to the energy of a discrete level in the continuum.

Energy of the Final State in Ry	Photoionization Cross Section from The "$1s_o$" State in $10^{-18}cm^2$	Photoionization Cross Section from The "$2p_o$" State in $10^{-18}cm^2$
2.72564	∞	0
2.726	2.782(-1)	8.753(-5)
2.8	1.937(-2)	1.253(-3)
3.0	1.011(-2)	2.384(-3)
3.2	7.704(-3)	3.103(-3)
3.4	6.475(-3)	3.663(-3)
3.6	5.699(-3)	4.129(-3)
3.79	5.176(-3)	4.513(-3)
4.0	4.741(-3)	4.887(-3)
4.2	4.417(-3)	5.204(-3)
4.4	4.153(-3)	5.490(-3)
4.6	3.933(-3)	5.751(-3)
4.8	3.746(-3)	5.989(-3)
5.0	3.585(-3)	6.208(-3)
5.2	3.444(-3)	6.411(-3)
5.31	3.373(-3)	6.516(-3)
5.31670	∞	6.522(-3)
5.317	3.035(-1)	6.588(-3)

Table 6.13a

Energy of the Final State in ϒ Ry	Photoionization Cross Section from The "$1s_o$" State in $10^{-18}cm^2$	Photoionization Cross Section from The "$2p_o$" State in $10^{-18}cm^2$
5.4	2.134(-2)	7.698(-3)
5.6	1.300(-2)	8.780(-3)
5.8	1.062(-2)	9.531(-3)
6.0	9.347(-3)	1.014(-2)
6.2	8.512(-3)	1.067(-2)
6.4	7.904(-3)	1.113(-2)
6.6	7.433(-3)	1.155(-2)
6.8	7.052(-3)	1.192(-2)
7.0	6.734(-3)	1.227(-2)
7.2	6.463(-3)	1.258(-2)
7.4	6.228(-3)	1.287(-2)
7.6	6.021(-3)	1.314(-2)
7.79	5.845(-3)	1.338(-2)
7.79648	∞	1.339(-2)
7.797	2.327(-1)	1.346(-2)
7.8	9.305(-2)	1.358(-2)
8.0	1.716(-2)	1.508(-2)

Table 6.13b

Photoionization cross-sections for transitions from the bound states "$1s_o$" and "$2p_o$" to the $m_f = -1$ Coulomb-modified continuum at $B = 10^7$G.

Energy of the Final State in ϒ Ry	Photoionization Cross Section from The "$1s_o$" State in $10^{-18}cm^2$	Photoionization Cross Section from The "$2p_o$" State in $10^{-18}cm^2$
1.02009	0	∞
1.021	1.268(-5)	5.738(-2)
1.2	1.774(-4)	3.403(-3)
1.4	2.565(-4)	2.041(-3)
1.6	3.152(-4)	1.428(-3)
1.8	3.637(-4)	1.055(-3)
2.0	4.056(-4)	7.970(-4)
2.2	4.428(-4)	6.075(-4)
2.4	4.764(-4)	4.629(-4)
2.6	5.072(-4)	3.502(-4)
2.8	5.357(-4)	2.613(-4)
3.0	5.622(-4)	1.909(-4)
3.2	5.870(-4)	1.354(-4)
3.4	6.104(-4)	9.208(-5)
3.6	6.324(-4)	5.889(-5)
3.79	6.523(-4)	3.535(-5)
3.793	6.526(-4)	∞
3.794	6.650(-4)	2.755(-2)
4.0	8.486(-4)	1.647(-3)
4.2	9.367(-4)	9.908(-4)
4.4	1.007(-3)	6.751(-4)

Table 6.14a

Energy of the Final State in ϒ Ry	Photoionization Cross Section from The "$1s_o$" State in $10^{-18}cm^2$	Photoionization Cross Section from The "$2p_o$" State in $10^{-18}cm^2$
4.6	1.068(-3)	4.821(-4)
4.8	1.102(-3)	3.531(-4)
5.0	1.173(-3)	2.640(-4)
5.2	1.219(-3)	2.026(-4)
5.4	1.261(-3)	1.618(-4)
5.6	1.302(-3)	1.369(-4)
5.8	1.339(-3)	1.248(-4)
6.0	1.375(-3)	1.233(-4)
6.2	1.409(-3)	1.307(-4)
6.39	1.440(-3)	1.447(-4)
6.392	1.441(-3)	∞
6.393	1.452(-3)	1.371(-2)
6.4	1.475(-3)	4.911(-3)
6.6	1.639(-3)	9.363(-4)
6.8	1.733(-3)	6.379(-4)
7.0	1.811(-3)	5.133(-4)
7.2	1.880(-3)	4.536(-4)
7.4	1.942(-3)	4.291(-4)
7.6	1.999(-3)	4.271(-4)
7.8	2.053(-3)	4.412(-4)
8.0	2.103(13)	4.675(-4)

Table 6.14b

Photoionization cross-sections for transitions from the bound states "$1s_o$" and "$2p_o$" to the $m_f = 0$ Coulomb-modified continuum at $B = 10^7$G.

Energy of the Final State in ^{Y} Ry	Photoionization Cross Section from The "$1s_o$" State in 10^{-18} cm^2	Photoionization Cross Section from The "$2p_o$" State in 10^{-18} cm^2
1.96090	∞	0
1.961	5.513(-1)	5.984(-5)
2.0	2.790(-2)	1.181(-3)
2.2	1.131(-2)	2.890(-3)
2.4	8.367(-3)	3.876(-3)
2.6	6.953(-3)	4.628(-3)
2.8	6.083(-3)	5.249(-3)
3.0	5.480(-3)	5.780(-3)
3.2	5.030(-3)	6.247(-3)
3.4	4.679(-3)	6.662(-3)
3.6	4.394(-3)	7.037(-3)
3.79	4.169(-3)	7.360(-3)
4.0	3.958(-3)	7.686(-3)
4.2	3.786(-3)	7.971(-3)
4.4	3.636(-3)	8.233(-3)
4.6	3.503(-3)	8.474(-3)
4.72	3.431(-3)	8.611(-3)
4.72564	∞	8.617(-3)
4.726	2.840(-1)	8.708(-3)
4.8	2.292(-2)	9.992(-3)

Table 6.15a

Energy of the Final State in ϒ Ry	Photoionization Cross Section from The "$1s_o$" State in $10^{-18}cm^2$	Photoionization Cross Section from The "$2p_o$" State in $10^{-18}cm^2$
5.0	1.347(-2)	1.137(-2)
5.2	1.095(-2)	1.230(-2)
5.4	9.626(-3)	1.306(-2)
5.6	8.763(-3)	1.371(-2)
5.8	8.138(-3)	1.427(-2)
6.0	7.655(-3)	1.478(-2)
6.2	7.265(-3)	1.524(-2)
6.4	6.941(-3)	1.566(-2)
6.6	6.665(-3)	1.605(-2)
6.8	6.425(-3)	1.640(-2)
7.0	6.214(-3)	1.673(-2)
7.2	6.026(-3)	1.703(-2)
7.31	5.932(-3)	1.718(-2)
7.31670	∞	1.719(-2)
7.317	3.086(-1)	1.726(-2)
7.4	2.404(-2)	1.844(-2)
7.6	1.558(-2)	1.963(-2)
7.8	1.314(-2)	2.048(-2)
8.0	1.182(-2)	2.117(-2)

Table 6.15b

Photoionization cross-sections for transitions from the bound states "$1s_o$" and "$2p_o$" to the $m_f = 1$ Coulomb-modified continuum at $B = 10^7$G.

Energy of the Final State in γ Ry	Photoionization Cross Section from The "$1s_o$" State in $10^{-18}cm^2$	Photoionization Cross Section from The "$2p_o$" State in $10^{-18}cm^2$
1.16075	∞	0
1.161	1.062(-1)	1.450(-2)
1.2	1.255(-2)	1.496(-1)
1.4	8.089(-3)	1.418(-1)
1.6	6.362(-3)	7.912(-2)
1.8	6.479(-3)	4.193(-2)
2.0	7.202(-3)	2.215(-2)
2.2	7.640(-3)	1.168(-2)
2.4	7.459(-3)	6.083(-3)
2.6	6.779(-3)	3.093(-3)
2.8	5.891(-3)	1.511(-3)
3.0	5.039(-3)	6.941(-4)
3.2	4.352(-3)	2.884(-4)
3.37873	∞	1.131(-4)
3.379	6.345(-3)	2.332(-3)
3.4	4.511(-3)	1.795(-2)
3.6	4.435(-3)	2.414(-2)
3.8	4.153(-3)	1.551(-2)
4.0	4.295(-3)	9.475(-3)
4.2	4.636(-3)	5.768(-3)
4.4	4.894(-3)	3.528(-3)
4.6	4.921(-3)	2.177(-3)

Table 6.16a

Energy of the Final State in ϒ Ry	Photoionization Cross Section from The "$1s_o$" State in $10^{-18}cm^2$	Photoionization Cross Section from The "$2p_o$" State in $10^{-18}cm^2$
4.8	4.732(-3)	1.364(-3)
5.0	4.432(-3)	8.751(-4)
5.2	4.082(-3)	5.798(-4)
5.4	3.758(-3)	3.997(-4)
5.51588	∞	3.289(-4)
5.516	4.095(-3)	8.530(-4)
5.6	3.517(-3)	9.852(-3)
5.8	3.346(-3)	8.063(-3)
6.0	3.206(-3)	5.206(-3)
6.2	3.162(-3)	3.311(-3)
6.4	3.155(-3)	2.139(-3)
6.6	3.115(-3)	1.412(-3)
6.8	3.013(-3)	9.539(-4)
7.0	2.865(-3)	6.603(-4)
7.2	2.697(-3)	4.684(-4)
7.4	2.528(-3)	3.406(-4)
7.61	2.362(-3)	2.505(-4)
7.61436	∞	2.490(-4)
7.615	2.600(-3)	8.375(-4)
7.8	2.224(-3)	4.740(-3)
8.0	2.110(-3)	3.273(-3)

Table 6.16b

Photoionization cross-sections for transitions from the bound states "$1s_o$" and "$2p_o$" to the $m_f = -1$ Coulomb-modified continuum at $B = 10^9$G.

Energy of the Final State in γ Ry	Photoionization Cross Section from The "$1s_o$" State in $10^{-18}cm^2$	Photoionization Cross Section from The "$2p_o$" State in $10^{-18}cm^2$
2.52522	0	∞
2.526	3.781(-4)	9.369
2.6	2.032(-2)	4.045(-1)
2.8	6.493(-2)	3.504(-3)
3.0	5.300(-2)	1.011(-2)
3.2	3.691(-2)	2.066(-2)
3.4	3.084(-2)	2.574(-2)
3.6	3.127(-2)	2.539(-2)
3.8	3.370(-2)	2.373(-2)
4.0	3.493(-2)	2.159(-2)
4.2	3.351(-2)	1.923(-2)
4.4	2.967(-2)	1.679(-2)
4.6	2.454(-2)	1.439(-2)
4.8	1.932(-2)	1.215(-2)
4.81222	1.901(-2)	∞
4.813	1.900(-2)	7.622
5.0	4.613(-2)	3.258(-2)

Table 6.17a

Energy of the Final State in ϒ Ry	Photoionization Cross Section from The "$1s_o$" State in $10^{-18}cm^2$	Photoionization Cross Section from The "$2p_o$" State in $10^{-18}cm^2$
5.2	4.505(-2)	1.412(-2)
5.4	2.841(-2)	2.350(-2)
5.6	2.056(-2)	2.352(-2)
5.8	1.970(-2)	2.068(-2)
6.0	2.205(-2)	1.782(-2)
6.2	2.455(-2)	1.541(-2)
6.4	2.515(-2)	1.333(-2)
6.6	2.337(-2)	1.145(-2)
6.8	2.000(-2)	9.723(-3)
6.99	1.635(-2)	8.241(-3)
6.9974	1.622(-2)	∞
6.998	1.623(-2)	6.926
7.2	3.490(-2)	1.578(-2)
7.4	3.140(-2)	1.224(-2)
7.61	1.954(-2)	1.868(-2)
7.8	1.511(-2)	1.766(-2)
8.0	1.488(-2)	1.502(-2)

Table 6.17b

Photoionization cross-sections for transitions from the bound states "$1s_o$" and "$2p_o$" to the $m_f = 0$ Coulomb-modified continuum at $B = 10^9$G.

Energy of the Final State in ϒ Ry	Photoionization Cross Section from The "$1s_o$" State in $10^{-18}cm^2$	Photoionization Cross Section from The "$2p_o$" State in $10^{-18}cm^2$
0.674613	∞	0
0.675	3.027(1)	9.448(-2)
0.8	1.478	1.093
1.0	7.441	9.028(-1)
1.2	4.803(-1)	6.280(-1)
1.4	3.396(-1)	4.311(-1)
1.6	2.522(-1)	3.006(-1)
1.8	1.929(-1)	2.135(-1)
2.0	1.506(-1)	1.541(-1)
2.2	1.195(-1)	1.127(-1)
2.4	9.610(-2)	8.350(-2)
2.6	7.827(-2)	6.263(-2)
2.8	6.452(-2)	4.760(-2)
3.0	5.378(-2)	3.667(-2)
3.16	4.682(-2)	3.006(-2)
3.16075	∞	3.003(-2)
3.161	2.181(-1)	6.909(-2)
3.2	6.542(-2)	4.236(-1)
3.4	5.113(-2)	3.641(-1)
3.6	4.265(-2)	1.950(-1)
3.8	3.805(-2)	1.027(-1)
4.0	3.511(-2)	5.611(-2)
4.2	3.234(-2)	3.212(-2)
4.4	2.915(-2)	1.935(-2)

Table 6.18a

Energy of the Final State in γ^2 Ry	Photoionization Cross Section from The "$1s_o$" State in $10^{-18}cm^2$	Photoionization Cross Section from The "$2p_o$" State in $10^{-18}cm^2$
4.6	2.568(-2)	1.233(-2)
4.8	2.227(-2)	8.347(-3)
5.0	1.924(-2)	6.005(-3)
5.2	1.671(-2)	4.563(-3)
5.37	1.496(-2)	3.743(-3)
5.37873	∞	3.708(-3)
5.379	1.821(-2)	7.232(-3)
5.4	1.557(-2)	3.191(-2)
5.6	1.428(-2)	4.043(-2)
5.8	1.288(-2)	2.614(-2)
6.0	1.219(-2)	1.633(-2)
6.2	1.188(-2)	1.033(-2)
6.4	1.155(-2)	6.694(-3)
6.6	1.100(-2)	4.472(-3)
6.8	1.025(-2)	3.099(-3)
7.0	9.413(-3)	2.238(-3)
7.2	8.594(-3)	1.686(-3)
7.4	7.850(-3)	1.320(-3)
7.51	7.480(-3)	1.171(-3)
7.51588	∞	1.164(-3)
7.516	8.103(-3)	1.878(-3)
7.61	7.235(-3)	1.419(-2)
7.8	6.785(-3)	1.143(-2)
8.0	6.383(-3)	7.466(-3)

Table 6.18b

Photoionization cross-sections for transitions from the bound states "$1s_o$" and "$2p_o$" to the $m_f = 1$ Coulomb-modified continuum at $B = 10^9$G.

§6.4 Conclusions

We have calculated the photoionization of the "$1s_o$" and "$2p_o$" states of atomic hydrogen in magnetic fields between 10^7 and 10^9G, at photon energies $h\nu = I_x + \beta$ where I_x is the (field-dependent) ionization threshold and $0 \leq \beta \leq 8$Ryd.

The model used, treats the bound states accurately, but approximates Coulomb effects in the continuum by decoupling the motion of the ejected electron along the field lines from its motion perpendicular to the field. The results are in general very different from those obtained ignoring Coulomb effects in the continuum completely (Landau model).

In general the photoionization cross-section is much smaller than in the field free case, until very high energies. As in the Landau model there are discrete states (for the motion perpendicular to the field lines) embedded in the continuum, and there are threshold resonances associated with these. Depending on the azimuthal quantum and parity of the initial and final states, the cross-section at these thresholds behaves in both models as k_f or k_f^{-1}. There are secondary maxima in the cross section not associated with threshold resonances and we have shown that these arise even in the simple Landau model. They appear to be associated with the details of the motion of the electron along the field lines, and since apart from an energy independent factor this is the same in our Coulomb continuum model as in the Landau model, they should occur at the same energies in both models, given the same bound state wave functions. Our calculations indicate that they should be more readily observable in photoionization of the "$1s_o$" state. We note that since the (ℓ, $m_f = 0, \pm 1$) levels are, unlike the Landau case, no longer degenerate in the presence of a Coulomb interaction, one should expect to see three times as many resonances as had been naively supposed; further when spin splittings are included, all of them will be doublets.

It is believed that some progress has been made towards establishing the behaviour of the photoionization cross-section of hydrogen in a magnetic field. However, these models do not include the effects of broadening due to the motion of the residual ion, and treat the effect of the Coulomb field on the continuum levels in an approximate fashion.

CHAPTER 7

CONCLUSIONS

In summary, the absorption of atomic hydrogen in magnetic fields in the range $10^7 \leq B \leq 10^9$G, has been studied at some length and it is believed that significant progress has been made towards describing, with some accuracy, the motion of the electron in both the bound and the free states in this range of field strengths. The bound states have been described by simple sets of cylindrical and unperturbed hydrogenic functions. The resulting energies are compared and it is found that the cylindrical functions best describe the system at high fields ($B \geq 5 \times 10^8$G), whilst for lower fields, the bound states still retain their spherical symmetry. The energies corresponding to the cylindrical wavefunctions also compare favourably with those of other authors, and the simplicity of these wavefunctions enables other matrix elements to be calculated analytically. This is illustrated in the calculation of bound-bound transition probabilities and oscillator strengths for all allowed transitions between 14 low lying levels of hydrogen, results for which are presented, and compared with the limited results of other authors.

The free states have also been studied in detail, and we consider two models for the continuum: (i) the pure Landau continuum which is believed to be an accurate description of the free state of the hydrogen atom in a region where the magnetic interaction is much larger than that of the Coulomb interaction and (ii) the Landau continuum modified by the Coulomb attraction of the nucleus in a plane perpendicular to the direction of the magnetic field. Wavefunctions describing the discrete states which exist in the plane perpendicular to the field direction, and the corresponding energy eigenvalues, have previously been calculated for the Landau continuum - these are just the states of the free electron in a magnetic

field, where the spacing between the energy levels is $\hbar\omega_c$ a.u. throughout. The wavefunctions and energies for the Coulomb modified continuum are calculated on solving a two point boundary value equation using numerical techniques. It is shown that the Coulomb field does, in fact, have a significant effect on the Landau continuum, especially, as expected, at the lower end of the range of field strengths considered here, and this, in turn, has a dramatic effect on the nature of the photoionization cross sections. It is seen, particularly at lower fields, that the energy spacing near to threshold departs from the $\hbar\omega_c$ a.u. of the Landau continuum, and approaches the value of $1.5\,\hbar\omega_c$ a.u., which is the spacing predicted by the semi classical WKB approximation, for a particle in a Coulomb and magnetic field at zero energy. However, as one departs from the ionization threshold, this spacing decreases until the Landau limit is eventually reached. It is, also shown that the wavefunctions in both types of continua, have different characteristics near the origin, and that the effect of the Coulomb interaction is to draw the wavefunction to smaller ρ, thus increasing the number of oscillations in the region of overlap with the bound states, at lower field strengths.

Much has also been achieved in attempting to establish the behaviour of the photoionization cross-sections. The formula for these cross-sections is derived, and evaluated for absorption from the lowest even and lowest odd parity bound states in our cylindrical basis. The threshold behaviour of the cross section has been discussed, and is the same in both the models we consider. A resonance is seen at the energies corresponding to each discrete level. The primary differences found between the cross sections where the final state is in the Landau continuum and those where the final state is in the Coulomb modified continuum, are found to be (i) that there is no degeneracy of energy levels in the Coulomb modified continuum, and as a result of this, three times as many resonances are seen than in the Landau continuum, and (ii) that due to the different nature of the wavefunctions in the region of overlap with the bound states, the

cross-sections in the Coulomb modified case, are much smaller than in the Landau case. Other features of the cross sections have also been discussed in detail.

Our continuum models do not include the effects of broadening due to the motion of the residual ion, and treat the effect of the Coulomb field on the continuum states in an approximate fashion. It has been shown here that, on replacing the plane wave by the more accurate distorted wave in the z direction, to include the effect of the Coulomb field, the threshold behaviour is unchanged. The fact that the coupling of the motion in the z direction with that in the (ρ, ϕ) plane has a broadening effect has been noted by Rau (1980). Clearly the problem is a complex one, with many more factors needing to be considered. It is believed that some progress has been made with the solution of a simple case, but there is much scope for further research in this field.

Appendix I

Details of Computer Programs

§AI.1 Program HYDROGN

This program calculates the energy eigenvalues and corresponding eigenvectors of a hydrogen atom in a uniform, static magnetic field, and also bound-bound transition probabilities, wavelengths and oscillator strengths. The wavefunctions are represented by a basis of unperturbed, hydrogenic functions, discussed in Chapter 2. A block diagram of the program is given in figure AI.1 and the structure is outlined below:

HYDROGN: main routine in which input is read (see table AI.1)

EIGEN: sets up the matrix containing the Hamiltonian matrix elements and calls the NAG routine F02ABF to calculate the eigenvalues and eigenvectors by the methods described in Chapter 2

RMAT: computes the matrix elements of r^2

THREEJ: computes the product of two Wigner 3_j symbols:

$$\sqrt{(2\ell_i+1)(2\ell_j+1)}\begin{pmatrix}\ell_i & \ell_j & 2\\ 0 & 0 & 0\end{pmatrix}\begin{pmatrix}\ell_i & \ell_j & 2\\ m_i & -m_j & 0\end{pmatrix}$$

BOUND: calculates the bound-bound transition probabilities, oscillator strengths and wavelengths for transitions specified by IX and IY (see input data)

ONEJ: computes the product of two Wigner 3_j symbols:

$$\sqrt{(2\ell_i+1)(2\ell_j+1)}\begin{pmatrix}\ell_j & 1 & \ell_i\\ 0 & 0 & 0\end{pmatrix}\begin{pmatrix}\ell_j & 1 & \ell_i\\ -m_j & \mu & m_i\end{pmatrix}$$

where $\mu = 0, \pm 1$ and $\ell_j = \ell_i \pm 1$

RMAT1: computes the integrals $I_3(j,k)$ given by equation (2.93).

FAC: calculates factorials

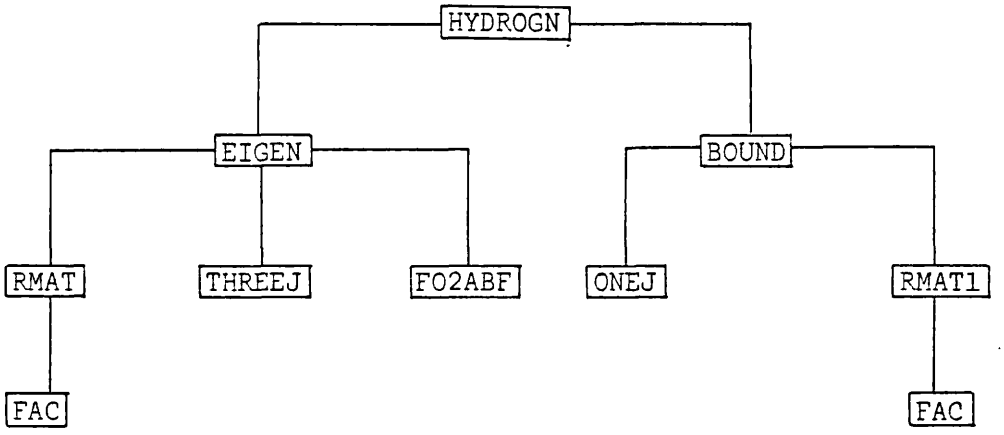

Fig. AI.1

Block Structure of program HYDROGN

Input Data

Input data for program HYDROGN is described in table AI.1. The energy eigenvalues and corresponding wavefunctions are calculated for even and odd parity states with given magnetic quantum numbers M1 and M2. Only transitions between states of different parity are allowed, and so if transition probabilities, oscillator strengths and wavelengths are required, additional data is read in, specifying the particular states of each parity, for the transition.

Input Variable	Description	Format
NS	Number of s,p,d,f and g states in the basis	I5
NP		I5
ND		I5
NF		I5
NG		I5
GAM	Measure of the field strength ($\gamma = \hbar\omega_c$)	E15.6
M1	Magnetic quantum number of even parity states	I5
M2	Magnetic quantum number of odd parity states	I5
NSL	Principle quantum numbers of the lowest s,p, d,f and g states to be included in the basis	I5
NPL		I5
NDL		I5
NFL		I5
NGL		I5
ITRANS	= 1 if transition probability required	I5
NNDO*	Number of transition probabilities required	I5
IX*	Column of the even parity eigenvector matrix required for the transition probability calculations	I5
IY*	Column of the odd parity eigenvector matrix required for the transition probability calculations	I5
NON*	= 1 if the state with the lowest energy in the transition has even parity = 2 if the state with the lowest energy in the transition has odd parity.	I5
NUPPER*	Principle quantum number of the state with highest energy in the transition	I5
NLOWER*	Principle quantum number of the state with lowest energy in the transition.	I5
LUPPER*	Angular momentum quantum number of the state with highest energy in the transition.	I5
LLOWER*	Angular momentum quantum number of the state with the lowest energy in the transition.	I5

Table AI.1

Input data for program HYDROGN. Variables marked with * are only read if ITRANS = 1

§AI.2 Program CPOLAR

The description of this program will be kept to a minimum as it is described in some considerable detail by Kara, 1980. Basically, the energy eigenvalues and corresponding eigenvectors of a hydrogen atom in a uniform static magnetic field are calculated, and also the bound-bound transition probabilities, wavelengths and oscillator strengths are determined. The wavefunctions are represented by a basis of cylindrical functions of the form

$$\chi^{(m,\pi)}_{\alpha\beta\delta} = z^{\alpha}\rho^{\beta}e^{-\delta r^2}e^{im\phi}$$

as described in chapter 3.

A block diagram of the program is shown in fig.AI.2 and the structure is outlined below:

CPOLAR: main routine where input is read and the matrices containing the Hamiltonian matrix elements and overlap integrals are generated.

BODD, BEVEN: Evaluates all the integrals given by tables 3.2 and 3.3, except for the common factors $J(B,\Delta)$ and $K(\alpha_o,\Delta)$, when $A > 2$ and $B > 1$.

NAGR : Calls all NAG routines needed to calculate the required eigenvalues and eigenvectors (details given below).

BBCPOL: Calculates transition probabilities, oscillator strengths and wavelengths for four transitions in the length ($\Delta m = 0, \pm 1$) and velocity ($\Delta m = 0$) forms. The following routines are called to evaluate the matrix elements of $r_{o,\pm 1}$ and ∇_o.

BEVNR1: Evaluates $\langle X_j | r_{\pm 1} | X_k \rangle$ given by equation (3.73) for even B. RBEVEN is called to calculate the integral over r.

BODDR1: Evaluates $\langle X_j | r_{\pm 1} | X_k \rangle$ given by equation (3.73) for odd B. RBODD is called to calculate the integral over r.

BEVNRO : Evaluates the integrals occurring in $\langle X_j | r_o | X_k \rangle$ and $\langle X_j | \nabla_o | X_k \rangle$ given by equations (3.76) and (3.83) for even B. RBODD is called to calculate the integral over r.

BODDRO : Evaluates the integrals occurring in $\langle X_j | r_o | X_k \rangle$ and $\langle X_j | \nabla_o | X_k \rangle$ given by equations (3.76) and (3.83) for odd B. RBEVEN is called to calculate the integral over r.

The NAG routines used to calculate the eigenvalues and eigenvectors are F01AEF, F01AGF, F02BEF, F01AHF and F01AFF. A description of these routines is set out in table AI.2.

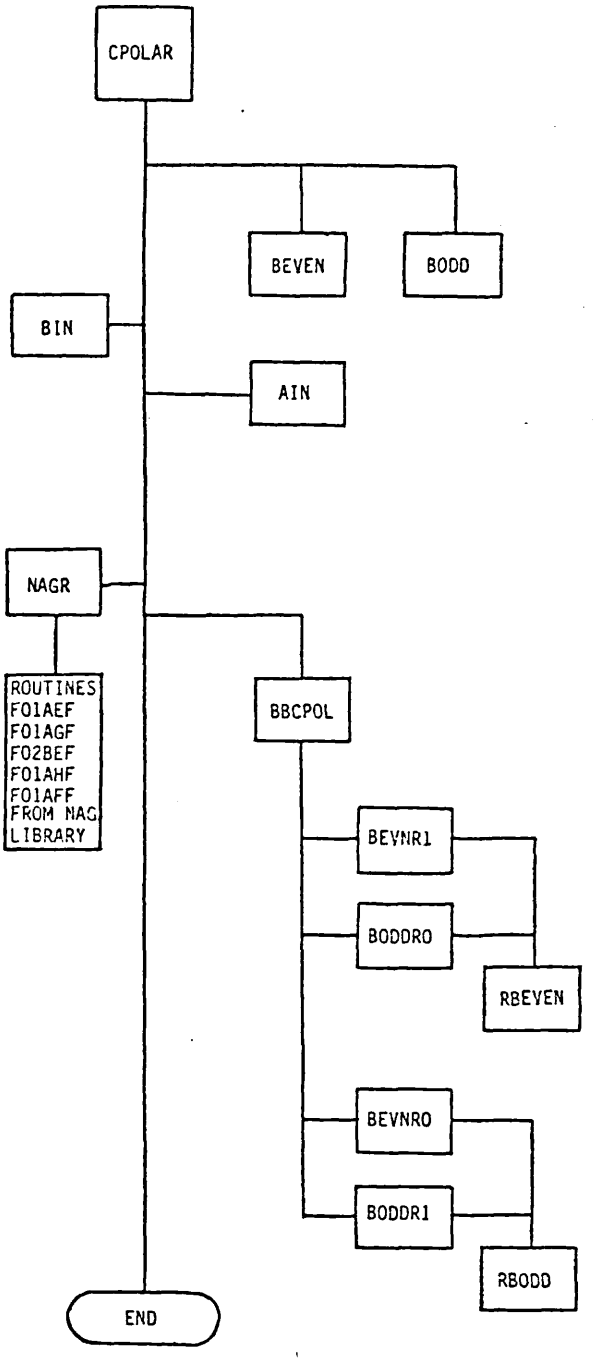

Fig. AI.2
Block Structure of program CPOLAR

NAG Routine	Description
F01AEF	Reduces the eigenproblem $A\underline{x} = \lambda S\underline{x}$ to the standard symmetric eigenproblem $P\underline{z} = \lambda \underline{z}$. P is of the form $L^{-1} AL^{-T}$.
F01AGF	Reduces the previously calculated real symmetric matrix P to tridiagonal form, denoted by PP.
F02BEF	Calculates eigenvalues of the problem $PP\underline{y} = \lambda \underline{y}$ in a given interval, and the corresponding eigenvectors.
F01AHF	Derives the eigenvectors of P from those of PP corresponding to the previously calculated eigenvalues.
F01AAF	Derives the eigenvectors of $A\underline{x} = \lambda S\underline{x}$ from those of the problem $P\underline{z} = \lambda \underline{z}$.

Table AI.2

Description of NAG library routines used in CPOLAR.

§AI.3 Program WFPLOT

This program solves the two point boundary value problem

$$u''(\rho) = V(\rho, \varepsilon)\, u(\rho) \quad ; \quad u(0) = u(\infty) = 0 \qquad \text{(AI.1)}$$

where an initial estimate for the eigenvalue, ε, is given. The method of solution is to reduce equation (AI.1) to a system of first order differential equations:

$$u_1'(\rho) = u_2(\rho) \qquad \text{(AI.2)}$$
$$u_2(\rho) = V(\rho, \varepsilon)\, u_1(\rho)$$

and solve these by a numerical, Runge-Kutta technique. The input data is described in table (AI.3). The methods by which the inward and outward integrations are started are described in Chapter 6.

Input Variable	Description	Format
NSTEP	Number of steps in the interval $[0.11, R2/2]$ at which the function $u_{out}(\rho)$ is to be evaluated.	I5
LAMBDA	Initial estimate for the eigenvalue EPS.	E15.6
GAM	Measure of the field strength ($\gamma = \hbar\omega_c$)	E15.6
M	Magnetic quantum number of the continuum state.	I5
ICOUL	Value of charge on nucleus (=0 for pure Landau continuum)	I5
R2	Outer limit for wavefunction calculation	E15.6

Table AI.3

Input data for program WFPLOT

Structure of the Program

WFPLOT: The main routine in which the input data is read and LANDAU is called to perform the calculations.

LANDAU: Calculates the values of $u(\rho)$ at each point in the interval [0,R2], the number of points being determined by NSTEP (input data).

The exact value of the eigenvalue is also obtained such that the first derivative of $u(\rho)$ agrees to four decimal places at the matching point ρ_o (which is set to $R2/2$ for convenience). The structure of this routine is described in figure (AI.3), where

$$\text{DELEPS} = (\text{ANORM})^2 \left\{ \frac{u'_{in}(\rho_o)}{u_{in}(\rho_o)} - \frac{u'_{out}(\rho_o)}{u_{out}(\rho_o)} \right\}$$

with $$\text{ANORM} = \left\{ \frac{N_{out}}{(u_{out}(\rho_o))^2} + \frac{N_{in}}{(u_{in}(\rho_o))^2} \right\}^{-\frac{1}{2}},$$

$$N_{out} = \int_o^{\rho_o} (u_{out}(\rho))^2 d\rho$$

and $$N_{in} = \int_{\rho_o}^{R2} (u_{in}(\rho))^2 d\rho$$

(cf. equations (6.20) and (6.23))

OUT: Evaluates $u(\rho)$ at the points 0.09, 0.10 and 0.11, given the initial gradient, according to the series expansion of equation (6.37).

IN: Evaluates $u(\rho)$ at the three points R2, R2-h_o and R2-2h_o, where h_o is the steplength determined by NSTEP, given the initial gradient, according to equation (6.39).

The following routines from the NAG library are also used:

D01ABF: Calculates the inward and outward integrations for each steplength h_o using a Runge Kutta technique. The routine is called (NSTEP + 3) times for the outward integration to ρ_o, and NSTEP times for the inward integration to ρ_o.

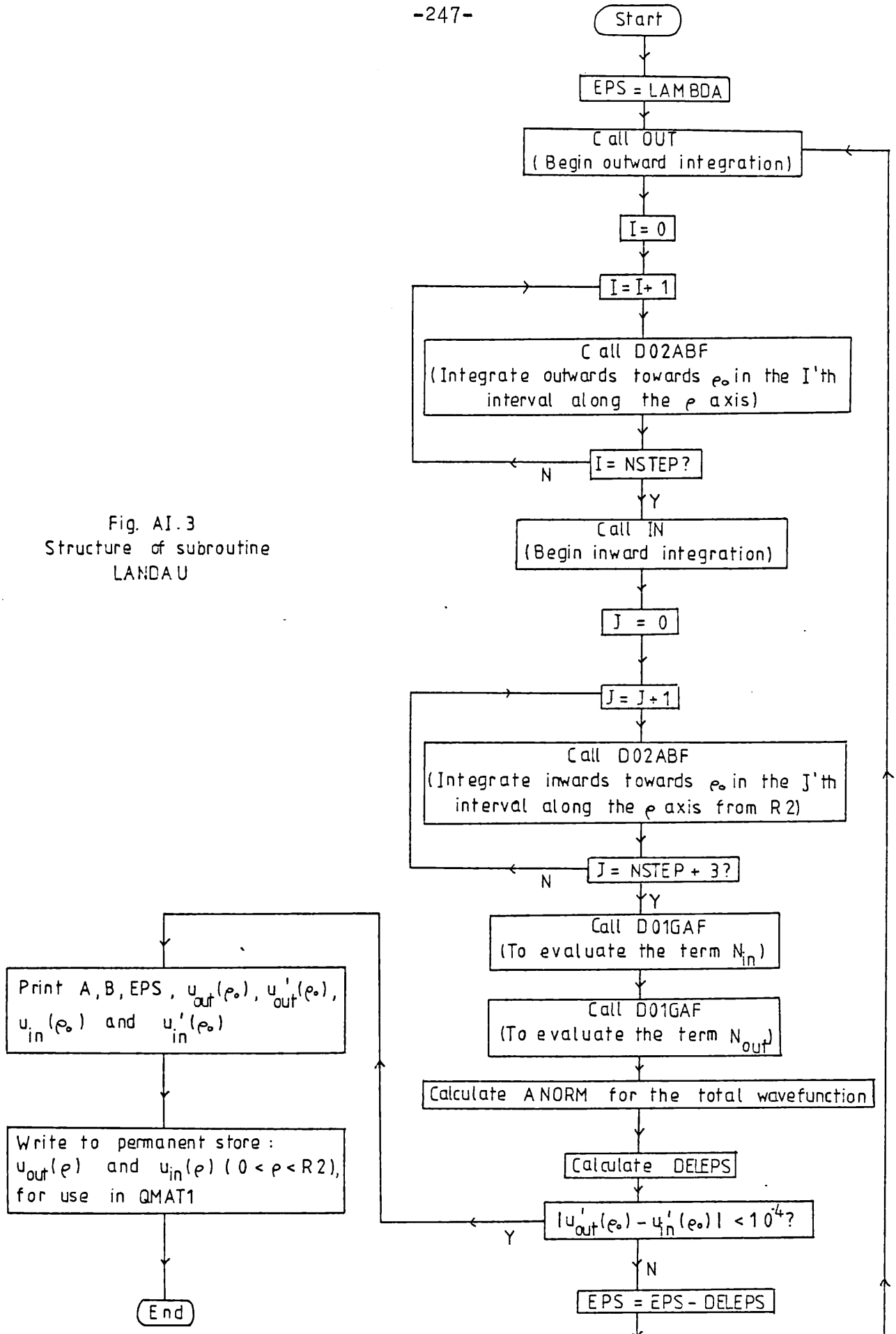

Fig. AI.3
Structure of subroutine
LANDAU

D01GAF: Used to evaluate N_{in} and N_{out}.

One of the following routines (as appropriate) is required for each call to D01ABF:

AUXOUT: Sets F(1) = $u_{out}(\rho)$ and F(2) = $u_{out}'(\rho)$ at a particular value of ρ .

AUXIN: Sets F(1) = $u_{in}(\rho)$ and F(2) = $u_{in}'(\rho)$ at a particular value of ρ .

§AI.4 Program QMAT

Program QMAT calculates the total photoionization cross-section given by equation (5.7). The bound state is of the form given by equation (5.8) and the continuum contains pure Landau levels. All the matrix elements occurring in this cross-section are evaluated analytically. The structure of the program is outlined in figure AI.4.

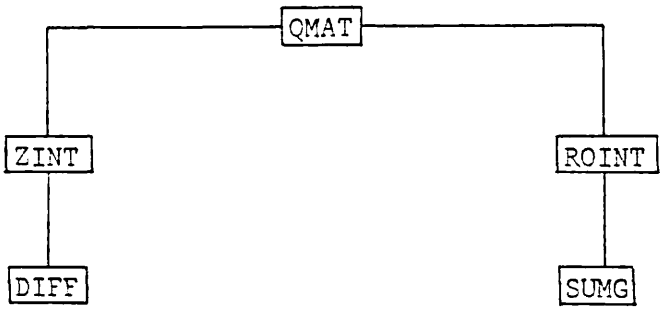

Fig.AI.4.

Block diagram of program QMAT.

The main routine is

QMAT: Input data is read and all calculations apart from the integrals over z and ρ occurring in the matrix elements, are carried out. A flow chart describing the structure of this routine is given in figure AI.5.

The variables used in this flow chart are defined as:

QMATR - the matrix element $|\langle \psi_i | r_\mu | \psi_f \rangle|^2$ (see §5.3)

$$\text{TOTQM} - \sum_{\ell=\ell_{min}}^{\ell_{max}} |\langle \psi_i | \sum_{\mu=-1}^{1} r_\mu | \psi_f \rangle|^2$$

PCS - total photoionization cross-section.

For other variables not defined here, see table AI.4

ZINT: Computes, analytically, the integral over z which occurs in the matrix element $\langle \psi_i | r_\mu | \psi_f \rangle$ and stores the result in Z. This is the same as the expression for Z given by equation (5.24). This subroutine calls the function DIFF to calculate the differential in equation (5.24).

DIFF: Calculates $\frac{d^\alpha}{dx^\alpha}(e^{-x^2/2})$ for $\alpha = 0,1.....8$ (see appendix III).

ROINT: Computes analytically the integral over ρ, given by equation (5.32). The subprogram SUMG is called.

SUMG: Calculates $\frac{\Gamma(a-p+1)}{\Delta^{a-p+1}}$ recursively.

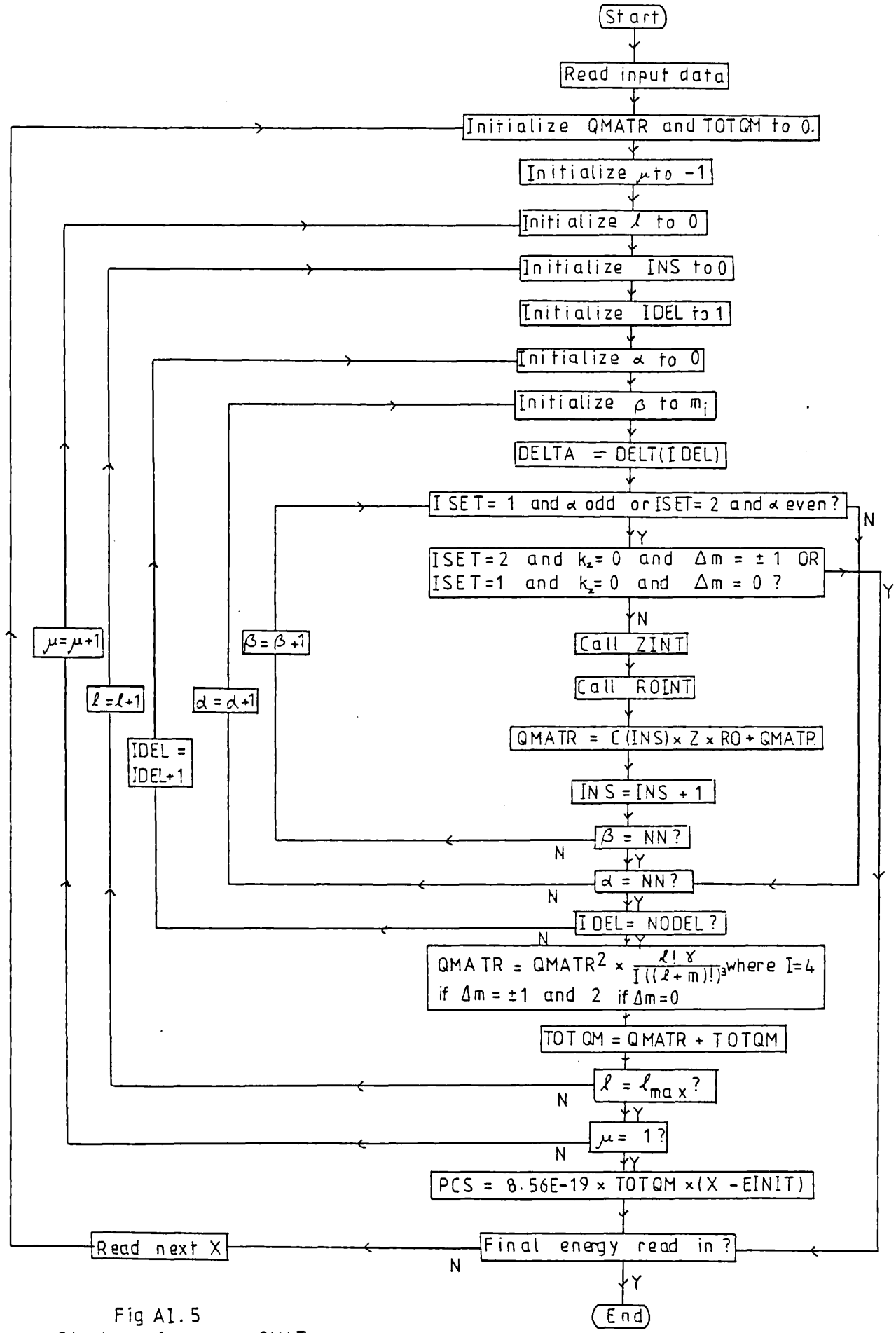

Fig AI.5
Structure of program QMAT

INPUT DATA

The input data for program QMAT is described in table (AI.4)

Input Variable	Description	Format
NODEL	Number of δ's to be included in the initial state wavefunction.	I5
NN	Maximum value of α and β to be included in the initial state wavefunction.	I5
ISET	= 1 if initial state has odd parity. = 2 if initial state has even parity.	I5
MI	Magnetic quantum number of initial state.	
GAM	Defines field strength ($\gamma = \hbar\omega_c$).	E15.6
EINIT	Energy eigenvalue for the initial state (computed by CPOLAR).	
DELT(I), I = 1,..NODEL	The values for δ which are to be included in the initial state wavefunction.	E15.6
IDIM	The total number of terms in the initial state wavefunction.	I5
C(I), I=1,..IDIM	The values of the coefficients of the initial state wavefunction (computed by CPOLAR).	E15.6
NIMP	Number of values of the final state energy for which the photoionization cross-section is to be calculated.	I5
X	Value of the energy of the final state in γ Ry.	E15.6

Table AI.4

Input data for program QMAT.

§AI.5 Program QMAT1

This program calculates the photoionization cross-section given by equation (5.7), but the sum over m_f is not included. Only the contribution to the final state with magnetic quantum number MF is computed, but the sum over all possible continuum levels for this m_f is included. The bound state is of the form given by equation (5.8) and the continuum model is that described in chapter 6. The wavefunctions of the continuum state are calculated in numerical form and so, in this program the ρ integral is calculated numerically. The structure of the program is outlined in figure AI.6. A more detailed description will be given elsewhere, (Kara, 1981).

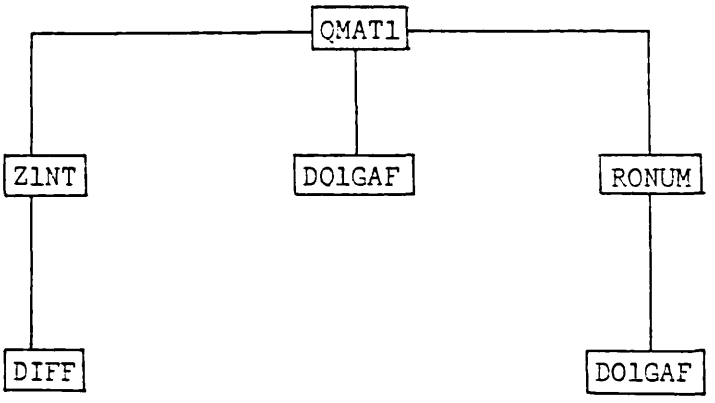

Fig.AI.6.

Block diagram of program QMAT1

The main routine is

QMAT1: Input data is read and all calculations, apart from the integrals over z and ρ occurring in the matrix elements, are carried out. The structure of this routine is similar to that of program QMAT (described in the previous section). The only differences being that the sum over ℓ is now replaced by a sum over the wavefunctions of the discrete continuum states,

whose principle quantum numbers and energies depend on the strength of the magnetic field, and the sum over m_f (ie. μ) is not included.

ZINT: The same routine as that used in program QMAT.

DIFF: Also the same routine as that used in program QMAT.

RONUM: Calculates the integral $\int_0^\infty \rho^{\beta+3/2} e^{-\delta\rho^2} u(\rho) d\rho$, where the numerical calculations are carried out by the NAG routine DOIGAF.

The following routine from the NAG library is called:

DO1GAF: This is called to carry out, by the numerical method described by Gill and Miller, 1972 , the integral over ρ (in RONUM) and the normalization constant of the total final state wavefunction given by equation (6.3) (in QMAT1).

Input Data

The input data for program QMAT1 is described in table (AI.5).

Input Variable	Description	Format
NODEL	As in table (AI.4)	I5
NN		I5
ISET		I5
MI		I5
MJ	Magnetic quantum number of the final state.	I5
GAM	As in table (AI.4)	E15.6
EINIT		E15.6
DELT(I)		E15.6
IDIM		I5
C(I)		E15.6
NNOLEV	Number of continuum levels to be included in the cross section.	I5
ENERGY(I)	Values of the NNOLEV energy eigenvalues of the continuum states.	E15.6
NNXU	Number of points at which the wavefunction of the final state is given.	I5
XX(I)	Values of ρ at which $u(\rho)$ is given.	E20.13
UU(I)	Values of $u(\rho)$ at the NNXU points.	E20.13
NIMP	As table (AI.4).	I5
X1	Energy of final state for which photoionization cross-section is to be calculated.	E15.6

Table AI.5

Input data for program QMAT1.

Appendix II

Evaluation of the Integral $\int_o^\infty e^{-ax^2} x^b \, dx$

We have, from Dwight, equations 860.15 and 860.16,

$$I_{a,b} = \int_o^\infty e^{-ax^2} x^b \, dx = \begin{cases} \dfrac{\left(\frac{a-1}{2}\right)!}{2b^{(a+1)/2}} & \text{if a is odd} \\ \dfrac{(a-1)!!\ \sqrt{\pi}}{2^{(a/2)+1}\ b^{(a+1)/2}} & \text{if a is even} \end{cases} \qquad \text{(AII.1)}$$

with a an integer and where p!! is defined as

$$(2n)!! = 2.4.6.\ldots\ldots\ldots 2n \qquad \text{(AII.2)}$$

and $(2n-1)!! = 1.3.5.\ldots\ldots.(2n-1).$

The values of this integral for $1 \leq a \leq 9$ are given in table AII.1 for easy reference.

If $\int_{-\infty}^{\infty} e^{ax^2} x^b \, dx$ is required, it should be noted that, if b is odd, then $x^b e^{-ax^2}$ is an odd function and so the integral will be zero. If b is even, however, the value of this integral will be $2.I_{a,b}$.

a	$I_{a,b}$
1	$\frac{1}{2b}$
2	$\frac{\sqrt{\pi}}{2b^{3/2}}$
3	$\frac{1}{2b^2}$
4	$\frac{3\sqrt{\pi}}{b^{5/2}}$
5	$\frac{1}{b^3}$
6	$\frac{15\sqrt{\pi}}{16b^{7/2}}$
7	$\frac{3}{b^4}$
8	$\frac{105\sqrt{\pi}}{32b^{9/2}}$
9	$\frac{12}{b^5}$

Table AII.1

Values of $I_{a,b}$ for $1 \leq a \leq 9$

APPENDIX III

Expansion of the First Nine Hermite Polynomials

The Hermite polynomial $He_n(x)$ can be written

$$He_n(x) = (-1)^n e^{x^2/2} \frac{d^n}{dx^n} (e^{-x^2/2}) \quad .$$

The polynomial representations of $\frac{d^n}{dx^n}(e^{-x^2/2})$ are given below for $0 \leq n \leq 8$. These are the only values of n required in programs QMAT and QMAT1 for the initial state wave functions considered here, as the maximum value for α taken, in the basis set, is 7.

n	$\frac{d^n}{dx^n}(e^{-x^2/2})$
0	$e^{-x^2/2}$
1	$-xe^{-x^2/2}$
2	$(x^2-1)e^{-x^2/2}$
3	$(-x^3+3x)e^{-x^2/2}$
4	$(x^4-6x^2+3)e^{-x^2/2}$
5	$(-x^5+10x^3-15x)e^{-x^2/2}$
6	$(x^6-15x^4+45x^2-15)e^{-x^2/2}$
7	$(-x^7+21x^5-105x^3+105x)e^{-x^2/2}$
8	$(x^8-28x^6+210x^4-420x^2+105)e^{-x^2/2}$

Table (III.1)

REFERENCES

Akimoto O and Hasegawa H 1967 J. Phys. Soc. Japan 22 181

Bethe H A and Salpeter E E 1977 "Quantum Mechanics of One- and Two-Electron Atoms" (Plenum)

Bhaduri R K, Nogami Y and Warke C S 1977 Astrophys. J. 217 324

Brandi H S 1975 Phys. Rev. A 11 1835

Brandi H S, Koiller B, Lins de Barros H G P and Miranda L C M 1978 Phys. Rev. A 18 1415

Brandi H S, Santos R R and Miranda L C M 1976 Lett. Nuovo Cimento 16 6

Brandi H S and Koiller B 1978 Can. J. Phys. 56 1545

Blumberg W A M, Itano W M and Larson D J 1979 Phys. Rev. A 19 139

Blumberg W A M, Jopson R M and Larson D J 1978 Phys. Rev. Lett. 40 1320

Burgess A 1964 Mem. R. Astr. Soc. 1964 69 (part 1)

Burke P G 1976 in "Atomic Processes and Applications" (ed. Burke P G and Moisieiwitsch B L) Ch. 7, (North Holland)

Bateman Manuscript Project, California Institute of Technology 1954 Vol 1, Higher Transcendental Functions, ed. Erdelyi A

Cabib D, Fabri E and Fiori G 1972 Nuovo Cimento 10 B 185

Clark C W and Taylor K T 1980 J. Phys. B 13 L737

Condon E U and Shortley G H 1963 "The Theory of Atomic Spectra" (Cambridge Univ. Press)

Dalgarno 1961 in "Quantum Theory" Vol 1: Elements, Bates D R (ed.) (Academic Press)

Dingle R B 1952 Proc. Roy. Soc. A 211 500

Dwight H B 1947 "Tables of Integrals and Other Mathematical Data" (MacMillan)

Economou N B, Freeman R R and Liao P F 1979 Phys. Rev. A 18 2506

Edmonds A R 1965 "Angular Momentum in Quantum Mechanics" (Princeton Univ. Press)

Edmonds A R 1970 J. de Physique C4 31 71

Edmonds A R 1973 J. Phys. B 6 1603

Eyring H, Walter and Kimball 1957 "Quantum Chemistry" (Chapman and Hall)

Francis J G F 1961 Computer J. 4 265

Froberg C E 1965 "Introduction to Numerical Analysis" (Addison-Wesley)

Fonk R J, Tracy D M, Wright D and Tomkins F S 1978 Phys. Rev. Lett. 40 1366

Garstang R H 1977 Rep. Prog. Phys. 40 105

Garton W R S and Tomkins F S 1969 Astrophys. J. 158 839

Gay J C, Delande and Biraben F 1980 J. Phys. B 13 L729

Gill P E and Miller G F 1972 Computer J. 15 80

Gill P E and Murray W 1974 NPL Report NAC 37

Glasser M L and Kaplan J I 1975 Phys. Lett. 53A 373

Goldstein H 1950 "Classical Mechanics" (Addison-Wesley)

Hartree D R 1955 "The Calculation of Atomic Structures" (Chapman and Hall)

Hylleraas and Undheim 1930 Zeits. F. Physik 65 759

Kara S M 1980 Comp. Phys. Comm. 20 221

Kara S M 1981 to be submitted to Comp. Phys. Comm.

Kara S M and McDowell M R C 1980 J. Phys B 13 1337

Kara S M and McDowell M R C 1981 J. Phys. B (in press)

Kelly H P 1963 Phys. Rev. 6 91

Kemble E C 1958 "The Fundamental Principles of Quantum Mechanics with Elementary Applications" (Dover)

Kemp J C 1970 Astrophys. J. 162 L69

Kemp J C, Swedlund J B, Landstreet J D and Angel J R P 1970 Astrophys. J. 161 L77

Lambert J C 1973 "Computational Methods in Ordinary Differential Equations" (Wiley)

Landau L D and Lifshitz E M 1975 "Quantum Mechanics" (Pergamon Press)

Lawson J D 1979 Atomki Kozlemenyak 21 195

Lu K T, Tomkins F S and Garton W R S 1978 Proc. Roy. Soc. A 364 421

Macdonald 1933 Phys. Rev. 43 830

Mayers D F 1962 in "Numerical Solution of Ordinary and Partial Differential Equations", Fox L (ed) p 16-27 (Pergamon Press)

Meuller R O, Rau A R P and Spruch L 1975 Phys. Rev. A 11 789

NAG Mark 7 Fortran Manual

Pavlov-Verevkin V B and Zhilinskii B I 1980 Phys. Lett. 75 A 279

Peach G 1967 Mem. R. Astr. Soc. 71

Peach G 1970 Mem. R. Astr. Soc. 73 part 1

Peters and Wilkinson 1965 Numer. Math 7 362

Pokatilov E P and Rusanov M M 1969 Sov. Phys. - Solid State 10 2458

Powell J L and Crasemann B 1961 "Quantum Mechanics" (Addison-Wesley)

Praddaude H C 1972 Phys. Rev. A 6 1321

Rau A R P 1979 J. Phys. B 12 L193

Rau A R P 1980 Comments Atom. Mol. Phys. 10 19

Ruder H, Wunner G, Herold H and Reinecke M 1981 Astrophys. J. (in press)

Ruderman M 1972 Ann. Rev. Astr. and Ap. 10 427

dos Santos R R and Brandi H S 1976 Phys. Rev. A 13 1970

Schiff L I 1955 "Quantum Mechanics" (McGraw-Hill)

Schmitt W, Herold H, Ruder H and Wunner G 1981 Astrophys. J. (in press)

Simola J and Virtamo J 1978 J. Phys. B 11 3309

Smith E R, Henry R J W, Surmelian G L and O'Connell R F 1973 Astrophys. J. 179 659

———————— 1975 Astrophys. J. 182 651

Starace A F 1973 J. Phys. B 6 585

Surmelian K and O'Connell R P 1974 Astrophys. J. 190 741

Wallis R and Bowlden H J 1958 J. Phys. Chem. Solids 7 78

Wigner E P 1948 Phys. Rev. 73 1002

Wilkinson J H and Reinsch C 1971 "Handbook for Automatic Computation"
Vol II: Linear Algebra (Springer-Verlag)

Wunner G. 1980 Astrophys. J. 240 971

Wunner G, Ruder H and Herold H 1981 Astrophys. J. (in press)

Wunner G, Ruder H, Schmitt W, Herold H and McDowell M R C 1981a
Mon. Not. R. Astrom. Soc. (in press)

Yafet Y, Keyes R W and Adams E N 1956 J. Phys. Chem. Solids 1 137